NATIONAL TECHNICAL UNIVERSITY OF ATHENS

Interdepartmental Master's Program

«Ship and Marine technology»

Master Thesis:

«Assessment of offshore wind energy in the Greek Seas based on CERRA reanalysis data»

Natalia Elona Koutri

Environmental Engineer

Supervisor:
Dr. Takvor Soukissian, Research Director, Hellenic Centre for Marine Research

Athens 2024

Table of contents

Synopsis and structure of the work

Climate change, is an urgent threat to both our planet and human well - being. Overpopulation combined with globalization has contributed to increased energy needs, lack of natural resources and available editable (onshore) space, as well as to enlarged greenhouse emissions, constituted to catastrophic consequences on the environment. In respect of the above, several targets have been established globally, for the decarbonization of the energy mix as part of climate change mitigation, where wind energy, mainly onshore, already plays a major role in the required energy transition.

The great potential resources of the oceans on a global scale, hold the potential to satisfy both current and future energy requirements. Offshore energy can be harnessed in various ways and the available space for the potential development of energy technologies, is much greater compared to onshore. Complex geomorphological schemes, affect the magnitude of wind speed, thus offshore wind energy outweighs compared to onshore, presenting stronger wind speeds and lower variability measures.

The importance of wind climatology analysis, is well - established and undisputed. Climate change impacts on the wind climate, as well as the corresponded variability within a year and from year - to year, have direct impacts on human life. The statistical assessment and modeling of speed, direction, and power density of wind, are widely used concerning among others, the evaluation of potential areas for the development of wind farms. Wind resources and the corresponded variability, initiate the fundamental factors for the design, maintenance and the selection of potential sites, for the development of an offshore wind farm. Areas present either low wind speeds or high variability coefficients, lead to unbalanced profits, due to the fact that the potential energy outcome is uncertain and unstable. Moreover, the extreme wind speeds, provoke damages on the structures and lead to economic unsustainable deployment and operation.

In this study, the analysis of the offshore wind characteristics in the Greek Seas, was performed using Matlab and the dataset derived from the most recent (2022) reanalysis results, i.e., Copernicus European Regional Reanalysis (CERRA), featuring high spatial (5.5 km x 5.5) and temporal resolution. The data specifically relate to wind speed at 100 meters height above the sea level, for a 36 – year period (1985 – 2020). Three main aspects of the Greece's offshore wind climate have been examined, namely wind speed, direction and wind power density, on three temporal scales; annual, monthly and seasonal. Specifically, the aforementioned aspects have been assessed in terms of their spatial distribution at the selected temporal scales. The analysis also includes, the estimation of annual and inter – annual variability, the long – term linear trends for both the mean wind speed and the extreme wind speeds, i.e. 95^{th} and 99^{th} percentiles for the three selected temporal scales.

The high offshore wind resources in the Greek Seas, due to the Etesians over the Aegean in summer, ensuring a steadier energy production throughout a year and therefore Greece constitutes one of the most favorable areas in the Mediterranean for the development of offshore wind farms. Nevertheless, despite the significant wind potential that both the Aegean and the Ionian Sea presenting, several factors had hindered the development of offshore wind farms in Greece for many years now.

The intense tourist activity, specifically in summer months, areas facing issues of national security or characterized by intense coastal activities, the lack of submarine network to support capacity needs, technical limitations emerging from the sea depth and distance from the

coastline, unstable economic situation due to economic crisis, as well as, the lack of a robust legislative framework, constituted the main reasons. In July 2022, the Greek Parliament passed the Law no.4964/2022, articles 65 – 80, towards the advancement of offshore wind energy and restructuring associated licensing procedures.

On October of 2023, the Hellenic Hydrocarbons and Energy Resources Management Company published the National Offshore Wind Farms Development and Programme, in respect of the law no. 4964/2022, for the definition and prioritization of the potential sites for the development of offshore wind farms, in the Greek Seas. The 23 potential areas that emerged, corresponded to 30 polygons spatially distributed all over the Aegean and Ionian Seas. In respect of the above, this study also includes, the assessment of the performance of the NREL wind turbine, with rated power 15 MW, for the offshore areas in Greece. Furthermore, a more extensive analysis was performed for the 30 selected sites (polygons), including the statistical analysis of wind speed and wind power density, the annual and inter – annual variability, the long – term linear trends, and the assessment of the performance of the wind turbine, in an annual scale.

The structure of this work is the following: In chapter 1, a general information about the offshore renewable energies is presented, as well as an analytic description of the National OWF Development and Programme, including the methodology used for the evaluation and prioritization of the potential areas for the installation of offshore wind farms over the Greek Seas. In chapter 2, the description of the data used for the statistical analysis of Greece's offshore wind climate is performed. Following, in chapter 3, the theoretical background and the methodology used in this work are presented. In chapter 4 the numerical results as regards wind speed, wind direction and wind power density are presented and discussed. Finally, chapter 5 includes the results regarding the assessment of the NREL – 15 MW offshore wind turbine performance for the Greek seas, as well as for 30 selected sites that are candidates for offshore wind farm development.

Keywords: [*Offshore wind energy, Greek Seas, annual and inter – annual variability, offshore wind turbine, linear trends, CERRA reanalysis]*

Σύνοψη και δομή της εργασίας

Η κλιματική αλλαγή αποτελεί μία επιτακτική απειλή τόσο για τον πλανήτη, όσο και για την ανθρώπινη ευημερία. Ο υπερπληθυσμός σε συνδυασμό με την παγκοσμιοποίηση συνέβαλλαν στην αύξηση των ενεργειακών αναγκών, στην έλλειψη των διαθέσιμων φυσικών πόρων και των αξιοποιήσιμων χερσαίων χώρων, καθώς και στην αύξηση των εκπομπών των αερίων του θερμοκηπίου στην ατμόσφαιρα, με αποτέλεσμα μια πληθώρα από περιβαλλοντικές επιπτώσεις. Αναφορικά με όλα τα παραπάνω, αρκετοί στόχοι έχουν τεθεί παγκοσμίως, για την απανθρακοποίηση του ενεργειακού μείγματος και κατ' επέκταση τον μετριασμό της κλιματικής αλλαγής, όπου η αιολική ενέργεια, κυρίως στην ξηρά, ήδη παίζει καθοριστικό ρόλο στην ενεργειακή μετάβαση που απαιτείται.

Οι ενεργειακοί πόροι των ωκεανών παγκοσμίως, είναι δυνατό να ικανοποιήσουν τόσο τις τρέχουσες όσο και τις μελλοντικές παγκόσμιες ενεργειακές απαιτήσεις. Η υπεράκτια ενέργεια μπορεί να αξιοποιηθεί με διάφορους τρόπους και ο διαθέσιμος χώρος για την πιθανή ανάπτυξη ενεργειακών τεχνολογιών, είναι πολύ μεγαλύτερος σε σχέση με αυτόν που έχει απομείνει στην ξηρά. Επιπλέον, οι υπεράκτιοι άνεμοι στους ωκεανούς, είναι ισχυρότεροι συγκριτικά με αυτούς της ξηράς, λόγω της έλλειψης πολύπλοκων γεωμορφολογιών που επηρεάζουν την ταχύτητα και την μεταβλητότητα του ανέμου.

Η σημασία της ανάλυσης και μελέτης του ανεμολογικού κλίματος μιας περιοχής, είναι πλέον καθιερωμένη και αδιαμφισβήτητη. Οι επιπτώσεις της κλιματικής αλλαγής στο ανεμολογικό καθεστώς, αλλά και η μεταβλητότητα του ανέμου από έτος σε έτος και εντός κάθε έτους, έχουν άμεσες επιπτώσεις στην ανθρώπινη ζωή. Η στατιστική ανάλυση και η μοντελοποίηση της ταχύτητας, της διεύθυνσης και της πυκνότητας αιολικής ισχύος του ανέμου, χρησιμοποιούνται ευρέως, μεταξύ άλλων, και ως παράγοντες για την αξιολόγηση εν δυνάμει περιοχών που προορίζονται για την εγκατάσταση αιολικών πάρκων. Το ανεμολογικό κλίμα μιας περιοχής και η αντίστοιχη μεταβλητότητα, αποτελούν θεμελιώδεις παράγοντες τόσο για την επιλογή των δυνητικών περιοχών ανάπτυξης, όσο και για τον σχεδιασμό και την συντήρηση των αιολικών πάρκων. Περιοχές που παρουσιάζουν είτε πολύ χαμηλές ταχύτητες ανέμου, είτε υψηλές τιμές μεταβλητότητας, δεν προτιμώνται, καθώς οδηγούν σε αβέβαιες εκτιμήσεις της παραγόμενης ενέργειας και συνεπώς του σχετικού κέρδους.

Σε αυτήν τη μελέτη, η ανάλυση του υπεράκτιου αιολικού κλίματος της Ελλάδας, πραγματοποιήθηκε με τη χρήση του λογισμικού Matlab και του πιο πρόσφατου (2022) συνόλου δεδομένων επανανάλυσης (Copernicus European Regional Reanalysis (CERRA)), το οποίο χαρακτηρίζεται από υψηλή χωρική (5.5 km x 5.5) και χρονική διακριτότητα. Τα δεδομένα συγκεκριμένα σχετίζονται με την ταχύτητα του ανέμου στα 100 m ύψος από την επιφάνεια της θάλασσας, για μία χρονική περίοδο 36-ετών (1985-2020). Η στατιστική ανάλυση πραγματοποιήθηκε για τρεις πτυχές του ανέμου, την ταχύτητα, την διεύθυνση και την πυκνότητα αιολικής ισχύος, σε τρείς χρονικές κλίμακες, την ετήσια, την μηνιαία και την εποχιακή. Η ανάλυση περιλαμβάνει επίσης, τη χωρική κατανομή των μέσων τιμών των προαναφερόμενων μεταβλητών, καθώς και των αντίστοιχων μέσων ετήσιων και υπηρετήσεων μεταβλητοτήτων, τις γραμμικές τάσεις της μέσης ταχύτητας του ανέμου, αλλά και των ακραίων ταχυτήτων, δηλαδή των 95% και 99% ποσοστημορίων, στις τρεις εξεταζόμενες χρονικές κλίμακες.

Οι υπεράκτιες ελληνικές περιοχές παρουσιάζουν υψηλότερο διαθέσιμο αιολικό δυναμικό το καλοκαίρι σε σύγκριση με την υπόλοιπη Μεσόγειο, εξασφαλίζοντας σταθερότερη παραγωγή ενέργειας καθόλη τη διάρκεια του έτους και ως εκ τούτου, αποτελούν από τις πιο ευνοϊκές περιοχές της Μεσογείου για την ανάπτυξη υπεράκτιων αιολικών πάρκων. Ωστόσο, παρά το

υψηλό διαθέσιμο αιολικό δυναμικό που εμφανίζουν τόσο το Αιγαίο, όσο και το Ιόνιο Πέλαγος, αρκετοί παράγοντες εμπόδιζαν την ανάπτυξη τέτοιων τεχνολογιών στην Ελλάδα για πολλά χρόνια. Η έντονη τουριστική δραστηριότητα και οι παράκτιες δραστηριότητες, ειδικά τους καλοκαιρινούς μήνες, περιοχές που αντιμετωπίζουν προβλήματα εθνικής ασφαλείας, η έλλειψη υποβρύχιου δικτύου ικανού να καλύψει τις ενεργειακές απαιτήσεις, τεχνικοί περιορισμοί που σχετίζονται με το βάθος και την απόσταση από την ξηρά, η ασταθής οικονομική κατάσταση της χώρας λόγω της οικονομικής κρίσης, αλλά και η έλλειψη ενός ισχυρού νομοθετικού πλαισίου, αποτελούσαν τους κύριους λόγους. Τον Ιούλιο του 2022, η Βουλή των Ελλήνων ψήφισε μία νέα νομοθεσία (Ν.4964/2022, άρθρα 65 - 80) ειδικά προσανατολισμένη στην προώθηση της υπεράκτιας αιολικής ενέργειας και στην αναδιάρθρωση των σχετικών διαδικασιών αδειοδότησης.

Τον Οκτώβριο του 2023, η Ελληνική Εταιρία Διαχείρισης Υδρογονανθράκων και Ενεργειακών Πόρων, δημοσίευσε το Εθνικό Πρόγραμμα Ανάπτυξης Υπεράκτιων Αιολικών Πάρκων, αναφορικά με τον νόμο 4964/2022, για τον προσδιορισμό και την προτεραιοποίηση των εν δυνάμει περιοχών ανάπτυξης υπεράκτιων αιολικών πάρκων, στις Ελληνικές θάλασσες. Προέκυψαν 23 εν δυνάμει περιοχές, οι οποίες αντιστοιχούσαν σε 30 πολύγωνα, χωρικά κατανεμημένα κυρίως σε όλο το εύρος του Αιγαίου, αλλά και κάποια στο Ιόνιο. Σε σχέση με τα παραπάνω, στην παρούσα μελέτη περιλαμβάνεται επίσης, η αξιολόγηση της απόδοσης της ανεμογεννήτριας NREL, ονομαστικής ισχύος 15 MW, για το σύνολο των υπεράκτιων περιοχών της Ελλάδας. Επιπλέον, πραγματοποιήθηκε η εκτενής ανάλυση των 30 επιλεγμένων θέσεων (πολύγωνων), στην οποία συμπεριλαμβάνονται, η στατιστική ανάλυση της ταχύτητας και της πυκνότητας αιολικής ισχύος του ανέμου, η εκτίμηση των μέτρων μεταβλητότητας (ετήσιας και υπερετήσιας), οι γραμμικές τάσεις και η αξιολόγηση της απόδοσης της προαναφερόμενης ανεμογεννήτριας.

Η παρούσα εργασία ακολουθεί την εξής δομή: Στο κεφάλαιο 1, παρουσιάζονται γενικές πληροφορίες για τις υπεράκτιες ανανεώσιμες πηγές ενέργειας, καθώς και μία αναλυτική περιγραφή του Εθνικού Προγράμματος Υπεράκτιων αιολικών πάρκων, όπου περιγράφεται η μεθοδολογία που χρησιμοποιήθηκε για την αξιολόγηση και προτεραιοποίηση των πιθανών περιοχών για την ανάπτυξη αιολικών πάρκων. Στο κεφάλαιο 2, δίνεται η περιγραφή των δεδομένων που χρησιμοποιούνται για την στατιστική ανάλυση του υπεράκτιου αιολικού κλίματος της Ελλάδας. Στην συνέχεια, στο κεφάλαιο 3, παρουσιάζεται το θεωρητικό υπόβαθρο και η μεθοδολογία που χρησιμοποιήθηκε σε αυτήν την μελέτη. Στο κεφάλαιο 4, δίνονται και συζητούνται τα αριθμητικά αποτελέσματα που αφορούν, την ταχύτητα, τη διεύθυνση και την πυκνότητα αιολικής ισχύος, του ανέμου. Τέλος το κεφάλαιο 5, περιλαμβάνει τα αποτελέσματα της αξιολόγησης της απόδοσης της υπεράκτιας ανεμογεννήτριας NREL – 15 MW στις ελληνικές θάλασσες, αλλά και τα αποτελέσματα από την εκτενή ανάλυση των 30 επιλεγμένων υποψήφιων τοποθεσιών για την ανάπτυξη υπεράκτιων αιολικών πάρκων.

Λέξεις Κλειδιά: [*Υπεράκτια αιολική ενέργεια, Ελληνικές θάλασσες, ετήσια-υπερετήσια μεταβλητότητα, υπεράκτια ανεμογεννήτρια, γραμμικές τάσεις, δεδομένα επανανάλυσης CERRA]*

Table of figures

List of tables

List of Abbreviations and Acronyms

ATT: Attenuator

CERRA: Copernicus European Regional Reanalysis

CV: Coefficient of variation

CP: Coefficient of power

DA: Data Assimilation

DJF: December, January, February

EU: European Union

OTEC: Ocean Thermal Energy Conversion

ORE: Offshore Renewable Energy

OW: Offshore wind

OWE: Offshore wind energy

OWT: Offshore Wind Turbines

OWSC: Oscillating Wave surge

OWC: Oscillating Wave Column Converters

ENE: East to northeast

EMEC: European Marine Energy Centre

ECMWF: European Centre for Medium Range Weather Forecasts

ECVs: Essential Climate Variables

FPV: Floating Photovoltaics

GHG: Greenhouse Gas

GW: Gigawatt

GWh: Gigawatt hours

HEREMA: Hellenic Hydrocarbons and Energy Resources Management Company

HAWT: Horizontal Axis Wind Turbines

hPa: Hector pascal = 100 Pascals

IAV: Inter-annual variability

IEA: International Energy Agency

JJA: June, July, August

kW: kilowatt

NE: Northeast

NDP – OWF: National OWF Development and Programme

NNE: North to northeast

NW: Northwest

NNW: North to northwest

NWP: Numerical Weather Prediction

MAM: March, April, May

MAV: Mean annual variability

MW: Megawatt

OWF: Offshore Wind Farm

OWFODA: OWF – Organized Development Areas

SEIA: Strategic Environmental Impact Assessment study SE: Southeast

SON: September, October, November

SE: Southeast

SSE: South to southeast

SW: Southwest

SSW: South to southwest

SSF – RES: Spatial and special frameworks for renewable energy sources

Std: Standard Deviation

PRO: Pressure retarded osmosis

RED: Reverse electro dialysis

TRL: Technology Readiness Level

TSE: Theil and Sen estimator

TWh: Terawatt hours

UERRA: Uncertainty in Ensemble of Regional Reanalysis

UK: United Kingdom

US: United States

VAWT: Vertical Axis Wind Turbines

WEC: Wave Energy Converter

WD: Wind direction

WPD: Wind power density

WS: Wind Speed

WSW: West to southwest

MWh: Megawatt hours

OE: Ocean Energy

WNW: West to northwest

WT: Wind Turbine

1. Introduction

1.1. General introduction to offshore renewable energy

Our seas and oceans have a great potential to become significant sources of clean energy, since ocean is a permanent, inexhaustible, and clean source of energy. The available ocean energy resources on a global scale, hold the potential to satisfy both current and future energy requirements. This reality has swiftly captured the attention of researchers and engineers, who are keenly interested in its exploitation, with the aim of producing clean and renewable energy. The Offshore Renewable Energy (ORE) can be availed in many ways, such as, harnessing offshore wind (OW) to produce energy, i.e. Offshore Wind Energy (OWE), by extracting Ocean Energy (OE) from waves, tidal/sea currents, thermal salinity gradients [1] and offshore solar energy.

Accordingly, there are multiple ways to exploit ocean's reserved energy and therefore, offshore renewable energy technology encompasses a range of clean energy technologies, each at different stages in their development. In general EU is a global leader in renewable energy offshore technology and industries [2] .

Furthermore, ORE has the potential to uphold EU's global leadership, by creating new employment opportunities, strengthening energy security, and concurrently contributing to the reduction of the greenhouse gas (GHG) emissions and the environmental protection. Overall, the advancement of research and technology in energy production, could play a pivotal role, not only in the current economy but also in achieving the environmental and energy security objectives of EU by 2050 [3].

Harnessing energy from the ocean seems ideal in various aspects, and comes with its share of challenges and issues, some of which are presented below:

- Higher technology costs compared to onshore, along with challenging access to financing for wave and tidal technologies, which are at a less developed stage compared to offshore wind.
- Challenges in the EU's offshore grid transmission infrastructure both within countries and across borders.
- Obstacles related to inadequate access to suitable port facilities or lack of specialized installation and maintenance capabilities.
- Elaborate licensing and consenting procedures that result in increased costs and project delays.
- Limited research and information exchange, hindering a better understanding and development, especially regarding the environmental impacts of ocean energy.
- Lack of a balanced economy; see also [3, 4].

1.2. Expectations of offshore renewable energy in Europe

In this section, expectations in Europe regarding various forms of ORE are briefly examined by providing a more in – depth analysis of OWE, which is the main interest in this research. European laboratories and industries are actively advancing various technologies to harness the energy potential of seas, for generating green electricity. These include, besides the

aforementioned, floating offshore wind, floating photovoltaic installations, and the utilization of algae for biofuel production. The geographical advantage of being physically connected to the North, the Mediterranean, the Atlantic the Baltic and the Black Seas, is a significant factor that Europe's position led the way to achieve climate neutrality by 2050.

According to the European Commission's estimations, EU aims to achieve specific targets in the ORE energy sector. By 2020, the goal was to install at least 60 GW of offshore wind and at least 1 GW of ocean energy. Looking ahead to 2050, the ambitious targets are set at 300 GW of OWE and 40 GW for OE. It's important to recognize that each sea basin in Europe possesses distinct characteristics, including geological conditions and the current stage of the ORE development. Consequently, different technologies are better suited for different basins. Some estimations for particular European seas are listed below, according to [2]:

- The North Sea, possesses significant and extensive natural potential for OWE, especially for fixed – bottom wind turbines, attributed to its shallow waters, and localized opportunities for wave and tidal energy.

- The Baltic Sea, has also a high natural potential of OWE and some localized potential for wave energy.

- The EU's Atlantic Ocean, has prospects for both bottom fixed and floating OWE. Additionally, there are opportunities for tidal and wave energy development.

- The Mediterranean Sea, has potential mostly for floating OWE, due to the great water depths.

- The Black Sea is suitable for both types of OWE, but also includes some promising wave and tidal energy development areas.

Although OWE development is more mature and advanced compared to tidal and wave technologies, wave and tidal power exhibit much higher power density than wind and solar power i.e., they offer greater power availability per unit volume. However, the utilization of ORE also depends on the efficiency, maturity and cost – effectiveness of the corresponding technologies [5]. At the moment, offshore wind energy systems are much more mature than other ORE technologies; see also next sections. It is also important to emphasize the fact that the EU holds a very strong position in the global ranking of developing technologies and innovations, particularly in the field of energy from waves and tides since 70% of the globally utilized ocean energy relies on technologies and patents originating from Europe [2].

In order to compare technological development among technologies from different ORE, the European Commission has defined various technology maturity levels, which are presented below [6]:

– TRL 1, basic principles observed

– TRL 2, technology concept formulated

– TRL 3, experimental proof of concept

– TRL 4, technology validated in lab

- TRL 5, technology validated in relevant environment (industrially relevant environment in the case of key enabling technologies)

- TRL 6, technology demonstrated in relevant environment (industrially relevant environment in the case of key enabling technologies)

- TRL 7, system prototype demonstration in operational environment

- TRL 8, system complete and qualified

- TRL 9, actual system proven in operational environment (competitive manufacturing in the case of key enabling technologies; or in space)

1.2.1. Wave energy

The propagation of ocean waves, particularly those generated by wind (sea surface wind waves), presents a valuable source of energy that can be harnessed and converted into electricity through specific technologies. Wave power density, varies across different locations and time periods throughout the year. Specifically, wave power density in coastal areas, is observed to be approximately a quarter to half of the corresponding in open ocean [5]. Furthermore, the temporal variability of wave energy, it is intricately linked to wind variability, introducing great uncertainties in estimations and forecasts.

Although intense sea-state offshore areas are ideal for wave energy availability, the reality is quite different [7], since Wave Energy Converters (WECs), are subject to high installation and maintenance costs to withstand such extreme conditions. Consequently, it is most practical and preferable to deploy WECs in coastal areas, where lower magnitudes of wave power flux observed.

To address the challenge of effectively extracting, transporting, and storing wave energy, Borthwick [8], mentioned that over 50 types of WECs were in development at the time, many of them studied theoretically, numerically and even at prototype scale. This diversity may be seen as advantageous, while it posed a potential drawback, since the wide array of technologies, each employing different techniques for different sea circumstances, makes it challenging to compile and enhance them uniformly, hindering the scalability of WECs for commercial purposes.

There are several highly developed technologies for wave energy aimed at achieving the EU's goals for ocean energy (wave and tidal), by 2050. The most advanced technologies are the point absorber and Oscillating Wave Column (TRL-9), followed by the Attenuator and Overtopping (TRL – 8) and the Oscillating wave surge converter (OWSC) and rotating mass (TRL- 7) [9].

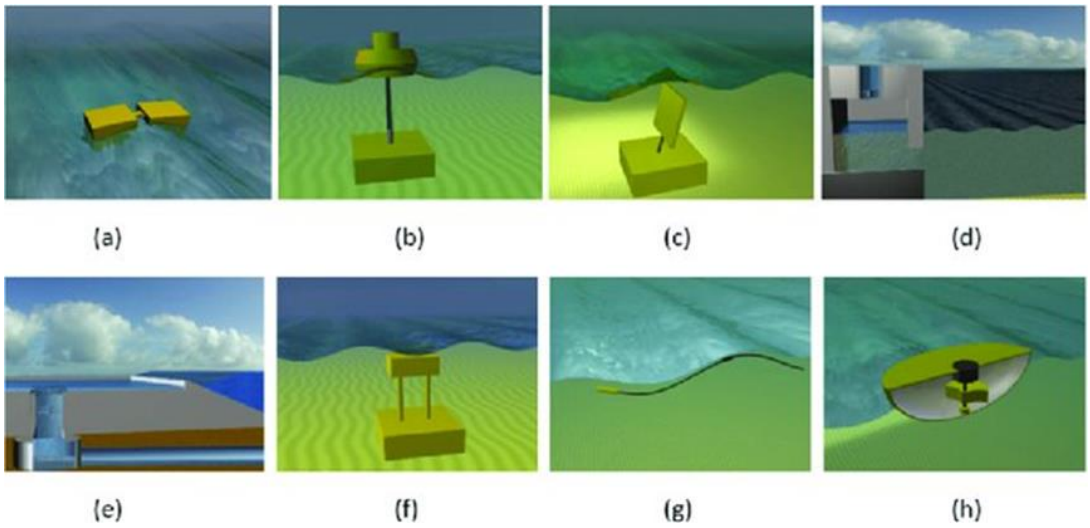

Figure 1. Types of WECs: (a) attenuator, (b) point absorber, (c) oscillating wave surge converter, (d) oscillating water column, (e)overtopping device, (f) submerged pressure differential, (g) bulge wave, (h) rotating mass (Source: [10])

Some notable wave energy converters demonstrations are provided below:

- In July 2011, the Mutriku wave energy plant in the Basque country, Spain, was officially launched with financial support from the European Commission's Seventh Framework Programme. The plant, situated on a 100m section of the breakwater facility's outer wall. Generating 296 kW, it provides electricity for 250 households and contributes to an annual reduction of 600 tons of carbon emissions. In 2019, the plant became part of the Biscay Marine Energy Platform (BiMEP), a facility supporting research and demonstrations of utility – scale floating marine renewable energy devices in open seas. By February 2020, the power plant had reached a significant milestone, producing a cumulative output of 2GWh since its installation, [11, 12].
- In BiMEP have been deployed various wave energy devices, with the most recent being Wello's Penguin 2, rotating mass device, deployed in 2021 and having a capacity of 1MW. The aforementioned located 1.5km off the Spanish Northen coast, [11, 13].
- Wave energy devices, including the Wapepiston full – scale demonstration system with a capacity of 200kW, have been implemented at the Platform Oceanica de Canarias (PLOCAN) test site in the Canary Islands [11].
- In 2022 Sweden's copower Ocean, WEC, installed in Northen Portugal [5, 14].

1.2.2. Energy from tides and currents

The overall available tidal energy has immense potential, especially in specific regions of Europe such as the UK and France. Additionally, its high predictability [1], combined with its higher energy density compared to OW, rendered tidal energy an appealing prospect for researchers over an extended period. There is also optimism that tidal energy might become cost – effective by 2050 [15].

Tidal energy is a leader among emerging OE sources, having been implement on a large scale, particularly with notable tidal barrages in France and Korea [9]. This form of energy can be

harnessed through various methods, including tapping into tidal currents, capitalizing on the horizontal movement of water, leveraging the vertical change of water through tidal range, and utilizing ocean circulation currents [5]. Apart from France in Europe, specific bay topographies can result in significant tidal ranges at the entrance, leading to powerful tidal currents. Examples of such locations include, Cook Strait in New Zealand [16], and the Pentland Firth in the UK [17].

However, the widespread adoption of tidal energy has been constrained by factors such as the limited availability of suitable locations, and the considerable local environmental impacts associated with processes during the installation. Furthermore, additional challenges in the advancement of tidal energy include substantial water depths, large distances for submarine cable transmission which increases the cost, and adverse effects resulting from cavitation [4].

The technologies that have been developed are at various technological stages, such as Horizontal and Vertical axis turbines, TRL – 9 and TRL – 7 respectively, and Tidal Kite with TRL – 8 [11]. It is crucial to note that although tidal barrages remain the most potent ORE technology, the environmental impacts that their structure can potentially cause, primarily in the submarine environment during installation and operation, are hindering their multiple utilization.

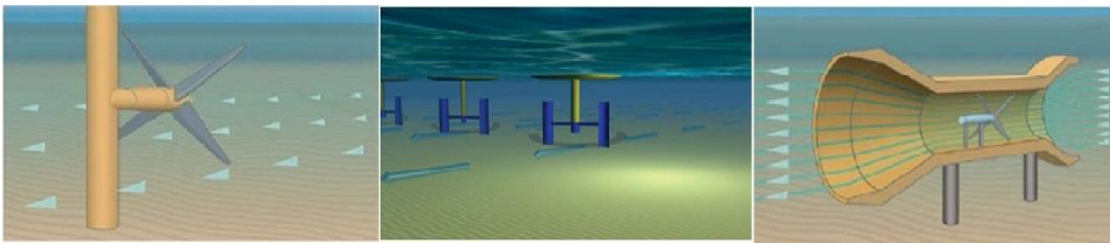

Figure 2. Horizontal axis, vertical axis and Venturi type device, three of many tidal energy technologies. (Source: [18])

Some notable tidal energy technologies' installations along Europe, are given below:

- In 2019, the European Marine Energy Centre (EMEK) in Orkney, Scotland, achieved the successful installation of the second-generation Spanish tidal platform 'ATIR', boasting a 2 MW capacity. Furthermore, by the close of 2023, EMEC made a significant announcement regarding the delivery of a 9.6 MW tidal turbine array as part of the new EU project EURO – TIDES [19].
- In 2023, Swedish Minesto, has completed the onshore testing on its tidal energy kite system Dragon 12. The 1.2 MW capacity device was installed for commercial use in Faroe Islands [20].
- In 2023, an additional Nova M100 (100kW) was incorporated into the existing grid – connected tidal power station in the Bluemull Sound, UK.

1.2.3. Thermal gradient energy

Ocean Thermal Energy Conversion (OTEC) utilizes the thermal gradient between the consistently cold deep sea – water (at depths of 800 – 1000m, remaining at a constant temperature of around 4°C, at 1000m) and the warmer surface water to generate electricity

through a heat engine. For effective operation, the temperature difference between these layers must exceed 20 °C, with surface temperatures ideally around 25°C. However, as these conditions are only prevalent in a belt around the Equator within tropical regions, OTEC is not considered feasible for development in the EU, except in specific overseas islands [11].

This form of ORE is consistently accessible and presents a substantial reservoir of potential resources, offering a high capacity for energy production. The capacity factor, which is the ratio of the actual electrical energy produced during a specific time period to the theoretical maximum electrical energy that could be produced in the same duration, is notably high [5].

A notable project, despite the fact that European seas, as mentioned earlier, do not meet the thermal differentials required for OTEC technologies, is the project carried out in 2022. A collaborative group named PLOTEC, consisting of members from Austria, Italy, Portugal, Spain, and the UK, secured funding under the Horizon Europe Framework Program. The funding was destined for the design and simulation of an OTEC platform engineered to withstand the challenging conditioned inherent in tropical weather. The platform will be culminating in a physical deployment at the PLOCAN test facility in Gran Canarian in 2024 [5, 21].

1.2.4. Salinity gradient energy

Salinity gradient energy can be harnessed from the chemical potential created by the meeting of seawater and fresh water. This energy is generated through methods such as pressure retarded osmosis (PRO), where a 5kW pilot plant was installed in Norway in 2009. In this method, a membrane is used to separate seawater from fresh water, and they are then combined through osmosis, allowing the extraction of energy from the ensuing physical flow. Another method is through Reverse Electro Dialysis (RED), where salt ions are transported through membranes to generate an electrical charge [22]. In 2014, a pilot – scale RED plant began its operation in the Netherlands.

Both of the aforementioned examples faced challenges over time due to expensive membranes used. This is one of the reasons why these technologies have not advanced significantly, as well as regarding that the environmental impacts of these technologies are not precisely known.

In European sea basins, testing facilities that accommodate both individual devices and arrays can be found in Scotland, the UK, Spain, and France. Additionally, a demonstration plant utilizing RED is implemented on a test grid in the Netherlands, reaching a TRL – 7 [11].

1.2.5. Floating solar energy

The development of offshore solar energy technologies, i.e. offshore floating photovoltaics (FPV) stands in an early stage. The current floating solar photovoltaic capacity in the EU reaches a total capacity of 50 kW, with the first European FPV project (North Sea 1), installed in the Netherlands in 2019; proving the ability of the structure to withstand waves up to 10 m high. A significant project of 250 kW capacity, is planned in the Canary Islands and a growing number of projects also plan to conduct a synergy of FPV with other ocean renewable energies [9].

Figure 3. Offshore floating photovoltaic (FPV); (Source:[23])

In addition, ORE can be used to directly power sectors of the Blue Economy such as aquaculture or seawater desalination. In 2020, a prototype of offshore desalination plant coupled with wave energy, was installed in the Canary Islands. Moreover, MUSICA project plans to couple wind, solar photovoltaic and wave energy, to power aquaculture and desalination in the island of Chios, in Greece [9, 24].

1.3. Offshore wind energy

1.3.1. General

Figure 4. Offshore wind farm (Source: [25])

The magnitude of wind speed depends, among other factors, on the roughness and morphology of the land it blows upon. Compared to onshore wind, the OW is stronger, and its variability is much lower, consequently, the expected offshore OWE production is much higher. Furthermore, the availability of space in the oceans for the installation of wind farms is significantly greater [1].

The utilization of OWE is notably the most advanced category of ORE concerning technology, development, policy framework and installed capacity [4]. Two key-factors influencing the amount of energy from OWE, are wind speed and air density. Evaluations of mean annual wind energy, indicated that onshore and offshore energy resources globally, have the potential to ideally provide 900,000 TWh/ year [5].

For the recognition and prioritization of a potential area for the development of offshore wind farms (OWF), regarding its wind potential, the most important factors that should be considered are the mean offshore wind speed, the wind power density and their associated variability at various time scales.

The exponential growth that OWEs has experienced globally, particularly in Europe, both in terms of research and installations, can be attributed to the numerous advantages it holds over onshore wind energy. The most significant of these advantages are outlined below:

- OWE is safe, environmentally friendly, clean, non – polluting renewable energy and widely distributed.
- Compared to nuclear energy, OWE is safer.
- OW, and consequently offshore wind power, is much higher that onshore and exhibits lower variability.
- Considering that the land surface (which constitutes 13% of the global land) with economically viable wind power is rapidly becoming saturated, the extensive spatial availability in oceans, becomes imperative for the installation of OWFs; including a wide spectrum of technologies, such as fixed – bottom wind turbines (WTs), suitable for shallow waters and floating, designed for deeper waters. In regions with deep waters, such as Greece, technical limitations emerge for the development of OWFs, and therefore the advancement of well – known traditional fixed – bottom WTs, is not an option, while floating WTs facilitate.
- Offshore wind turbines (OWTs) have greater nominal power and taller constructions, compared to onshore turbines, thus the amount of energy produced per turbine is also higher. Earlier studies, estimated that for a 3.0 MW OWT with a hub height of 100 m height above the sea, the global wind power was around 39 TW [1, 26]. Nowadays, in active offshore parks wind turbines with an average nominal power of 3 to at least 10 MW are already installed (in Netherlands [27] and an 18 MW prototype was installed in China), with the aim of further increasing in the coming years.
- Finally, visual and auditory disturbance is lower compared to onshore installations, since OWFs are installed at a considerable distance from the coastline, and therefore the WTs have the potential for further size and nominal power expansion.

Despite the advantages that make OWE more attractive compared to other ORE, there are various difficulties and disadvantages that should be taken into consideration during the planning of an OWF. Here are some examples:

- The main drawback of OW is the increased installation cost compared to onshore. Shipbuilding facilities are required for turbine assembly, and specialized vessels are also needed for their transportation to the installation area.
- Apart from wind availability, distance from shore and water depth are currently the most important technical and financial constraints in the selection of potential sites for the development of an OWF. As distance from shore and depth increase, the costs of underwater electrical grid connections, installation and maintenance also increase.
- OWTs construction requires higher expertise in infrastructure, installation, electrical connection, as well as the use of materials with higher corrosion resistance, since significant parts of OWTs are constantly exposed to the harsher weather conditions in oceans, such as to salinity, waves and strong winds [28].
- Licensing procedures take many years, and bureaucratic processes are usually complex.
- Strong social reactions, mainly due to a lack of knowledge, are primarily related to concerns about effects on the environment and the disruption of everyday life routine, particularly in terms of visual and noise disturbances.
- There is lack of sufficient subsea infrastructure capable of supporting the amount of electricity that can be generated by these technologies.
- There are certain environmental impacts [29, 30], primarily concerning noise during the installation of fixed – bottom turbines. Recommendations to the mitigation of the effects on mammals and sea turtles during pre – installation operations, are included in [31].

1.3.2. Offshore wind turbines

WT technology is highly mature, and the experience and expertise gained from research and innovation on onshore WTs, increased the development speed rates of modern designs with featuring aerodynamical efficient blades as well as economical blade designs and tower structures, sturdy control systems [5].

The knowledge acquired from onshore WTs was the pylon for the design and development of OWTs. Nowadays OWTs characterized by a three – blade horizontal axis, facing the wind (upwind), and are equipped with a pitch control system. Similar to onshore WTs, Horizontal Axis Wind Turbines (HAWT), have been dominant in OWT so far. However, studies have been made conducted to explore the possibility of Vertical Axis Wind Turbines (VAWT) stableness and predominance over HAWT, primarily for floating installations [32].

The advancement of offshore development allows the installation of larger WTs, primarily due to the option of transporting these turbines by ship, compared to onshore installations where road transports and their appropriate configuration, are required. However, a key challenge for future progress, is the design and production of cost-effective ultra – large WTs with rated power exceeding 20 MW, requiring additional research and development efforts, particularly focusing on new blade materials and optimized designs.

The fundamental differences between OWT and onshore WTs are primarily due to the installation environment. Ocean, with its stronger winds and intense waves, imposes additional loads, compared to onshore WTs; and therefore, the foundations of OWT are the main technical and economic challenges, as it is estimated to account for one – third of the total cost [33].

The foundation technologies of WTs vary and mainly depend on the depth of water and the mineralogical composition of the seabed; and categorized as follows; see more in [5].

Shallow or intermediate waters (0 – 60m)

Bottom – fixed foundations, technologically mature and widely utilized in the Northern Seas, correspond to these depths. Their design and installation are straightforward and they categorized depending on depth and seabed nature, as shown below:

- Gravity Based Structures: Concrete - based structures primarily used for depths up to 10m.
- Monopile. Cylindrical steel tubes, preferred for water depths 20 to 40m due to economic considerations. The most commonly used foundations in shallow and intermediate water depths, because of their simple manufacturing and design.
- Jacket Foundations. Four metal piles connected by a lattice, provides strength and stability in water depths up to 70m. In water depths up to 30m, Jacket and Tripod foundations main strong competitors of monopile.
- Tripod: Three–leg structures made of cylindrical steel tubes, The depth of pile penetration and the base width adjusts based on environmental and soil conditions.

Deeper Waters (deeper than 60m)

The immerge need of more financially viable OWTs, caused by increased sizes and costs of bottom – fixed foundations, as well the technical limitations of deep-water depths, had led to the growing interest in floating OWTs installations. Various floating designs arisen, such as spar, semi – submersible, or tension leg platform.

Spar and semi – submersible floating has been tested at the sea, while tension leg platform prototypes due to complex and high costs in transportation and installation, are yet to undergo such testing. Several bottom – fixed and floating OWTs foundations garnered extensive experience from the oil and gas sector's commercial – scale deployments. However, designing OWT foundations and support structures requires distinct skills, and furthermore design methodologies from other sectors, may not directly apply to ORE [5].

In recent offshore wind leasing processes, floating OWFs constituted the 60% of submitted bids, showing a notable trend towards floating installations. Moreover, it is expected that floating OWE will significantly contribute, reaching 100 – 150 GW of the targeted 350 GW OW capacity by 2050 [27].

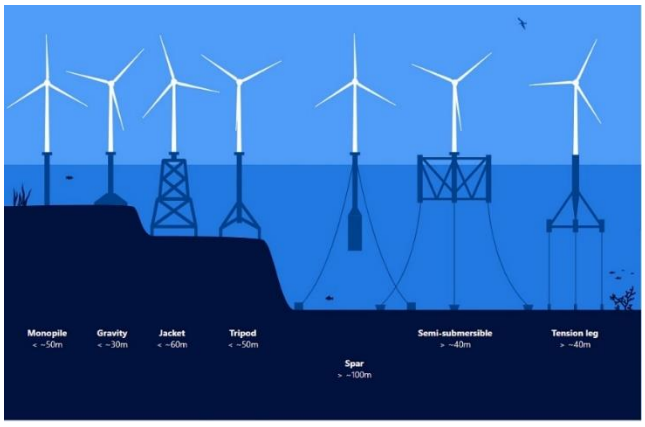

Figure 5. Example of typical foundation types and applicable water depths. (Source: [34]).

1.4. Current status of offshore wind energy in Europe

Europe has established a robust presence in the technology and industry of OWE. In particular, the OWE industry has gained a first mover advantage, notably with the installation of Vindeby OWF on the southern coast of Denmark in 1991, in deploying fixed bottom wind turbines. Furthermore, at the end of 2022, a significant percentage (50%) of the global installed OWE capacity was produced in Europe [9].

Europe currently possesses a noteworthy 255 GW of installed wind power capacity, out of which 30GW is situated offshore, with an additional 2.5 GW capacity of OWE, compared to 2021, achieving an increased record of 4% [27]. The aforementioned, coupled with the anticipation of capacity factors for new OW projects in 2022 being around 50% and an average power of 8 MW, underscore the ongoing growth and investment in offshore wind projects.

Challenges due to adverse weather conditions in oceans, such as strong waves, wind and currents, difficulties in connections with the grid, unfavorable material transportations, etc., contributed to enormous costs and delays on the development of OWF installations. Nevertheless, over the last 15 years, in new installations, high-capacity factors and consistent cost reduction, has been observed.

Furthermore, European Commission in 2020 [2], reported that the existing installed OWFs, were producing clean, environmentally friendly energy, competitive and sometimes more cost - effective than energy derived from fossil – fuels.

Europe still holds a leading position, in OWE research and technological development, although, in 2022, 23 countries including 10 EU Member states, did not reported any wind installations [27]. The challenges need to be addressed both domestically and in EU level, include: significant delays due to permits, bureaucracy, the unstable domestic economy, social reactions concerning environmental impacts, others related to the influence on other coastal activities, and technical limitations mainly concerning countries in the Mediterranean Sea, where despite their favored atmospheric and oceanographic conditions, are characterized by deeper waters, which prevent the development of well – known technologies, i.e. fixed – bottom OWFs.

The forefront countries of OWFs installations are depicted in Figure 6, and a more extensive analysis is presented below; see more in [27, 35].

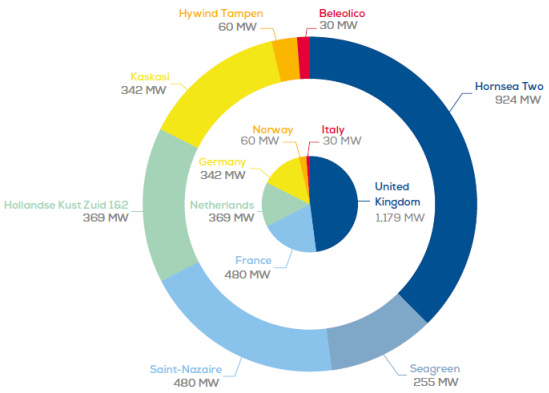

Figure 6. New offshore wind farms in Europe in 2022. (Source: Wind Europe, Wind energy in Europe: 2022 Statistics and the outlook for 2023 – 2027 [27])

- Italy: After a delay of 14 years, in May of 2022, Italy has successfully installed the initial offshore wind farm in the Mediterranean. Beleolico di Taranto, consists of 10 turbines with a total capacity of 30 MW.

- UK: Nearly half of the European offshore installations were located in the UK, contributing to a new connected capacity of 1.2GW by the end of 2022, incorporating an additional 110 turbines into the grid. This establishes the UK as the country with the highest offshore installed capacity in 2022. Furthermore, has completed the Hornsea II project, consisting of a total of 165 turbines with a total capacity of 1386 MW. It serves as an extension of Hornsea I, which had 174 turbines with a total capacity of 1218 MW.

- France: Has successfully installed its first large – scale commercial offshore wind farm, Saint Nazaire. Installed with monopiles, it consists of 80 turbines with a capacity of 6MW each, amounting to a total capacity of 480 MW. The wind farm is located at a distance of 12 – 20 km from the coast in waters approximately 20m deep. Moreover, within the next three years, France is projected to deploy three floating projects with a combined capacity of 85 MW in the Mediterranean Sea.

- Germany: Connected to the grid an offshore farm named Kaskaki in the North Seas, with a total capacity of 342 MW.

- Norway: On August 23, 2023, the floating offshore wind farm Hywind Tampen, the world's largest floating windfarm, was connected for full commercial operation. It consists of 11 turbines, each with a capacity of 8.6MW, totaling 95MW. However, due to grid limitations, only 88MW can be transmitted. The wind farm will supply approximately 35% of the annual power needs of five oil platforms in the surrounding area, covering the energy that cannot be transferred to the grid.

- The Netherlands: Installed 369 MW from the Hollandse Kus Zuid 1 & 2 offshore wind farm. The final turbines were installed in June 2023, and the park is expected to commence operation within 2024, boasting a total capacity of 770MW with a total amount of 70 turbines.

- Sweden: Deployed an additional 2.4 GW of offshore wind capacity.

- Finland: Added an extra 2.4 GW of offshore wind capacity.

1.5. Current status in Greece

Greece has a highly advantageous geographical position compared to other European countries regarding OWE. The Mediterranean OW tends to decrease during summer, while in Greece, due to Etesians, high magnitudes of wind speed occur, which contribute to a steadier OWE production throughout a year; and therefore, the Greek Seas emerging as one of the most favorable areas, in the Mediterranean, for the development of OWFs.

As of late 2022, Greece added the significant amount of 3 GW onshore wind capacity, nevertheless, until today, the development of OWFs, is still absent from the national wind

market. Several factors have hindered the development of OWE in Greece for many years now, despite the significant wind potential in various regions of both the Aegean and the Ionian Sea [36-39].

The intense tourist activity as well as other intense coastal activities, specifically in summer months, combined with strong social reactions, which led to relevant authorities hindering the licensing process, with the perception that the potential installation of OWF would reduce the tourism rates and affect other coastal activities.

The lack of submarine network to support capacity needs, as well as areas that raise issues of national security, and inevitably, were not exploitable.

Depth and distance from the coastline, constitute the most challenging technical parameters, due to Greece's small continental shelf and deep waters, resulting limited effective water depths for the OWFs installations, been located very close to shore, and therefore, increase social reactions. Consequently, the majority of potential sites, may necessitate floating foundations, leading to economically unsustainable deployment and operation.

Greece's unstable economic situation due to economic crisis, played a crucial role in the stagnation of state subsidies, hindering investors from daring to embark on the development of OWFs.

The initial identification of a potential area for the development of an OWF, constitutes from prior assessments in order to moderate or completely avoid all the aforementioned barriers, within a legislative framework. In respect of that, the primarily aspect of the delayed development of OWFs in Greece, appears to be due to the absence of a robust legislative framework. Nevertheless, in July 2022, the Greek Parliament passed the new legislation (Law no.4964/2022, articles 65 – 80), specifically geared towards the advancement of OWE and streamlining associated licensing procedures [40].

1.5.1. National offshore wind farms development programme by HEREMA

Greece's legislation in 2022 (Law no.4964/2022, articles 65 – 80), noted that the initial steps in development of OWE, was primarily the identification of potential areas for the development of OWFs.

National Offshore Wind Farm Development Programme (NDP – OWF) [41], was entrusted to the Hellenic Hydrocarbons and Energy Resources Management Company (HEREMA). In compliance with Article 67, paragraphs 1 – 3 of Law 4964/2022, HEREMA performed an analysis of Greece's maritime areas, with the aim of the preliminary determination of potential areas for the development of OWFs.

The NDP – OWF and the potential Organized Development Areas (potential OWFODA) were officially published on October 31 of 2023. The potential OWFODA emerged on the suggestions of the national energy planning and objectives, environmental and biodiversity protection planning, existing Spatial and Special Frameworks for Renewable Energy Sources (SSF – RES), suggestions from consultations with the Spatial Planning Directorate of the Hellenic Ministry of Environment and Energy, opinions from relevant public authorities to prevent conflicts with other maritime uses in Greek territory, and international best practices, approaches and conditions; see more in [41].

Several criteria applied, including, exclusion criteria to avoid areas, which according to global practices indicate either acceptance or rejection, evaluation criteria for prioritizing medium – and long – term development areas and criteria for additional assessment of the prevailing areas, in next stages.

HEREMA established 20 exclusion criteria for the initial exclusion of potential OWF development areas:

- Excluding coastal waters by, excluding marine areas within a distance of 1 NM (1.852 m) from the baseline (exclusion of coastal waters).
- Four exclusion criteria related to environmental conditions.
- One exclusion criterion concerning cultural actions.
- Two exclusion criteria related to infrastructure networks.
- One exclusion criterion related to production zones.
- Three exclusion criteria resulting from proposals of the Department of Spatial Planning.
- Four exclusion criteria resulting from discussions with competent authorities.
- Two exclusion criteria derived from technical parameters; see also.

The regions remained then categorized, into areas for medium – term development of OWFs, i.e., until 2030 – 2032, and areas designated for long – term development of OWFs, i.e., from 2032 onwards. The evaluation criteria that applied, concerned, water depth and wind speed limits, grid connection availability/capacity, and the estimated capacity of each area, regarding the in between distance of the WTs. For medium-term installation, emerged 10 potential OWFODA primarily suitable for floating installations, and 13 for long- term installation, also mainly designated for floating deployment.

Two more potential OWFODA emerged using the same criteria, in NDP – OWF 2023, for the development of fixed – bottom pilot OWF projects, i.e., Pilot 1 & 2, with potential capacity of up to 600 MW and a total area of 353 km^2. The final boundaries of the pilot projects, will be determined after the approval of Hellenic National Defense General Staff and Civil Aviation Authority, due to surveillance radar, Alexandroupolis airport and the air navigation system located close to Pilot 1&2, which fall under the aforementioned authorities, respectively.

In sequenced stages, additional evaluation criteria will be examined, involving constraints from rules of requirements that can be met by mitigating specific impacts on a case-by-case basis, indicating more extensive technical and environmental assessments, for individual areas, in order to determinate the most suitable sites and optimize investment decisions for the efficient design and installation of the OWFs, specialized to the characteristics of each area.

1.5.2. The criteria applied in NDP – OWF 2023

Exclusion Criteria

The first criterion applied, referred to the exclusion of marine areas within a distance of 1 NM (1.852 m) from the baseline (exclusion of coastal waters).The initial exclusion criterion automatically incorporated several rules from SSF – RES, which are included in the 1,852 m. Excluded areas encompass areas appertain in the water quality program and protective zones, within a distance of 1500 m from the shore, protected zones including, archaeological and cultural monuments, historic sites, and monasteries; areas closer than 1000 m from industries and high-voltage lines (354 m), organized areas for the development of tertiary sector activities,

such as tourist ports and thematic parks (1000 m), as well as distances from cities with a population over 2000 people (1000 m), and isolated residences, with a minimum distance of 500 m. Due to this constraint, the areas remaining for potential OWFs installation corresponded to a total area of 98,501 km^2.

Four exclusion criteria related to environmental conditions, including areas of absolute nature protection, National Forests protection, regions designated as natural monuments, as well as, Ramsar wetlands and habitats included in the Natura 2000 network.

One exclusion criterion pertained to cultural heritage protection, including monuments listed on the World's Cultural Heritage Catalog and archaeological sites and monuments.

Two more exclusion criteria applied, related to infrastructure networks, covering telecommunication facilities and aviation related activities, as well as production zones, specifically aquaculture including fish farms.

Department of Spatial Planning, proposed three more exclusion criteria encompassing established marine and submarine parks, diving parks, confirmed passenger navigation routes, enclosed bays with a width less than 1500 m, geopark areas, and landscapes of particular natural beauty.

Four more exclusion criteria emerged from discussions with competent authorities, including shooting ranges and military exercise fields, prohibited areas due to national security, shipwrecks and their protection zones, submarine cables, telecommunication networks, and gas pipelines.

According to HEREMA, after the application of the 17 aforementioned criteria, a total 65,051 km^2 emerged for further study, with the corresponding 799km^2 for bottom – fixed, 16,955km^2 for floating, and 155km^2 for either bottom – fixed or floating installations of OWFs, respectively.

Therefore, the final two exclusion criteria are derived from technical parameters, specifically concerning specified depths and wind speeds for the potential areas, ensuring the sustainability of the project, which were used both to exclude areas and in the subsequent phase of the study.

Evaluation Criteria

For the prioritization of the most favorable areas that emerged from the exclusion criteria, 4 evaluation criteria applied. The areas designed for development until 2030 (medium -term), were fulfilled at least three out of four criteria, while regions designed for long – term development, i.e. 2032 an onwards, fulfilled only two out of four. The evaluation criteria that applied in the NPD – OWF, are presented below:

<u>Depth of water</u>

Following international practices, HEREMA set depth as an exclusion criterion considering depths that exceeded 1,000m. The areas that corresponded to depths greater than the mentioned threshold were initially excluded.

Regarding the prioritization of the areas into medium – term and long – term development zones, the depth criterion was applied again, due to the fact that depth is a decisive factor in construction costs, affecting the entire project lifecycle. The majority of identified areas, corresponded to depths ranging from 70 – 250m, while there were areas that align with depths ranging from 500 to 1000m.

Based on international standards, areas with depths ranging from 60 – 500m are promoted for medium – term OWF development, while for long – term development, depths from 500 – 1,000 m are considered suitable. According to the NDP – OWF, areas with average depth below 350 m, are deemed appropriate for floating OWTs in the medium – term development phase.

Wind Speed

Based on technical characteristics, the full performance of OWTs, typically succeeds with wind speeds exceeding 12m/s. The currently OWTs are usually characterized by, cut – in speed of 4 m/s; thus, the minimum permissible limit of the mean annual wind speed for a selected site was nominated higher. Regarding the areas of interest, wind speeds predominantly ranging between 8 and 8.5 m/s, while there are areas with higher wind speed magnitude in range of 8.5 – 9.0 m/s with corresponding depths in range 70 – 250 m and areas with average annual winds speeds exceeding 9 m/s, observed at depths of 70 – 250 m.

HEREMA excluded areas with average annual wind speeds below 6.5m/s for fixed – bottom OWFs, while for floating OWFs, set the threshold at 8m/s. Considering the aforementioned and international literature a mean annual wind speed greater than 9 m/s, was set as a threshold for the the medium – term development of floating OWFs.

Grid Connection Availability/Capacity

The aim of this criterion, was to meet the immediate needs for the transmission and absorption of the energy generated into the grid. The prioritization of the potential areas regarding this criterion was made of based on the distance between the nearest side of the potential park, and the available connection points. Therefore, areas designated for floating OWFs, with connection points within a radius of 50 km, were prioritized for medium – term development, while for fixed – bottom OWFs, it sufficed the existence of electrical infrastructure in the area of interest.

Estimated power in relation to the distance of the wind turbines

Areas were proposed based on the estimated power capacity exceeding 300 MW, with a corresponding area size larger than 60 km^2.

1.5.3. Potential organized development areas

National Energy and Climate plan, has set a target of a total 2 GW capacity from OWFs, up to 2030. The results of the NDP – OWF, showed that since the total capacity of medium-term potential areas corresponded to 4.9 GW, this goal is not impossible.

The areas emerged for the potential development of OWFs, covered a total expanse of 2.359 km^2 and corresponded to the significant amount of 11.8 GW capacity. Regarding Greece's bathymetry conditions, the majority of the potential areas is suitable for floating technologies, with a total estimated capacity of 10.4 GW, while for fixed – bottom OWTs, the estimated capacity was 1.4 GW; the detailed position of potential floating and bottom – fixed OWFs, is presented in Figure 7.

For bottom – fixed OWFs a significant spatial dispersion along the Greek Seas was notable, in contrast with the floating, formed in compact regions in the southern Aegean, eastern Crete Isl. and the eastern and western Cyclades. The most favorable potential regions for fixed – bottom OWFs tend to be in the central Aegean and Crete Isl., where higher values of wind speed

observed. A total amount of 23 areas emerged from the NPD – OWF and more specific 30 potential sites (polygons) around the Greek Seas, as shown in Figure 8.

Among the 23 potential development areas, 10 locations, as shown in Figure 9, were identified for development in the medium – term, i.e., until 2032 and covered a total area of 978 km^2, corresponded to a total estimated capacity of 4.9 GW. Diapontian Islands, Crete-2A, and Gulf of Patras, were designated for fixed- bottom installations, due to the existence of required grid capacity at nearby interconnection points. The remaining 7 areas were destined for floating installations.

Moreover, 13 areas were identified for long – term exploitation, as showed in Figure 10, with an estimated total capacity of approximately 7 GW. Saint Efstratios-1A, is designed for long – term fixed – bottom installation, due to the lack of available network capacity, while the reimaging 12 areas, are designed for floating OWFs.

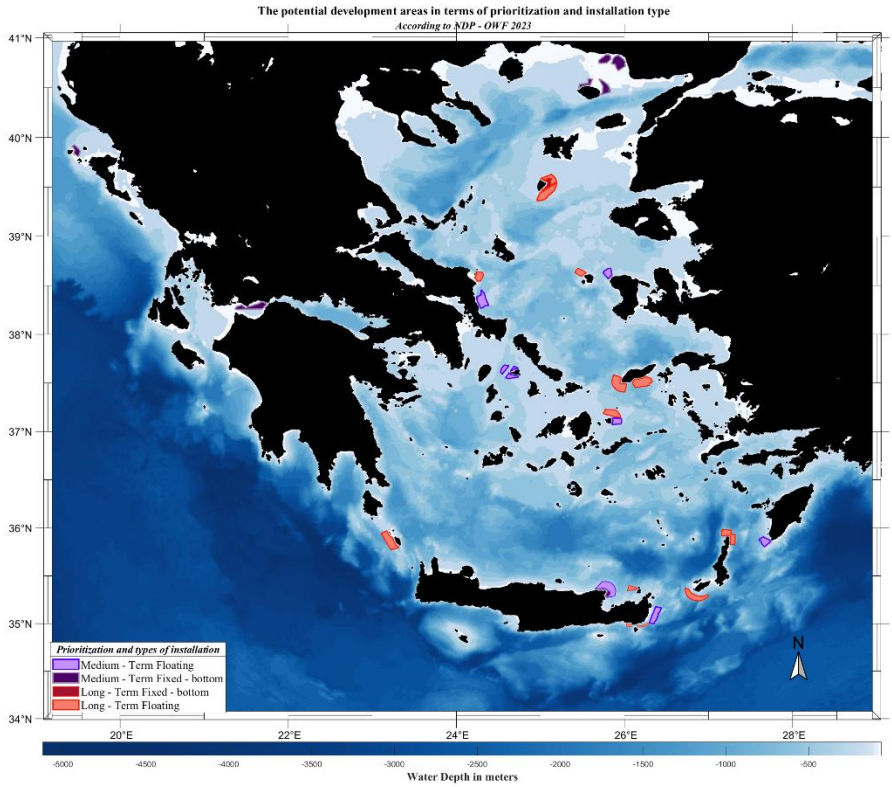

Figure 7.Locations of the potential areas for the development of OWFs, in terms of prioritization and installation type, in the Greek Seas. [12]

[1] The coordinates of the polygons were selected by the published NDP – OWF 2023 [40]

[2] Bathymetry dataset by NOAA National Centers for Environmental Information. 2022: ETOPO 2022 15 Arc-Second Global Relief Model. NOAA National Centers for Environmental Information. DOI: 10.25921/fd45-gt74. Accessed [01/2024].

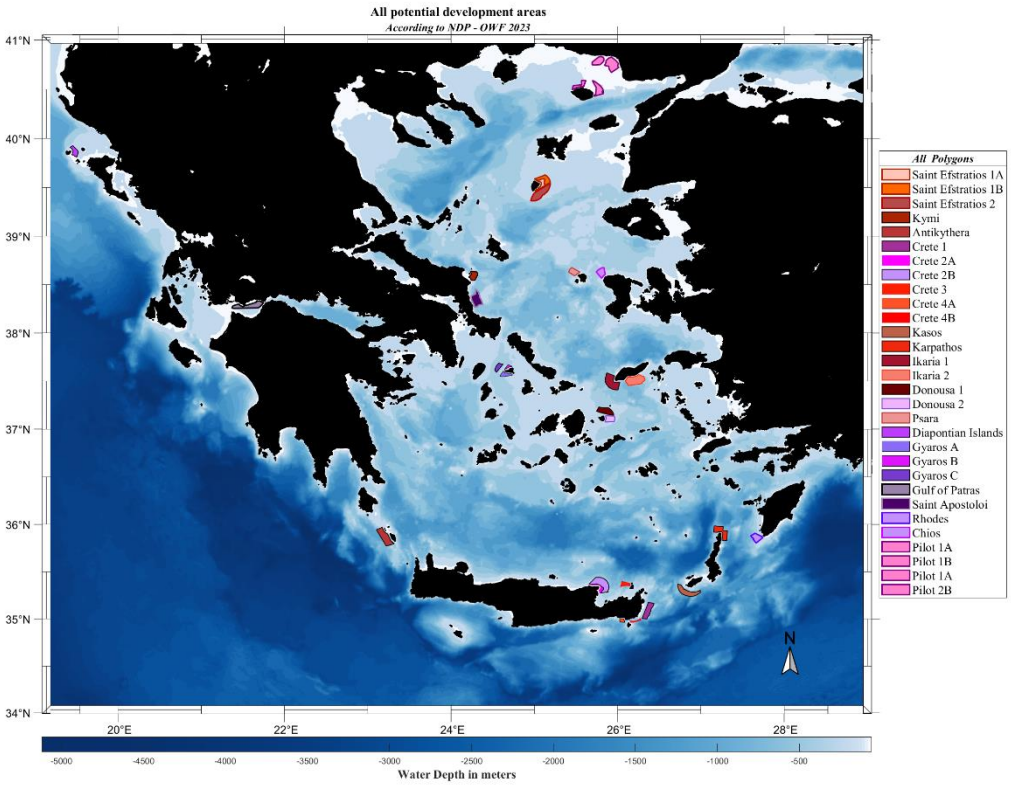

Figure 8. All the potential areas for the development of OWFs, in the Greek Seas

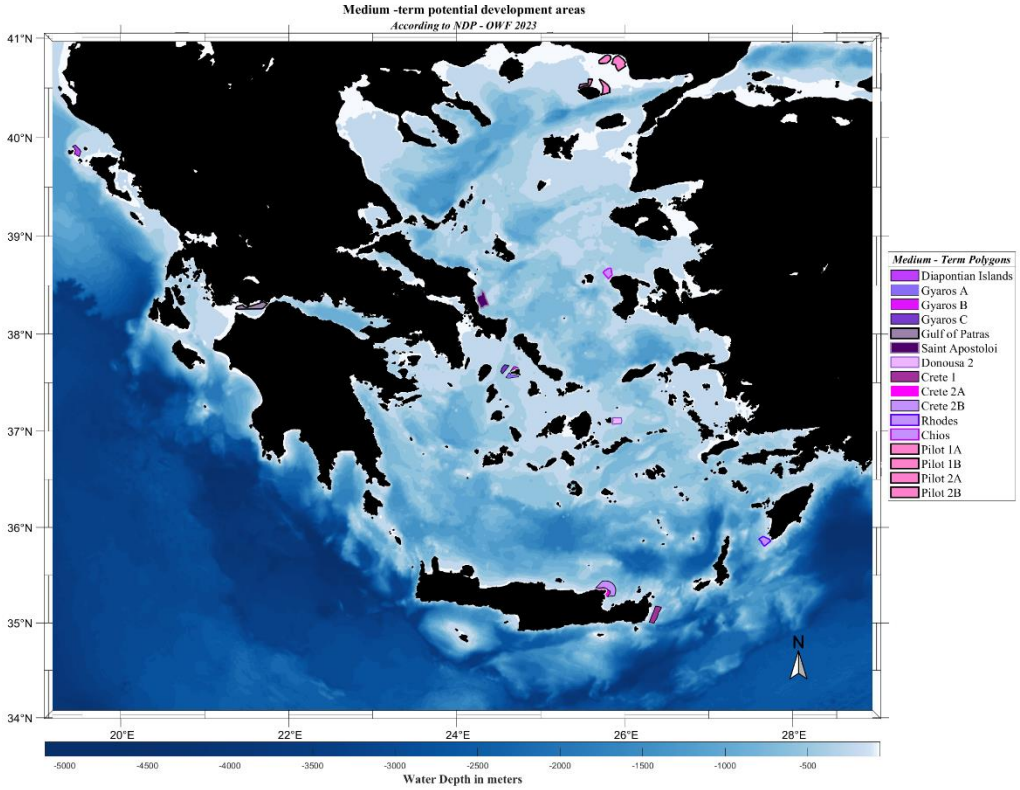

Figure 9. Medium – term potential areas for the development of OWFs, in the Greek Seas

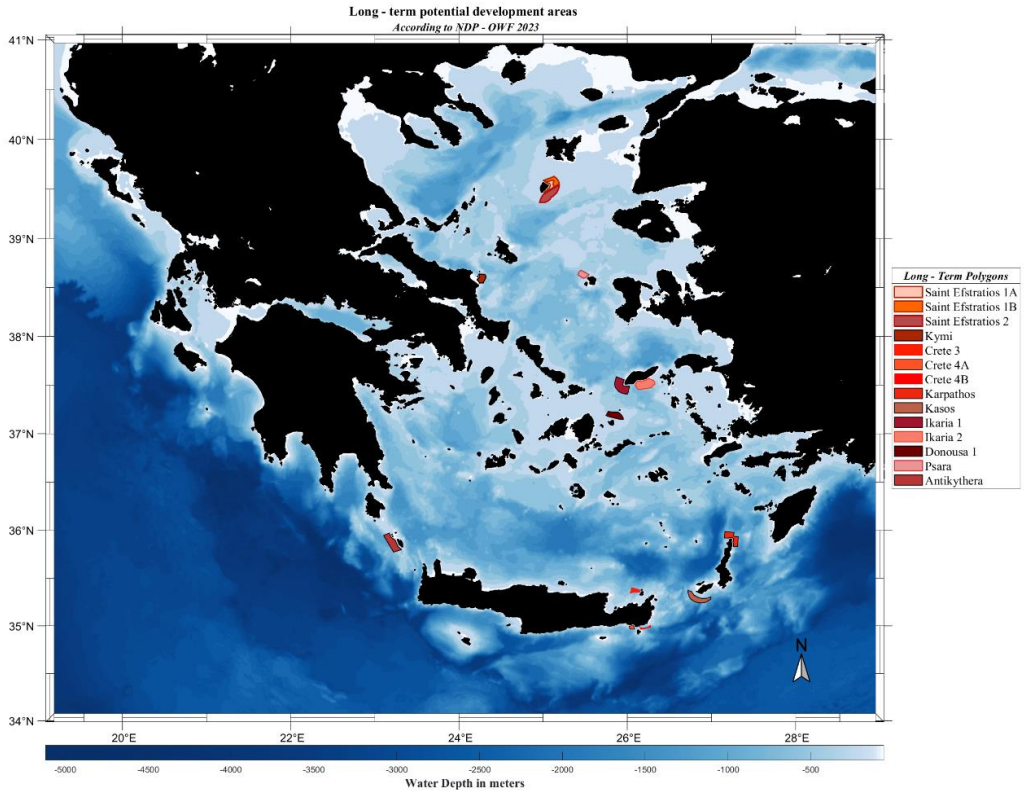

Figure 10. Long – term potential areas for the development of OWFs, in the Greek Seas

2. Data description

Weather forecasting relies on current atmospheric and earth surface assessments using models who incorporate principles of mathematics and physics, to analyze present data. The dataset that emerges from this operation, is used on evolving atmospheric and surface states [42].

Atmospheric reanalysis reconstructs and analyzes historical weather conditions by integrating observations from the past (in - situ, surface, and satellite remote sensing), with short – term forecasts from the latest Numerical Weather Prediction (NWP) models; offering consistent representation of the atmospheric state by assimilating observational data into a meteorological model, adjusted to replicate observed conditions as closely as possible. A consistent data assimilation (DA) system is used, unaffected by changes in methodology or techniques, while a previous forecast model with newly available observations in an optimal way produces better estimations of the state of the atmosphere.

Higher horizontal resolution, more sophisticated DA schemes and the benefit from the continuous development of forecast models, are the main advantages of reanalysis. Furthermore, they vary in several aspects, including the selection of observations that are integrated into the system, the choice of the model employed, as well as, the methods of estimating and correcting error statistics.

The datasets emerge from reanalysis systems, are among the most utilized, across various research domains, such as studies of atmospheric dynamics, analysis of climate variability and evaluation of NWPs errors, to involve modelling and assimilation capabilities [43, 44], while they find application in industrial contexts, such as wind power assessments for potential OWFs installations and observing long- term trends in climate monitoring studies [45].

ERA – Interim and its next generation ERA5 [46], with horizontal spatial resolution 31 km, produced by the European Centre for Medium Range Weather Forecasts (ECMWF), constitute as the most highly prevalent and widely employed reanalysis datasets [47], due to their enhanced and consistent recording of numerous Essential Climate Variables (ECVs); and extensively utilized, among other applications, in studies focusing on wind climate assessment [37, 38, 48, 49].

In order to resolve smaller – scale processes, in 2019 the Uncertainty in Ensemble of Regional Reanalysis (UERRA) [50] project, offered a high – resolution regional reanalysis over Europe with a spatial horizontal resolution up to 11km.

In the early 2020s, based on the limited area HARMONIE – ALADIN (NWP) model and an improved DA system (in a 3 – hour cycling mode), the most recent regional climate reanalysis released, within the framework of the Copernicus Climate Change Service. Copernicus European Regional Reanalysis (CERRA) [52], serves various purposes, including research, climate services, or even policy development [42] and has already applied in various approved studies [51-53].

The uniqueness of CERRA lies in its integration of a deterministic component with ensemble DA. This integration allows for periodic updates of the background error covariance matrix, a key element in the assimilation process. The background error covariance matrix captures uncertainties and errors associated with evolving weather systems, which consistently refreshes flow dependent information in the background error covariance matrix, ensuring that the assimilation process adapts to the dynamic nature of weather patterns; also, the ERA5 reanalysis is used for boundary conditions, aim to more accurately capture the changing errors

associated with evolving weather systems. This improvement is expected to result in more representative analyses and forecasts by better accounting for the dynamic nature of weather patterns and their associated uncertainties [54].

CERRA, is designed to create a pan – European reanalysis for the European region and its surrounding sea areas, as shown in Figure 11.

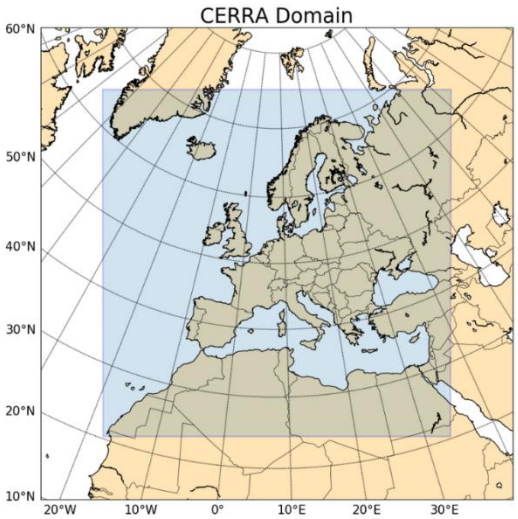

Figure 11. The spatial domain of the Copernicus European Regional Reanalysis (CERRA) system represented by the highlighted region in blue shading. (Source:[55])

The high horizontal spatial resolution (5.5 km x 5.5 km), allows CERRA for a better description of topographic and physiographic features, combined with the increased number of observations assimilated in the system, provides a significant added value to the dataset compared to the current state of the global reanalysis [55].

In terms of vertical resolution, features 106 model levels, extending from the surface up to 1hPa, while most of the data is post – processed and saved on 29 selected pressure levels, due to limited save space and hybrid – sigma coordinates of grid, which not align with standard pressure levels, making their use complex. Several variables are stored at 11 height levels, between 15 – 500m, serving applications in the wind energy sector [42].

Moreover, the gridded dataset, demonstrates reasonable temporal consistency conducted at 00 UTC, 03 UTC, 06 UTC, 09 UTC, 12 UTC, 15 UTC, 18 UTC, and 21 UTC, covering a wide time span, ranging from the early 1980s to the present, including monthly operational updates in near real time.

In the present study, the assessment of the existing offshore wind climate using Matlab and the most recent reanalysis dataset CERRA, accessed from the Copernicus Climate Data Store (https://cds.climate.copernicus.eu/ [50]), provided free of charge and combined with its high temporal and spatial resolution, is presented in the following sections. The study, includes the statistical analysis of three main aspects of wind (speed, direction and power density) at 100 m height above the sea level, which considered as the typical height of the rotor of an OWT [5]. The gridded dataset concerns a 36-year period (1985 – 2020), with a 3 – hour timestep. The area studied is defined by a rectangle with 19°E – 30°E & 34°N – 40°N, as captured in Figure 12, including the entire offshore areas of Greece.

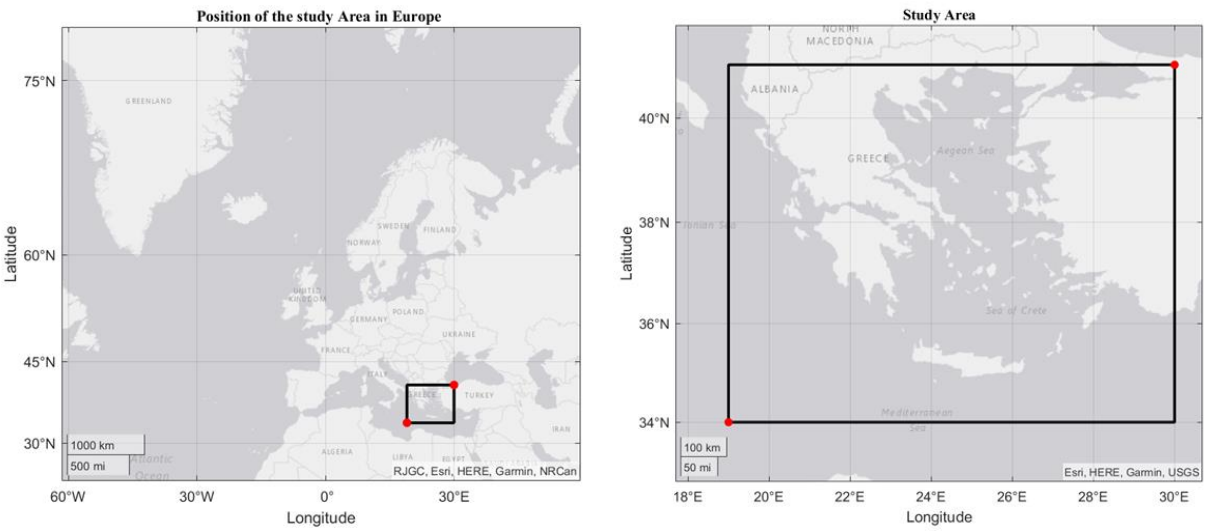

Figure 12. Position of the area of interest in Europe (left figure); Study Area: The Greek Seas (right).

3. Theoretical background and methodology

3.1. The importance of wind climate assessment

As demonstrated by numerous previous studies, the importance of wind climatology analysis is well – established and undisputed. The statistical assessment and modeling of wind speed, along with the study of the associated wind direction, are widely used concerning among others, the retrieval of offshore wind speeds from satellite data, weather forecasting along shipping lanes, optimization of ship routing [56], and bird migration routes [57, 58].

Consequences arising from climate change, affect over time, both of the global climate structure and meteorological conditions, as well as the human life. In respect, temporal lengthy data, for the evaluation of long – term variability, as well as the trends of current wind speed considered imperative [59-61].

Atmospheric pollution constitutes one of the factors that accelerates climate change; Can, et al. [62] mentioned that, higher wind speeds are likely to facilitate the spread of pollutants, while as observed by Pogumirskis, et al., [63] an increased probability of wind blowing from a specific direction can be linked to a higher likelihood of air pollution. In respect, the assessment of mean wind speed and direction, as well as the corresponded variability and long-term trends, contribute to the creation of atmospheric pollution scattering patterns.

The erosion of sandy shorelines, affects the nearshore communities socioeconomically and consists a direct result of wind speed and direction, due to their impact on wave climate, resulting storm surges from the frictional wind stress on the sea surface. Thus, the identification of the areas with the wind characteristics affect vulnerable shorelines is considering crucial [64, 65].

The definition of the frequency and intensity of extreme wind events is crucial, as they are responsible for physical destruction, injuries, loss of life, and economic damage [66].

Both wind speed and direction constitute as fundamental factors regarding the design, construction and stability of structures [67], as well as for the energy assessments of buildings. He Y., et al [68] mentioned that establishing accurate wind profiles in all wind directions is crucial for the development of reliable and precise building energy assessments, due to the substantial differences in vertical wind speed between the upper and lower layers.

Global efforts have been directed towards the decarbonization of the energy mix as part of climate change moderation; while the amount of energy generated, relies on weather patterns and wind speeds, which themselves can be influenced by climate change [59]. Analyzing wind aspects is essential in planning the development of an OWF, evaluating their contribution to global energy system decarbonization, as well as a main factor for the definition of the levelized cost of energy. Furthermore, long – term changes of wind aspects have direct impacts in the energy production and therefore in the accurate prediction of profits [60]. Modeling wind direction is becoming increasingly significant, particularly in applications evolving technology of floating wind turbines [69], and micro-siting of OWFs [70, 71].

In order to access accurately the offshore wind climate, long – time series of wind data is needed. The most reliable source of obtaining such data is considered to be in - situ measurements of wind characteristics; yet, spatial and temporal limitations arise, due to their high cost. Satellite – based measurements, or NWP models, as well as by combining measurements from different satellites through the implementation of suitable interpolation schemes for a larger spatiotemporal analysis compared to individual satellite datasets, consist more cost – affective sources of wind data [72].

The precise analysis of offshore wind climate across various spatial scales, requires the existence of substantial data samples with suitable sampling frequencies. Each of the aforementioned wind data resources, comes with its set of advantages and limitations; thus, individual satellite measurements provide a variety of spatial and temporal scales, nevertheless, their accuracy is questionable near shores and narrow straits; on the other hand, regarding NWP models, due to their variety, offer the benefit of selection, based on their performance in the area of interest. Reanalysis products offer access to wind data time series enabling the examination of long – term variability and the identification of significant changes on a multiannual time scale.

For a comprehensive wind climate analysis, as well as, for the evaluation of potential areas for the installation of an OWF with an operational life close to 30 years, the ideal duration of the wind aspects datasets, recommend time – series span several decades. Currently, only a few datasets provide such extensive temporal coverage coupled with a large – scale spatial resolution.

3.2. Greece’s offshore wind climate

Both the Aegean and the Ionian Seas are characterized by distinctive coastlines and complex topographies. The Aegean, is surrounded by three sides of intricated topographies, the continental Greece, the southern Balkans and the Turkish coastlines, combined with the existence of a vast number of islands which exhibit various sizes and contribute to the variability of OW [73]. Georgiou,et al. [74], highlighted that the geographical and oceanographic features of the Aegean Sea play a crucial role in its rapid responses to meteorological changes.

Furthermore, in the southern Aegean, Crete Isl. due to its high mountain ranges, causes the creation of wind channels between the surrounding area islands, as well as, channeling and wind interactions between the coastal valleys and the mainland [75].

The most characterized wind system in the Greek Seas are Etesians, which stands out as one of the most prominent wind patterns globally. Etesians are persistent northern winds of the lower atmosphere, with a regional scale, that occur over the Aegean Sea and the eastern Mediterranean in the latest part of June and disperse in the end of September [76].

The duration of the Etesians over the Greek Seas lasts a few months with very strong wind speeds and mainly a constant wind direction, provided by the channel created by the mountains in Greece, Turkey and Southern Balkans [77]. Nevertheless, wind direction differs in different regions; northern Aegean is mainly characterized by north winds, the central by north to north - east winds (NNE) while in the Ionian Sea their considered west or northwest (NW).

Various factors including alterations in midlatitude circulation, shifts in jet stream patterns, fluctuations in the Indian summer monsoon, and climate change, can impact the behavior of Etesian winds [78].

Previous studies [37-39] indicated that the Aegean Sea is considered one of the windiest regions in the Mediterranean basin; the study of Dafka, Toreti [78], using EURO – CORDEX data, indicated a significant increase to the Etesians frequency and intensity over the 21 century specifically, more intense in June to September and frequent in May, June and September. Nevertheless, the most recent studies based on climate model projections, emerged with decreasing projections for the coming decades, for both of wind power density and variability, mainly at the southern parts of the Aegean; see more in [60].

The methodology followed for the analysis of the three main aspects of wind climate in Greece, including the spatio – temporal long – term variability, as well as the linear wind speed trends, for the annual, monthly, seasonal and decadal time scale, are presented in the following sections.

3.3. Statistical analysis for wind speed and direction

3.3.1. Analysis in the annual scale

Climate variables such as wind, adhere to the definition of random variables, thus each observation differs from the next. Information about the predominant wind climate is typically conveyed through annual and seasonal low–order statistical characteristics of wind speed and wind direction, such as mean values and variances, along with other statistical parameters that quantify the corresponding temporal variability. Spatial variability is commonly expressed by a specific coefficient of variation (CV), like mean annual or inter – annual variability, offering a unique and static, baseline for comparative analysis in the spatial domain [79].

For the statistical analysis of wind speed, using the basic time index t, corresponding to the 3 – hour intervals, $t \rightarrow u(t_i) = u_i$, by the terminology of [76], will represent the time series of wind speed.

Three temporal scales were selected for the spatial analysis of the variable; annual, monthly and seasonal, each employing distinct tools, catering to diverse application needs and unveiling various facets of wind speed.

In addition to the aforementioned temporal scales, the spatial analysis of wind speed's corresponding variability, was examined in an annual and in a long – term scale, i.e., decadal time scale, due to the fact that long – term changes of wind speed and relative variability, are important in real life situations, as mentioned in previous sections.

In respect of all the above, the scale of t_i is hours, and the standard low – order statistical moments were considered, such as mean value of wind speed. Mean is a measure of the central location of the data, which estimation is straightforward, computed by adding all the values of the variable for a specific coordinate, and divide it by the number of data values in a specific coordinate. In respect, the annual mean wind speed for a particular year j is,

$$m_{u,Y=j} = \frac{1}{N}\sum_{i=1}^{N} u_i \,, \qquad [1]$$

where N being the number of observations of the year, i.e. the number of the corresponding hours in a year j.

Form the sequence of the above annual mean wind speeds for a series of years $m_{u,Y}(j)\,, j = 1,2,..J.$, the mean annual wind speed is denoted as follows:

$$m_{u,Y} = \frac{1}{J}\sum_{j=1}^{J} m_{u,j}(j), \qquad [2]$$

where J is the total number of years (36).

In order to assess the variability of a variable, variance σ^2 and standard deviation σ, are measures commonly used. The difference between each wind speed value and the annual mean wind speed for a year j is computed. The annual standard deviation, is used as one of the descriptive measures of variability in this study, for a specific year and it is estimated as follows:

$$\sigma_{m_{u,Y=j}} = \sqrt{\frac{1}{N}\sum_{i=1}^{N}\left(u_{i,Y(j)} - m_{u,Y=j}\right)}, \qquad [3]$$

where N is the number of observations of the specific year and $m_{u,j}$ is the annual mean wind speed for a specific year as mentioned before.

Therefore, from the sequence of the above annual mean wind speeds for the 36 – year period, the $\sigma_{m_{u,Y}}$ estimated as follows:

$$\sigma_{m_{u,Y}} = \sqrt{\frac{1}{J}\sum_{j=1}^{J}(m_{u_i,Y=j} - m_u)}. \quad [4]$$

Median is an alternative measure of central location that offers robustness in compare with the mean, due to the fact that remains unaffected by extreme values of wind speed, whether high or low. Represented by the 50th percentile, median stands as the central value within the dataset, providing insight into the central tendency of the wind speed data. Estimating the median involves arranging wind speed values in ascending order, with the exactly centered value, corresponding to median. This signifies that 50% of the wind speeds are lower than the value of the median, and the remaining 50% are higher. The estimated median for a specific year, i.e. annual median wind speed and the sequence of the annual median wind speeds for a series of years is used for the estimation of the median annual wind speed, akin to the corresponding mean annual wind speed. Furthermore, the 95th and 99th percentiles estimated for specific year j.

The individual variability of wind speed is expressed in a spatial domain by the CV which is a relative measure of the dispersion of data points around the mean [38, 79]. It provides insights into the wind speed variability within each year, and is also referred as mean annual variability (MAV). MAV is defined as the ratio of the annual standard deviation to the annual mean value of wind speed $m_{u,Y=j}, j = 1,2,..,J$, and is denoted as,

$$CV = \frac{1}{J}\sum_{j=1}^{J}\frac{\sigma_{u,Y}(j)}{m_{u,Y(j)}}, \quad [5]$$

where $\sigma_{u,Y}(j)$ denotes the annual standard deviation of the wind speed for a year $j, j = 1, 2 \ldots J$.

Interannual Scale

On the other hand, the ratio defined as the standard deviation $\sigma_{m_{u,Y(j)}}$ of the annual mean wind speed sequence $m_{u,Y=j}$, to the overall mean wind speed value m_u, provides a measure of the corresponding variability of wind speed from year to year. Inter – annual variability (IAV), is,

$$IAV = \frac{\sigma_{m_{u,Y(j)}}}{m_u}. \quad [6]$$

Regarding the wind direction, only the mean values were estimated for the corresponding temporal scales. The estimation of mean wind directions is not straightforward, due to the fact that wind direction belongs to vectorial data, which have a starting point and a direction. The statistical analysis and the comparing between this kind of data is quite different from the methodology used for linear data, such as wind speed, and notions like “higher” or “decreased” do not apply in the compare and evaluation of circular data.

For the calculation of the mean annual, mean monthly and mean seasonal direction of wind, the methodology provided by Soukissian [69] used, where $\vartheta(t_i) = \theta_i, i = 1,2,\ldots.n,$ represents the time series of wind direction and t is the basic time index corresponded to the 3 – h intervals; thus, the mean wind direction is given:

$$\bar{\vartheta} = \begin{cases} tan^{-1}(S/C), if\ C > 0, S > 0 \\ tan^{-1}(S/C) + \pi, if\ C < 0 \\ tan^{-1}(S/C) + 2\pi, if\ S < 0, C > 0 \end{cases}, \quad [7]$$

where, C and S are estimated as follows; see more in [69].

$$C = \sum_{i=1}^{n} cos(\vartheta_i), S = \sum_{i=1}^{n} sin(\vartheta_i). \quad [8]$$

3.3.2. Analysis in the monthly scale

In this temporal scale, the examined variable was the mean value of the 3 – h intervals for each month of the available time series. Using the same methodology as for the annual scale, months will be representing by the letter m and the estimation of monthly mean wind speed $m_{u,Y,M}(j,m)$, for a particular year j and month m is given:

$$m_{u,Y=j,M=m} = \frac{1}{K}\sum_{i=1}^{K} u_i, \quad [9]$$

where K is the total number of the 3 – h intervals for a particular month m and year j.

Furthermore, the mean monthly wind speed for a particular month m, $m_{u,M=m}$, estimated from an appropriately selected subsequence of $m_{u,Y,M}(j,m)$. For example, the mean monthly wind speed for January, is given by the sequence of monthly mean values of January for a series of years, and is denoted as,

$$m_{u,M=m} = \frac{1}{J}\sum_{j=1}^{J} m_{u,M=m}(j)\ \ for\ m = 1,2,..M, \quad [10]$$

where $m_{u,M=m}(j), j = 1,2,\ldots 36$, denotes the sequence of monthly mean values for the particular month m, for the entire series of years.

The monthly standard deviation for specific month m and year j is estimated as follows:

$$\sigma_{m_{u,Y=j,M=m}} = \sqrt{\frac{1}{K}\sum_{i=1}^{K}\left(u_{i,Y,M} - m_{u,Y=j,M=m}\right)}, \quad [11]$$

where $u_{i,Y,M}$ are the observations of wind speed for a specific month and year and $m_{u,Y=j,M=m}$ is the monthly mean wind speed for a year j and month m. Therefore, the standard deviation of the sequence of the above monthly mean wind speeds for a month m and year $j, j = 1,2,..J$ is denoted as follows:

$$\sigma_{m_{u,Y(j),M(m)}} = \sqrt{\frac{1}{J}\sum_{j=1}^{J}\left(m_{u_i,Y=j,M=m} - m_{u,M=m}\right)}, \quad [12]$$

where $m_{u_i,Y=j,M=m}$ are the monthly mean values and $m_{u,M=m}$ is the mean monthly value of wind speed for a particular month m. As follows the corresponding median, 95th and 99th percentiles were estimated.

3.3.3. Analysis in the seasonal scale

In this temporal scale, the examined variable is the mean value of the 3 – h intervals for each season of the available time series. Using the same methodology, seasons will be representing by the letter s, on behalf of one of the four seasons within a year, which are defined as follows:

- Winter: December, January, February (DJF)
- Spring: March, April, May (MAM)
- Summer: June, July, August (JJA)
- Autumn: September, October, November (SON)

Therefore, the estimation of seasonal mean wind speed $m_{u,Y,S}(j,s)$, for a particular year j and season s is,

$$m_{u,Y=j,S=s} = \frac{1}{L}\sum_{i=1}^{L} u_i\,, \quad [13]$$

where L is the total number of 3 – h intervals correspond to season s and year j.

The mean seasonal wind speed for a particular season s, $m_{u,S=s}$, is estimated from the corresponded subsequence of $m_{u,Y,S}(j,s)$. For each season $s = 1,..,S$, the mean seasonal wind speed will be estimated from the sequence of seasonal mean wind speeds for the selected season s, for the 36 – year period, as follows:

$$m_{u,S=s} = \frac{1}{J}\sum_{j=1}^{J} m_{u,S=s}(j) \quad , for\ s = 1,2,3,4 \ , \qquad [14]$$

where $m_{u,S=s}(j), j = 1,2, \dots 36$, denotes the sequence of the seasonal mean values for the particular season s, for the selected series of years.

The seasonal standard deviation for particular season s and year j is estimated as follows:

$$\sigma_{m_{u,Y=j,S=s}} = \sqrt{\frac{1}{L}\sum_{i=1}^{L}(u_{i,Y,S} - m_{u,Y=j,S=s})}, \qquad [15]$$

where $u_{i,Y,S}$ are the observations of wind speed for a specific season and year, $m_{u,Y=j,S=s}$ is the seasonal mean wind speed for a year and season s and L are the corresponded 3 – h intervals of the specific season s in a year j. Therefore, the standard deviation of the sequence from the above seasonal mean wind speeds for season s, for the 36 - years J, is estimated as follows:

$$\sigma_{m_{u,Y(j),S(s)}} = \sqrt{\frac{1}{J}\sum_{j=1}^{J}(m_{u_i,Y=j,S=s} - m_{u,S=s})}, \qquad [16]$$

where $m_{u_i,Y=j,S=s}$ are the seasonal mean values and $m_{u,S=s}$ is the mean seasonal value of wind speed for a particular season s. As follows, the corresponding median, 95th and 99th percentiles were estimated for the seasonal statistical analysis.

3.3.4. Wind speed trends

For a concluded analysis of the wind climate in a specific region, the estimation of the wind speed trend, is essential. The estimation of the linear trend provides a measurement of the tendency of the sequence of the mean wind speeds, in the examined time scale, to increase, decrease, or remain constant. A resistant and robust method named Theil and Sen estimator (TSE) [81, 82], applied for the estimation of slopes, i.e. the ratio of the linear trend. The preference of TSE method depended on the resistance presents to outliers along its high asymptotic efficiency, widely used as a non – parametric method for trend analysis in the hydrology and meteorology [83].

The TSE method, provides the estimation of the slopes for every possible pair of points, by ultimately estimate a total number of slopes, equivalent to:

$$\binom{n}{2} = \frac{n(n-1)}{2}, \quad [17]$$

where n is the size of the sample and the final non- parametric slope $\hat{b}_1$ is defined as the spatial median of the total slopes, as follows:

$$\hat{b}_1 = median\{\hat{B}\}, \hat{B} = \left\{ b_{ij} | b_{ij} = \frac{u_{j-}u_i}{t_j - t_i}, t_i \neq t_j, 1 \leq i < j < n \right\}, \quad [18]$$

where all the possible combinations of mean wind speed values $u_{j,}u_i$ and t_j, t_i, $j > i$, $i = 1,2, \dots, n-1$ and $j = 2,3, .., n$.

Regarding the trend line, the intercept $\hat{b}_0$ is estimated by the equation proposed by Conover, W.J.[84]:

$$\hat{b}_0 = u_m - \hat{b}_1 \cdot t_m, \quad [19]$$

where u_m and t_m are the medians of the measurements and of the response variables correspondingly.

For the evaluation of the trends of the extreme wind speeds over the Greek seas, the 95th and the 99th percentiles for specific year were estimated, for the corresponded temporal scales. The sequence of the above series of the 95th and 99th percentiles of wind speed for a series of 36 - years, were $j = 1,2, \dots, J$, then used for the estimation of the linear trend of the extreme wind speeds.

3.4. Wind power density

The available wind power density (WPD) over the Greek Seas, concerning the fact that Greece is one of the prevailing areas of the Mediterranean basin, in terms of OWE, expected to arise with high values, as it is linked to the cube of the available wind speed, as follows:

$$WPD = \frac{1}{2}\rho \cdot u^3, \quad [20]$$

where, ρ is the air density considered to be constant and equal to 1.2258 kg/m^3.

For the statistical analysis of wind power density, following the same methodology as in the previous section, the basic time index t used, corresponding to the 3 – hour intervals, $t \rightarrow u(t_i) = u_i$, thus, the annual mean wind power density for a particular year j is denoted as follows:

$$\overline{P_{u,Y=J}} = \frac{1}{2N}\sum_{i=1}^{N} \rho u_i^3, \quad [21]$$

where N is the corresponded hours to a specific year j.

The sequence created from the annual mean wind power densities $P_{u,j}(j)$, was used for the estimation of the mean annual wind power density, for the entire series of examined years, denoted as:

$$\overline{P_{u,Y}} = \frac{1}{J}\sum_{j=1}^{J} P_{u,j}(j). \quad [22]$$

The estimation of the annual standard deviation, the standard deviation of the sequence of the annual mean wind power densities, as well as the corresponded median measures, was also performed. For the evaluation of the variability of wind power density within a year and from year to year, the coefficients of variations used in the previous section, modified as follows:

$$CV_{WPD} = \frac{1}{J}\sum_{j=1}^{J} \frac{\sigma_{P_{u,Y(j)}}}{P_{u,Y(j)}}, \quad [23]$$

where $\sigma_{\mathrm{P_{u,Y(j)}}}$ denotes the annual standard deviation of the wind power density for year $j, j = 1, 2 \ldots J$ and $\mathrm{P_{u,Y(j)}}$ is the annual mean wind power density.

The estimation of variability of wind power density ratio from year to year, i.e., IAV is denoted as follows:

$$IAV_{WPD} = \frac{\sigma_{P_{u,Y}}}{P_u}, \quad [24]$$

where $\sigma_{\mathrm{P_{u,Y}}}(j)$ denotes the standard deviation of the annual mean wind power density sequence $\overline{P_{u,Y=j}}$, to the overall mean wind power density value P_u.

Regarding the monthly scale, following the previous section's methodology the monthly mean wind power density for a particular year j and month m is estimated as follows:

$$\overline{P_{u,Y=J,M=m}} = \frac{1}{2K}\sum_{i=1}^{K}\rho u_i^3, \quad [25]$$

where K is representing the corresponded hours for the month m in the year j; thus, the sequence of the monthly mean wind power densities $P_{u,j,m}(j)$ emerged from the previous equation, is used for the estimation of the mean monthly wind power density, as follows:

$$\overline{P_{u,Y,M}} = \frac{1}{J}\sum_{j=1}^{J} P_{u,j,m}(j). \quad [26]$$

The seasonal mean wind power density estimated for every season s and year j, where L is the corresponded hours for the season s within the year j:

$$\overline{P_{u,Y=j,M=m,S=s}} = \frac{1}{2L}\sum_{i=1}^{L}\rho u_i^3. \quad [27]$$

As well as the corresponded mean seasonal wind power density, emerged from the sequence of seasonal means $P_{u,j,s}(j)$ in a series of years $j = 1,..J$.

$$\overline{P_{u,Y,S}} = \frac{1}{J}\sum_{j=1}^{J} P_{u,j,s}(j). \quad [28]$$

3.5. Performance assessment of the NREL-15 MW offshore wind turbine

The wind climate of a potential area for the development of OWFs, changes within a year, or from year to year, or even due to climate change, creating uncertainties to the estimated produced energy and therefore, to the economic efficiency of the prospective installed OWF. Thus, beyond the statistical analysis of the wind climate, the assessment of the performance of potential installed WTs, is necessary.

There are several aspects that should be examined regarding the performance assessment of potential WTs; including the estimated produced energy, estimations involving the operational limits and the evaluation of specialized factors, in order to compare the efficiency of the selected turbine between the potential development areas. The available wind resource of a potential area, is a crucial parameter for designing and selecting the most suitable WT model, in the development of an OWF. For the proper operation of a WT, the brake of the rotor in the drive train, stops the procedure of the turbine for either extremely low or high values of wind speed. The thresholds that represent a significant portion of industrial WTs are characterized by cut –

in speeds, i.e. the minimum wind speed at which WT operates, at 4 m/s, and cut – out at 25 m/s, i.e. the maximum wind speed at which the WT will perform.

In respect of all the above, a 15 – MW offshore wind turbine was chosen, the NREL 15 – MW [85], produced by National Renewable Energy Laboratory of the US and Technical university of Denmark; while funded by the US Department of Energy Office of Energy and Renewable Energy wind and water technologies office; and created based on a previous version of the IEA – 15MW [86]. With corresponded operational limits, cut – in speed 4m/s and cut – out speed 25 m/s.

3.5.1. Evaluation of the wind turbine performance

The power curve of a WT, constitutes the identity of the machine and associates the characteristics of the potential development area with the characteristics of the WT. The power curve of the NREL – 15 MW, is presented in Table 1, including the power output, the corresponded values of coefficient of power (C_P) and the distributed wind speeds.

The C_P factor, represents the ratio of the power absorbed from the WT, to the available WPD of the area of interest; the percentage that emerge provides the ratio absorbed by the WT, from the available WPD of the examined area and is estimated as follows:

$$C_P = \frac{P_T}{P_w} \quad [29]$$

The maximum theoretical efficiency that a WT can have, is called Benz limit and corresponds to a $C_p \sim 59{,}3\%$.

One of the aspects examined for the performance assessment of the selected WT in this study, was the estimation of the produced energy, performed for both the 30 sites, as well as for the entire area of the Greek Seas, in an annual scale.

The estimation of the annual energy that the selected WT could produce in the Greeks seas within a specific year, as well as in for the series of 36 – years, $j = 1, \dots J$, is the straightforward calculation of the mean power output of the WT, by combining its power curve with the available wind speed time series [79]. In respect of all the above, the annual mean produced energy for a specific year j, is estimated as follows:

$$\bar{E}_{w,Y=j} = \frac{1}{N}\sum_{i=1}^{N} E_w(u_i), \quad [30]$$

where N is the size of the sample, corresponded to the 3 – hour intervals for the specific year j. As follows, the mean annual wind energy output estimated from the sequence of the above annual mean energies is denoted as:

$$\overline{E_{w,Y}} = \frac{1}{J}\sum_{j=1}^{J} E_{u,j}(j), \quad [31]$$

for the 36 – year period examined, where $j = 1, \dots J = 36$.

An additional factor that should be taken into account for the development of OWFs, is the capacity factor (CF) of a WT in the area of interest. The CF factor represents the ratio between the total energy produced by the WT and the energy could be produced if the WT was operating in full capacity for all the corresponded hours for the series of years examined.

For the estimation of the CF factor of the NREL WT, in the Greek seas, both the energy estimated for a specific year j, and the energy emerged from the WT while operating in its full capacity (15000 kW), were used. The sequence emerged, from the above ratios then used for the estimation of the mean annual CF in the Greek seas, for the 36 – year period, where $j = 1, \dots J = 36$:

$$CF = \frac{1}{J}\sum_{j=1}^{J} \frac{\overline{E_{w,Y}}}{\overline{EFC_{w,Y}}}, \quad [32]$$

$EFC_{w,Y}$ is the energy emerged from the full capacity operation of the WT, in the examined time scale, while $\overline{E_{w,Y}}$ is the total energy produced by the WT.

Table 1. Power curve of the NREL -15MW wind turbine

WS (m/s)	**Power** (kW)	C_P (%)
3	0	0
4	720	0.406007508
5	1239	0.357719682
6	2271	0.379442585
7	3817	0.401614683
8	5876	0.414184048
9	8450	0.418322017
10	11536	0.416329121
11	15000	0.406719267
12	15000	0.313277398
13	15000	0.246401158
14	15000	0.19728256
15	15000	0.160398028
16	15000	0.132163902
17	15000	0.110185903
18	15000	0.092822933
19	15000	0.078924529
20	15000	0.067667918
21	15000	0.058454092
22	15000	0.050839908
23	15000	0.044492754
24	15000	0.039159675
25	15000	0.034645974

3.5.2. Time percentages within the operational limits of the wind turbine

Extreme high or low values of wind speed, could potentially reduce the efficiency of the WT, cause damage to the turbine, compromised its proper functioning, or even lead to complete destruction. These issues result in the unreliability of the OWF operation, as well as to increased costs for the maintenance or even the replacement of individual components of the turbine. In respect of that, the selection of the potential area for the installation of an OWF, is directly related to the corresponded time percentages of wind speed within the operational limits of the potential installed model.

The estimation of the time percentages of wind speed within the operational limits of the NREL – 15 MW, estimated for the three temporal scales; the annual time percentages denoted as follows:

$$P_{r[4\leq u_{100,i}\leq 25]} = \frac{\sum_{i=1}^{N} 1_B[4 \leq u_{100,i} \leq 25]}{N}, \quad [33]$$

where $P_{r[4\leq u_{100,i}\leq 25]}$ represents the probability of the wind speed within the operational limits, N, is the number of hours, corresponded to the 3 – h intervals of the 36 years and 1_B, is the indicator function of the incident.

The same methodology applied for the next two temporal scales, for the corresponded sizes of samples. For example, for the estimation of the monthly time percentages, the probability of the occurrence $4 \leq u_{100,i} \leq 25$ for a specific month m, will be estimated by the wind speeds of the corresponded incidents for the specific month m, for the 36 – year period, where $j = 1, \ldots J = 36$, denoted as:

$$P_{r[4\leq u_{100,M,i}\leq 25]} = \frac{\sum_{i=1}^{K} 1_B[4 \leq u_{100,M,i} \leq 25]}{K}, \quad \text{m} = 1,..\text{M} \quad [34]$$

where K, is representing the corresponded hours for the month m for the 36 years.

Regarding seasonal time percentages, respectively:

$$P_{r[4\leq u_{100,L,i}\leq 25]} = \frac{\sum_{i=1}^{L} 1_B[4 \leq u_{100,S,i} \leq 25]}{L}, \quad \text{s} = 1,..\text{S} \quad [35]$$

where L, is representing the corresponded hours for the season s for the for the 36 years.

3.6. Definition of the 30 polygons according the spatial distribution of CERRA

In order to compare the performance of the NREL – 15 MW between the 30 selected sites, all the above applied, in selected points, considered representative for the entire area of each polygon. Each grid point of the CERRA dataset, represents approximately 30 km^2, while some of the examined polygons exhibit intricate corners or schemes, due to the complex geomorphology of the nearby islands. The above combination led to limited options of potential examination spots in some areas.

In order to identify the available quantity of points for each examined site, each polygon demarcated by a quadrangular, which created by utilizing the maximum and minimum values of longitude and latitude, respectively. The points confined in this frame were initially considered representative for each area. An additional segmentation was performed, discarding points that were outside the boundaries of each polygon, within the square limits. The aforementioned process, is presented for one of the 30 sites in Figure 13.

From the remain available points, one was selected, considered representative of the entire examined site. An extensive analysis then conducted in an annual scale for each area, including the statistical analysis of wind speed, WPD, the corresponded trends and variability, as well as, the assessment of the performance of the NREL – 15MW turbine, in order to compare both the wind climate of the 30 areas and the WT's efficiency.

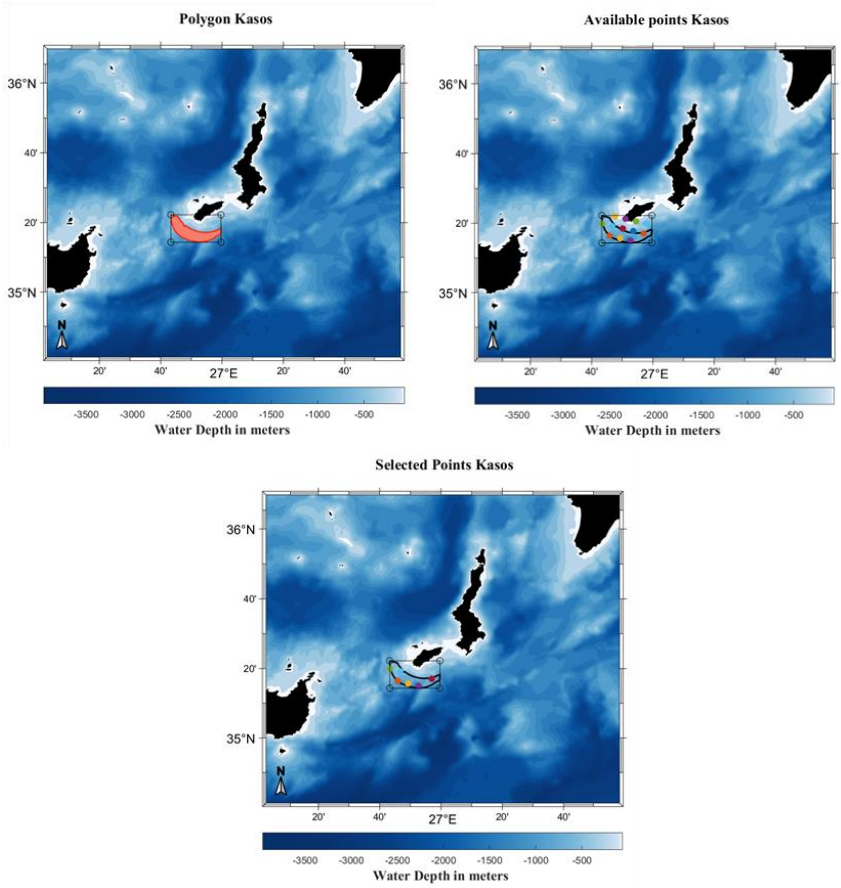

Figure 13. The definition of points corresponded to each polygon, according to CERRA spatial analysis

4. Numerical results

4.1. Wind speed and direction

4.1.1. Annual Scale

The spatial distribution of mean annual wind speed is illustrated in Figure 14, aligning with anticipated wind patterns based on previous studies [36]. The estimations from [36-38], suggested that the highest values of mean annual wind speed were observed in the central Aegean, which is supported in this study, however, it was not the prevailing area.

The results regarding the spatial distribution of mean annual wind speed, indicating elevated values across the entire range from the northern to the western regions of the Aegean. The most significant wind speeds were observed along the eastern coasts of Crete Isl. and the surrounding marine area, while the overall highest value (~ 10 m/s) was noticed at the point 35.12° N 26.53° E; the corresponding statistical measures and mean annual direction are given in Table 2 and in Figure 15, the time series of the regions presented the highest and the lowest mean annual values are depicted, respectively.

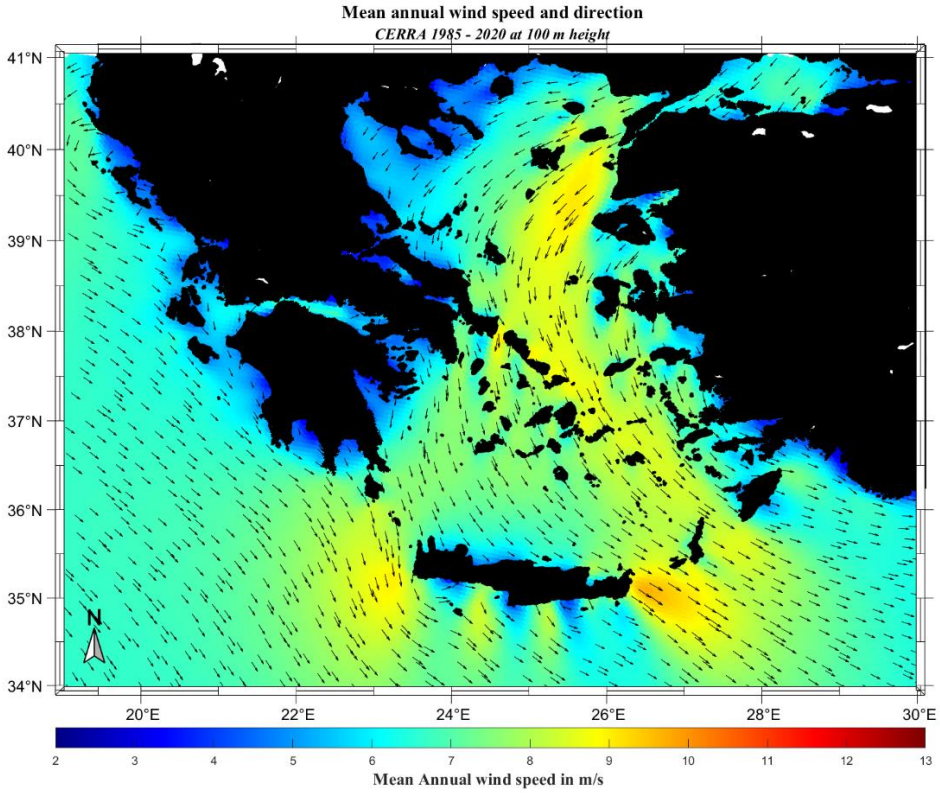

Figure 14 . The spatial distribution of mean annual wind speed and direction in the Greek Seas [3].

[3] Matlab, along with the M_map toolbox, was employed for generating the maps of this study; see more in [87].

The second – highest mean annual wind speed was observed at the southeastern tip of the island of Evvoia, in the cape of Kafireas, also known as Cavo D'Oro, with values exceeding 9 m/s. Significant wind speeds were noticed in the northern Aegean, near Saint Efstratios Isl. and the surrounding sea areas (~ 8 - 9 m/s). One of the windiest areas was the region of central Aegean, in the southeast shores of Andros Isl., exceeding wind speed values close to 9 m/s.

Similarly notable wind speed values were observed in the western coasts of Crete Isl., covering the surrounding sea area, reaching the coasts of Antikythera Isl., with values ranging from 8 to 9 m/s. In the Ionian Sea, mean annual values were generally lower compared to the Aegean, approximately around 7 m/s.

Lower wind speeds were typically observed in proximity to coastlines, which may be attributed to the data spatial resolution limitations in combine with the complex topography and coastlines of Greece. Consequently, the obtained results may exhibit reduced accuracy near coastal areas and in very narrow straits. The lowest wind speeds were observed near eastern coasts of Halkidiki and North Evvoia.

Table 2. The statistical parameters of selected areas in the Greek seas.

Sea Areas	**Coordinates** °	**WS** m/s	**Median** m/s	**Std** m/s	**MAV** %	**IAV** %	**WD** °
East Crete	35.12° N 26.53° E	9.67	9.70	0.40	47.83	4.23	327
Cavo D'Oro	37.91° N 24.65° E	9.09	8.68	0.48	56.29	5.28	264
E. Saint Efstratios	39.38° N 25.60° E	9.08	9.04	0.32	50.46	3.58	231
SE Andros	37.74° N 25.04° E	9.00	8.83	0.45	51.63	5.04	290
E. Halkidiki	40.53° N 24.18°E	4.16	3.43	0.18	71.01	4.44	85.15

Regarding the spatial distribution of mean annual direction, the results agreed with previous studies [36, 38]. The wind climate in the Aegean Sea for the annual time scale, was largely shaped by northeast (NE) winds, mainly in the northern Aegean. Wind in the central Aegean Sea blows from the north, and in the southern to the southeastern Aegean, where the highest wind speed values appeared, the wind direction was northwest (NW). On the other hand, in the Ionian Seas the prevailing wind direction was mainly NW, except for certain circular patterns observed in the northern Ionian, over the Diapontian Islands, where different wind directions were observed.

The spatial distribution of MAV, is presented in Figure 16, where the highest variability observed near the coastal areas of both the Aegean and Ionian Seas. The values range from 40 to 96%, with the overall high values appeared along the southern coasts of the Peloponnese; for more statistical details refer to Table 3. The lowest MAV values observed along the western coast of Crete Isl. (34.84 °N 22.74°E, 43.20%) and the surrounding sea areas; results that are in agreement with Soukissian [36]. The eastern shores of Halkidiki, the eastern region of the Dodecanese Islands as well as the surrounding sea areas, presented high values of MAV, respectively; statistical moments of all the aforementioned regions are presented in Table 3.

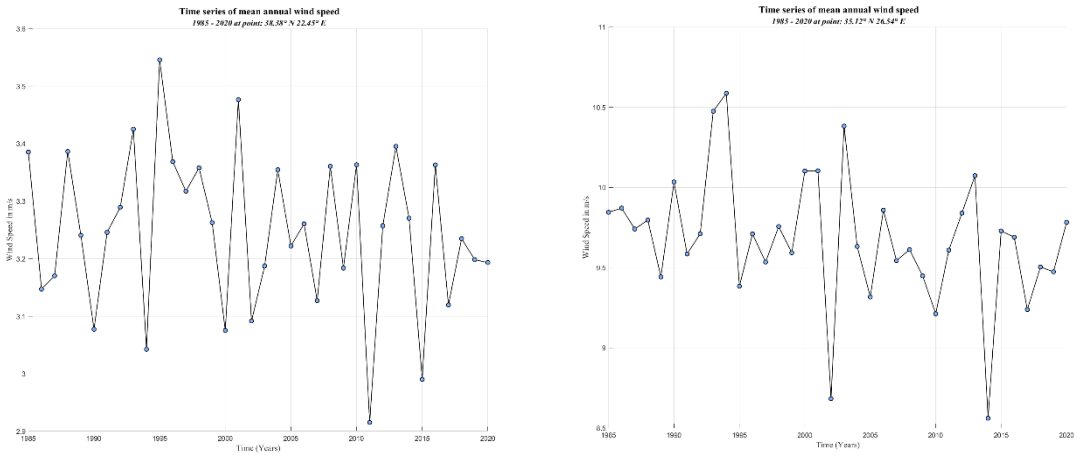

Figure 15. Timeseries for the locations exhibit the minimum (left figure, Gulf of Korinthos) and maximum (right, east of Crete Isl.) values of mean annual wind speed, for the 36 – year period 1985 - 2020.

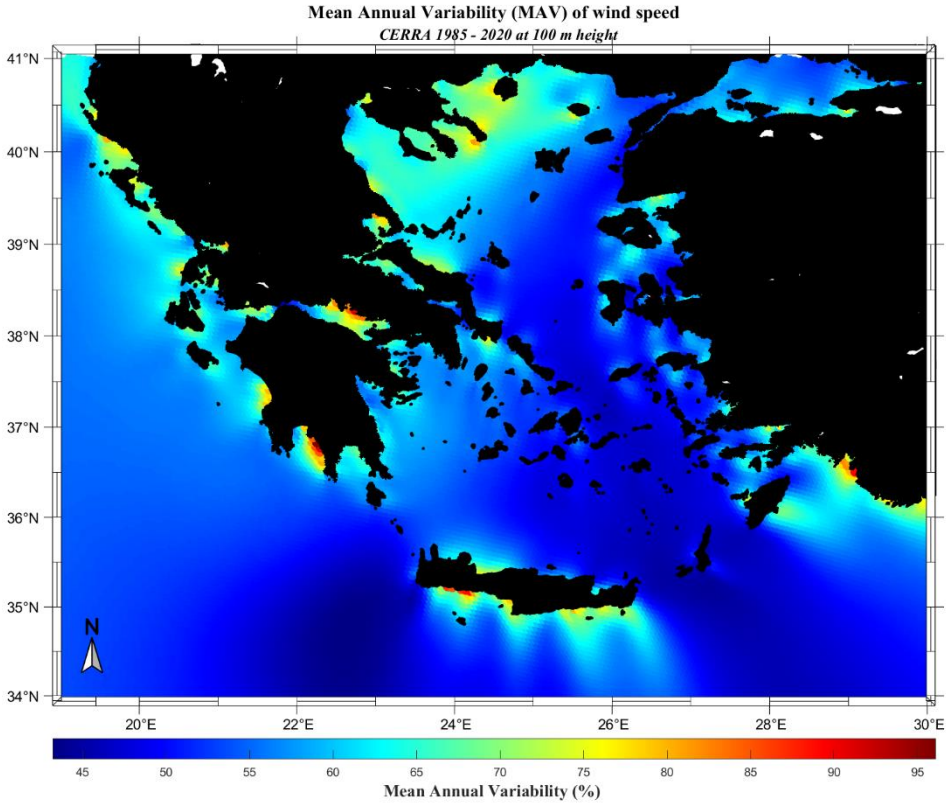

Figure 16. The spatial distribution of mean annual variability of wind speed in the Greek seas.

Regarding interannual variability as presented in Figure 17, it was evidenced by the spatial distribution of IAV, that the Ionian Sea exhibited higher values compared to the Aegean Sea. The highest value of IAV was observed along the southern coasts of Crete Isl., with the overall highest value exceeded 6 % (35.17 °N 24.25 °E). Eastern shores of Rhodes Isl., as well as north offshore areas of Gyaros Isl., were also areas presented high IAV values, close to 6 %, respectively.

Table 3. The statistical parameters of the areas with the highest and lowest MAV, in the Greek Seas.

Sea Areas	Coordinates °	WS m/s	Median m/s	Std m/s	MAV (%)	IAV (%)
North coasts of Peloponnese	36.83° N 22.25° E	3.45	2.38	0.20	96.10	5.78
North Evvoia	38.69° N 23.86° E	4.02	2.82	0.22	84.93	5.60
East coasts of Halkidiki	40.25° N 24.36° E	4.46	3.38	0.21	77.93	4.79
East of Diapontian islands	40.03° N 19.76° E	4.10	3.19	0.18	74.18	4.51
SW Crete	34.84° N 22.74°E	8.30	8.07	0.23	43.20	2.85

The spatial distribution of IAV over Ionian Sea in general displayed higher values, compared to Aegean; nevertheless, the overall highest value in this region did not exceed 4.5 %. The regions with the lowest variability were the surrounded areas of Antikythera Isl., with values ~ 2 %, and western coasts of Crete Isl., including the areas over the southern part of Kythera Isl. ~2%, as well as the southern part of Lesvos Isl., with values ~ 3 % respectively.

Table 4. The statistical moments of the areas with the highest and lowest IAV, in the Greek Seas.

Sea Areas	Coordinates °	WS m/s	Median m/s	Std m/s	MAV %	IAV %
South coasts of Crete	35.17° N 24.25° E	6.34	4.54	0.39	81.14	6.23
SE coasts of Rhodes	36.06° N 28.43° E	6.20	5.32	0.36	65.16	5.95
North Gyaros	37.87° N 24.58° E	8.78	8.10	0.51	61.28	5.82
East of Diapontian Islands	40.03° N 19.76°E	4.10	3.19	0.18	74.18	4.51
North of Antikythera	36.00° N 23.14°E	8.12	7.86	0.16	51.42	1.91

Crete Isl., emerged with different statistical parameters and patterns in each coast, since high values of wind speed noted in the west and east coasts of the island, while in the north and south, lower values observed, with higher variability coefficients. Noteworthy was, that the highest values of wind speed, with corresponded low variability, observed in offshore areas characterized by extremely deep waters, which are not considered for the development of OWFs.

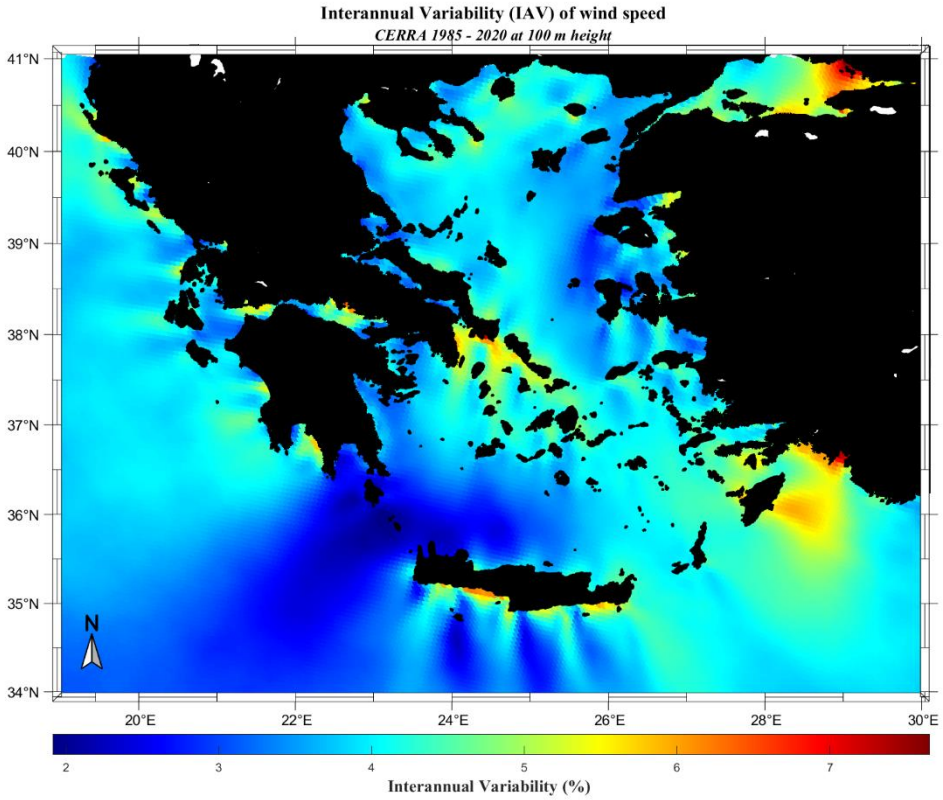

Figure 17. The spatial distribution of inter – annual wind speed variability in the Greek seas.

4.1.2. Monthly time scale

The spatial distribution of mean monthly wind speed and direction for January up to December is presented in Figure 18. The highest mean wind speed values occurred in July, reasonable due to the fact that this is one of the months Etesians blow over the Greek Seas, which often attains values exceeding 15 m/s and wind gusts over 20 – 25 m/s [75].

Regarding mean January's wind speed and direction, the highest values of wind speed associated with east and NE directions, observed in the North Aegean, in agreement with Prezerakos [88]; mentioned that the collapse of Persian trough emerges northeasterly winds during the cold seasons over the Aegean. The overall highest wind speed for the particular month was located in the offshore area near east coasts of Lemnos Isl. (> 10 m/s) covering the sea area over Saint Efstratios Isl. and south areas of Samothrace Isl.

Significant values appeared in the offshore areas of east (with the corresponding NW wind direction) and west coasts of Crete Isl. including the extended area up to the south coasts of Antikythera Isl. with values ranging from 9 to 10 m/, as well as in central Aegean with its north winds, with wind speeds in range between 8 and 10 m/s.

In general, in the Aegean Sea higher wind speeds were observed, where the majority presented values exceeding 8 m/s, compared to the Ionian Sea with its NW winds and speeds ranging from 5 – 7 m/s.

The lowest values of wind speed were observed near coastal areas, east offshore areas of Halkidiki with the overall mean wind speed noted in the northern parts of the Ionian, at point 39.98° N 19.63° E; statistical moments are presented in Table 5.

Table 5.The statistical parameters of the areas with the highest and lowest values of mean monthly mean for January, in the Greek seas.

Sea Areas	**Coordinates** °	**WS** m/s	**Median** m/s	**Std** m/s	**WD** °
East of Limnos	39.94°N 25.84°E	10.09	9.84	1.24	191
SN of Samothrace	40.20°N 25.53°E	9.93	9.68	1.38	188
South coasts of Crete	35.35° N 23.22° E	9.74	9.79	0.95	305
Halkidiki	40.53° N 24.18°E	5.44	5.45	0.87	235
East of Diapontian islands	39.98° N 19.63° E	4.41	5.48	1.05	160

Increased monthly mean wind speeds were observed in February compared to January, particularly over the Aegean Sea, with values exceeding 8 m/s; The highest values followed the patterns of the previous month, emerged in the same regions (north and central Aegean, east and west coasts of Crete Isl.) with higher magnitudes. Once again, the Ionian Sea presented calmest wind conditions compared to the Aegean.

Regarding wind direction, in February the main difference from January was noticed in the Ionian Sea, where mainly in the south region, winds observed western, while towards the norther area, they became south – southeast (SSE).

Wind directions in March generally maintained the consistent patterns observed in the previous months. A noticeable decrease was presented for the wind speeds compared to the two preceding months, in the entire offshore area of Greece. Despite this overall reduction, there were instances of high wind speeds observed in specific offshore areas; notably in the northern Aegean including the sea areas between Samothrace and Lemnos islands, with the overall highest wind speed recorded at point 39.86°N 25.75°E, ~ 9.5 m/s, as well as the extended area between the west coasts of Crete and Antikythera islands, with corresponding wind speed exceeding 9m/s.

In April, a further decrease was noticed, with the highest values ranging from 8 to 9m/s. The overall maximum wind speeds, were also noted at the so far prevailing areas. Regarding wind direction in the northern Aegean, winds are predominantly from the east, while in the central Aegean, they shift to NW directions. In the Ionian, the patterns remained consistent with previous months, maintained their westerly orientation, while a more pronounced northerly direction observed in the southern Ionian Sea, to the offshore areas off the western coasts of Crete Isl.

Even lower wind speeds were observed in May, for both of the Aegean and Ionian Seas, with the highest values around 8.5 m/s, observed near the coastal areas east of Crete Isl. and the surrounding offshore areas, inclined more towards the southeast and the southern coasts of Kasos Island. In general, May emerged with the overall lowest wind speeds that have been observed so far. Concerning wind direction, a notable difference compared to previous months was observed in the northern Aegean, where offshore of Halkidiki, winds from the northeast

transform into southeast, over Samothrace Isl., indicating the creation of flows due to the islands in the region and their topography. Moreover, the high wind speeds that so far observed in the northern Aegean have started to “shift” towards the central region.

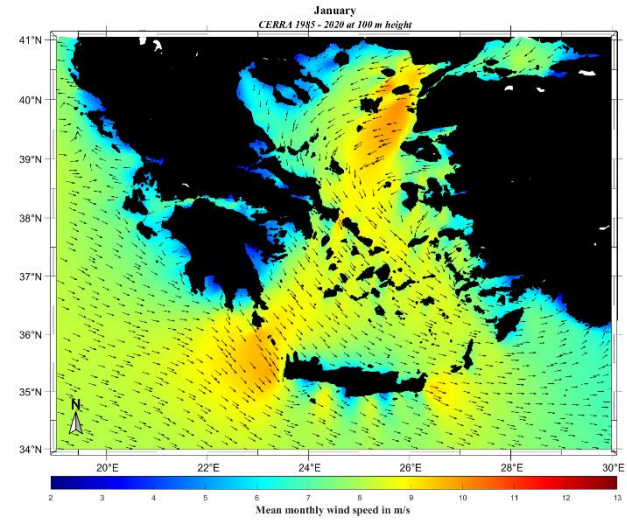

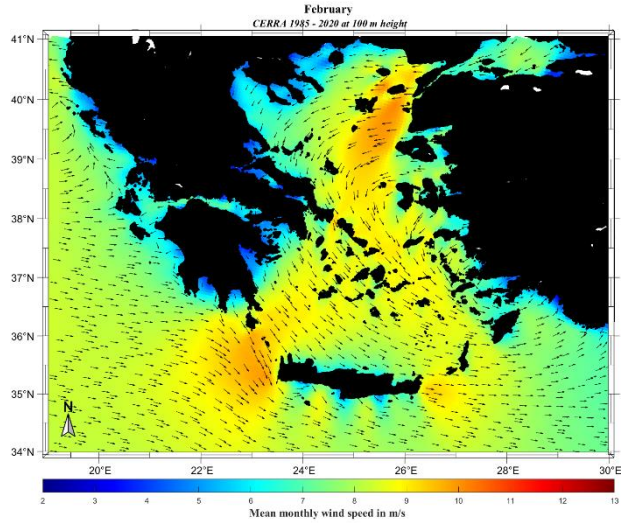

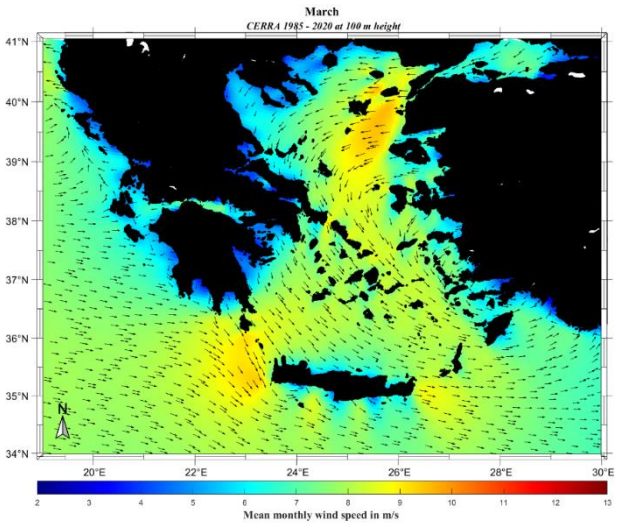

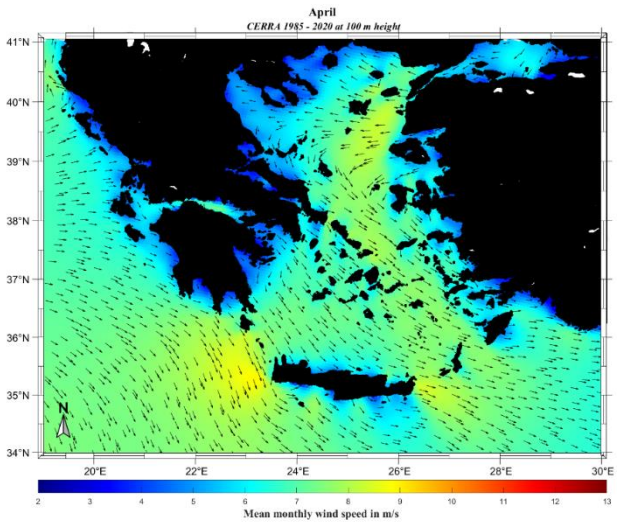

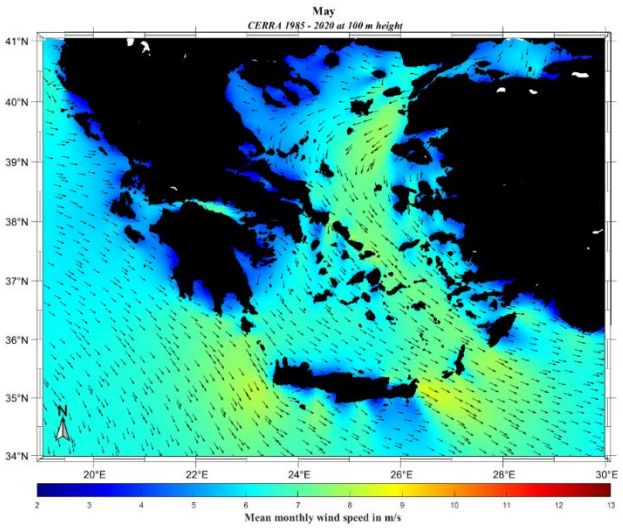

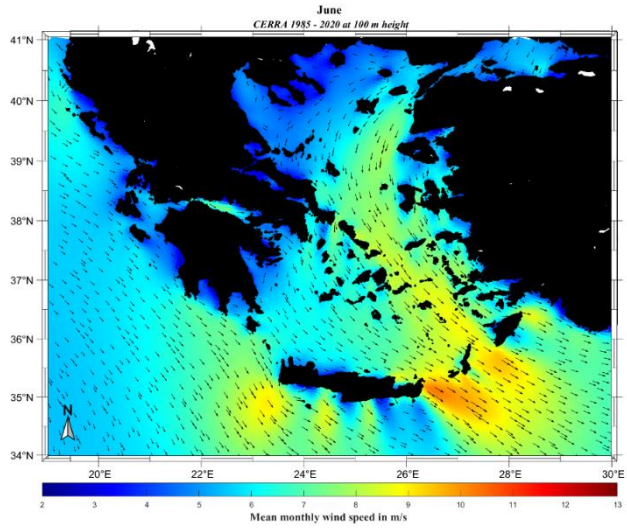

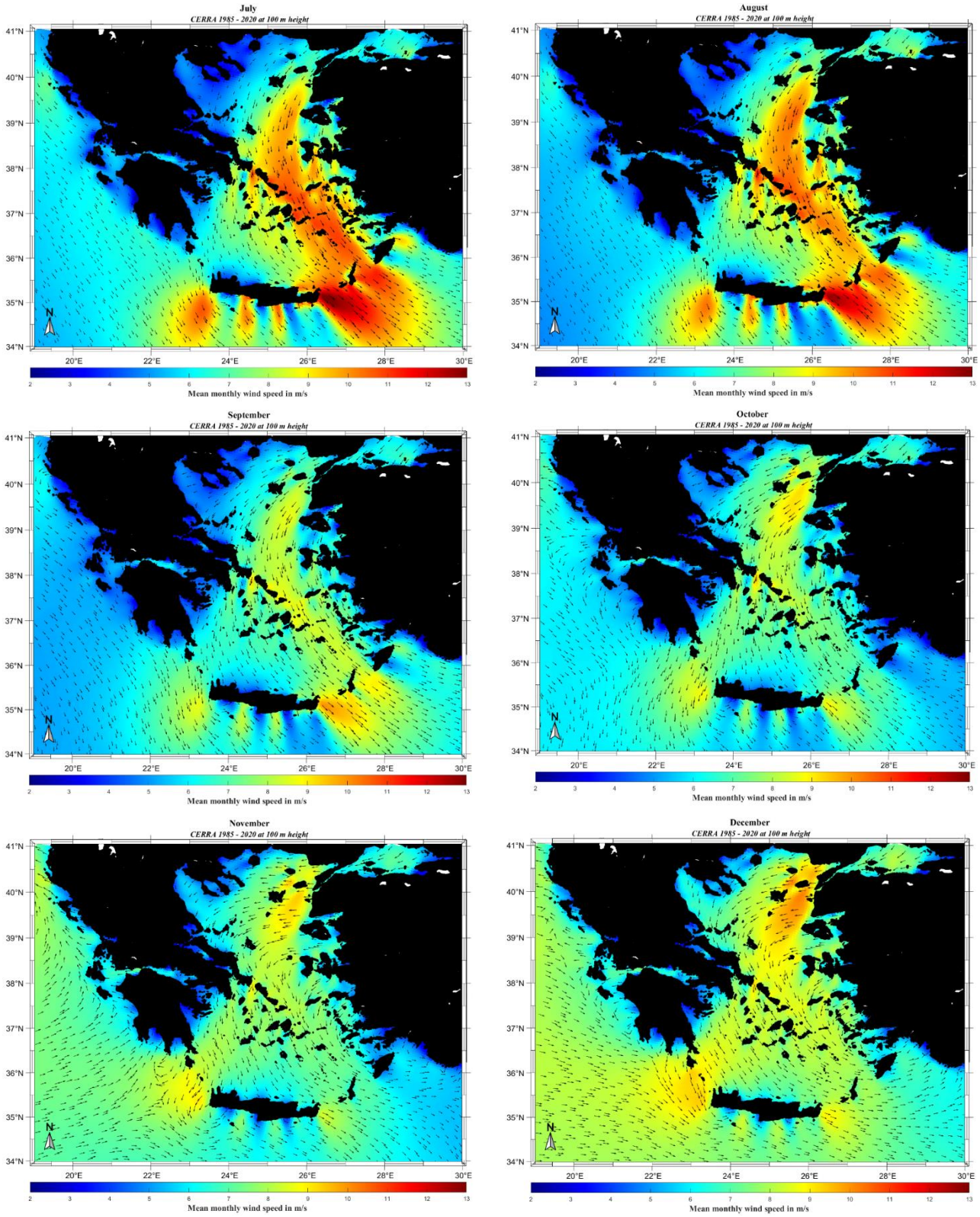

Figure 18. The spatial distribution of mean monthly wind speed and wind direction in the Greek seas.

In June, a significant increase in wind speeds was observed, compared to May throughout the entire "spinal column" of the Aegean, with the highest values, appeared east of Crete Isl., up to Kasos and south of Karpathos Islands. This increase aligned with the anticipated onset of the

Etesians during this month [76]. The overall windiest area was observed around the coordinate 35.11°N 26.59°E, with mean wind speed approximately at 10.27 m/s. Additionally, elevated wind speeds were also observed SW of Rhodes Isl.(~ 9 m/s) and in the central Aegean SE of Naxos, possible due to the absence of a high-pressure area over the Balkans, which localizes and confines the Etesians more to the south and east of the Cyclades, particularly around Naxos Isl. [88].

The Ionian Sea, exhibited lower wind values ranging from 5 to 7 m/s, accompanied by corresponding NW wind directions. More details for the statistical parameters of some chosen areas in the Greek Seas, are presented in Table 6.

Table 6. The statistical parameters of the areas with the highest and lowest values of mean monthly mean for June, in the Greek seas.

Sea Areas	**Coordinates** °	**WS** m/s	**Median** m/s	**Std** m/s	**WD** °
East coasts of Crete	35.11°N 26.59°E	10.15	9.84	1.70	317
South of Rhodes	35.70°N 27.75°E	9.46	9.57	1.30	320
Tillos	35.24° N 27.12° E	9.24	9.37	1.28	318
Halkidiki	40.25° N 24.36°E	3.08	3.09	0.41	59

Regarding wind direction during June in the Aegean Sea, as anticipated, conformed to the directional patterns of the Etesians, i.e., north to NE winds in the north Aegean, transitioning to NNW in the central Aegean and further into NW winds in the southeastern regions. In July, due to the Etesians, the wind speeds reached their peak values, compared to all of the rest months. A surge of increased in the mean wind speeds noticed throughout the entire Aegean and there were also observed higher values in the Ionian Sea, with the highest observed in the northern parts. The overall maximum values, reaching 13 m/s, were observed at the eastern coasts of Crete Isl. and the surrounding areas across Kasos and Karpathos islands, as well as, within the straits between the complex of Crete, Karpathos and Rhodes islands, respectively; where acceleration in flow emerging in these areas, attributed to the channeling of the flow between the three aforementioned islands.

The entire central and eastern Aegean experienced speeds exceeding 10 m/s, with notably high speeds NW of Gyaros and NE of Andros, Tinos, Mykonos islands, as well as in the eastern coasts of Naxos Isl., where wind speeds exceeded 11 m/s. In the northern Aegean, wind speeds from 9 to 11 m/s emerged, while regarding the Ionian, the lowest wind speed values were observed, ranging from 5 to 7 m/s, with the highest noted in the surrounding areas of Diapontian Islands.

Noteworthy was that in the southern coasts of Crete Isl. both significant high and low values of wind speed exhibited, showing the statistical variability between the coasts of the island. This phenomenon is attributed to the wind circulation between the valleys and the mountains of Crete; in which wind moving towards from the valleys to the open sea, attains extremely high values of speed; while weaker flow from south to north prevails in the areas where the high mountains of Crete Isl. are located, leading to the formation of three areas of small – scale anti – cyclonic vortices, i.e., circular patterns that rotate in opposite directions [75].

Similarly high wind speeds were observed in August, where the Aegean Sea once again surpassed the Ionian Sea (3 – 6 m/s), with corresponding NW directions. Wind speeds in the

Ionian Sea were notably lower both compared to the Aegean and with the wind speeds noted in the Ionian for the previous months.

Table 7. The statistical parameters of the areas with the highest and lowest values of mean monthly mean for July, in the Greek seas.

Sea Areas	Coordinates °	WS m/s	Median m/s	Std m/s	WD °
East coasts of Crete	35.12°N 26.53°E	13.18	13.30	1.48	326
South Rhodes	35.68°N 27.87 °E	11.23	11,23	0.91	318
South of Kasos	35.30°N 27.07°E	11.12	11.19	1.01	323
East Naxos	37.01°N 25. 76°E	11.04	11.26	1.32	293
Tinos	37.73°N 25.10°E	10.95	11.14	1.62	290
Halkidiki	40.25° N 24.36°E	3.10	3.13	0.28	208

Regarding the Aegean Sea, the highest wind speeds were once again observed east of Crete Isl., covering the entire marine area from Kasos to Karpathos and Rhodes islands (~ 11 m/s), with corresponded NW wind directions. The northern central Aegean was also one of the windiest regions, with the highest speeds appeared in the extended area between west coasts of Andros and the offshore areas west of Gyaros islands, as well as in the entire northeastern part of the Cyclades complex.

Higher values were also observed in the northern Aegean, with the overall highest located in the west areas of Lesvos Isl. and in the eastern parts of the Aegean, with the maximum wind speeds of this region, located south of Ikaria Isl. (~11 m/s), with corresponded NNW directions.

Table 8. The statistical parameters of the areas with the highest and lowest values of mean monthly mean for August, in the Greek seas.

Sea Areas	Coordinates °	WS m/s	Median m/s	Std m/s	WD °
E. coasts of Crete	35.12°N 26.53°E	12.74	13.10	1.24	319
Cavo D'Oro	37.82°N 24.62 °E	11.23	11,61	1.96	267
South of Kasos	35.22°N 26.99°E	11.12	11.47	0.91	320
SE Andros	37.73°N 25.10°E	10.95	11.53	1.54	289
E. Diapontian islands	39.92°N 19.08°E	3.67	3.56	0.46	7.96
Halkidiki	40.25° N 24.36°E	3.41	4.03	0.45	213

In September, a general decrease was observed compared to the previous two months with wind speeds in range from 5 to 10 m/s, while the overall highest were reaching 10 m/s on the eastern coasts of Crete Isl. An increase was noted in the northern Ionian compared to the summer months (JJA), while a decrease was observed in the northern parts of the central Aegean, where the speeds, which approached values close to 12 m/s in the previous two months, fell to 8 - 9 m/s. There was also a reduction in the Ionian Sea, characterized by winds around 5 m/s, while a decreased observed in the surrounding area of Diapontian Islands, where in August wind

speeds exceeded 7.5 m/s, while in September values decreased to 6 m/s, respectively. Regarding the wind direction, both in the Aegean and the Ionian, the usual patterns were observed.

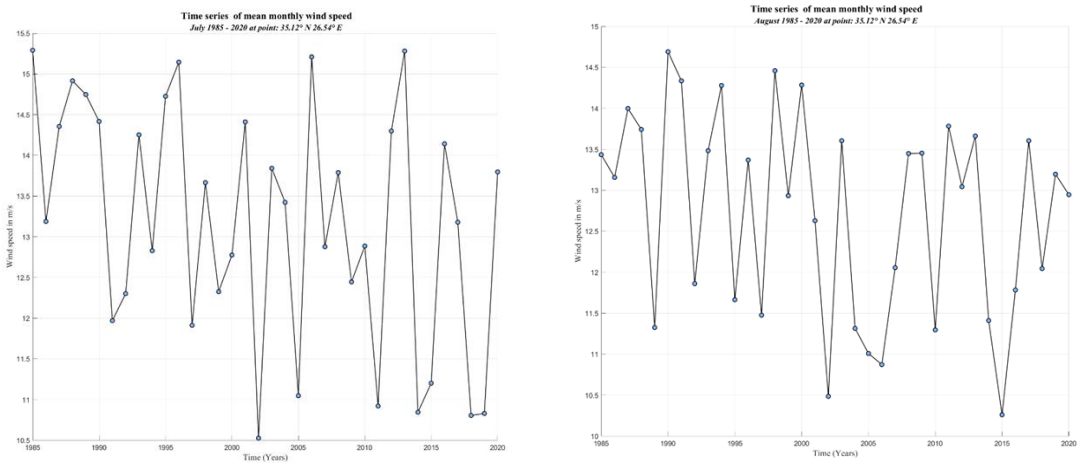

Figure 19. Timeseries for the location exhibit the maximum (east of Crete) value of mean monthly wind speed for July (left) and August (right), for the 36 -year period 1985 – 2020.

In October, a reduction in wind speeds was observed in the areas that presented the highest speeds for the previous months. The prevailing area was located in the strait of Cavo D'Oro including the surrounding area, with values approximately close to 9.5 m/s. Increased speeds were noted in the northern Aegean, with the highest values located east of Saint Efstratios Isl., covering the entire area up to Lesvos Isl., characterized by wind speeds exceeded 9 m/s, as well as, in the Gulf of Patras where wind speed values from 4 to 5 m/s have been observed for the prior months, while for October exceeded 6 m/s. Regarding to the Ionian Sea, higher wind speeds noted, compared to the previous two months, nevertheless, still lower than Aegean's. Generally, the entire northern, central, and southeastern Aegean was characterized mainly by speeds exceeding 8 m/s. The lowest speeds were once again observed near the coasts of Halkidiki.

Table 9. The statistical parameters of the areas with the highest and lowest values of mean monthly mean for October, in the Greek seas.

Sea Areas	**Coordinates** °	**WS** m/s	**Median** m/s	**Std** m/s	**WD** °
Cavo D'Oro	37.91°N 24.65°E	9.38	9.30	1.60	263
E. of Limnos	39.81°N 25.73 °E	9.18	9.37	1.16	226
E. of Saint.Efstratios	39.50°N 25.51°E	9.14	9.29	1.19	235
E. coasts of Crete	35.03°N 26.50°E	8.77	8.90	1.25	312

November, in general, presented an interesting pattern regarding wind direction, that was not observed in any of the previous months. The northern Aegean was characterized by east directions, the northern – central by NE, while the southern Aegean by NW. The most noteworthy aspect concerns the Ionian Sea, which typically experiences NW winds,

nevertheless, SW directions observed in the Ionian, which combined with the NW winds of the central Aegean, created over the southern Peloponnese up to western coasts of Crete Isl., formations similar to anti – cyclonic vortices.

Regarding wind speed, there was a general increase observed in November, mainly in the Ionian Sea, where compared with previous months wind speeds (6 – 8 m/s), higher values appeared, ranging from 8 to 9 m/s. The areas with the highest and lowest values of wind speed for this month are presented in Table 10.

Table 10. The statistical parameters of the areas with the highest and lowest values of mean monthly mean for November, in the Greek seas.

Sea Areas	**Coordinates** °	**WS** m/s	**Median** m/s	**Std** m/s	**WD** °
South Samothrace	40.23°N 25.60°E	9.46	9.53	1.39	177
E. coasts of Crete	35.03°N 26.50°E 35.12°N 23.53°E	8.97 8.99	9.03 8.82	1.16 1.14	236 241
Cavo D'Oro	37.96°N 24.66°E	8.82	8.46	1.52	243
Gulf of Itea	38.37°N 22.44°E	3.01	3.02	0.46	146

Table 11. The statistical parameters of the areas with the highest and lowest values of mean monthly mean for December, in the Greek seas.

Sea Areas	**Coordinates** °	**Wind speed** m/s	**Median** m/s	**Std** m/s	**Direction** °
East Limnos	39.90°N 25.76°E	10.18	10.02	1.32	188
South Samothraki	40.23°N 25.60°E	10.17	10.03	1.41	186
East of Saint Efstratios	39.38°N 25.34°E	9.65	9.33	1.20	200
West coasts of Crete	35.38°N 23.29°E	9.37	9.32	0.75	285
South Kythera	36.06°N 23.04°E	9.35	9.33	0.69	289
South coasts of Peloponnese	37.44°N 21.41°E	5.62	5.65	0.84	200
East Halkidiki	40.46°N 24.29°E	5.60	5.50	0.97	232

December emerged with increased wind speeds, with the higher increase located in the northern Aegean, where values exceeded 10 m/s. Once again, in the extended area between west coasts of Crete and south coasts of Peloponnese, high values emerged with corresponding NW and NNW directions. Similarly high wind speeds noted in the northern – central Aegean. Regarding wind direction, in the northern Aegean observed NE, shifted to NNE in the central Aegean and eventually NW in the southeastern part of Greece.

Regarding the Ionian Sea, wind speeds increased, compared to previous months, primarily from the east and northeast, ranging between 5 to 8.5 m/s. The highest values of wind speed were observed in the western maritime areas of the Ionian islands, and similar patterns, as mentioned

before for Peloponnese and Crete, were observed in the western coasts of Peloponnese and certain regions of the Ionian Sea, indicating the presence of anti – cyclonic circulations.

The spatial distribution of wind speed and direction in the Greek seas from January to December, showed significant variations between individual months. Specifically, the available wind speed resources followed a circular (seasonal) pattern which starts in December with relatively high values (exceeding 11m/s in a large part of the Aegean and around 8 m/s in the Ionian), while in February increased wind speed values were observed, both in the northern and central Aegean, as well as in the Ionian, with corresponding WNW wind directions. The pattern continues with a gradual decrease for March and April, reaching the lowest values in May. In May, the highest values were shifted from the north to the central Aegean, which was the month with the overall lowest wind speed values. Increased wind speeds observed again in June, with the overall highest in July and August, with corresponding wind directions north and NE in the northern part of the Aegean, NW in the southeastern and NW in the Ionian, respectively. The highest values of wind speeds, were distributed mainly in the southeastern and central Aegean, with the Ionian emerged the lowest, during the months of Etesians. An abruptly decrease noted in September, with a subsequent increase again in the northern Aegean in October and November, as well as in the Ionian, restarting the circular pattern in December.

4.1.3. Seasonal time scale

The spatial distribution of mean seasonal wind speed and direction in the Greek Seas, is presented in Figure 20, from winter to autumn. Regarding winter the entire Greek offshore areas, emerged with high values of wind speed, ranging from 7 to 10 m/s. Furthermore, winter presented the overall smoother spatial distribution, compared to the other seasons. The higher values were observed in the northern Aegean, exceeding 10 m/s, where the prevailing areas, were east of Lemnos Isl. and the surrounding areas up to Samothrace and down to Saint Efstratios islands, with corresponded east and NE winds; as well as, on both offshore areas near west and east coasts of Crete Isl., where wind exceeded 9 and 8 m/s, with corresponding NNW and west directions, respectively.

In the eastern - central Aegean wind speeds ranged between 8 to 9 m/s, while in the Gulf of Patras, exceeded 7 m/s. In general, winter could be characterized as the season with the smoother spatial distribution of wind speeds and circulation systems, since the only unexpected situation occurred in the northern Ionian Sea, where circular patterns that rotated in opposite directions were generated, in contrary with the otherwise northwest – directed Ionian circulation.

Regarding spring, a notable decrease was noted, as expected due to the monthly analysis, over the Greek Seas. The observed values did not exceed 9 m/s; the overall highest wind speed was observed near west coasts of Crete Isl. and the surrounding areas of the point 35.30°N 23.21°E, with corresponded wind speed close to 8.75 m/s and NNW wind direction (292°). Among the areas that the lower wind speeds have been observed, was the east offshore region of Diapontian Islands in the north Ionian Sea with values ~ 4.5 m/s and corresponding SSW wind direction (55 °), probably due to the anticyclone generated in the area, on the contrary to the west offshore side of these islands, where wind speeds exceeded 7 m/s, with corresponded WSW directions.

Summer, represented by the windiest months within a year, as estimated in the previous section. Therefore, emerged with the overall highest wind speed values regarding seasonal analysis, noted in the Aegean Sea; while in the Ionian decreased wind speeds observed, with an exception

in the areas near Diapontian Islands and west of Kerkyra Isl., where higher wind speeds were presented, compared to previous seasons, with corresponded NW directions.

The areas with the highest speeds were, west (with the overall higher exceeding 12 m/s at point 35.12°N 26.53°E with corresponding NW direction) and east offshore areas of Crete Isl., including the surrounding areas of Kasos, southeast of Karpathos and southwest of Rhodes, fulfilled the straits of this complex of islands with great wind speed resources.

In the northern central and eastern Aegean, values of wind speed exceeded 10 m /s, with the highest values observed in the strait of Cavo D'Oro and at the offshore areas of northern Cyclades; as well as, in Ikaria and east of Amorgos islands, respectively. Northern Aegean presented primarily north wind directions and lower values of wind speed, while in central and southeastern Aegean NNW and NNW directions were observed, respectively.

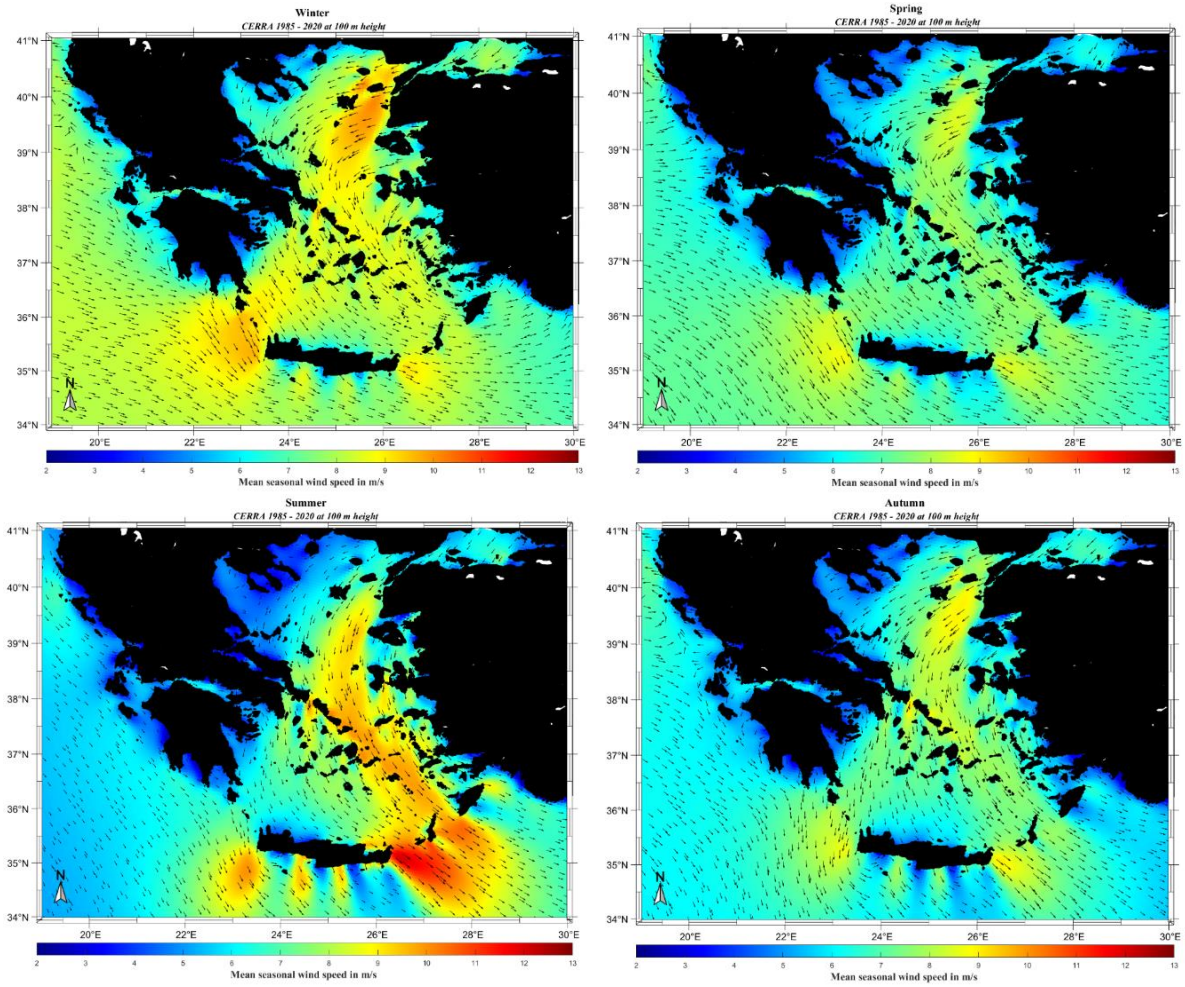

Figure 20. The spatial distribution of mean seasonal wind speed and wind direction in the Greek seas.

A decrease emerged in Autumn, which complete the seasonal circle behavior of wind speeds observed in the Greeks seas. East and west coasts of Crete Isl. and specific regions of the central (overall highest in the strait of Cavo D'Oro, 37.91°N 24.65°E ~9 m/s with corresponding direction 256°) and northern Aegean (east of Saint Efstratios Isl.) were the windiest areas observed for this season, with values lower than 9 m/s. Both in the north Aegean and the Ionian

seas, wind speed started to increase when the values observed on the rest regions started to decrease. The lowest values were located in the offshore area east of Rhodes and near shores of Halkidiki.

4.2. Wind speed linear trends

4.2.1. Annual Scale

In this section the wind speed trends regarding the annual scale are presented, where the obtained results describe whether the statistical characteristics of wind speed tend to increase (positive values of the slope), decrease (negative values of the slope), or remain almost constant (slope values close to zero), in the corresponded exanimate time scale.

In respect of the above, the spatial distribution of the linear slope of the annual mean wind speeds $m_{u,Y}(j), j = 1,..,J$ is presented for the period 1985 – 2020 in Figure 21.

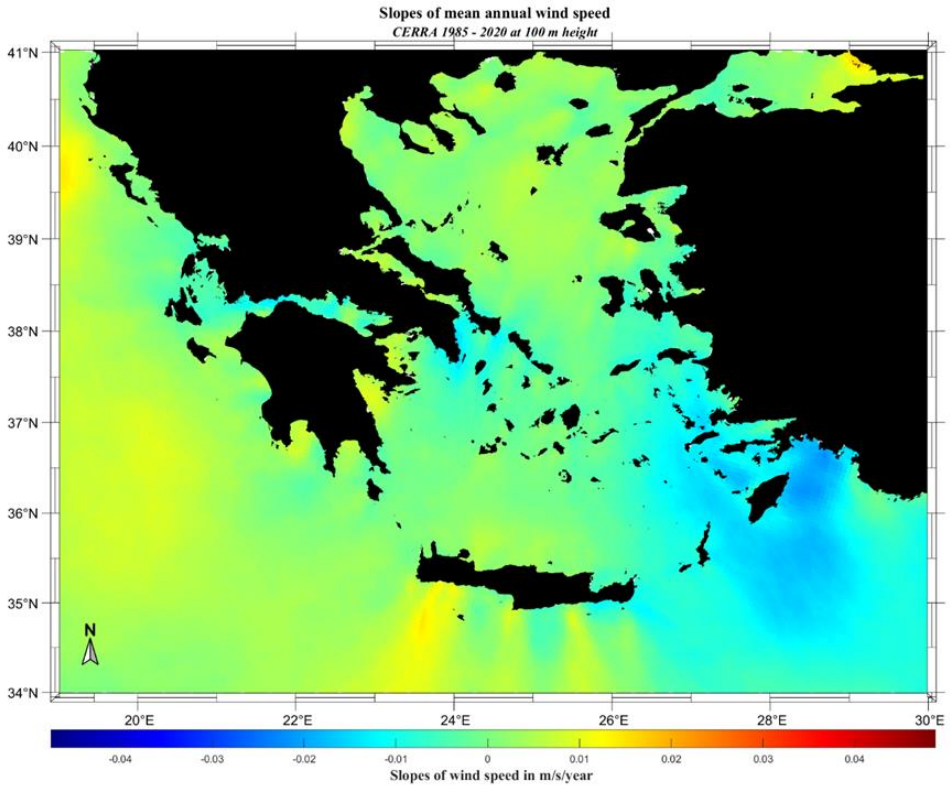

Figure 21. The spatial distribution of the linear slope of mean annual wind speed in the Greek seas.

The largest positive value of slope, i.e., positive trend, observed in the Ionian Sea, at point 39.76°N 19.07°E, with value 0.0147 m/s/year, located in the offshore areas NW of Diapontian Islands. In general, the highest values for the exanimated scale, were noticed in the Ionian Sea, with the highest positive slopes in the northern parts, while in the southern Ionian slopes were ~ 0.0093 m/s/year. The second spot with the highest positive slopes was observed in the

offshore areas south of Crete Isl., specifically south of Gaydos Isl. (0.0142 m/s/year), as well as in the south coasts of Crete Isl.

In the northern Aegean in general, positive slopes were observed, with the highest located in the northern offshore areas of Saint Efstratios Isl., with values ~ 0.068 m/s/year around the point 39.71°N 24.92°E and the surrounding sea areas. Negative slopes were presented both SE of Rhodes Isl., covering the straits between Kasos and Karpathos islands, with the overall negative slope located in the offshore areas around the spot 36.26°N 28.38°E (-0.021 m/s/year); as well as, in the northern offshore areas of the island covering the entire area between the complex of Tilos, Symi, Rhodes islands, with the highest negative slope located at the point 36.37°N 27.67°E (-0.018 m/s/year).

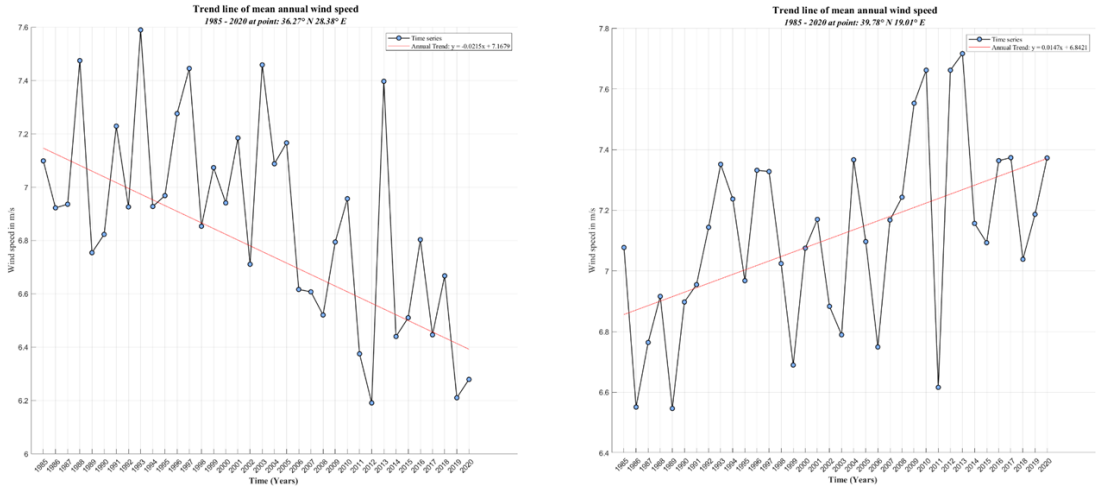

Figure 22. Trend lines for the locations emerged the maximum negative (left) and the maximum positive (right) slope for wind speed for the annual scale (1985 – 2020).

In general, significant negative values were observed in areas where the highest wind speed values were recorded in the previous sections, such as offshore areas near east coasts of Crete Isl. (-0.01m/s/year), west of Andros Isl. up to the strait of Cavo D'Oro, ranging from -0.008 to -0.01 m/s/year. Positive slopes observed mostly in the Ionian Sea and in northern offshore areas of the Aegean, while in the eastern -central and southeast parts, decreased tendencies of wind speed were observed; with an exception in the south part of the central Aegean, northern of Crete Isl. and in the straits between the islands located south of the surrounding area.

The results observed in Figure 21, indicated an overall increase tendency in the Ionian Sea, northern areas of Aegean and north of Crete Isl.; while a long – term decrease noted in the central, eastern and southeast parts of the Aegean. Previous studies results, using datasets with different spatial and temporal resolutions, were similar with the ones discussed; indicating the decrease in the central Aegean and the positive values in the Ionian [38], while Soukissian, T. and M.-A. Sotiriou [37], observed the overall highest slope in the SW coasts of Crete and the highest negative slope in Rhodes Isl.; either way the results of this study include both.

In Figure 22, the spatial distribution of the linear slope of 95th and 99th annual percentiles of wind speed in the Greek seas are presented, indicated similar results compared with the mean annual wind speeds slopes; nevertheless, the slopes for the extreme wind speed values were clearly greater.

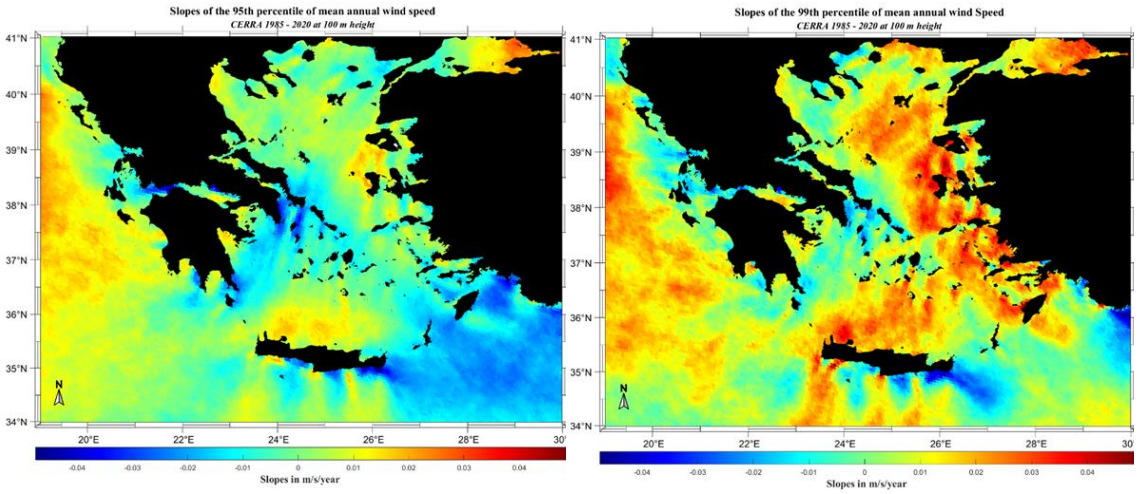

Figure 23. The spatial distribution of the linear slope of 95th (left figure) and 99th (right figure) annual percentiles of wind speed in the Greek seas.

Regarding the 95th annual percentiles of wind speed, both negative and positive higher values emerged; The highest slopes observed in the entire range of the Ionian Sea, with the overall maximum positive slope located in the offshore areas NW of Diapontian Islands, at point 40.01°N 19.05°E (0.0267 m/s/year); in the sea areas near south coasts of Crete Isl.(35.17°N 23.96°E, 0.020) and in the eastern Aegean between Psara and Chios islands; while the maximum negative slope observed in the offshore areas near SE coasts of Crete Isl., around 34.99°N 26.19°E (-0.045m/s/year) and in Gulf of Patras (38.31°N 21.55°E, - 0.037m/s/year).

Significant negative slopes also observed in the offshore areas of Kasos, Karpathos and SW Rhodes, as well as in the central Aegean with the maximum negative slope presented in the NE parts of Kea Isl. (- 0.034 m/s/year) and the extended area between Kea and Serifos (~ 0.027 m/s/year) islands, while negative values observed in the northern parts of Cyclades (~0.01 m/s/year).

On the other hand, the areas where the 99th annual percentiles slopes presented higher positive values were the SE coasts of Crete Isl., with the overall maximum value located at point 35.14°N 23.83°E (0.0488 m/s/year); the entire area of the Ionian Sea, ranging from 0.016 to 0.035 m/s/year; as well as in the northern and eastern part of the Aegean; with the areas where the 99th percentile of annual wind speeds tend to increase at the fastest rates, were the extended area between Lemnos, Chios and Psara islands (0.015 - 0.045m/s/year), the straits between the southeast islands of the Aegean (~ 0.029) and the northern part of Crete Isl. (0.035 m/s/year), indicated that the higher extreme wind speeds tend to increase, over time.

4.2.2. Monthly scale

The spatial distribution of the linear slope of the monthly mean wind speed $m_{u,M=m}(j), j = 1,..,J$, for January to December is presented in Figure 24. In January, a general increased tendency noted over the Greek seas, with the values of slopes ranging from - 0.036 to 0.0574 m/s/January, with the overall maximum positive value was located in the eastern Aegean near Turkish coasts, while the overall highest negative slope appeared in the Gulf of Patras (38.29°N 21.67°E, -0.0357m/s/January).

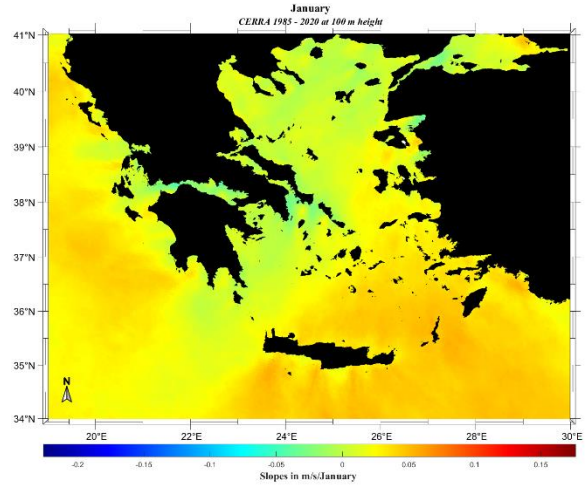
January
CERRA 1985 - 2020 at 100 m height
41°N
40°N
39°N
38°N
37°N
36°N
35°N
34°N
20°E
22°E
24°E
26°E
28°E
30°E
N
-0.2
-0.15
-0.1
-0.05
0
0.05
0.1
0.15
Slopes in m/s/January

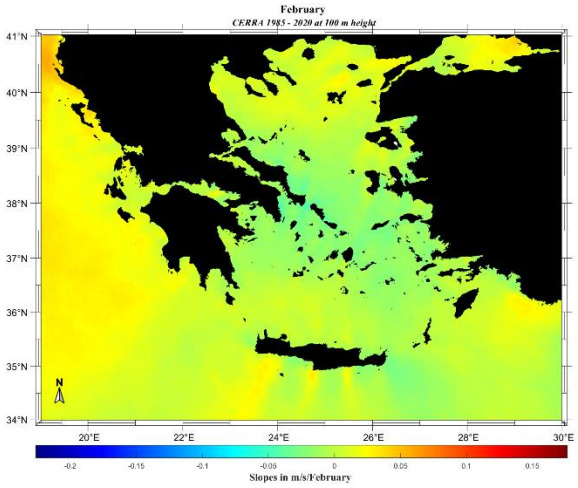
February
CERRA 1985 - 2020 at 100 m height
41°N
40°N
39°N
38°N
37°N
36°N
35°N
34°N
20°E
22°E
24°E
26°E
28°E
30°E
N
-0.2
-0.15
-0.1
-0.05
0
0.05
0.1
0.15
Slopes in m/s/February

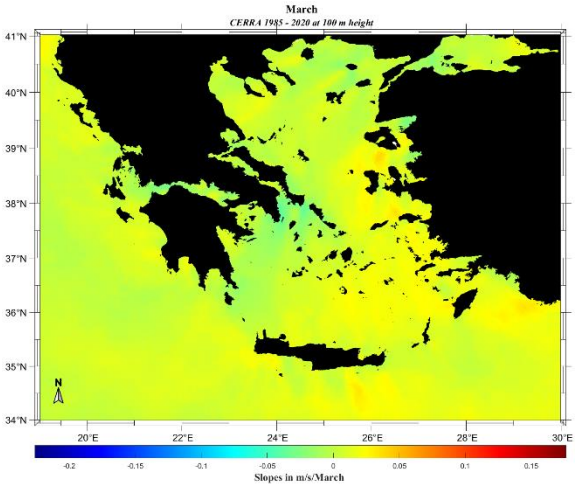
March
CERRA 1985 - 2020 at 100 m height
41°N
40°N
39°N
38°N
37°N
36°N
35°N
34°N
20°E
22°E
24°E
26°E
28°E
30°E
N
-0.2
-0.15
-0.1
-0.05
0
0.05
0.1
0.15
Slopes in m/s/March

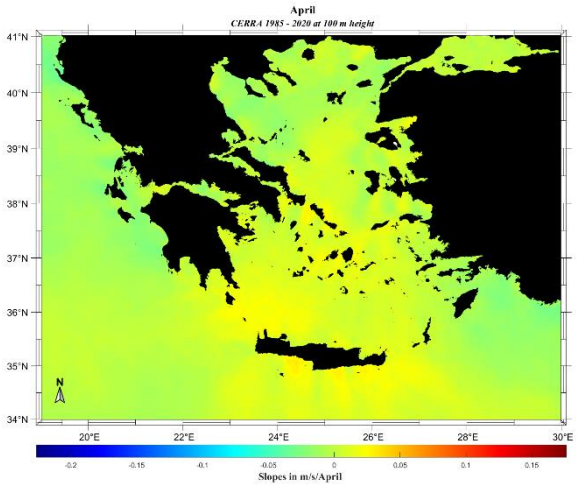
April
CERRA 1985 - 2020 at 100 m height
41°N
40°N
39°N
38°N
37°N
36°N
35°N
34°N
20°E
22°E
24°E
26°E
28°E
30°E
N
-0.2
-0.15
-0.1
-0.05
0
0.05
0.1
0.15
Slopes in m/s/April

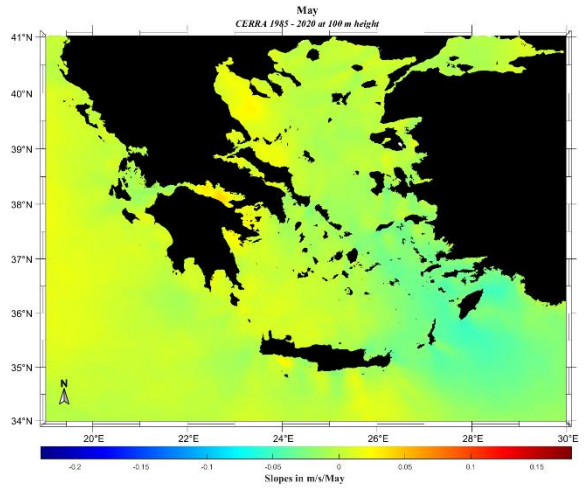
May
CERRA 1985 - 2020 at 100 m height
41°N
40°N
39°N
38°N
37°N
36°N
35°N
34°N
20°E
22°E
24°E
26°E
28°E
30°E
N
-0.2
-0.15
-0.1
-0.05
0
0.05
0.1
0.15
Slopes in m/s/May

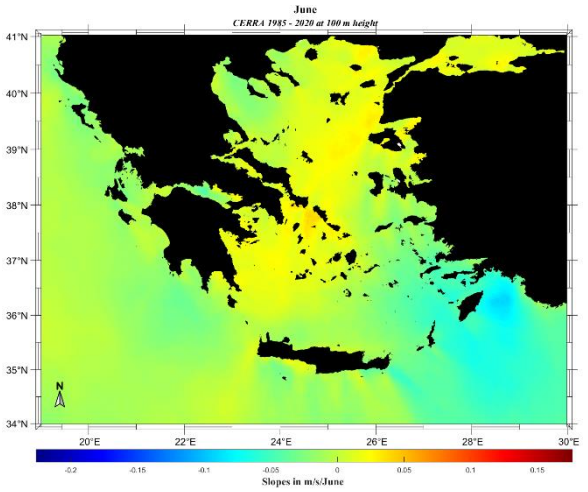
June
CERRA 1985 - 2020 at 100 m height
41°N
40°N
39°N
38°N
37°N
36°N
35°N
34°N
20°E
22°E
24°E
26°E
28°E
30°E
N
-0.2
-0.15
-0.1
-0.05
0
0.05
0.1
0.15
Slopes in m/s/June

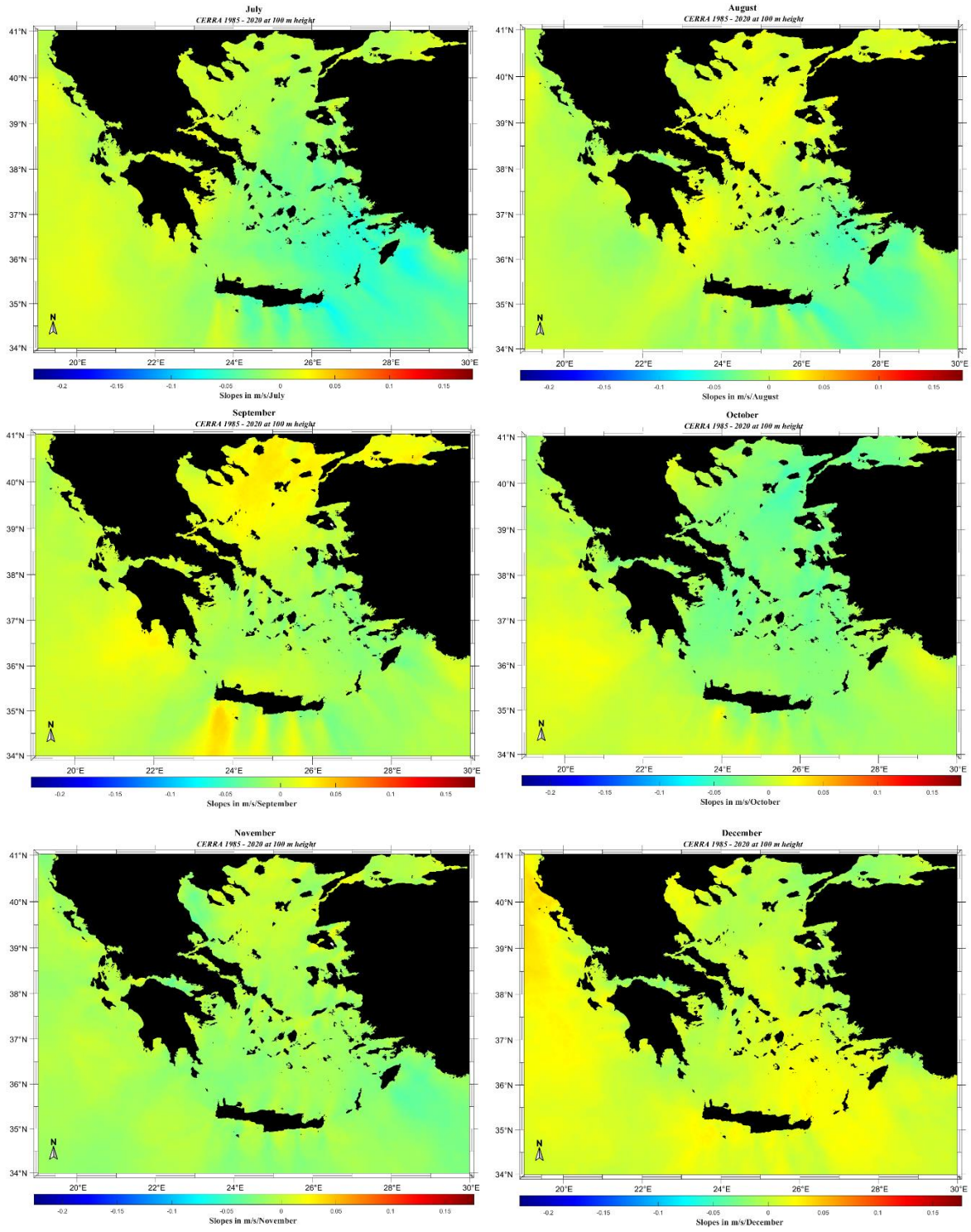

Figure 24. The spatial distribution of the linear slope of mean monthly wind speed in the Greek seas.

The areas with the highest positive values of monthly slopes for January, were the south parts of Crete Isl., near west offshore area of Gaydos Isl. around the point 34.92°N 23.71°, with slopes that exceeded 0.05 m/s/January; as well as the Ionian Sea, with the highest slopes located in the north and south areas with values ranging from 0.028 – 0.045 m/s/January.

In the extended area between Karpathos and Rhodes islands, high positive slopes that exceeded 0.055 m/s/January were observed, as well as in the northern offshore areas of Crete Isl., where low wind speeds have been noticed (~ 0.044 m/s/January). The areas showed tendency for decrease were, the central Aegean, with the maximum negative slopes located north of Gyaros Isl. covering the entire area up to the strait of Cavo D'Oro (~ -0.020 – 0.035 m/s/January); the Gulf of Patras, where the overall maximum negative slope observed around the point 38.28°N 21.73°E (- 0.034m/s/January), as well as in the northern Aegean, between Samothrace and Lemnos islands, where negative tendency spotted with values close to -0.001 m/s/January.

In February, decreased positive values, compared to January, were spotted all over the Ionian Sea, ranging from 0.028 – 0.057 m/s/February, with the highest values located in the northern parts of the Ionian, while in the Aegean positive slopes observed in specific areas south and in the offshore areas near north coasts of Crete Isl., with the higher located in the extended area between southwest coasts of Crete and Gaydos (0.0057 – 0.028 m/s/February); as well as in the east areas of Rhodes Isl. and in the northern Aegean between Samothrace and Lemnos islands.

Negative slopes for February noted in the entire region of central Aegean and eastern central Aegean, where the highest negative values appeared in the strait of Cavo D'Oro, around the point 37.97°N 24.60°E with slope -0.042 m/s/February; as well as in the north coasts of Tinos Isl. (37.69°N 25.03°E, -0.039 m/s/February), covering the entire area close to north coasts of this complex of islands and in the eastern Aegean, with values -0.027 in the offshore areas NE of Ikaria Isl.

In March greater uniformity was observed compared to the previous months, concerning the spatial distribution of slopes, in both of the Aegean and the Ionian Seas. In general, positive values of slopes appeared in the entire range of the Aegean, lower compared to February's and January's, with the overall maximum positive slope located in the NE Aegean, south of Lesvos Isl., in the surrounding areas of the point 38.82°N 26.20°E (0.039 m/s/March) and north of Samos Isl. (37.85°N 26.53°E, 0.036 m/s/March). In the offshore areas east of Rhodes Isl., near the Turkish coasts, positive slopes close to 0.033 m/s/March were appeared, while in the northern areas of Crete Isl., values of the same order were noticed.

Moreover, a decrease was noticed in the central and south Ionian, where the highest positive slopes were observed in the previous months. The areas where the monthly wind speeds tend to decrease on March at the fastest rates, were the east coasts of Athens (37.86°N 24.07°E, -0.036), the areas covering the strait of Cavo D'oro down to west coasts of Andros Isl. (37.92°N 24.59°E, -0.036), the southwest areas of Kea Isl. around the spot 37.51°N 24.10°E, with slopes -0.024 and the areas near southeast coasts of Andros Isl. with values of 0.019 around the point 37.74°N 25.04°E.

Regarding April, the opposite spatial pattern was observed, compared to March. For example, in March in the south coasts of Crete Isl. were noticed with negative slopes in the spots that in April the higher positive slopes were observed (35.09°N 24.41°E, 0.0327), and in reverse. Furthermore, in the areas over the central Aegean in Cavo D'Oro, in March high negative slopes were emerged, while in April increasing tendency was appeared (37.91°N 24.65°E, 0.029 m/s/April).

In the Ionian Sea, positive slopes were appeared until this month, while in April, slightly negative values, ranging from – 0.013 to -0.022, were observed; also, in the extended area between Lesvos and Chios islands, where the maximum positive slopes were observed in March, emerged with negative values (-0.013 m/s/April).

As for May, the highest positive slopes appeared in the east offshore areas of Thessalian and in the Gulf of Korinthos, with the overall maximum values spotted around points 38.14°N 22.70°E (0.044 m/s/May) and 39.78°N 23.32°E (ranging from 0.028 m/s/May), respectively.

Furthermore, increasing tendency was observed in the areas close to south coasts of Crete Isl. (35.16°N 24.01°E (0.028 m/s/May), as well as in the Ionian Sea, with positive slopes around 0.013 m/s/May. In general, the areas where decreasing tendency was appeared, were the central (-0.021 m/s/May) and eastern parts of the Aegean, with the highest negative values observed in the surrounding area of SW Rhodes Isl. (35.81°N 27.91°E (-0.052 m/s/May), expended up to east side of Karpathos Isl., as well as the straits between the islands north of Rhodes, with values ranging from -0.027 to -0.038 m/s/May.

In June, the wind speeds tended to increase over the northern and central Aegean (0.0081 – 0.45 m/s/June), following the circulation patterns of the Etesians and in agreement with [79]; nevertheless, the values of positive slopes indicate a decrease in compare with the values observed in previous months. In the Ionian Sea observed either negative slopes or values close to zero, indicated constant conditions.

The area in which the higher increasing tendency values appeared, were, the north area of Gyaros Isl., around the point 37.82°N 24.62°E (0.041 m/s/June), as well as the west areas near coasts of Andros Isl., with slopes exceeding 0.040 m/s/June at the point 37.75°N 24.73°E. In the east Aegean, the northern offshore areas of Lesvos Isl. indicated strong tendency for increase (39.43°N 27.87°E (0.031 m/s/June), while in the southeastern part of the Aegean, negative slopes appeared, with the highest located in the eastern offshore areas of Rhodes Isl. (36.32°N 28.77°E (-0.093 m/s/June) and in the southeast seas close to the coast of Crete Isl. (~ - 0.046 m/s/June).

Lower both negative and positive slopes were observed for July in the Greek seas, with the Aegean emerged a general for decrease, while the Ionian showed lower increasing slopes in the entire area (0.008 – 0.015 m/s/July). The overall maximum positive slope observed in the area south of the northern tip of Evvoia, (38.17°N 23.16°E (0.023 m/s/July), as well as in the southwest areas near coasts of Crete Isl. (~ 0.011 m/s/July) and in the east and south coasts of Peloponnese (~0.015 m/s/July).

Negative values appeared in the entire central, east and southeast Aegean, where the overall maximum negative slope was located in the sea areas near east coasts of Crete Isl. (34.99°N 26.43°E (-0.0769 m/s/July), covering the extended south offshore area; in lower range negative slopes were observed in the straits between Kasos and Karpathos islands, as well as in the east and northern areas of Rhodes Isl., covering the extended offshore area and the straits between the complex of SE Aegean's islands, respectively.

Regarding August, positive slopes were observed in the entire north and central Aegean, while negative slopes maintained in the southeast Aegean, with the overall maximum negative, near the southeast coasts of Crete Isl. and the surrounding offshore areas (34.99°N 26.43°E (-0.057 m/s/August). The areas that also showed decreasing tendency, were the eastern and northern parts of Rhodes Isl., including the eastern offshore areas (-0.040 m/s/August) and the straits between the SE islands of the Aegean (-0.047 m/s/August), respectively.

In the Ionian Sea, slightly lower positive slopes were observed, compared to July, with the highest located in the offshore areas west of Diapontian Islands (0.015 m/s/August), while the overall maximum positive slope appeared in the northeast Aegean, covering the offshore areas NW of Lesvos Isl.

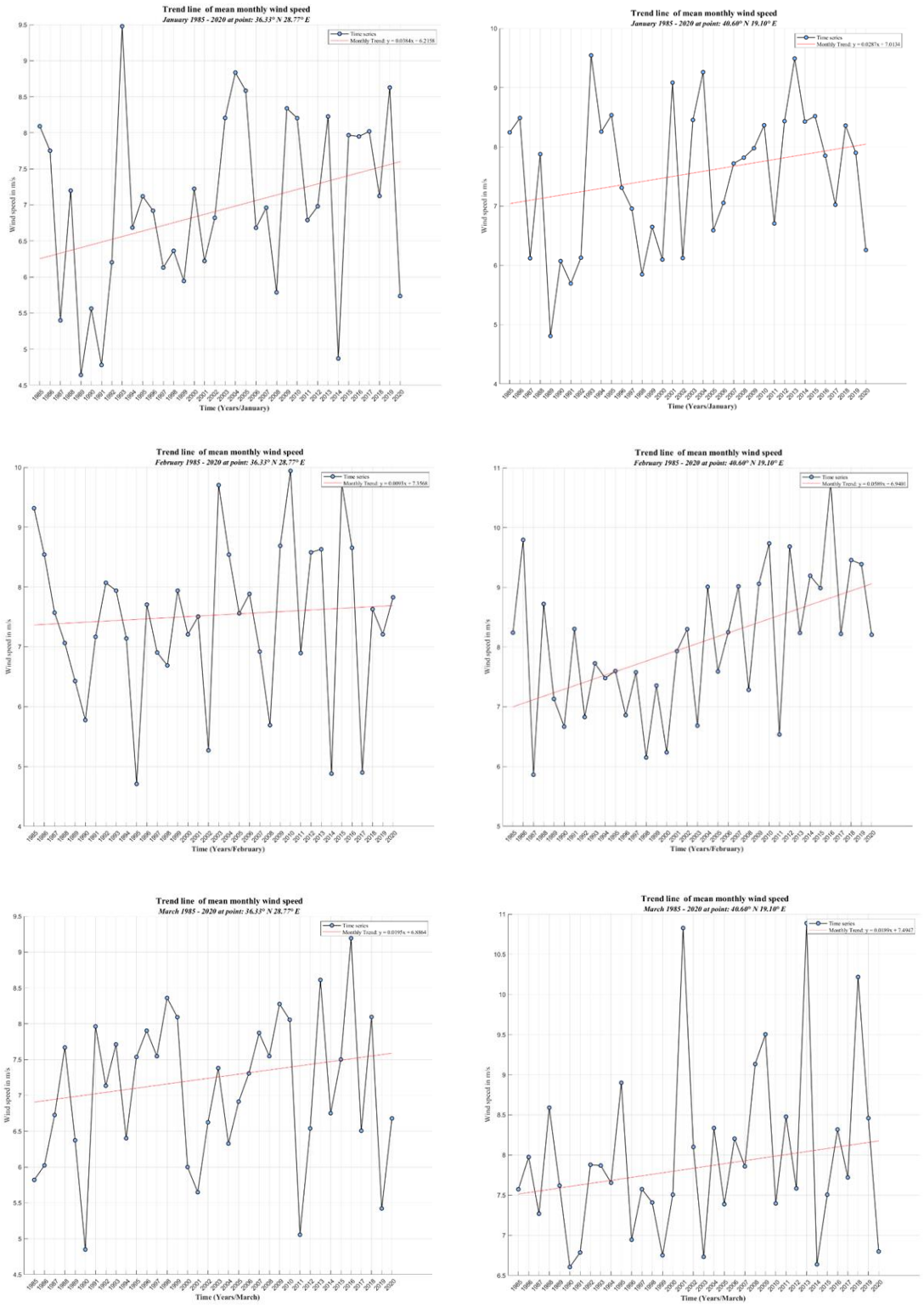

Figure 25. Trend lines for the locations exhibited the maximum negative (36.33°N 28.77°E, left) and the maximum positive (40.60°N 19.10°E, right) slope for mean monthly wind speed from January to March for the 36 – year period (1985 – 2020).

The spatial distribution of linear slopes of the monthly mean wind speeds for September, emerged with higher values, compared to the previous months. The areas with the highest

positive slopes were observed, in the extended area between near SW coasts of Crete Isl. and SW offshore areas of Gaydos Isl. (34.73°N 23.66°E (0.0421 m/s/September)), as well as in the west and south west areas near coasts of Peloponnese (0.028 m/s/September), in the south Ionian (0.011 m/s/September) and the entire offshore areas of the northern Aegean, ranging from 0.019 to 0.035 m/s/September.

In the central Aegean negative slopes appeared, with the overall maximum negative slope located east of Rhodes Isl. (36.11°N 28.38°E (-0.00313 m/s/September)); while the negative values were observed in the eastern Aegean, lower compared to August, with some areas emerging slopes close to zero, indicated constant behavior; such as, south of Rhodes Isl. and the extended area between Kasos and Karpathos islands, as well as the surrounding areas of Ikaria Isl., northern of Chios Isl. and in the eastern – central Aegean.

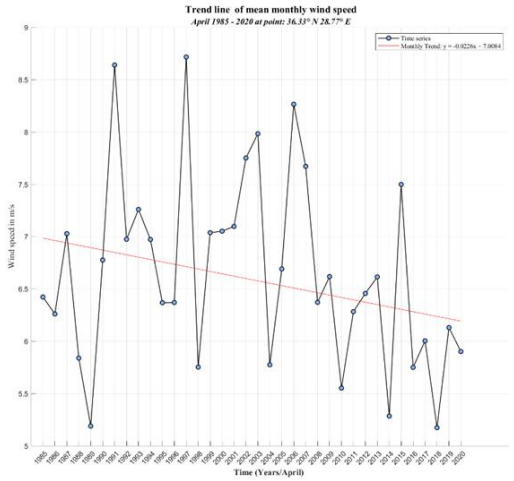

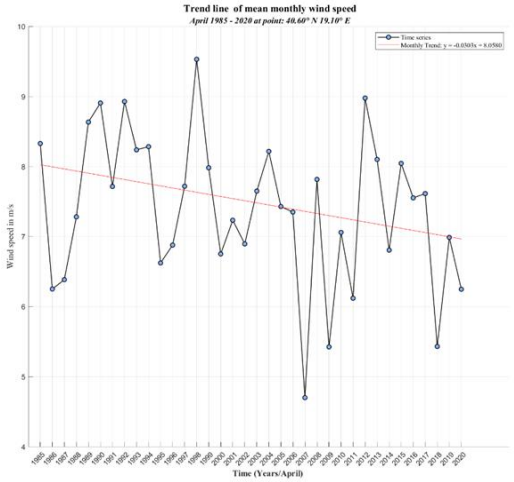

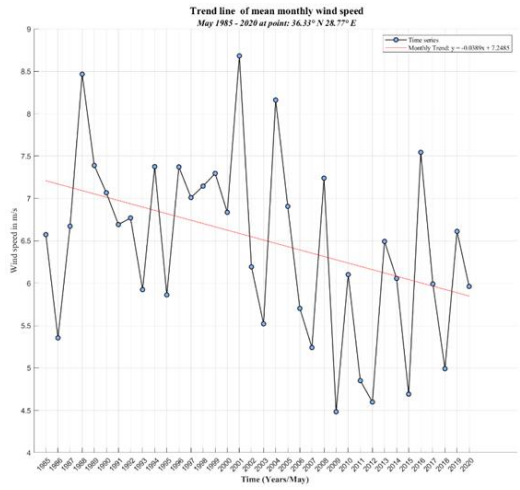

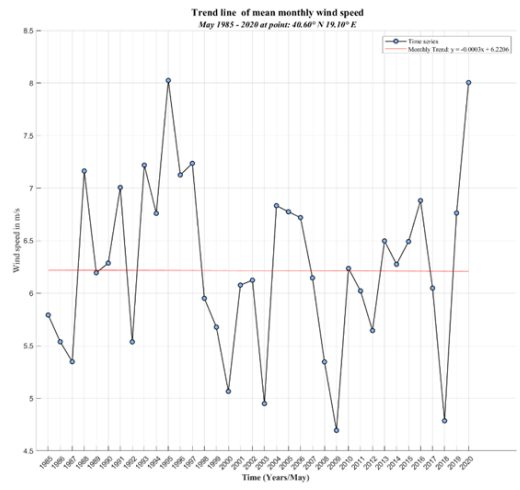

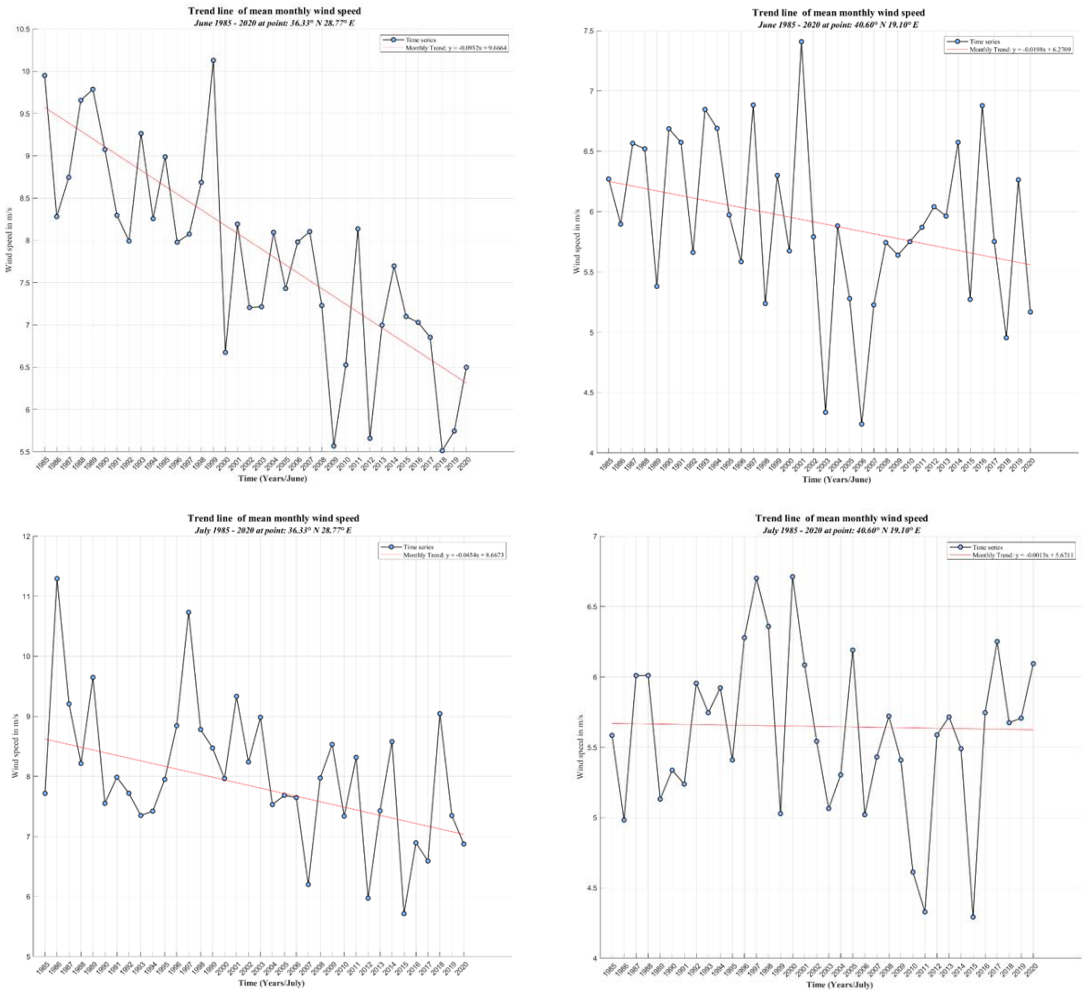

Figure 26. Trend lines for the locations exhibited the maximum negative (36.33°N 28.77°E, left) and the maximum positive (40.60°N 19.10°E, right) slope for the mean monthly wind speed from April to July for the 36 – year period (1985 – 2020).

Lower range slopes, appeared for October in the entire area of the Greek Seas, with the highest positive value located in the south Ionian (36.08°N 20.98°E (0.024 m/s/October)), while the overall maximum negative values observed east of Lemnos Isl., near the Turkish coasts covering the surrounding offshore areas (39.93°N 25.90°E (-0.050 m/s/October)). Moreover, positive slopes were located in the east offshore areas of Rhodes Isl., near the Turkish coasts and Kastelorizo Isl., as well as in the offshore areas south of Crete Isl.; while, negative slopes were observed in the entire Aegean and north Ionian.

Regarding November, negative slopes were observed with values ranging from negative slopes close to zero, (north of Gyaros Isl., -0.002), to higher negative slopes, located in SE Rhodes Isl. (35.74°N 28.26°E (-0.040 m/s/November)). In general, higher positive slopes were appeared in limited areas of the eastern Aegean, with the highest observed in areas south of Lesvos Isl. (39.05°N 26.07°E (0.019 m/s/November)).

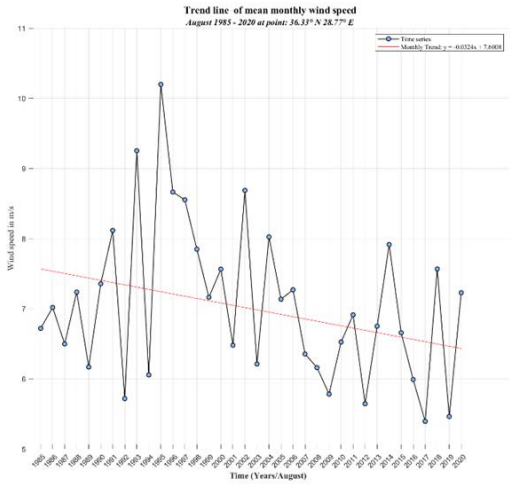
Trend line of mean monthly wind speed
August 1985 - 2020 at point: 36.33° N 28.77° E
Time series
Monthly Trend: y = -0.0324x + 7.6608
Wind speed in m/s
Time (Years/August)

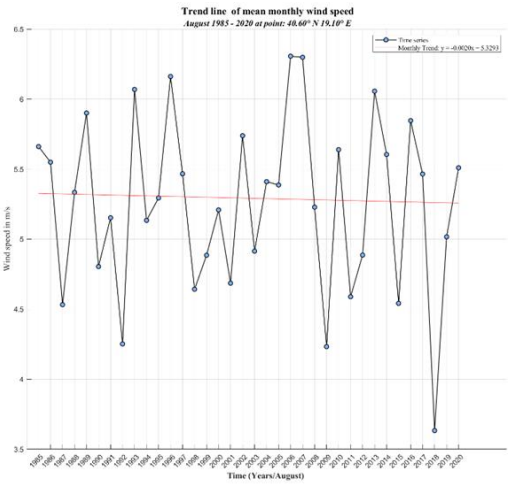
Trend line of mean monthly wind speed
August 1985 - 2020 at point: 40.60° N 19.10° E
Time series
Monthly Trend: y = -0.0020x + 5.3293
Wind speed in m/s
Time (Years/August)

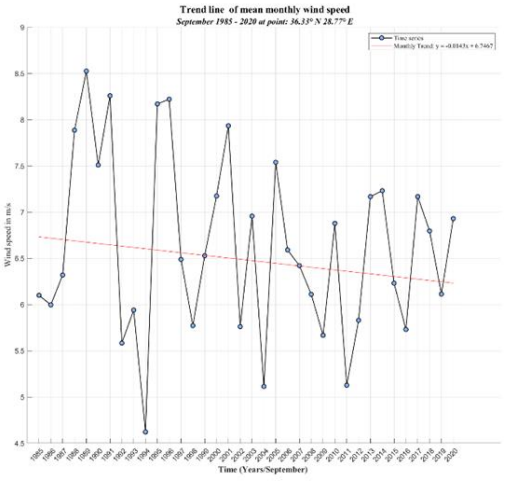
Trend line of mean monthly wind speed
September 1985 - 2020 at point: 36.33° N 28.77° E
Time series
Monthly Trend: y = -0.0843x + 6.7467
Wind speed in m/s
Time (Years/September)

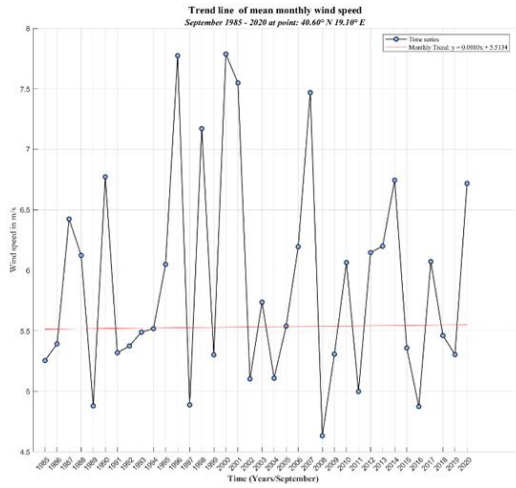
Trend line of mean monthly wind speed
September 1985 - 2020 at point: 40.60° N 19.10° E
Time series
Monthly Trend: y = 0.0080x + 5.5134
Wind speed in m/s
Time (Years/September)

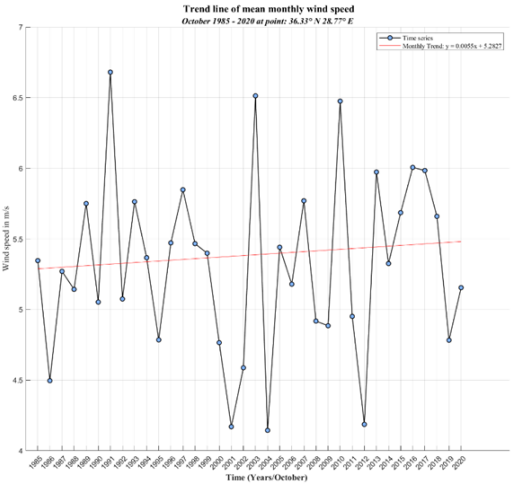
Trend line of mean monthly wind speed
October 1985 - 2020 at point: 36.33° N 28.77° E
Time series
Monthly Trend: y = 0.0055x + 5.2927
Wind speed in m/s
Time (Years/October)

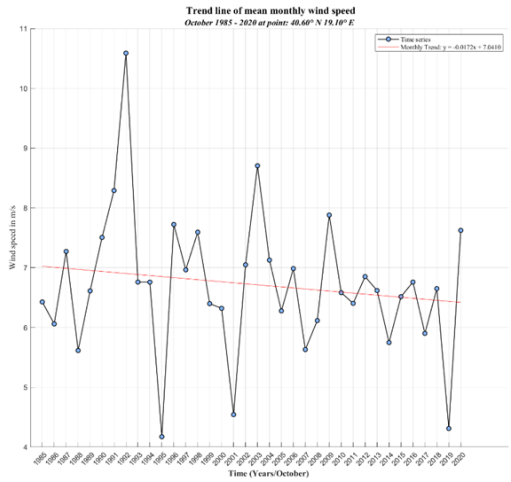
Trend line of mean monthly wind speed
October 1985 - 2020 at point: 40.60° N 19.10° E
Time series
Monthly Trend: y = -0.0172x + 7.0410
Wind speed in m/s
Time (Years/October)

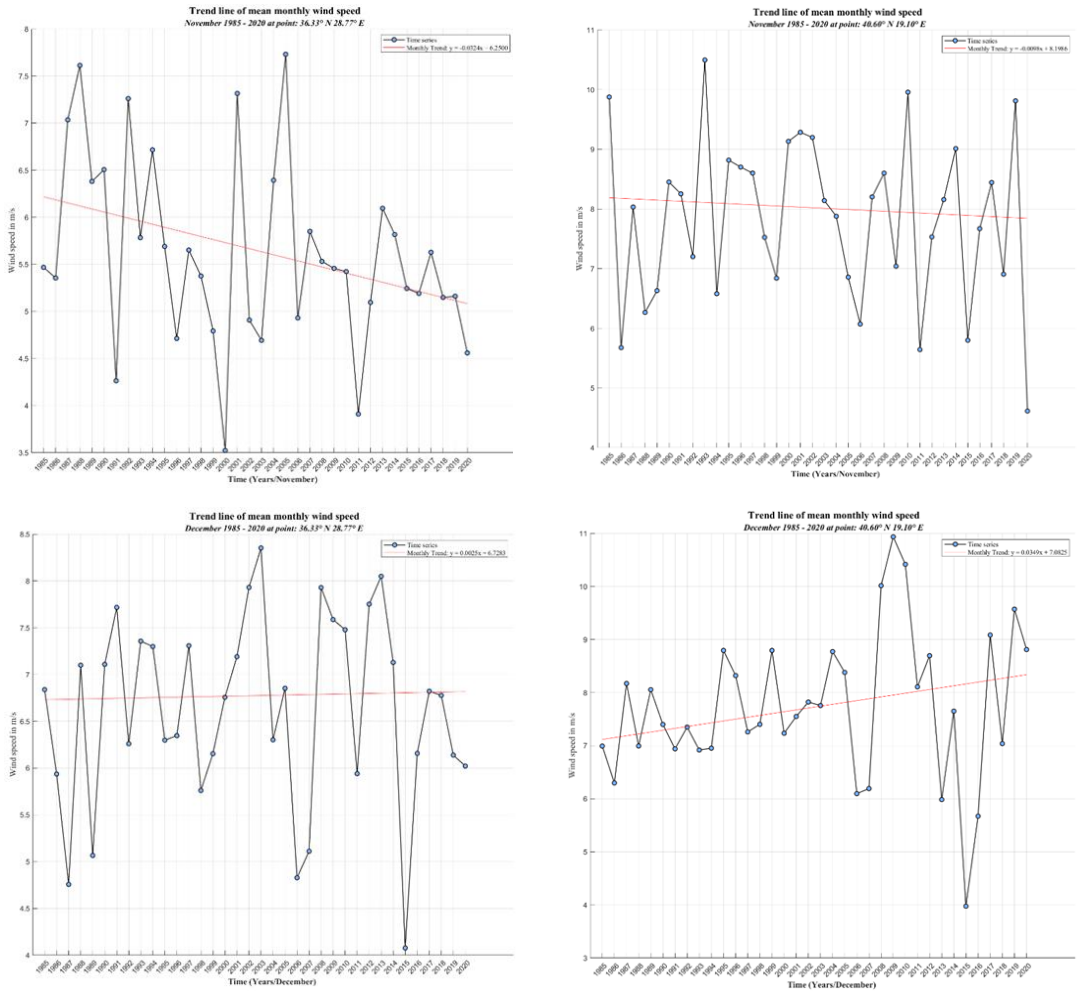

Figure 27. Trend lines for the locations exhibited the maximum negative (36.33°N 28.77°E, left) and the maximum positive (40.60°N 19.10°E, right) slope for mean monthly wind speed from August to December for the 36 -year period (1985 – 2020).

Regarding the spatial distribution in December, the highest positive slope was noticed in the Ionian (39.43°N 19.00°E (0.0427 m/s/December)), while Gulf of Korinthos showed the highest decreasing tendency (38.26°N 22.54°E (-0.0275 m/s/December)). Slopes close to zero were observed in the northern Aegean, indicated constant conditions, while the central, east and southeast Aegean, as well as the west and SW areas of Crete Isl., emerged with positive slopes in range 0.011 – 0.030 m/s/December. Noted that, negative slopes appeared in the eastern and southern parts of Peloponnese for this month.

The results of the monthly spatial distribution of linear slopes, indicated that the magnitude of slopes varies a lot from January to December, as showed in the trend lines presented in Figure 25,Figure 26 and Figure 27, for the areas exhibited the maximum negative and positive slopes, respectively. The overall maximum positive values of slopes were observed in the north Ionian in February (0.0589 m/s/February), while the lowest positive values observed in the NE Aegean in November (0.019 m/s/November). Regarding negative slopes, the area with the overall highest value, observed in June, east of Rhodes (-0.0932 m/s/June).

In the central Aegean a general tendency for decrease was observed, for February, May, July, October and November, while in the Ionian wind speeds emerged in general with positive

slopes, except from April. In general, November emerged as the month with the least significant values of slopes in the entire offshore Greek area.

Extreme monthly wind speed slopes

The spatial distribution of the linear slopes of the 95th and 99th percentiles of monthly wind speeds were depicted in Figure 28. In January, regarding the lower extreme wind speeds, emerged from the 95th percentiles, the areas with the highest positive slopes were observed in the eastern parts of the Aegean and in the Ionian Sea, with the overall maximum slope presented in the offshore areas east of Rhodes Isl. close to the Turkish coasts (0.1046 m/s/January). Increasing tendency emerged in the areas such as, the surrounding areas of Chios Isl. (~0.081 m/s/January), the extended area between Ikaria and Rhodes islands, along with the straits of the eastern Aegean's islands, ranging from 0.040 to 0.070 m/s/January, while in the surrounding areas of Crete Isl., significant positive slopes (0.020 – 0.081 m/s/January) were noticed, with the highest values observed in the southern and northern parts of the island.

The areas showed decreasing tendency were, Gulf of Patras (38.29°N 21.67°E, (-0.1393 m/s/January)), the area from SW coasts of Peloponnese, expanded up to south Kythera Isl., the south Ionian, ranging from -0.016 to -0.072 m/s/January, as well as regions in the central Aegean, as west of Andros Isl. (~ -0.041 m/s/January).

As for the spatial distribution of the 99th percentiles slopes, i.e. the highest extreme wind speeds, despite the fact that both negative and positive slopes emerged with similar spatial patterns, the slopes ranged in higher values, with significant differences noted in specific regions. For example, both the 95th and 99th slopes in the central Aegean, in the west areas near coasts of Andros Isl. emerged with negative slopes around -0.01 and -0.03, respectively; nevertheless, northern of Kea Isl., positive slopes emerged, which in the case, the higher extreme wind speeds, i.e. 99th percentiles, had higher increasing tendency over time (0.080 m/s/January), compared to the 95th (0.013 to 0.042 m/s/January). Furthermore, in the eastern parts of the Aegean, higher values of the 99th percentile were presented; in the extended area between Psara and Chios islands (~ 0.1359 m/s/January for the 99th and corresponding values for the 95th 0.083 m/s/January), in the offshore areas eastern of Rhodes Isl. (0.068 and 0.111 m/s/January for 95th and 99th, respectively); northwest areas of Skiros Isl., emerged with positive slopes in range 0.068 – 0.108 m/s/January, while in the case of 95th were ~0.028 m/s/January; indicated that the extremer wind speeds tend to increase in higher rates.

Negative slopes were presented positive values in specific regions compared to the values observed in the 95th, with the overall maximum negative values located in the Gulf of Korinthos and Patras, with slopes around -0.1367 and -0.1174 m/s/January, respectively. Higher negative slopes were appeared in the areas expanded from southwest coasts of Peloponnese, up to southeast parts of the Ionian Sea, ranging from -0.026 to -0.085 m/s/January.

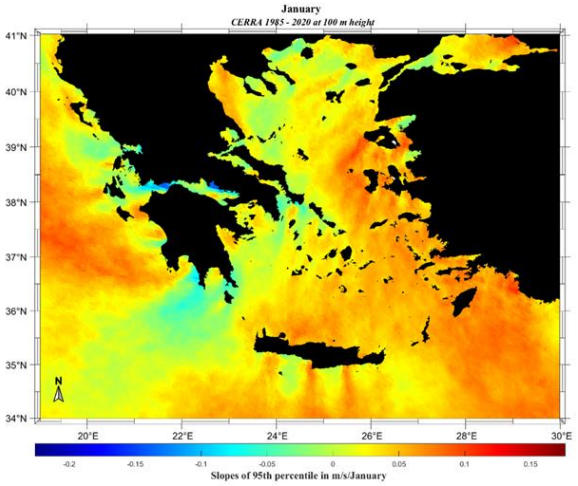
January
CERRA 1985 - 2020 at 100 m height
41°N
40°N
39°N
38°N
37°N
36°N
35°N
34°N
20°E
22°E
24°E
26°E
28°E
30°E
N
-0.2
-0.15
-0.1
-0.05
0
0.05
0.1
0.15
Slopes of 95th percentile in m/s/January

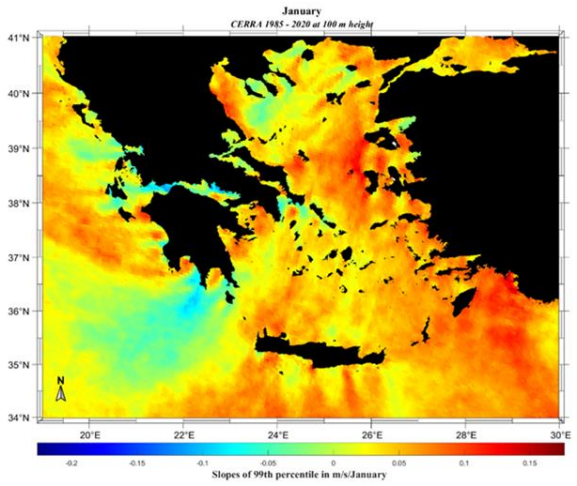
January
CERRA 1985 - 2020 at 100 m height
41°N
40°N
39°N
38°N
37°N
36°N
35°N
34°N
20°E
22°E
24°E
26°E
28°E
30°E
N
-0.2
-0.15
-0.1
-0.05
0
0.05
0.1
0.15
Slopes of 99th percentile in m/s/January

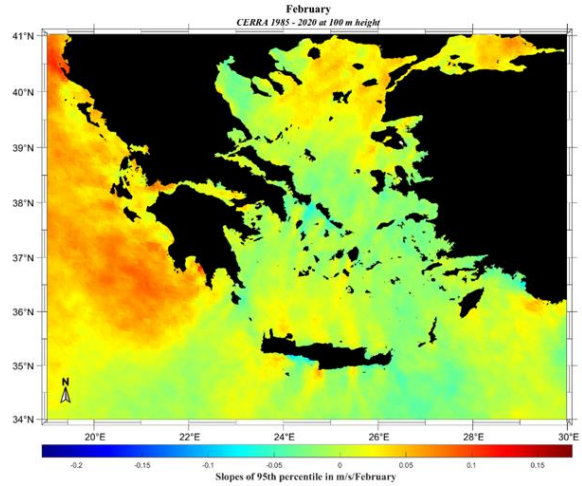
February
CERRA 1985 - 2020 at 100 m height
41°N
40°N
39°N
38°N
37°N
36°N
35°N
34°N
20°E
22°E
24°E
26°E
28°E
30°E
N
-0.2
-0.15
-0.1
-0.05
0
0.05
0.1
0.15
Slopes of 95th percentile in m/s/February

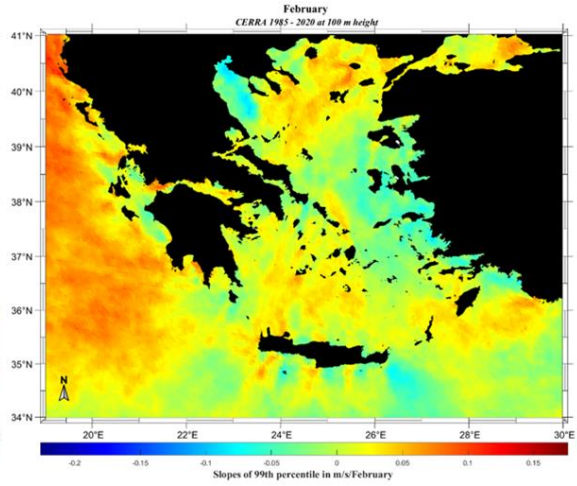
February
CERRA 1985 - 2020 at 100 m height
41°N
40°N
39°N
38°N
37°N
36°N
35°N
34°N
20°E
22°E
24°E
26°E
28°E
30°E
N
-0.2
-0.15
-0.1
-0.05
0
0.05
0.1
0.15
Slopes of 99th percentile in m/s/February

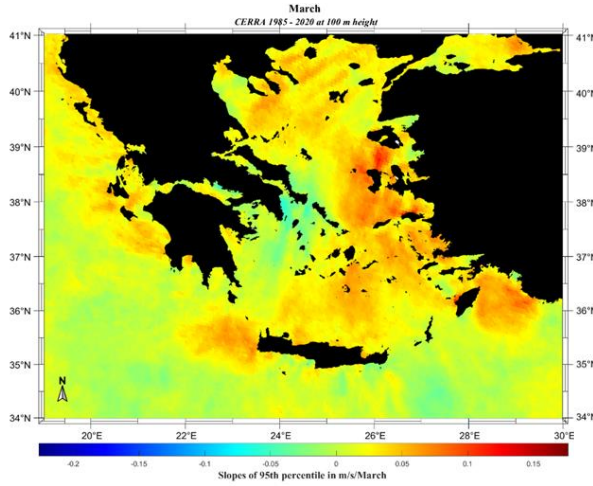
March
CERRA 1985 - 2020 at 100 m height
41°N
40°N
39°N
38°N
37°N
36°N
35°N
34°N
20°E
22°E
24°E
26°E
28°E
30°E
N
-0.2
-0.15
-0.1
-0.05
0
0.05
0.1
0.15
Slopes of 95th percentile in m/s/March

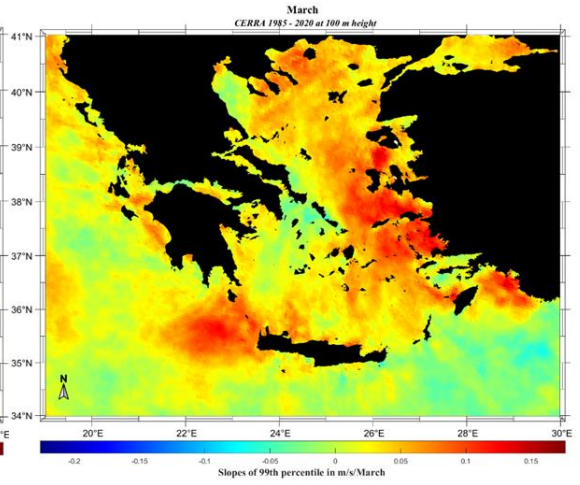
March
CERRA 1985 - 2020 at 100 m height
41°N
40°N
39°N
38°N
37°N
36°N
35°N
34°N
20°E
22°E
24°E
26°E
28°E
30°E
N
-0.2
-0.15
-0.1
-0.05
0
0.05
0.1
0.15
Slopes of 99th percentile in m/s/March

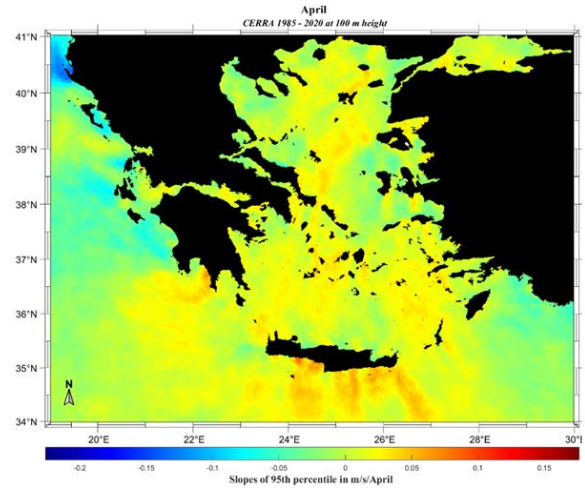
April
CERRA 1985 - 2020 at 100 m height
41°N
40°N
39°N
38°N
37°N
36°N
35°N
34°N
20°E
22°E
24°E
26°E
28°E
N
-0.2
-0.15
-0.1
-0.05
0
0.05
0.1
0.15
Slopes of 95th percentile in m/s/April

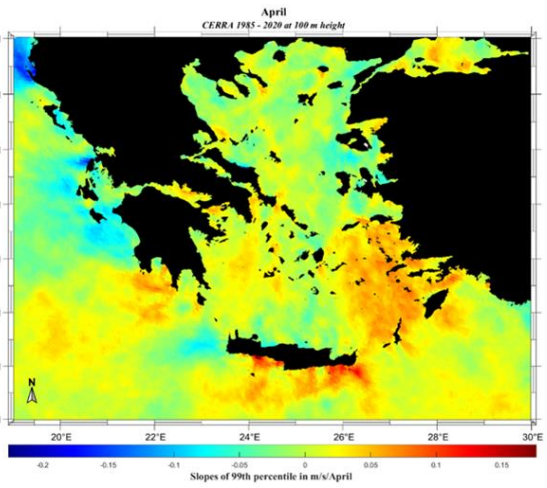
April
CERRA 1985 - 2020 at 100 m height
41°N
40°N
39°N
38°N
37°N
36°N
35°N
34°N
20°E
22°E
24°E
26°E
28°E
30°E
N
-0.2
-0.15
-0.1
-0.05
0
0.05
0.1
0.15
Slopes of 99th percentile in m/s/April

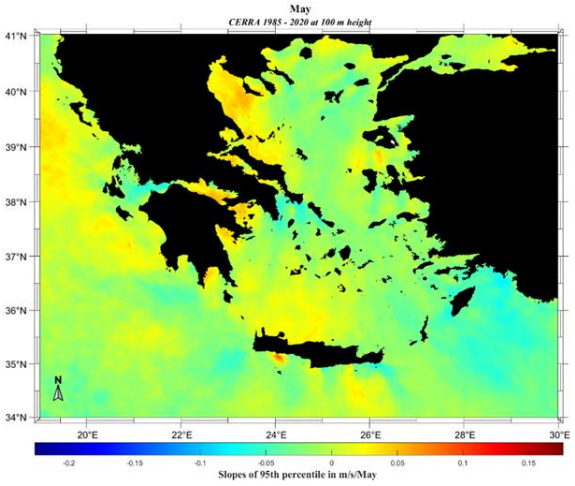
May
CERRA 1985 - 2020 at 100 m height
41°N
40°N
39°N
38°N
37°N
36°N
35°N
34°N
20°E
22°E
24°E
26°E
28°E
30°E
N
-0.2
-0.15
-0.1
-0.05
0
0.05
0.1
0.15
Slopes of 95th percentile in m/s/May

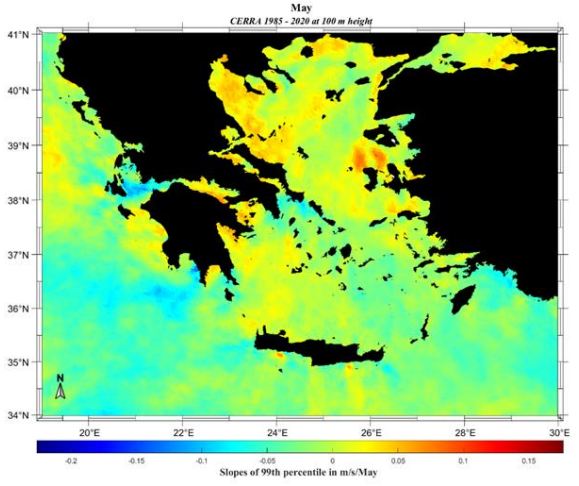
May
CERRA 1985 - 2020 at 100 m height
41°N
40°N
39°N
38°N
37°N
36°N
35°N
34°N
20°E
22°E
24°E
26°E
28°E
30°E
N
-0.2
-0.15
-0.1
-0.05
0
0.05
0.1
0.15
Slopes of 99th percentile in m/s/May

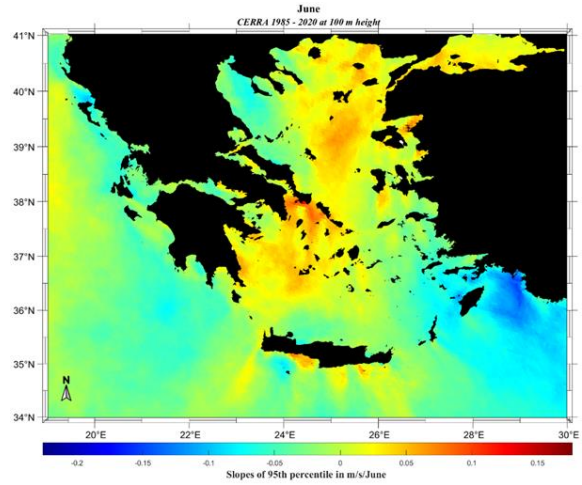
June
CERRA 1985 - 2020 at 100 m height
41°N
40°N
39°N
38°N
37°N
36°N
35°N
34°N
20°E
22°E
24°E
26°E
28°E
30°E
N
-0.2
-0.15
-0.1
-0.05
0
0.05
0.1
0.15
Slopes of 95th percentile in m/s/June

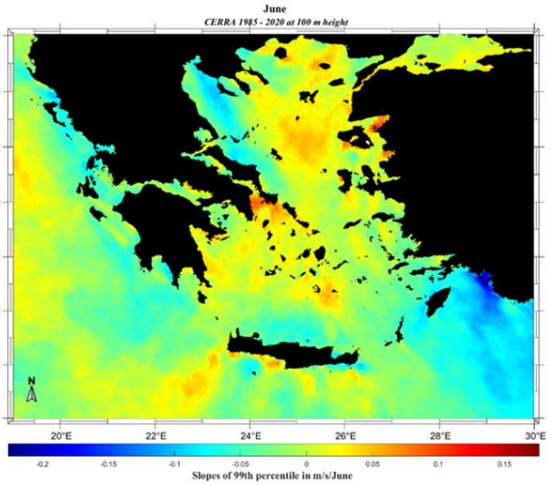
June
CERRA 1985 - 2020 at 100 m height
41°N
40°N
39°N
38°N
37°N
36°N
35°N
34°N
20°E
22°E
24°E
26°E
28°E
30°E
N
-0.2
-0.15
-0.1
-0.05
0
0.05
0.1
0.15
Slopes of 99th percentile in m/s/June

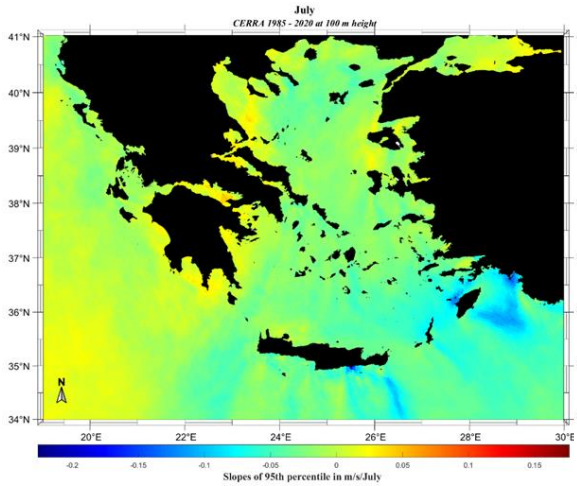
July
CERRA 1985 - 2020 at 100 m height
41°N
40°N
39°N
38°N
37°N
36°N
35°N
34°N
20°E
22°E
24°E
26°E
28°E
30°E
N
-0.2
-0.15
-0.1
-0.05
0
0.05
0.1
0.15
Slopes of 95th percentile in m/s/July

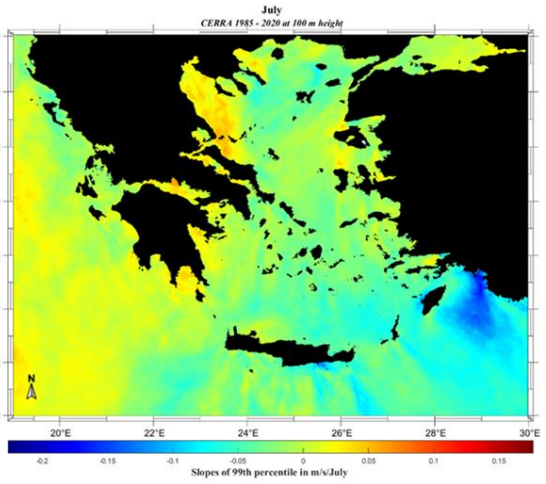
July
CERRA 1985 - 2020 at 100 m height
41°N
40°N
39°N
38°N
37°N
36°N
35°N
34°N
20°E
22°E
24°E
26°E
28°E
30°E
N
-0.2
-0.15
-0.1
-0.05
0
0.05
0.1
0.15
Slopes of 99th percentile in m/s/July

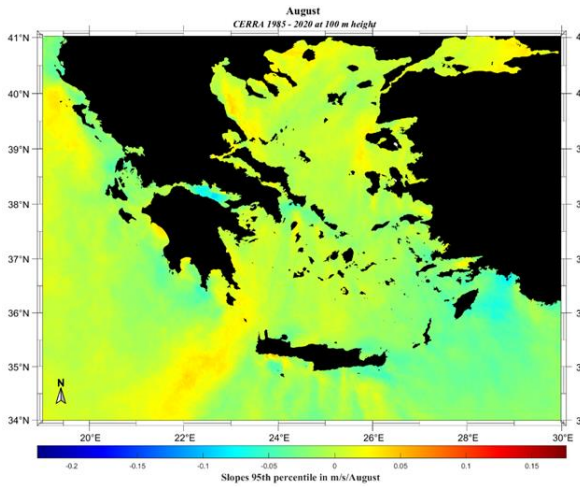
August
CERRA 1985 - 2020 at 100 m height
41°N
40°N
39°N
38°N
37°N
36°N
35°N
34°N
20°E
22°E
24°E
26°E
28°E
30°E
N
-0.2
-0.15
-0.1
-0.05
0
0.05
0.1
0.15
Slopes 95th percentile in m/s/August

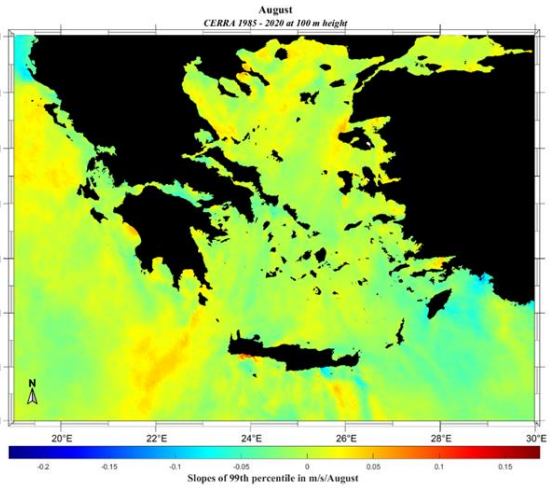
August
CERRA 1985 - 2020 at 100 m height
41°N
40°N
39°N
38°N
37°N
36°N
35°N
34°N
20°E
22°E
24°E
26°E
28°E
30°E
N
-0.2
-0.15
-0.1
-0.05
0
0.05
0.1
0.15
Slopes of 99th percentile in m/s/August

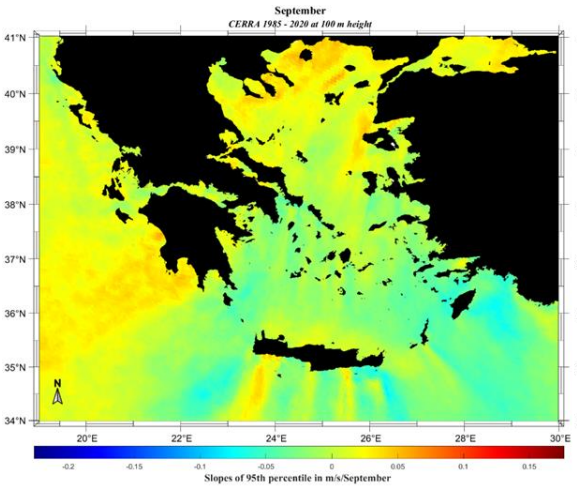
September
CERRA 1985 - 2020 at 100 m height
41°N
40°N
39°N
38°N
37°N
36°N
35°N
34°N
20°E
22°E
24°E
26°E
28°E
30°E
N
-0.2
-0.15
-0.1
-0.05
0
0.05
0.1
0.15
Slopes of 95th percentile in m/s/September

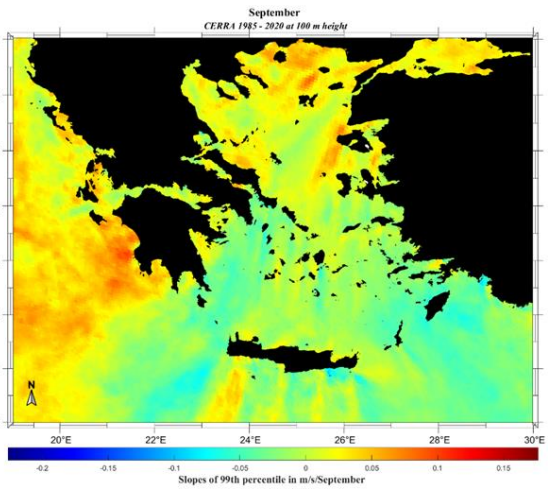
September
CERRA 1985 - 2020 at 100 m height
41°N
40°N
39°N
38°N
37°N
36°N
35°N
34°N
20°E
22°E
24°E
26°E
28°E
30°E
N
-0.2
-0.15
-0.1
-0.05
0
0.05
0.1
0.15
Slopes of 99th percentile in m/s/September

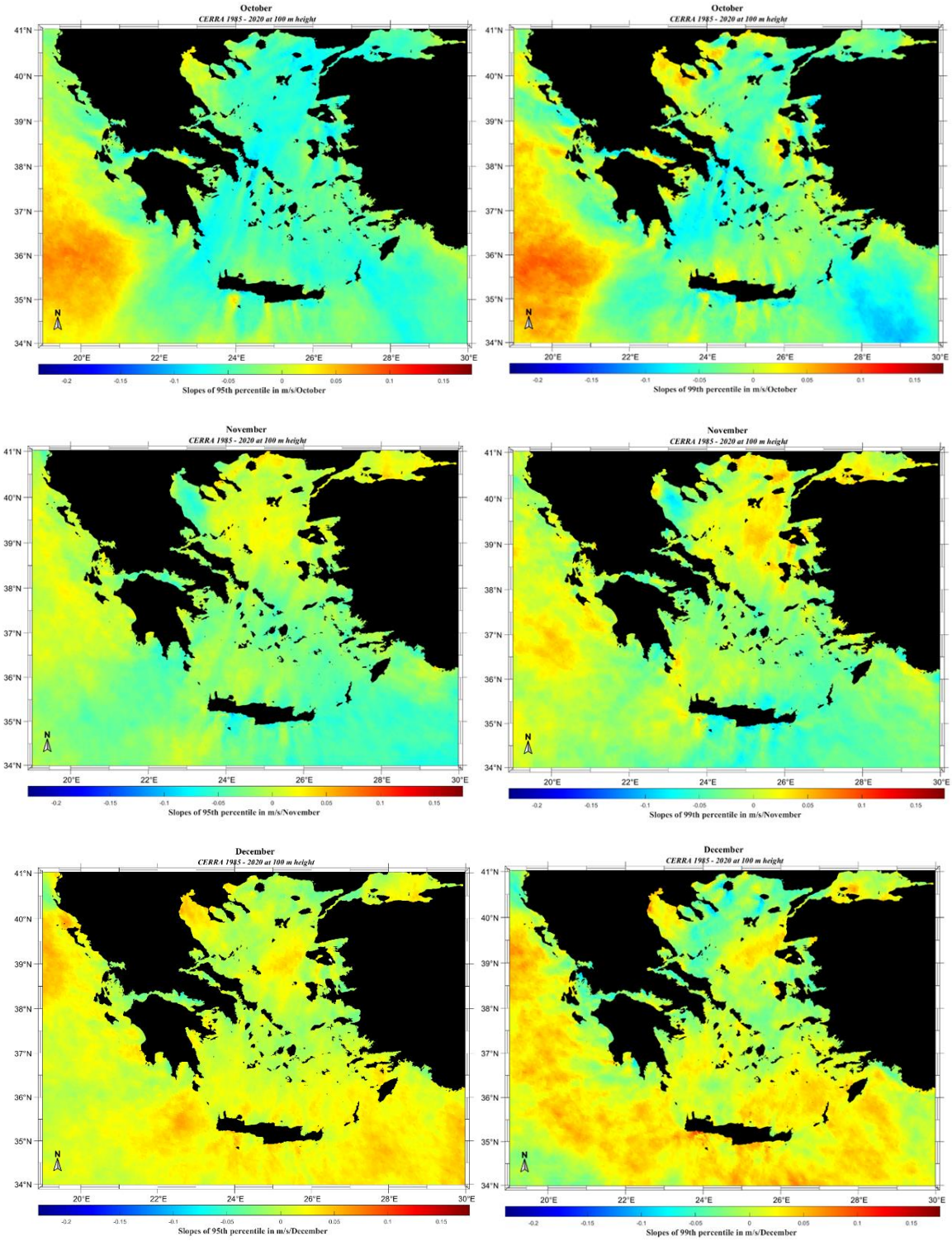

Figure 28. The spatial distribution of the linear slope of 95th (left figure) and 99th (right figure) monthly percentiles of wind speed in the Greek seas.

Regarding the 95th slopes in February, negative slopes were observed in regions where in January the higher positive values were noted; such as, the surrounding area of Chios and Psara islands, with negative slopes ranging from -0.016 to -0.033 m/s/February, with the highest negative slopes were observed in the south coasts of Crete Isl. (35.18°N 24.20°, -0.0829

m/s/February). In general, central and eastern Aegean appeared either values close to zero, indicated that the region's tendency is almost constant, or negative slopes, ranging from -0.020 to the highest observed (-0.075m/s/February) in the strait of Cavo D'Oro.

Positive slopes were observed in the entire area of the Ionian Sea, with the overall highest located in the northern parts (40.49° 19.21° 0.111 m/s/February), while high slopes were also noticed in Gulf of Patras (~ 0.048 m/s/February), in the northern Aegean with values ranging from 0.028 – 0.033 m/s/February, as well as in regions near south and north coasts of Crete Isl. (0.03 m/s/February), and near the Turkish coasts in the southeast part of Rhodes Isl., near Kastelorizo, with slopes close to 0.048 m/s/February.

The slopes of the 99th percentiles for February, appeared with slightly increased slopes compared to the 95th. Noted that again in this case, the spatial distribution between the two analyzed categories emerged with similar patterns. The main differences noticed on specific regions, where slopes, either negative or positive, emerged higher for the extremer wind speeds. For example, in the extended area between Karpathos and Rhodes islands, the tendency emerged from the 95th slopes indicated a steadiness in the area, while for the case of the 99th, positive slopes in range 0.020 – 0.035 m/s/February were noted. In the northern Aegean, in the offshore area south of Samothrace Isl., positive slopes close to 0.075 m/s/February were appeared, while regarding the 95th, lower slopes were noticed (0.020 m/s/February); as for the eastern part of the central Aegean, in the area between Psara and Chios islands, low positive values appeared for the 95th percentiles (~0.20 m/s/February), while the extremer wind speeds tended to decrease (-0.022 to -0.052 m/s/February).

The Ionian Sea appeared so far, as the area with the steadiest tendency for increase regarding the extreme wind speeds, nevertheless, in March different patterns appeared. The highest positive 95th slope (but in lower range compared to previous months), was located in the eastern parts of the Aegean, in the offshore area between Lesvos and Chios islands (38.60°N 25.75°,0.1211 m/s/March), while the highest 99th was appeared in the northern part of Samos Isl. (37.83°N 26.64°E, 0.1514 m/s/March). The overall negative slopes of the 95th and the 99th percentiles in March, were located in the central Aegean (38.00°N 24.11°E, -0.060 m/s/March and 37.70°N 24.97°E, -0.0567). The areas presented the highest positive slopes, were the northern and eastern Aegean and the extended area between Crete and Kythera islands, ranging from 0.067 to 0.1255 m/s/March. The areas emerged with decreasing tendency, were the central Aegean, as well as the southeast coasts of Crete Isl., with slopes around -0.023 m/s/March; as well as, the offshore areas in the south parts of Karpathos, Kasos and SE Crete islands, ranging from -0.331 to -0.577 m/s/March.

April, emerged with similar patterns, but in significant lower ranges. The overall maximum negative values were appeared in the northern parts of the Ionian, with slopes -0.134 and -0.172 m/s/April, respectively, while the overall maximum positive slopes were observed in the areas near south coasts of Crete Isl. with corresponding slopes 0.0813 and 0.1764 m/s/April (35.18°N 24.20°E); Crete Isl. emerged with high positive values in the area near its southeast coasts (34.93°N 26.23°E, 0.057 and 0.012 m/s/April, respectively), where negative slopes were noticed in the previous months.

In general, the areas presented higher positive slopes were, the extended area between Ikaria and Rhodes islands, including the entire central – southeastern parts of the Aegean (0.018 - 0.0.33 for the 95th percentile and 0.051 - 0.070 for the 99th percentile, respectively), while in the Ionian, negative slopes appeared, as well as in the west parts of Crete and south of Lemnos islands. Noted, that in the central Aegean, where the overall maximum negative values were located in the previous months, positive slopes emerged for both the 95th and the 99th in April (~0.014 and 0.038 m/s/April, respectively).

Regarding May, the spatial patterns were similar, with differences noted in specific regions and in the ranges of the slopes. For example, the overall highest positive slopes for the 95th percentile, appeared in the areas near south coasts of Crete Isl. (25.15°N 24.07°E, 0.0872 m/s/May), while for the 99th percentile, in the areas between Lesvos and Chios islands (38.65°N 25.76°E, 0.0886 m/s/May). The maximum negative slope, for the 95th was observed near the Turkish coasts in the southeastern parts of the Aegean (-0.084 m/s/May), while in the 99th in the south coasts of Peloponnese (-0.13 m/s/May). In general, low decreasing tendency was noticed in the entire region of the central and southeast Aegean, as well as in the south parts of the Ionian Sea; while positive slopes appeared in the offshore areas of Halkidiki and north of Crete Isl. for both of the 95th and 99th percentiles. A main difference was observed in the central Ionian, where the values of positive slopes of the 99th percentiles, were covered larger spatial area, compared to the 95th.

The spatial distribution regarding June, presented the highest values of positive slopes over the central Aegean, covering the area between the strait of Cavo D'Oro and the east coasts of Athens, with the overall maximum values for the 95th in the southwest coasts of Evvoia (0.1291 m/s/June) with corresponding slope for the 99th 0.087 m/s/June; while the maximum slope for the 99th was located near the coasts of Turkey, east of Lesvos Isl. (0.087 m/s/June), with corresponding slope for the 95th 0.057 m/s/June.

Furthermore, in both cases the areas emerged increasing tendency were, the northern and central Aegean, with the highest slopes appeared in the surrounding area of Saint Efstratios Isl. up to east areas of Skyros Isl. (0.013 – 0.067 m/s/June for 95th and 0.027 – 0.054 m/s/June for 99th) and the extended area between west Andros and east areas near coasts of Gyaros islands, with slightly lower slopes in the south parts of the island, respectively (0.045 – 0.082 m/s/June for the 95th and 0.049 – 0.060 m/s/June for 99th); while decreasing tendency were presented, near the coasts of the Ionian islands (-0.069 to -0.098 m/s/June), as well as in the southeastern parts of Aegean, with the maximum values appeared in the offshore areas east of Rhodes and north of Karpathos islands (ranging from -0.071 to -0.15 for 95th and -0.059 to -0.17 m/s/June for 99th). The east part of Crete Isl. presented negative slopes ~ 0.035 and -0.086 m/s/June, for both of the 95th and the 99th percentiles, respectively. In general, in June, the tendency of the extreme wind speed values, was presented an interesting behavior, thus the decrease that spotted in the 99th was located in the same regions as in the 95th, while, the increasing distribution is quite wider in the higher extreme speeds compared to the 95th.

Regarding the tendency of the extreme wind speeds in July, a total decrease was noted over the Aegean, while positive slopes were observed in the Ionian. The overall maximum negative slope for the 95th percentiles, was located near south coasts of Crete Isl. (-0.18 m/s/July), while for the extremer wind speeds, east of Rhodes Isl., near to the Turkish coasts (-0.17 m/s/July).

The overall highest positive slopes were observed for both the 95th and 99th, in Gulf of Korinthos (0.055 and 0.065 m/s/July). The western part of the Greek Seas, including the Ionian, the Gulf of Patras and Korinthos, the east parts of Thessalia, as well as the extended area from the east coasts of Peloponnese up to south Ionian, were presented increasing tendency, with higher values noted for the 99th percentiles (0.017 – 0.024 m/s/July and 0.015 – 0.059 m/s/July, respectively). As for the Aegean, and the eastern parts of the offshore Greek areas, the only region emerged increasing tendency, was northern from Chios Isl. up to Lesvos Isl. (0.022 for 95th and 0.043 m/s/July for 99th); while negative slopes were appeared for both cases, in the rest Aegean, ranging from -0.022 to -0.080 m/s/July for the 95th and from -0.007 to -0.090 m/s/July for the 99th percentiles, respectively.

August emerged with a general increasing tendency, except from the offshore areas covering the central and south - eastern parts of the Aegean. The overall maximum positive slopes for

the 95th percentiles, were observed east of Thessalia (0.053 m/s/August) and in the south - west coasts of Crete Isl. (0.087 m/s/August) for the 99th; while the corresponding maximum negative slopes were appeared in Gulf of Korinthos (-0.09 m/s/August for the 95th) and in the eastern offshores regions of Rhodes Isl., near the Turkish coasts (-0.102 m/s/August for the 99th). Each of the 95th and 99th presented increasing tendency in the northern Ionian, with lower positive slopes noted in the 99th compared to the 95th; in west parts of Crete Isl. with higher positive values for the 99th percentile, as well as in the northern and NE parts of the Aegean, including the surrounding areas of Lemnos, Samothrace, Lesvos and Chios islands.

Regarding September, high positive values were noted in the north Aegean, in the extended area between Samothrace and Lemnos islands, in the areas near coasts of Halkidiki (~0.058 m/s/September), as well as in both northern and in some south coasts of Crete Isl. (0.013 – 0.035 m/s/September). Significant higher positive slopes (0.020 – 0.103 m/s/September), compared to the 95th, observed for the extremer wind speeds, in the aforementioned regions, with the overall maximum, near the west coasts of Peloponnese. The eastern and the southern parts of the Ionian, presented increasing tendency, while regions such as central and southeast Aegean, appeared with negative slopes either for 95th and 99th percentiles, with the overall highest negative slopes located near the southeast coasts of Crete Isl. and the surrounding sea areas (-0.081m/s/September for the 95th and -0.096 m/s/September for the 99th, respectively).

In October, a total decrease was noted both in Aegean and in the northern parts of the Ionian, ranging from -0.006 to -0.0972 m/s/October for the lower extreme wind speeds, with the overall maximum negative in the south – west coasts of Crete Isl.; while for the 99th percentiles, the same spatial patterns were appeared in higher ranges.

Regarding the 95th percentiles, positive slopes appeared in the south parts of the Ionian in range 0.033 to m/s/October, as well as in the west areas of Halkidiki (0.013 m/s/October) and in some south areas of Crete Isl. ~0.024 m/s/October, while for the 99th percentile, higher positive values were observed in the first two aforementioned regions with corresponded values ~0.098 and 0.054 m/s/October, and lower for south regions of Crete Isl. ~0.011 m/s/October. High negative values were also observed in the central Aegean, in the northern parts of Kea Isl. with higher negative slopes noted for the 95th percentiles; for the extremer wind speeds the higher negative slopes appeared in the western and eastern parts of the Cyclades, while tendency towards an increase in extremer wind speeds (99th) was observed in the northern parts of the east Aegean, in the surrounding areas of west Chios up to Lesvos.

Regarding November, negative slopes were observed over the entire central, south and east Aegean, as well as in the south Ionian. Positive slopes appeared in the central and western parts of the Ionian, as well as in the northern parts of the Aegean, with higher values for the extreme winds. Higher negative slopes, compared to the 95th percentile observed in the areas near the SE coasts of Crete Isl., while in both cases, increasing tendency was noticed in the southeastern tip of Peloponnese, including the offshore area of Kythera Isl. for the 99th percentiles. The overall highest positive slopes for the 95th percentile, observed in the northern parts of the Aegean, near coasts of Halkidiki (0.048 m/s/November), while the maximum negative slopes appeared in the areas near the SW coasts of Crete Isl. (-0.106 m/s/November). As for the 99th percentiles, the maximum negative values appeared again in the SW coasts of Crete Isl., slightly higher (0.107 m/s/November), while the highest positive slopes observed in the south coasts of Lesvos Isl. (0.065 m/s/November).

December's highest positive slopes (0,065 m/s/December) were observed in the north Ionian, close to the eastern areas of Diapontian Islands, while the negative in Gulf of Korinthos -0.060. As for the extremer wind speeds trends, negative slopes were appeared south of Samothrace

Isl. in the northern Aegean (-0.101 m/s/December) and the overall highest positive (0.092 m/s/December), in the SW areas near coasts of Crete Isl.

In general, positive slopes were observed for both for the 95th and the 99th percentiles in the south and south east Aegean, ranging from 0.013 to 0.070 m/s/December and 0.33 to 0.92 m/s/December, with the highest observed in the extended area between west coasts of Crete and Kythera islands, as well as in the south offshore areas of Kasos and Karpathos and in southeast area of Rhodes for the 99th percentile; while in the areas near east coasts of Crete Isl., negative slopes noted - 0.0026 and -0.0087 m/s/December, respectively. Northern parts of the Aegean, appeared with decreased tendency, as well as the northern parts of the Central Aegean, while positive slopes observed in the SW offshore areas of Tinos Isl., and in the surrounding area of Amorgos Isl., mainly in the south offshore regions.

4.2.3. Seasonal scale

The spatial distribution of the linear slopes of the mean seasonal wind speeds is presented in Figure 29 with slightly differences between the 4 seasons. The overall maximum positive slope for winter, was presented in the NW areas of Diapontian Islands (~ 0.039 m/s/winter), while the maximum negative slope was located in the east parts of Athens around the point 37.97°N 24.01°E with values close to -0.029 m/s/winter. In general, the highest positive slopes were appeared in the Ionian Sea (0.017 – 0.039 m/s/winter), while lower but positive slopes were observed all over the Aegean ranging from 0.0018 to 0.034 m/s/winter, with the highest values noted in the SW areas near coasts of Crete Isl. and in the southeast Aegean, in the surrounding areas of Kasos and Karpathos islands.

Negative slopes, appeared in the central Aegean, in the extended area between east coasts of Evvoia and the surrounding area of the complex of Kea, Serifos and Gyaros islands, ranging from -0.012 to 0.039 m/s/winter, in the Gulf of Patras (-0.020 m/s/winter) and in the northern Aegean, in regions SE of Samothrace (-0.0042 m/s/winter) and NE of Lemnos (-0.0055 m/s/winter).

Regarding spring, the spatial patterns emerged for the linear slopes indicated a decreasing tendency in the regions where in winter the higher positive slopes appeared, with negative slopes observed in the SE Aegean, in the north areas of Rhodes Isl., as well as in the extended area between Rhodes, Kasos and Karpathos islands, with slopes ranging from -0.011 to -0.023 m/s/spring, while the overall maximum negative slope was located around the point 36.50°N 28.65°E ~ -0.024 m/s/spring. Central Aegean again emerged with decreasing tendency, with slopes in range between -0.007 to - 0.014 m/s/spring, as well as the east coasts of Crete Isl. (~ -0.005m/s/spring), the area between Samothrace and Lemnos islands in the northern Aegean (~ -0.011 m/s/spring) and the central and SE Ionian ranging from -0.008 to -0.022 m/s/spring.

The overall highest positive slopes were appeared in the south coasts of Crete Isl. (35.16°N 24.01°E ~ 0.021 m/s/spring), while other regions emerged with positive slopes were, the north, south and southeast areas near coasts of Crete Isl., the southern parts of the central Aegean, the extended area between Lesvos and Chios islands, as well as the northern Ionian.

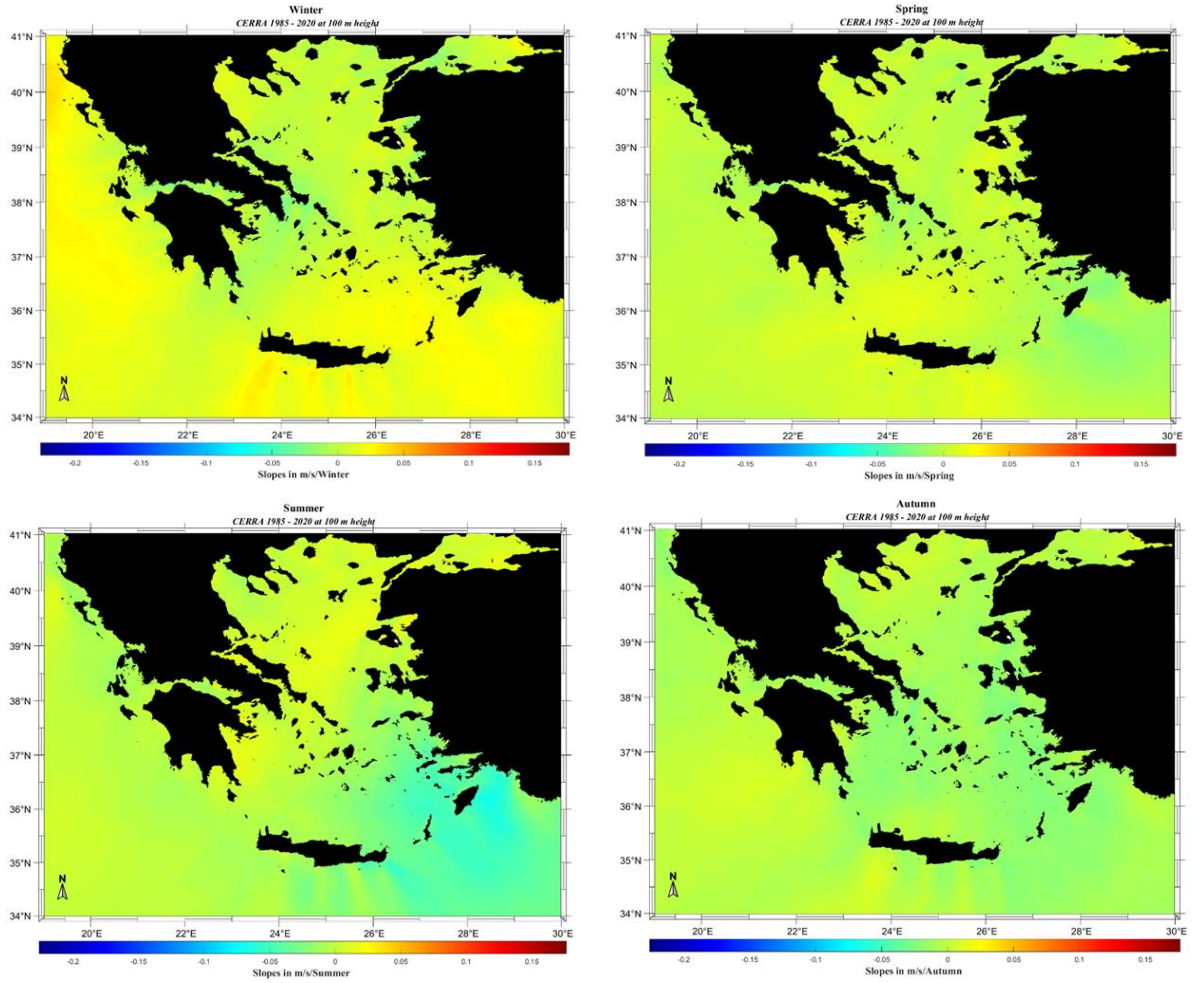

Figure 29. The spatial distribution of the linear slopes of mean seasonal wind speeds in the Greek seas.

The spatial distribution of linear slopes for mean summer wind speeds, indicated higher negative slopes in the southeast Aegean, including the areas from near east coasts of Crete Isl., up to east offshore areas of Rhodes Isl., where the overall maximum negative slope observed (36.19°N 28.47°E ~ -0.069 m/s/summer). Negative slopes also appeared in the west parts of Crete Isl., including the areas up to SW coasts of Peloponnese and the eastern regions of the Ionian, as well as in the eastern Aegean. The areas emerged with increasing tendency were, the central and northern Aegean ranging from 0.009 to 0.014 m/s/summer, with the overall maximum positive slope located east of Lesvos, near the Turkish coasts ~ 0.019m/s/summer.

Regarding autumn, negative slopes observed in the entire area of both the Aegean and the Ionian Seas, with the overall negative slope located in the south-eastern part of Chios Isl. (38.14°N 26.11°E –0.028 m/s/autumn. The areas that presented positive slopes were, the SW offshore areas of Crete Isl., as well as the SW areas from Peloponnese coasts in which the overall highest positive slopes were observed (0.0038 to 0.012 m/s/autumn).

Extreme seasonal wind speed slopes

The spatial distribution of the linear slopes for the 95th and 99th percentiles of mean seasonal wind speed from winter to autumn, is presented in Figure 30, where the patterns depicted, followed the patterns observed for the slopes of the seasonal mean wind speed, in the previous section. Regarding winter, the long – term trends emerged for the entire offshore Greece, for both the 95th and the 99th percentiles of seasonal wind speeds, were in general characterized by positive slopes. The regions presented decreasing tendency over time were noted in Gulf of Korinthos and Patras, for wind speeds in range between 15 – 17 m/s, the slopes were around -0.024 m/s/winter, while for the higher extreme wind speeds of this season (17 – 30 m/s), the overall negative slope was appeared in the Gulf of Patras (-0.0873 m/s/winter).

Significant negative values were observed in the extended area between the strait of Cavo D'Oro (-0.0383 m/s/winter for the 95th and -0.0127 m/s/winter for the 99th) and in the SE offshore areas of Kea Isl. (-0.014 m/s/winter for the 95th and -0.0028 m/s/winter for the 99th); while in the northern parts of the island, positive slopes were noticed (0.015 m/s/winter for the 95th and 0.035 m/s/winter for the 99th, respectively). In the SW areas near coasts of Peloponnese and in the northern Aegean close to south coasts of Halkidiki and the surrounding area, as well as south of Samothrace Isl., were observed negative slopes, in higher ranges for the extremer wind speeds.

The areas emerged with positive slopes for winter were, the eastern parts of Rhodes Isl., as well as the area between east Crete, Karpathos and Kasos islands; the northern Aegean, the extended area between Lesvos, Chios and Psara islands, where the highest slopes started from the SW coasts of Lesvos and landed up to the NW areas of Chios (0.022 – 0.048 m/s/winter), while for the higher extremes, landed up to the areas near NW coasts of Psara Isl. (0.030 – 0.048 m/s/winter).

The overall highest positive slopes, for both the 95th and the 99th percentiles, were located in the SW coasts of Crete Isl. (0.0719 and 0.0925 m/s/winter, respectively). In general, an increasing tendency was spotted in the surrounding areas of Crete Isl., including the northern parts of the island, with values ranging from 0.024 to 0.0719 m/s/winter for the 95th percentiles and from 0.025 to 0.0925 m/s/winter for the 99th percentiles, respectively; while a part of the SE offshore areas of Crete emerged with negative slopes. The western parts of the Ionian presented the highest positive slopes, compared to the rest area, with increased magnitudes of slopes noticed for the 99th percentiles.

Regarding the long – term trends of the extreme wind speeds for Spring, the positive tendency observed for winter in the Ionian and the south and southeast parts of the Aegean, was now shifted towards east and north areas of the Aegean. More specifically, the overall negative slope was appeared in the northern parts of the Ionian (-0.0439 m/s/spring for the lower extremes), where positive slopes observed for the winter, and in the central Ionian for the higher extremes (-0.0582 m/s/spring); while the highest positive slopes were located in the areas south of Lesvos Isl. for the 95th (0.053 m/s/spring) and NE of Ikaria Isl. with positive slope 0.1052 m/s/spring, for the 99th percentiles, where lower positive values emerged for winter.

In general, the areas emerged tend to increase at the fastest rates, were the south – central, eastern and northern areas of the Aegean, with slopes in range between 0.010 to 0.053 m/s/spring for the 95th percentiles and 0.015 to 0.1052 for the 99th percentiles, respectively. The higher extremes, presented an overall tendency for increase in the eastern parts of the Aegean, in the extended area between areas south of Lesvos Isl. and eastern parts of Rhodes Isl., while for the case of the 95th percentiles, negative slopes were appeared east of Rhodes Isl.

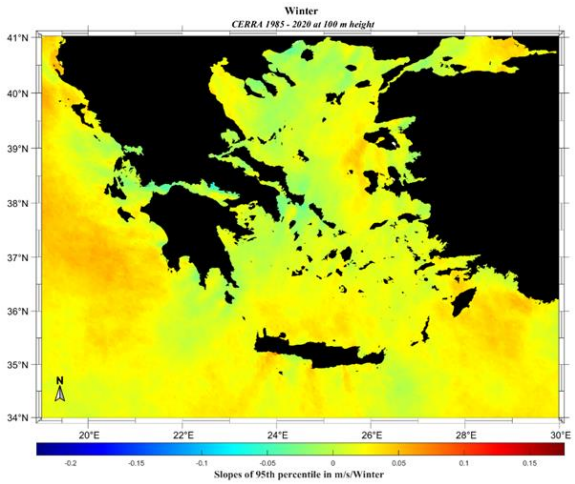
Winter
CERRA 1985 - 2020 at 100 m height
41°N
40°N
39°N
38°N
37°N
36°N
35°N
34°N
20°E
22°E
24°E
26°E
28°E
30°E
N
-0.2
-0.15
-0.1
-0.05
0
0.05
0.1
0.15
Slopes of 95th percentile in m/s/Winter

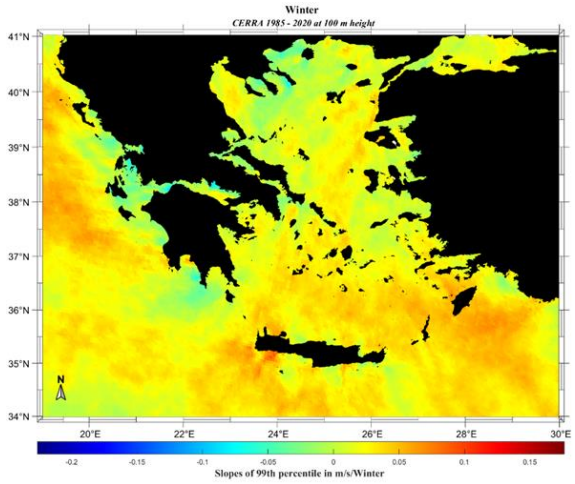
Winter
CERRA 1985 - 2020 at 100 m height
41°N
40°N
39°N
38°N
37°N
36°N
35°N
34°N
20°E
22°E
24°E
26°E
28°E
30°E
N
-0.2
-0.15
-0.1
-0.05
0
0.05
0.1
0.15
Slopes of 99th percentile in m/s/Winter

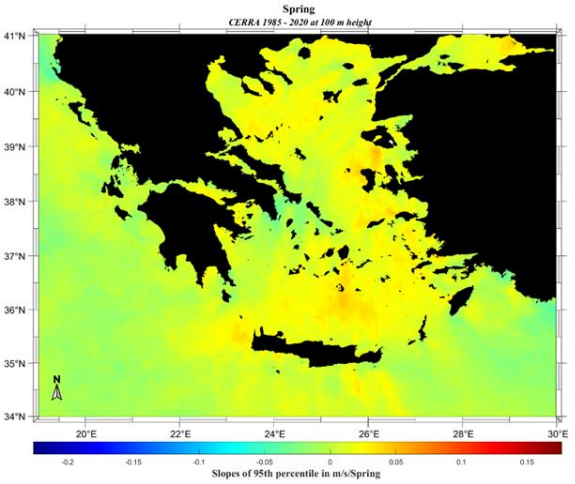
Spring
CERRA 1985 - 2020 at 100 m height
41°N
40°N
39°N
38°N
37°N
36°N
35°N
34°N
20°E
22°E
24°E
26°E
28°E
30°E
N
-0.2
-0.15
-0.1
-0.05
0
0.05
0.1
0.15
Slopes of 95th percentile in m/s/Spring

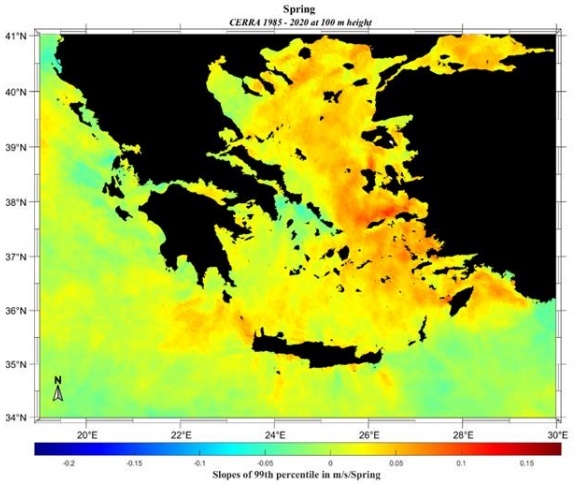
Spring
CERRA 1985 - 2020 at 100 m height
41°N
40°N
39°N
38°N
37°N
36°N
35°N
34°N
20°E
22°E
24°E
26°E
28°E
30°E
N
-0.2
-0.15
-0.1
-0.05
0
0.05
0.1
0.15
Slopes of 99th percentile in m/s/Spring

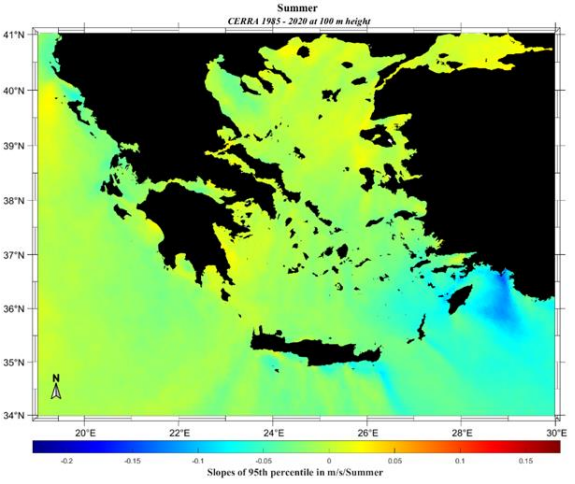
Summer
CERRA 1985 - 2020 at 100 m height
41°N
40°N
39°N
38°N
37°N
36°N
35°N
34°N
20°E
22°E
24°E
26°E
28°E
30°E
N
-0.2
-0.15
-0.1
-0.05
0
0.05
0.1
0.15
Slopes of 95th percentile in m/s/Summer

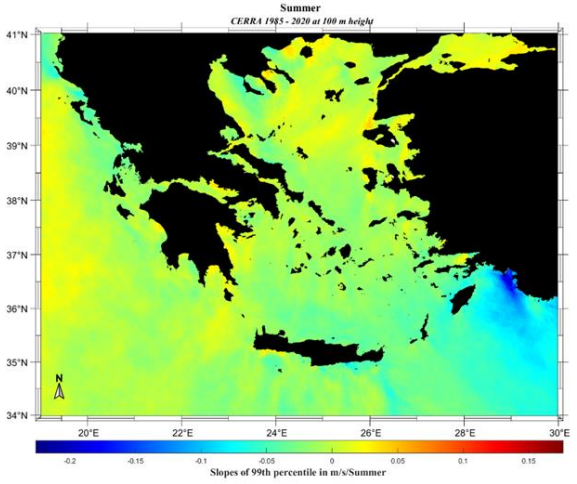
Summer
CERRA 1985 - 2020 at 100 m height
41°N
40°N
39°N
38°N
37°N
36°N
35°N
34°N
20°E
22°E
24°E
26°E
28°E
30°E
N
-0.2
-0.15
-0.1
-0.05
0
0.05
0.1
0.15
Slopes of 99th percentile in m/s/Summer

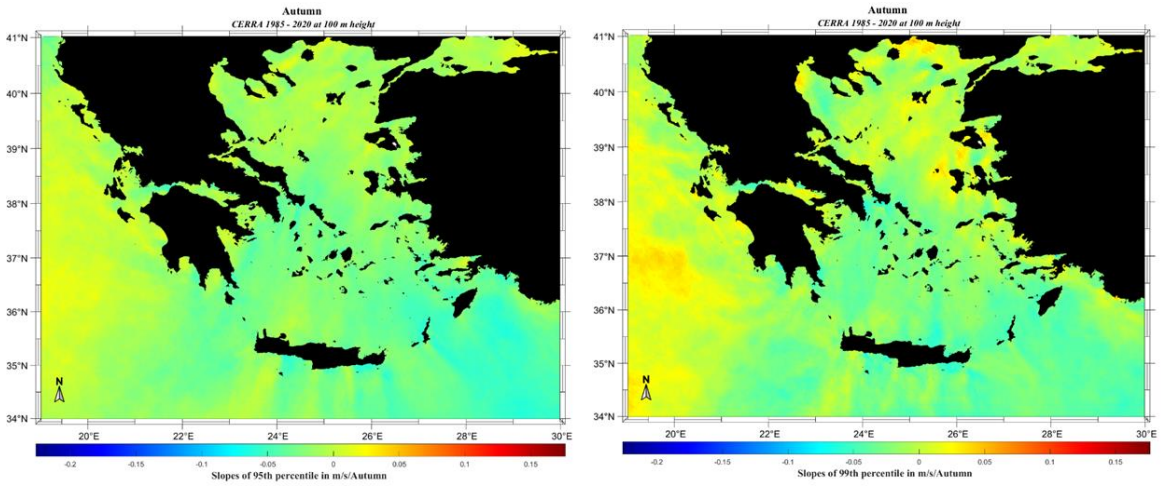

Figure 30. The spatial distribution of the linear slope of the 95th (left figure) and 99th (right figure) seasonal percentiles of wind speed, in the Greek seas.

In both cases, negative slopes were observed in the central Aegean, with the highest located in the offshore areas north of Gyaros Isl. and in the area between SE Andros Isl. and NE Tinos Isl.; the south parts of the extended area between Crete, Kasos and Karpathos islands were also emerged with negative slopes, while the western and northern offshore areas of Crete Isl. tended to increase.

Regarding summer, similar spatial patterns were emerged for both the 95th and the 99th percentiles. Decreasing tendency was observed for the entire areas of the central, south and east Aegean, with the overall maximum negative slopes located in the extended area between east of Rhodes Isl. and the Turkish coasts, ranging from -0.0347 to -0.1386 m/s/summer for the 95th and -0.043 to -0.2080 m/s/summer for the 99th, respectively. Furthermore, negative slopes were appeared in the SE areas near coasts of Crete Isl. (-0.059 and -0.028 m/s/summer, respectively), the areas between south Kasos and Karpathos islands, covering the entire area up to south coasts of Kos Isl. Lower range values were also observed in the central Aegean, as well as between Samothrace and Lemnos islands, in the south parts of the Ionian for the 95th and in the south for the 99th. The highest negative slope of the aforementioned area was located east of Diapontian Islands, while in west, positive slopes emerged (0.025 and 0.013 m/s/summer, respectively). The higher extremes, tend to increase over time in the western parts of the Ionian, with slopes in range 0.013 – 0.021 m/s/summer, while areas where positive slopes were observed were the north areas of Lesvos Isl., as well as the east offshore areas of Saint Efstratios Isl. and near coasts of Peloponnese.

As for autumn, decreasing tendency was observed in the entire area of the Greek Seas, with the overall maximum negative slope located SE of Rhodes Isl. (-0.064 and -0.070, respectively), while the overall positive in the south Ionian (0.021 and 0.042m/s/autumn). Positive slopes were emerged in areas near east coasts of Saint Efstratios Isl., west of Gaydos Isl., for the 95th percentiles; while regarding the higher extremes, in the extended area between Psara Isl. and Lesvos Isl., in the SE Ikaria Isl. and Samos Isl., as well as between Evvoia and Skyros Isl.

4.3. Wind power density

4.3.1. Annual time scale

The spatial distribution of mean annual wind power density (WPD) is presented in Figure 31 making it clear, that Aegean surpasses the Ionian Sea. Significantly high values of WPD were observed in the anticipated regions of the Aegean, including the northern, central and southeastern regions, similar results with Soukissian, Karathanasi, and Zaragkas [79]. In more detail, the overall highest WPD values were located offshore along the east coasts of Crete Isl., with values reaching 955 W/m^2. In the west coasts of Crete Isl. and the surrounding sea areas along Antikythera and south Kythera offshore areas, were also observed significant values of WPD, ranging from 600 to 750 W/m^2.

The second highest area of WPD values was the central Aegean, with the highest located in west areas of Andros Isl. (~ 953 W/m^2), including the surrounding areas of Gyaros Isl. Furthermore, high values were observed in the NE coasts of Andros Isl., in the surrounding area of Mykonos Isl., southeast areas of Naxos Isl., and lower but not negligible, in northeast Amorgos Isl. and surrounding areas of Astypalaia Isl.

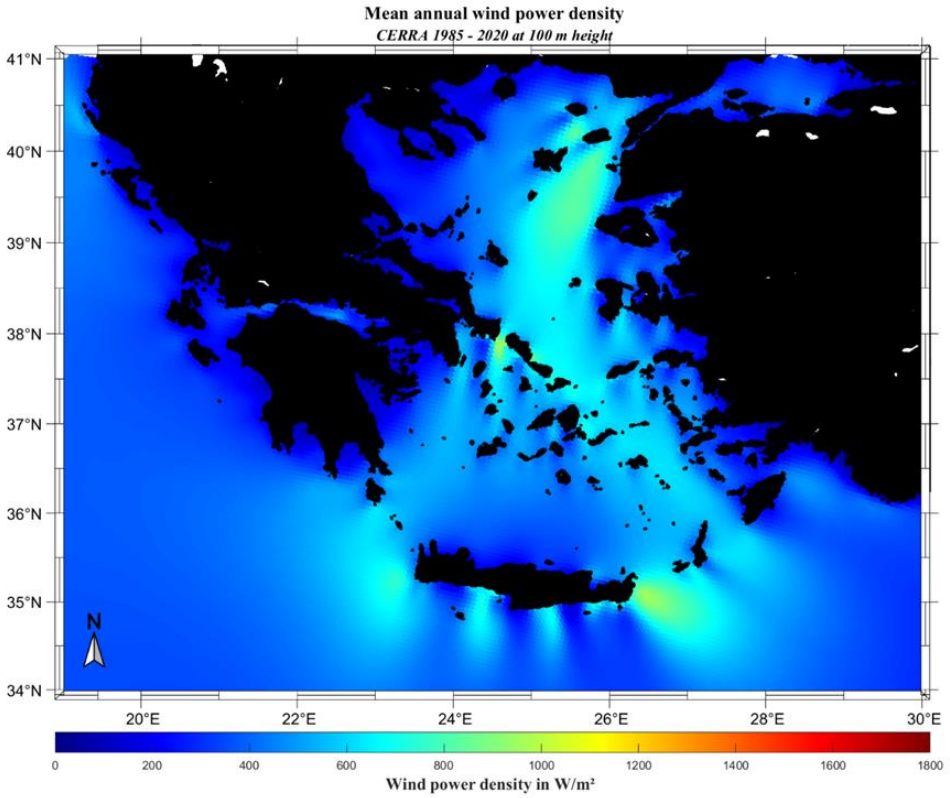

Figure 31. The spatial distribution of the mean annual wind power density, in the Greek seas.

WPD values ranging from 600 to 850 W/m^2, dominated in the entire northern Aegean, and reached peak values exceeding 800 W/m^2 along the southwest coasts of Samothrace Isl.,

covering almost the entire surrounding maritime sea and the extended area between east of Lemnos and the northern shores of the Psara Isl.

The lower values of WPD were observed in the east side of the Ionian Sea, in the surrounding coastal areas of Peloponnese and Halkidiki, as well as, in the south coasts of Crete Isl., due to the mountains of the island blocking the circulation of wind in certain regions of the island; and in southeast shores of Rhodes Isl. Including the surrounding sea areas. Furthermore, notable values of low WPD were noticed in south Lesvos Isl., where the corresponding wind speeds were usually high. More details about the statistical parameters of areas that presented interesting values of WPD are presented in Table 12.

The spatial distribution of MAV of WPD, is presented in Figure 32, where the highest variability percentages were observed near the coastal areas of both the Aegean and the Ionian Seas. The values were in range between 105 to 430 %, with the overall highest values appearing along the southern coast of the Peloponnese; for more statistical details refer to Table 13.

Table 12. The statistical parameters of the areas with the highest and lowest values of mean annual WPD, in the Greek seas

Sea Areas	**Coordinates** °	**WPD** W/m^2	**Median** W/m^2	**Std** W/m^2	**MAV** %	**IAV** %
East coasts of Crete	35.07°N 26.52°E 35.12°N 26.53°E	954.65 942.18	540 560	101.63 102.99	104.77 109.98	10.98 10.83
West Andros	37.86°N 24.64°E	953.75	389	161.98	131.60	13.79
South Samothrace	40.23°N 25.60°E	832.15	327	93.00	151.93	11.17
East Sain Efstratios	39.63°N 25.61°E	829.85	422	80.19	135.16	9.66
North Amorgos	36.96°N 25.75°E	698.59	418	72.11	112.98	10.32
East Diapontian	39.82°N 19.01°E	447.03	189	50.45	158.33	11.28
South Rhodes	35.93°N 28.08°E	285.94	113	35.02	178.11	12.25

Table 13. The statistical parameters of the areas with the highest and lowest values of MAV of WPD, in the Greek seas.

Sea Areas	**Coordinates** °	**WPD** W/m^2	**Median** W/m^2	**Std** W/m^2	**MAV** %	**IAV** %
East coasts of Crete	35.26°N 26.57°E	756.42	495	77.41	105.76	10.23
East Karpathos	35.63°N 27.18°E	446.67	297	45.31	106.40	10.14
East Naxos	37.01°N 25.76°E	674.53	415	66.94	111.59	9.92
North Amorgos	36.96°N 25.75°E	698.59	418	72.11	112.98	10.32
SW Ikaria	37.42°N 25.95°E	641.30	395	58.52	116.33	9.12
North Astypalaia	36.72°N 26.23°E	618.02	363	61.52	118.43	9.95
East Diapontian Islands	39.93°N 19.74°E	180.45	36.18	18.13	215.76	10.05
South Peloponnese	36.88°N 22.20°E	97.79	9.86	23.65	429.96	24.18

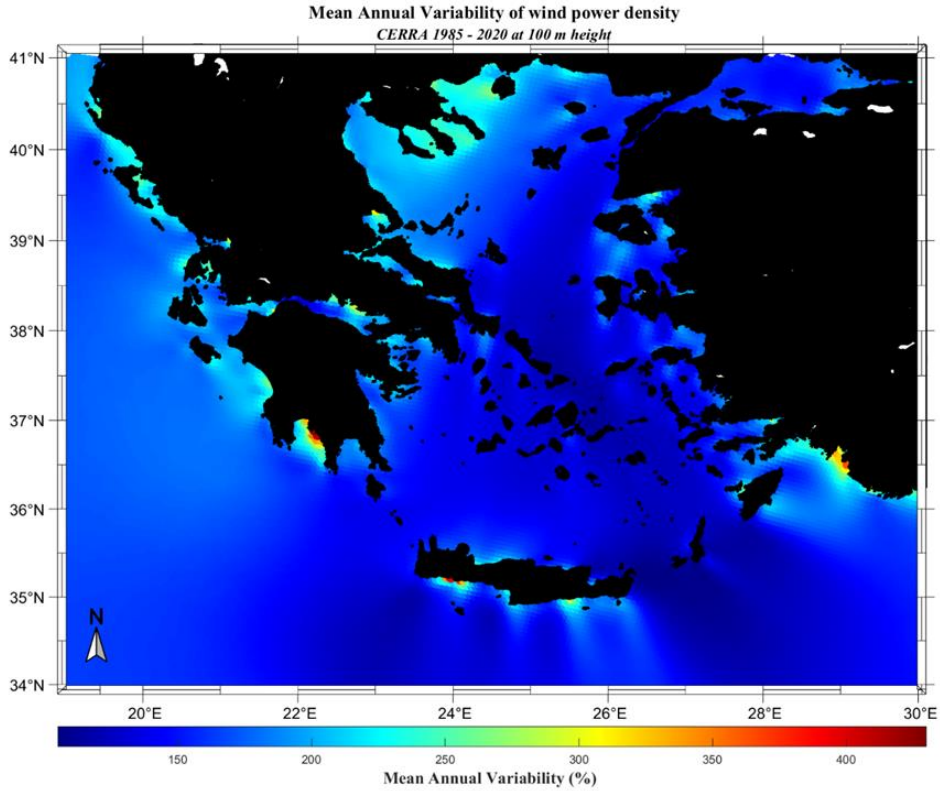

Figure 32. The spatial distribution of mean annual variability of wind power density in the Greek seas.

The lowest MAV values were observed along the east coasts of Crete (35.26 °N 26.57°E) and the surrounding sea areas; similar results with Soukissian, Karathanasi, and Zaragkas [79]. The second lowest area with low MAV values was located in the surrounding areas of east Karpathos coasts. North - central Aegean and specific, eastern of Naxos Isl., including the sea areas along north of Amorgos Isl., the north offshore areas of Mykonos Isl. and southeast of Andros Isl., were emerged with low MAV values ranging from 115 – 127%. In the straits of the central – eastern Aegean, were also presented low values of MAV, with the lowest appeared in the surrounding area of Ikaria Isl. South and eastern shores of Halkidiki, the eastern offshore region of Diapontian Islands in the Ionian and the surrounding sea areas, were presented high values of MAV, respectively; statistical parameters of some of the aforementioned regions are presented in Table 13.

Regarding inter – annual variability as presented in Figure 33, it is evident, that in general low values were presented, with the overall highest value of IAV observed along the southern coasts of Crete Isl., 25.52 % (35.22 °N 23.97 °E). South shores of Pelopponece, Gulf of Patras and Korinthos, as well as the offshore areas between Gyaros, Kythnos and Kea islands, were also presented higher IAV values, compared with the rest Aegean, ranging from 10 - 15 %, respectively.

The spatial distribution of IAV over the Ionian Sea in general displayed higher values, compared to the Aegean; nevertheless, the overall highest value in this region was located in the south Ionian and did not exceed 17 %. Regions with the lowest variability were, the surrounded areas of Antikythera Isl. with values ~ 6 % and the extended area between western part of Chios Isl. and the northern part of Astypalaia Isl., (~ 7 % and 9 %, respectively). The overall lowest value of MAV was observed in the northwestern parts of Crete Isl., including the sea areas around the

point 34.66 ° N 24.06 °E (~ 6 %); similar results as the findings of Soukissian, Karathanasi, and Zaragkas [79].

Table 14. The statistical parameters of the areas with the highest and lowest values of IAV of WPD, in the Greek seas.

Sea Areas	**Coordinates** °	**WPD** W/m^2	**Median** W/m^2	**Std** W/m^2	**MAV** %	**IAV** %
South of Crete	34.66°N 24.06°E	456.69	212	26.80	139.65	5.86
West Kythera	36.16°N 22.76°E	493.27	220	29.34	142.46	5.94
South Antikythera	35.78°N 23.27°E	547.19	273	34.30	138.67	6.26
West Chios	38.42°N 25.69°E	612.34	350	45.96	126.95	7.50
West Lesvos	39.06°N 25.69°E	653.34	335	50.91	133.87	7.79
Gulf of Patras	38.25°N 21.66°E	192.88	62.59	29.26	219.27	15.17
South Peloponnese	36.83°N 22.25°E	148.70	8.32	37.28	414.92	25.07
South coasts of Crete	35.22°N 23.97°E	146.79	13.46	37.47	396.07	25.52

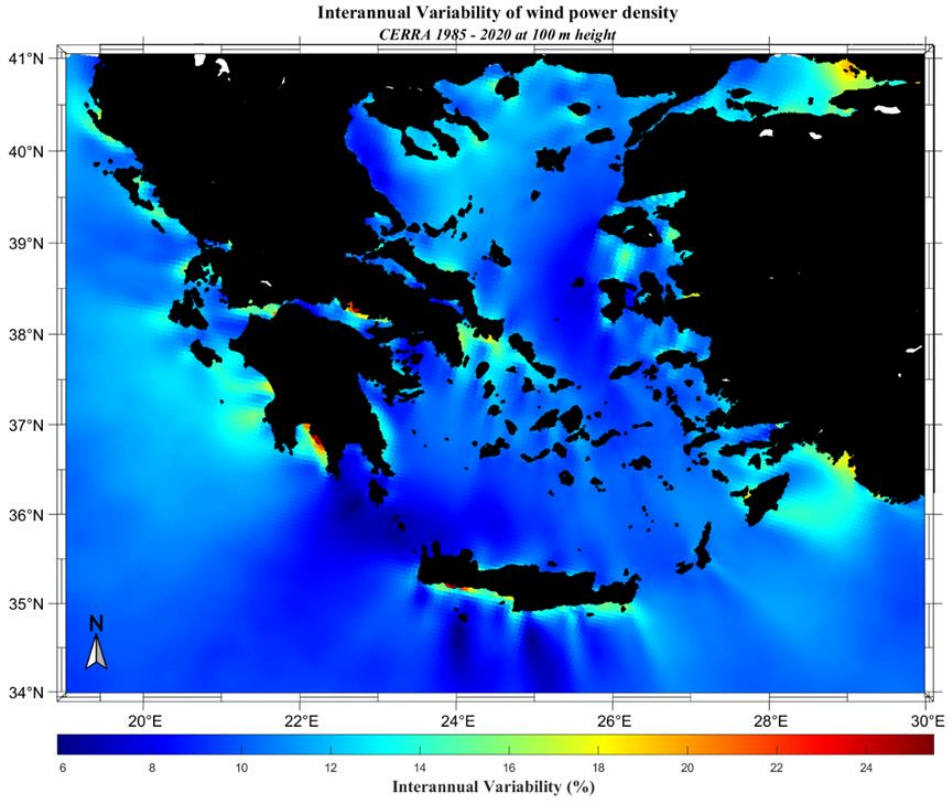

Figure 33. The spatial distribution of inter - annual variability of wind power density in the Greek seas.

4.3.2. Monthly time scale

The spatial distribution of mean monthly WPD from January to December is presented in Figure 34. Regarding mean January's WPD, higher values were observed all over the Aegean, compared to the Ionian Sea. WPD values in the Greek seas for this month, were ranging from 50 – 1265 W/m^2, with the majority of regions in the Aegean exceeded values of 600 W/m^2, while the Ionian presented values in range 500 – 600 W/m^2.

The higher values were observed in the north Aegean in range between 750 and 1265 W/m^2, especially in the sea areas south of Samothrace Isl. down to north shores of Lemnos Isl. covering the entire east offshore area of Saint Efstratios Isl.; similar results with [36, 79], where in winter the highest values the Greek seas were observed in the north Aegean ~ 1000 W/m^2.

Significant values were observed over the entire region of the central Aegean, ranging from 600 – 950 W/m^2, with the highest WPD values located in the strait of Cavo D'Oro, covering the entire area from west Andros Isl. up to west areas of Gyaros Isl. Both west and east areas near Crete coasts were also presented high values of WPD, covering the offshore areas up to south of Kythera Isl., and SE coasts of Karpathos Isl., respectively. More details about the areas presented interesting WPD values are presented in Table 15.

Table 15. The statistical parameters of the areas with the highest and lowest values of mean monthly WPD for January, in the Greek seas.

Sea Areas	**Coordinates** °	**WPD** W/m^2	**Median** W/m^2	**Std** W/m^2
South Samothrace	40.19°N 25.29°E	1265.7	1088	431
Saint Efstratios	39.50°N 25.51°E	1102.4	1073	310.36
Cavo D'Oro	38.01°N 24.62°E	940.99	921	259.68
West Crete	35.34°N 23.28°E	931.27	946.81	240.52
South Kythera	36.07°N 22.98°E	871.62	873.86	165.81
East coasts Peloponnese	37.43°N 22.77°E	80.43	77.17	20.90

The patterns of the spatial distribution for February in both the Aegean and the Ionian Seas present higher values in compare with January. Several areas exceeded 1000 W/m^2, such as North Aegean, the extended offshore areas between the complex of Samothrace, Lemnos and Saint Efstratios islands, as well as the offshore areas west of Crete Isl. and in the central Aegean in the strait of Cavo D'Oro.

Large values of WPD were also located in the entire region of central and northern areas of the eastern Aegean, with values ranging from 600 to 1000 W/m^2, while the overall highest was observed in the west offshore areas covering the straits between north Cyclades and the surrounding sea areas west of Gyaros Isl. and east of Kythnos Isl., as well as in the areas NE of Andros and Naxos islands, covering the surrounding area over Amorgos Isl.

Both of the areas near west and east coasts of Crete Isl., including the straits between Kasos and Karpathos islands, presented high values of WPD, reaching ~ 850 W/m^2 and in range 700

– 800 W/m², respectively. In the Ionian Sea, the highest values were noted in the northern sea areas ranging from 500 to 700 W/m², while lower values were observed north of Rhodes Isl., in the straits between the existing complex of islands in the area, in east coasts of Halkidiki, in north Evvoia and mostly in the eastern areas near coasts of Peloponnese; more statistical details are included in Table 16.

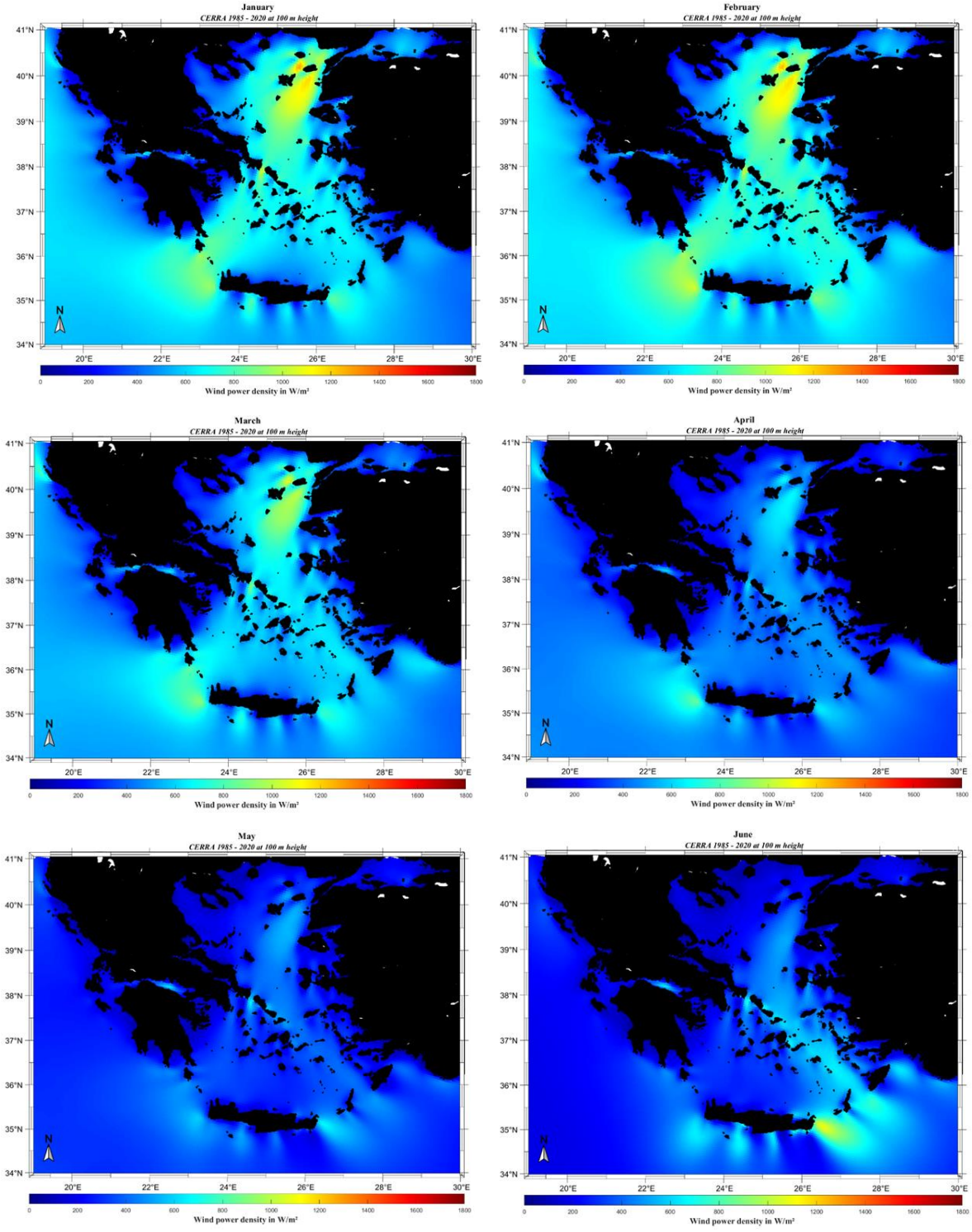

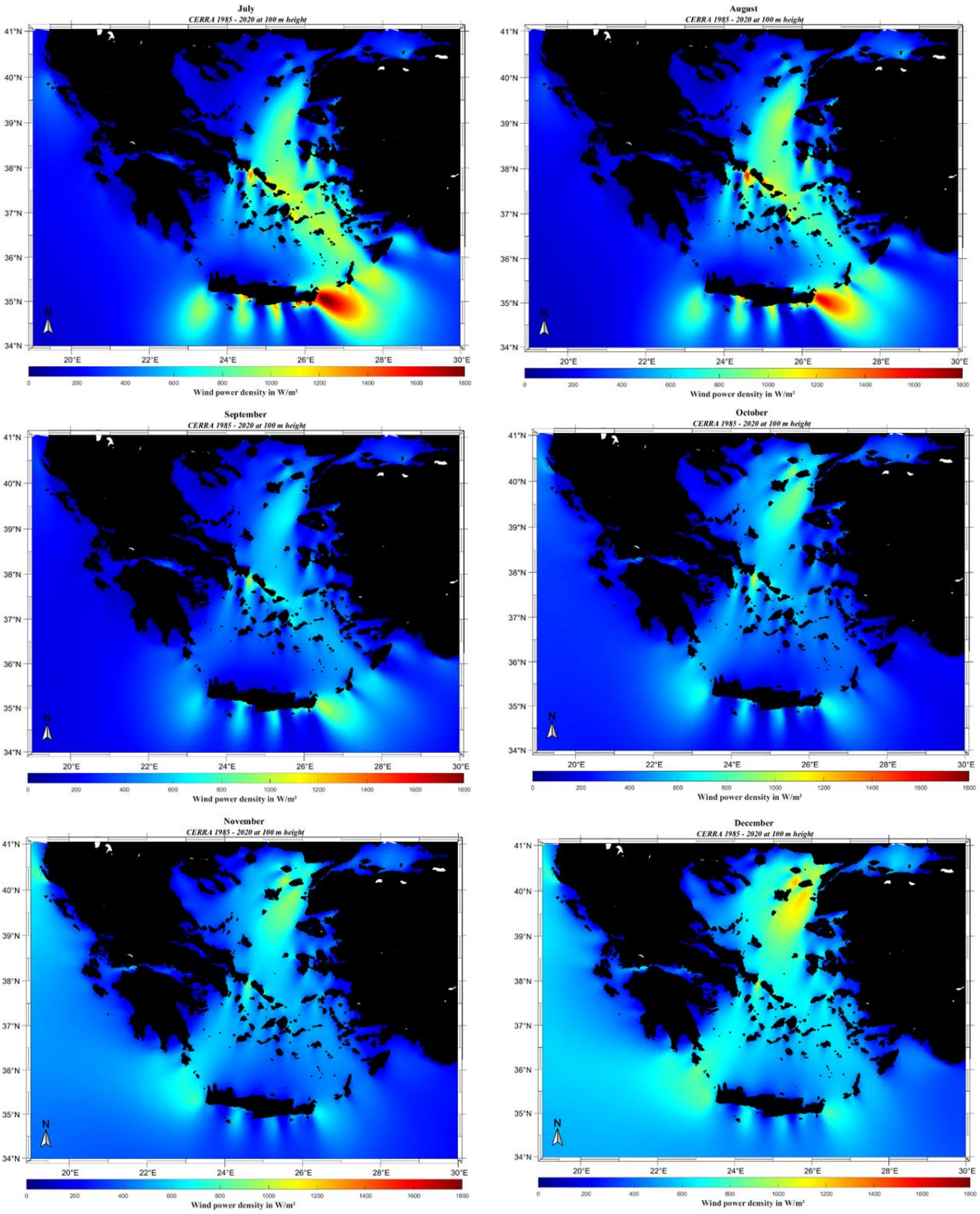

Figure 34. The spatial distribution of mean monthly wind power density in the Greek seas.

In the spatial analysis of WPD for March, a decrease was observed in the entire study area, with the lowest values presented in the Ionian Sea (~200 - 600 W/m²), with an exception of the northern areas with values exceeding 600 W/m². The areas in which the higher values were observed were, the northern Aegean, with the highest located in the offshore areas south of Samothrace Isl. (40.19°N 25.59°E, 1058 W/m²), in the central Aegean covering the straits between the northern Cyclades ranging from 500 – 880 W/m², as well as in the extended area

between west coasts of Crete and the offshore area up to west of Antikythera and south coasts of Kythera and Peloponnese, ranging from 650 to 900 W/m^2 .

Table 16. The statistical parameters of the areas with the highest values of mean monthly WPD for February, in the Greek seas.

Sea Areas	Coordinates °	WPD W/m^2	Median W/m^2	Std W/m^2
South Samothrace	40.19°N 25.59°E	1236.7	1185	385.03
Saint Efstratios	39.56°N 25.46°E	1122	1050	296.66
West Crete	35.33°N 23.34°E	1027	982.18	309.76
Cavo D'Oro	37.92°N 24.59°E	1010	938	416
Kythera/Antikythera	36.01°N 23.09°E	954	916	274
North coasts of Ikaria	37.57°N 25.93°E 37.56°N 25.99°E	809 835	766 793	238 244
North Ionian	40.34°N 19.24°E	810	812	348
NE Astypalaia	36.41°N 26.24°E	751	722	214

A significant decrease was presented in the entire offshore Greek area regarding April, with values of WPD ranging from 40 – 843 W/m^2. The range of values characterized the Ionian Sea, was 200 – 650 W/m^2, with the higher values presented in the northern Ionian; while in the Aegean values from 200 to 843 W/m^2 were observed, with the overall maximum located in the west area of Crete Isl. The extended area between south coasts of Kythera Isl. and west coasts of Crete Isl., was the area in which the highest values regarding this month were presented, ranging from 600 - 843 W/m^2. While in the north and central Aegean, where in the previous two moths the highest WPD were noticed, values did not exceed 670 and 570 W/m^2, respectively.

From the spatial analysis of May, a further diminish was observed over the Greek Seas, ranging from 40 to 664 W/m^2. The overall highest value was located in the east offshore areas of Crete Isl., (35.12 °N 26.53°E, 664.76 W/m^2), while the lowest was observed near the eastern coasts of Peloponnese at the point 37.61°N 23.19°E, ~ 45 W/m^2. In general, areas that dominated in the previous months, such as northern and central Aegean, as well as the eastern offshore areas of Crete Isl., emerged with lower values of WPD, ranging from 400 to 500 W/m^2; 200 – 550 W/m^2 and 300 – 570 W/m^2, respectively. While the highest values that were observed in the Ionian Sea, did not exceed 400 W/m^2.

In June, the values of WPD showed a decrease in the Ionian Sea, while in the Aegean compared to May, WPD was increased. In more detail, the highest values were observed in the southeastern Aegean ranging from 600 – 1091 W/m^2, with the overall highest value located in the east shores of Crete and the surrounding areas of the point 35.12°N 25.64 °E (1091 W/m^2). Increased values of WPD, compared to May and April were also observed in the straits between Kasos, Karpathos and SW shores of Rhodes islands, covering the entire surrounding area, ranging from 700 – 800 W/m^2. In the northern parts of Cyclades complex, in the central Aegean

up to eastern central and SE Aegean with values in range between 600 and 700 W/m^2. Regarding the Ionian, there was not a significant change in the spatial distribution of WPD from the previous months, as the values were still low and did not exceed 400 W/m^2.

As expected, the overall highest values of WPD observed in July, ranging from 50 to 1856 W/m^2; more statistical details are provided in Table 17. The Etesians operate over the Aegean Sea this month, and since the highest wind speeds were recorded in July in the east shores of Crete Isl., it was anticipated that the overall highest value of WPD will be around the same area, 35.07°N 26.52°E, ~ 1850 W/m^2.

Table 17. The statistical parameters of the areas with the highest values of mean monthly WPD for July, in the Greek seas.

Sea Areas	**Coordinates** °	**WPD** W/m^2	**Median** W/m^2	**Std** W/m^2
East Crete	35.07°N 26.52°E	1856	1882	449
West Andros	37.86°N 24.64°E	1352	1467	495
NE Tinos	37.73°N 25.10°E	1167	1195	332
North Amorgos	36.91°N 25.73°E	1147	1154	273
South Kasos	35.24°N 27.12°E	1118	1005	230
South coasts of Ikaria	37.50°N 26.04°E	1013	1061	256
SW Chios	38.03°N 26.14°E	918	927	297

The second area with the highest values of WPD was observed in the central Aegean, and more specifically, in the west shores of Andros Isl. including all the offshore areas of north and west Gyaros Isl., along east shores of Kythnos Isl.; northeastern shores of Andros, Tinos, Mykonos islands, as well as the northern offshore areas of Amorgos and Astypalaia islands, in range 900 – 1162 W/m^2. Furthermore, values that exceeded 1000 W/m^2 were also noted in the south east shores of Crete Isl., while in the western coasts lower values compared to the east side, nevertheless still high, ranging from 800 to 950 W/m^2.

The northern parts of the Aegean were also presented higher values than May and April, ~ 900 W/m^2, with the highest observed in the SN offshore areas of Psara Isl. and southern areas of Chios Isl. In northern Ionian, decreased values of WPD were noticed, ranging from 200 to 400 W/m^2, while the overall lowest values were located in the shores of Halkidiki and Peloponnese, respectively.

In August similar spatial patterns were observed in the Greek Seas, with the Aegean presented higher WPD values due to the Etesians, compared to the Ionian, which ranges between 100 – 300 W/m^2. The higher values were again observed in the eastern souths of Crete Isl., lower than July ~ 1680 W/m^2, expanding all over the offshore sea area of SW Kasos, Karpathos and Rhodes islands, as well as the areas near SE coasts of Crete Isl., with values exceeding 1400 W/m^2.

Increased values compared to July, observed in the central Aegean and more specific, in the extended areas between west and east shores of Andros Isl., up to north offshore areas of Serifos Isl. and in the northeastern areas of Tinos, Mykonos and Naxos islands, exceeding 1000 W/m^2 respectively. Moreover, higher values were observed in the northern Aegean, ranging from 600 to 900 W/m^2, with the highest values observed west of Psara Isl.; for more statistical parameters, refer to Table 18.

The spatial distribution patterns emerged for September were similar with those noticed in August, nevertheless, the WPD values were significantly decreased and similar with those that have been observed in March. The higher values were observed in the central Aegean west of Andros Isl. (37.86°N 24.64°E, ~ 1000 W/m^2), covering the surrounding area up to north Gyaros and east Kythnos islands. The areas near east coasts of Crete Isl. were the second region that presented high values of WPD along with the straits between Kasos and Karpathos islands, ranging from 600 – 980 W/m^2. Notable WPD values were also observed in the north shores of Cyclades, covering the area up to eastern central Aegean to WS and WN coasts of Ikaria Isl. in range 500 – 850 W/m^2; as well as the northern Aegean with values around 650 W/m^2. Regarding the Ionian Sea, values near 300 W/m^2 were noticed.

Table 18. The statistical parameters of the areas with the highest values of mean monthly WPD for August, in the Greek seas.

Sea Areas	**Coordinates** °	**WPD** W/m^2	**Median** W/m^2	**Std** W/m^2
East Crete	35.12°N 26.53°E	1625	1638	352
West Andros	37.86°N 24.64°E	1543	1570	556
SW Kasos	35.27°N 26.76°E	1107	1123	208
SE Naxos	36.97°N 25.69°E	1034	1064	244
NE Mykonos	37.52°N 25.42°E	1025	1057	244
West Lesvos	39.10°N 25.51°E	986	963	277
South shores of Ikaria	35.50°N 26.04°E	950	932	223

As for October, the spatially patterns noticed, were similar to March, with values ranging near September's WPD values, with an exception the increase that was observed in the northern Aegean. More specific, the highest WPD values for this month were observed in the central Aegean, covering the extended area between west coasts of Andros and east coasts of Kythnos islands, in range 600 - 1000 W/m^2; as well as the northern parts of Cyclades with values exceeding 700 W/m^2.

A decrease was noticed, compared to the previous months, in the eastern parts of the Aegean, with exceptions the east coasts of Crete Isl. and the areas near west coasts of Ikaria Isl., respectively. In the northern Aegean values were higher than those observed for September, with south of Samothrace Isl. (~ 850 W/m^2) and the extended area of south Lemnos Isl. up to east Saint Efstratios Isl., ranging from 700 to 860 W/m^2. Higher values were observed in the west coasts of Crete Isl. too, covering the entire offshore area up to south Kythera Isl., while an increase was noticed in the northern parts of the Ionian Sea.

Regarding November, the WPD values were clearly increased in the offshore area of Greece, ranging from 50 – 995 W/m^2. The areas in which the higher values of WPD presented were, the northern Aegean ranging from 750 to the highest value in the south offshore areas of Samothrace Isl. ~ 995 W/m^2; the central Aegean and the surrounding offshore areas of the northern Cyclades, in range 600 – 890 W/m^2; the west coasts of Crete Isl., including the extended area up to Kythera Isl., with approximately 750 W/m^2, as well as the offshore areas near east coasts of Crete Isl., with WPD ~700 W/m^2. Higher values were also observed in the Ionian Sea, compared to the previous moths, with the highest in the northern regions and more specific west of Diapontian islands ~ 650 W/m^2.

The spatial distribution of December exhibited with a further increase in both the Aegean and the Ionian Seas. The most significant values of WPD were observed in the northern and central parts of the Aegean, with values exceeded 1200 and 900 W/m^2, respectively. Areas that also corresponded to high values of WPD were near both west and east coasts of Crete Isl., with values ranging from 600 – 850 W/m^2, the straits between eastern Aegean's islands, as well as the northeastern part of the Cyclades in the central Aegean, in range 600 – 700 W/m^2.

The spatial distribution of WPD in the Greek seas from January to December had shown significant variations between individual months and follows the same patterns as the wind speed's monthly spatiotemporal distribution. Specifically, the available WPD resources follow the same circular (seasonal) pattern that was observed in terms of mean monthly wind speed. Started in December with relatively high values (exceeding 900 W/m^2 in a large part of the Aegean and around 550 W/m^2 in the Ionian), reaching the highest values for the months of winter in February, in the northern and central Aegean. When in spring (MAM) a gradual decrease of WPD was noticed with the overall lowest values observed in May. Increased values of WPD were again noticed for summer months (JJA), with the overall highest observed in July ~ 1900 W/m^2, followed by August. Once again, the Ionian presented lower values of WPD compared to the Aegean, while the highest WPD values were observed in offshore areas with deep waters, unsuitable for the development and the installation of an OWF.

4.3.3. Seasonal time scale

The spatial distribution of mean seasonal WPD is presented in Figure 35, from winter to autumn. Regarding winter, the entire region of the Greek seas emerged with high values of WPD, ranging from 50 to 1200 W/m^2. The higher values were observed in the northern Aegean, with values exceeding 1250 W/m^2, in the extended area between east of Lemnos and south Samothrace islands, as well as over the offshore areas east of Saint Efstratios Isl. Significant values of WPD were also observed in both of the offshore areas near west and east coasts of Crete Isl., where WPD exceeded 900 and 800 W/m^2, respectively. In the central eastern Aegean, WPD emerged with values in range between 700 and 980 W/m^2, while WPD that exceeded 600 W/m^2 were observed in the Gulf of Patras. In general, winter could be characterized as the season with the smoother spatial distribution of WPD, since high values were presented in both the Aegean and the Ionian Seas.

In spring, a notable decrease was observed over the Greek Seas. The values presented were not exceed 770 W/m^2; the overall highest WPD was located in the offshore areas near west coasts of Crete Isl., including the surrounding areas of the point 35.29°N 23.27°E, with corresponding WPD value of ~ 773 W/m^2. The east offshore region of Diapontian Islands in the north Ionian Sea, as well as, the offshore areas east of Rhodes Isl., with values ranging from 200 to 300 W/m^2,were the areas that presented from the lower values of WPD.

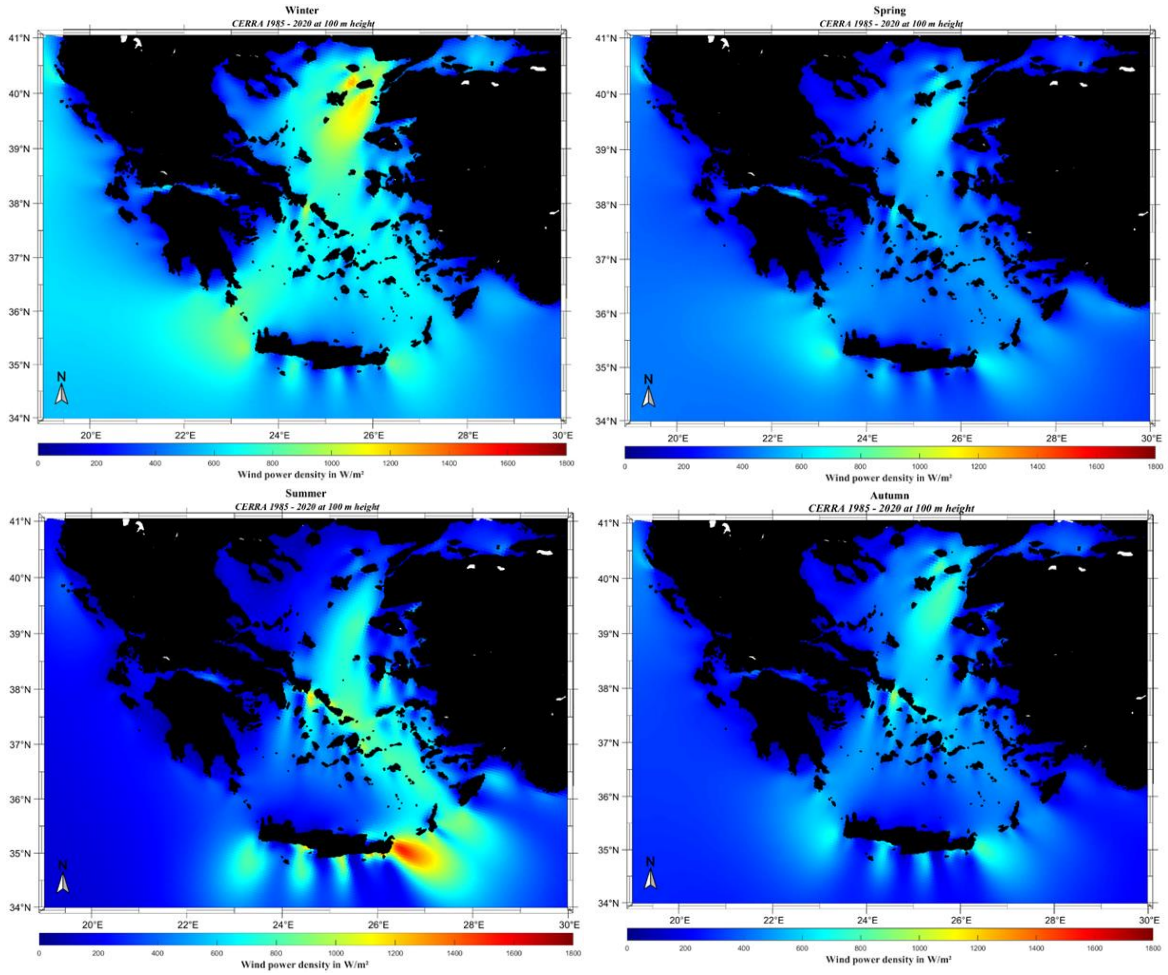

Figure 35.The spatial distribution of mean seasonal wind power density in the Greek seas.

Summer, represented by the windiest months within a year, thus as it was expected, the overall highest WPD values were noticed for this season in the Aegean Sea, compared with the decrease observed in the Ionian Sea (200 – 350 W/m^2). The areas in which the highest WPD values emerged were, the extended area between east coasts of Crete Isl. (with the overall higher exceeded 1500 W/m^2 at point 35.06°N 26.57°E), Kasos Isl., southeast of Karpathos Isl. and southwest of Rhodes Isl., equipping the straits of this complex of islands with great wind power potential, ranging from 800 – 1530 W/m^2. In the northern central and eastern Aegean, values of WPD were ranging from 700 to 1000 W/m^2, with the highest values observed in the strait of Cavo D'Oro and the offshore northern Cyclades, in Ikaria Isl., and east of Amorgos Isl., respectively. Northern Aegean presented lower values than eastern and central Aegean, corresponding to WPD values in range between 300 and 800 W/m^2, with the highest values observed in the southern offshore areas of Psara Isl., up to west coasts of Lesvos Isl.

Decreased WPD values were observed in autumn, completed the seasonal pattern that was already noticed in the previous sections in the Greek seas. Both of the offshore areas near east and west coasts of Crete Isl., and in specific regions of the central Aegean, with the overall highest WPD values located west of Andros Isl. (37.87°N 24.58°E ~960 W/m^2); as well as, in the northern Aegean, south of Samothrace Isl. (40.23°N 25.60°E ~855 W/m^2).

5. Evaluation of the NREL – 15MW wind turbine in selected areas

5.1. Mean annual energy production

The spatial distribution of the mean annual produced energy from the selected WT, is depicted in Figure 36, where the patterns emerged were similar to the spatial distribution of mean annual wind speed, that already presented in the previous section, in Figure 14. In general, clearly the Ionian Sea emerged with significant lower magnitude of produced energy potential, compared to the Aegean. The overall highest annual produced energy was observed in the areas near east coasts of Crete Isl., with the highest value at the point 35.16°N 26.55°E and corresponded estimated energy ~ 78,629 MWh/year, while the lowest values were noted near coasts of Halkidiki and Peloponnese, as well as in the Turkish coasts east of Rhodes Isl., with values close to 5,132 MWh/year.

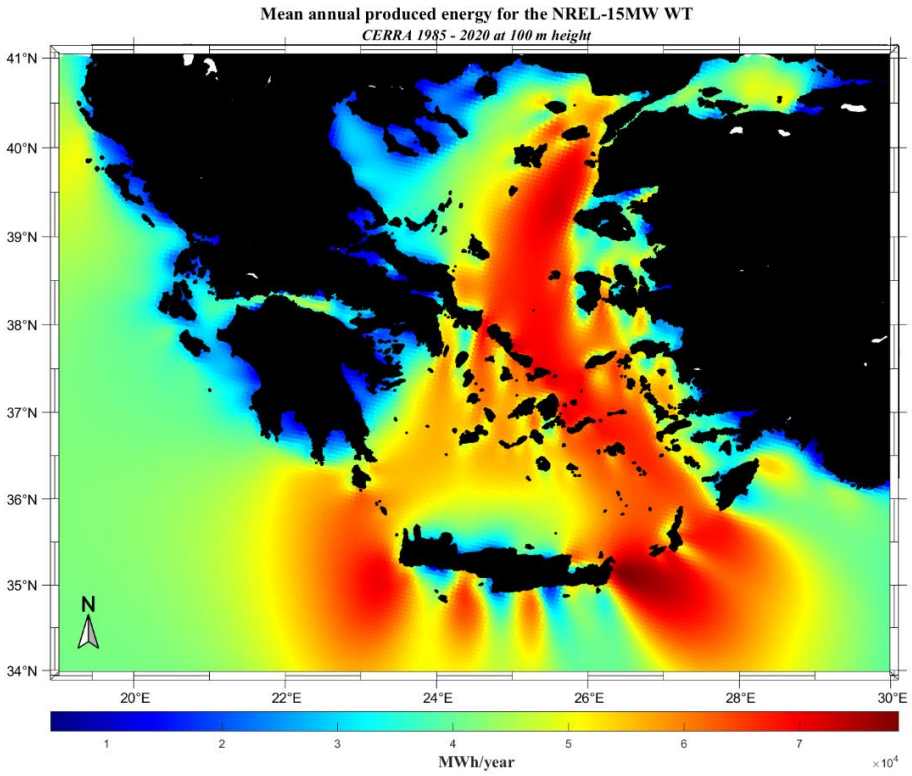

Figure 36. The spatial distribution of the mean annual produced energy for the NREL-15 MW wind turbine, in the Greek seas.

The surrounding areas of Crete Isl., including some regions of the northern and southern parts of the island, especially in the west and east areas, extending from coasts up to south Kythera and SW Rhodes islands respectively, were the areas in which the highest values of mean annual produced energy observed, ranging from 62,882 to 78,629 MWh/year, as well as in the northern parts of the Aegean, around the point 39.38° N 25.60°E with corresponded wind energy ~72,514 MWh/year. Significant high produced energy values were also emerged in the NE offshore

areas of Andros Isl., around the point 37.79° N 25.05° E, with values close to 72,055 MWh/year, while equivalent estimated production was noticed in the east areas of Mykonos, SE of Naxos and slightly lower in the surrounding areas of Astypalaia islands, as well as in the extended area between north of Gyaros Isl., and east offshore areas of Serifos Isl., respectively.

5.2. Mean annual capacity factor

In this section the mean annual CF was estimated and its spatial distribution in the Greek Seas, is presented in Figure 37. In general, the expected spatial patterns were emerged, similar to those that have been observed for the mean annual produced energy, with the overall maximum CF located in the eastern offshore areas of Crete Isl., ~60% (35.16 °N 26.55° 59.79%). The areas in which the higher CF values emerged were, the extended area between east Crete Isl., covering the straits between Kasos and Karpathos and SW Rhodes islands, with values that exceeded 50%; values higher than 50% were also emerged in the eastern parts of Cyclades down to Astypalaia Isl., as well as in the northern Aegean, in the extended areas between Lesvos and south Lemnos and Saint Efstratios down to Psara and Chios islands, respectively.

High CF values were also presented in the south and west coasts of Crete Isl., expanded up to south coasts of Peloponnese, with values ranging from 40 to 55%. Lower CF values compared to the Aegean, were observed in the Ionian Sea (30 – 38%), with the highest values located in the west areas of Diapontian Islands, while lower values appeared in the surrounding areas of coasts of Halkidiki ~16%, in the NW and some south regions near coasts of Crete Isl., ~22%, as well as in the SE coasts of Rhodes Isl., with values lower than 25%.

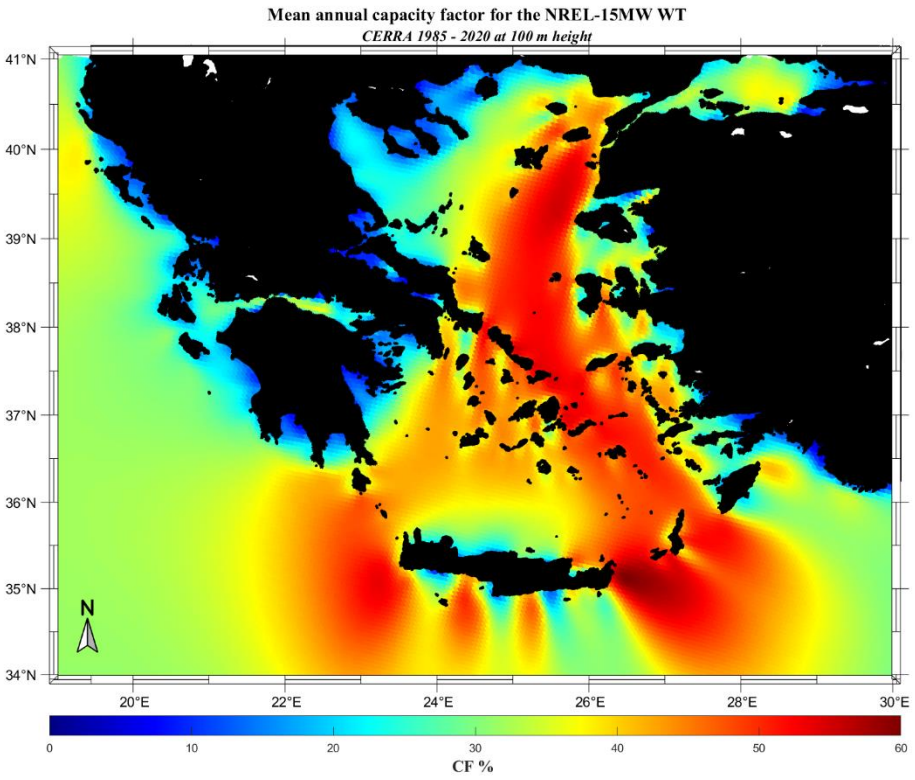

Figure 37. The spatial distribution of the mean annual CF for the NREL-15 MW wind turbine, in the Greek seas.

5.3. Time percentages within the operational limits of the wind turbine

5.3.1. Annual time scale

The spatial distribution of the annual time percentages of wind speed within the cut – in and cut – out limits, is presented in Figure 38, ranging from ~30 to 90 %. The overall highest percentage was observed in the areas extending between near west coasts of Crete Isl., (35.27°N 23.08°E 90.48 %) up to west Antikythera and south Kythera islands, ranging from 82 to 90 %. In general, high percentages were also observed in the entire Aegean, including the offshore areas between Saint Efstratios and Lemnos islands (72 – 80 %), as well as, in the northern parts of the central Aegean, with the northern and eastern parts of Cyclades complex, exceeded 80%. Furthermore, in the east and SE Aegean, including the straits between eastern Aegean's islands and in the east parts of Crete Isl., including the extended area between Crete, Kasos and Karpathos islands, ranging from 71 to 85%.

Lower time percentages were observed in the Ionian compared to the Aegean Sea, ranging from 62 to 75 %, with the higher values observed in both the northern and the southern areas of the Ionian. Areas near coasts of Halkidiki (42 – 65 %) and Peloponnese (38 – 69%), were also emerged with lower percentages. Noted that despite that both west and east areas near coasts of Crete Isl., emerged with the overall maximum percentages, lower values were also observed both in the north and south, SE coasts of the island (45 – 69%). Moreover, areas in which lower percentages also noticed were, the eastern parts of Rhodes Isl. (~58%), east parts of Gyaros Isl. (~72 %) and north of Kea Isl. (~62%).

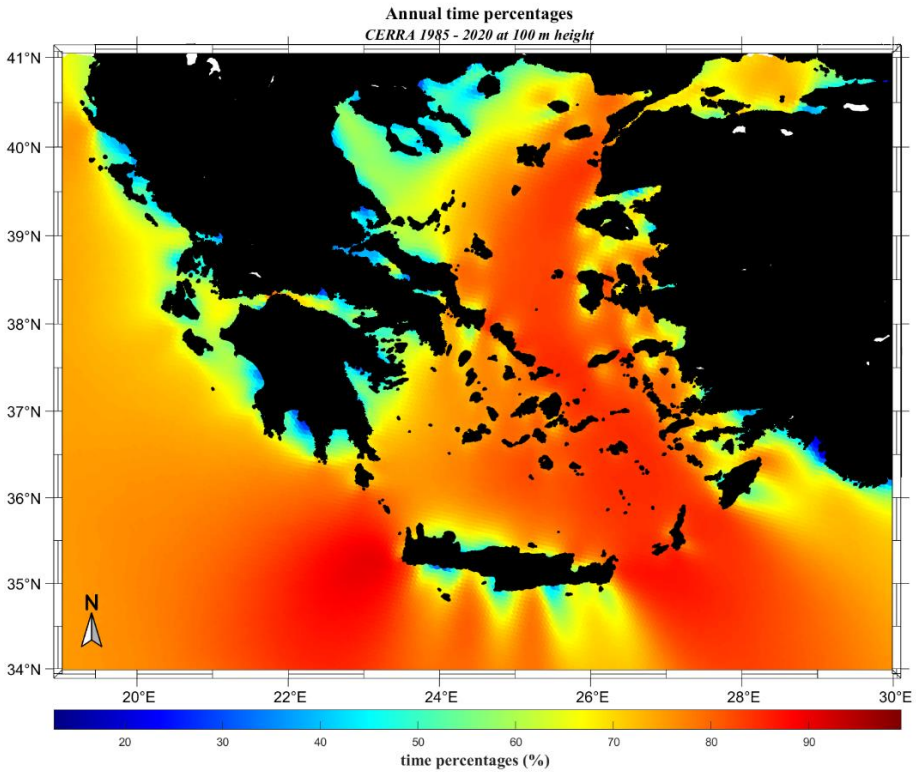

Figure 38. The spatial distribution of annual time percentages within the operational limits of the NREL 15 MW WT.

5.3.2. Monthly time scale

Regarding the spatial distribution of the monthly time percentages, depicted in Figure 39, as anticipated, elevated values were presented in the Greek Seas, for July and August. For this time scale, the variability observed between January to December, for the mean monthly wind speed, as it was expected, was also emerged in the particular spatial analysis, following the same spatiotemporal patterns. During January and February, notable wind speeds have been observed in both the Aegean and the Ionian seas, indicated that for the majority of these areas the time percentages will emerge high, respectively.

In general, higher percentages observed for January, compared to February, while for both January and February, the overall highest percentage observed in the areas near west coasts of Crete Isl., with values close to 91 and 88 %, respectively. The areas in which the higher percentages emerged were, the extended offshore areas between west coasts of Crete Isl., the south coasts of Peloponnese (82 – 91 % and 78 – 88%, respectively), as well as, the areas near east coasts of Crete Isl., up to the surrounding areas of Kasos, Karpathos and SW Rhodes (79 – 80% and 78 – 83 % respectively). In the northern areas of the central Aegean as well as, in the eastern parts, values exceeding 80% were observed, while in the Ionian, high percentages were noticed, ranging from 77 – 81%, for both of the aforementioned months.

In March, similar spatial patterns to those observed in February emerged, with percentages spanned in the same regions, and exhibited an equivalent magnitude to that observed in February. Regarding April, a spatially decrease was observed, as expected, with the higher values located in the extended area between west Crete Isl., and south coasts of Kythera Isl., (79 – 88 %), as well as in the extended area between near east coasts of Crete and Kasos (81 – 84%), while notable lower percentages observed in the south coasts of Crete Isl., with the lower located in both southwest and southeast coastal areas (59 % and 49 %, respectively).

In the Ionian Sea, decreased percentages were noted, ranging from 60 – 79%, as well as in the northern Aegean, with values from 45 to 80%. The central Aegean emerged with high percentages (~80%) in the northern parts of Andros and Tinos islands, as well as in the surrounding areas of Astypalaia Isl.; nevertheless, lower values were presented in the western regions of the central Aegean ranging from 50 to 72%, with the overall lowest observed in the offshore area between Kea Isl., and Evvoia.

The spatial distribution regarding May, was emerged with a total decrease in the percentages in the Greek Seas compared to the previous months, with the highest percentages located again in the west and east coasts of Crete Isl., (87% and 84 %, respectively). June, presented similar spatial patterns, with greater values of percentages; the extended area between the west coasts of Crete and Kythera, exceeded values of 90%, while in the offshore areas near east coasts of Crete Isl., up to south regions of Kasos and Karpathos islands, values ranging from 85 to 90 %, were observed.

The Ionian offshore areas presented lower percentages compared to the Aegean, for both May and June, in a range between 35 – 76 % and 42 – 78 %, respectively, while in the east offshore areas of Peloponnese, as well as in the western parts of the central Aegean lower percentages (50 – 68%) were noticed. Areas in which higher values observed were, the north parts of Cyclades complex, including the northern parts of Andros, Tinos, Mykonos islands (79 – 80%), east Naxos Isl. ~78 % and the surrounding areas of Astypalaia Isl., exceeding 85%.

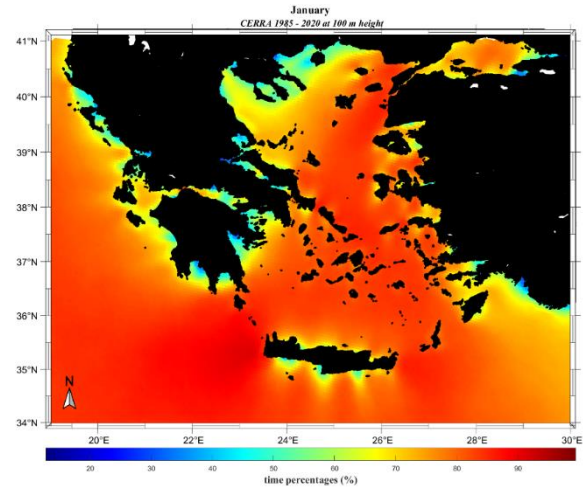
January
CERRA 1985 - 2020 at 100 m height
41°N
40°N
39°N
38°N
37°N
36°N
35°N
34°N
20°E
22°E
24°E
26°E
28°E
30°E
N
20
30
40
50
60
70
80
90
time percentages (%)

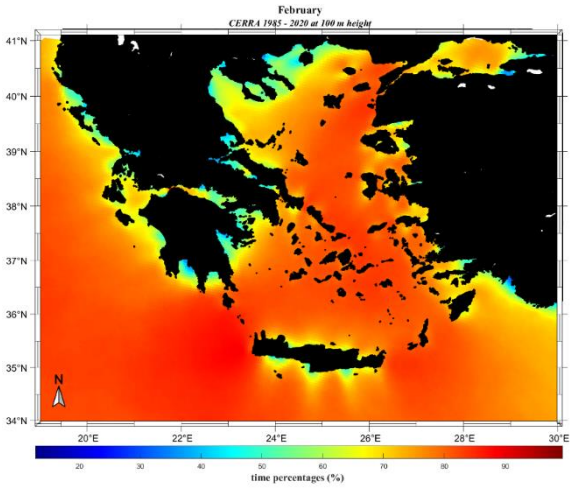
February
CERRA 1985 - 2020 at 100 m height
41°N
40°N
39°N
38°N
37°N
36°N
35°N
34°N
20°E
22°E
24°E
26°E
28°E
30°E
N
20
30
40
50
60
70
80
90
time percentages (%)

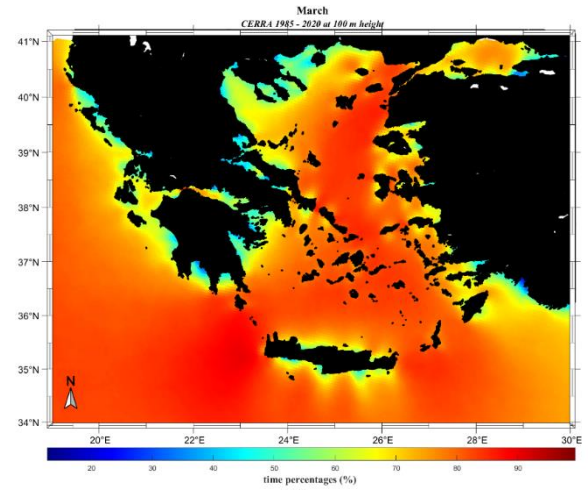
March
CERRA 1985 - 2020 at 100 m height
41°N
40°N
39°N
38°N
37°N
36°N
35°N
34°N
20°E
22°E
24°E
26°E
28°E
30°E
N
20
30
40
50
60
70
80
90
time percentages (%)

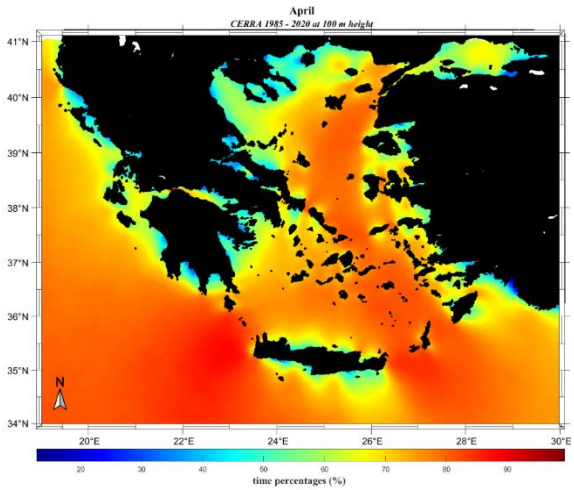
April
CERRA 1985 - 2020 at 100 m height
41°N
40°N
39°N
38°N
37°N
36°N
35°N
34°N
20°E
22°E
24°E
26°E
28°E
30°E
N
20
30
40
50
60
70
80
90
time percentages (%)

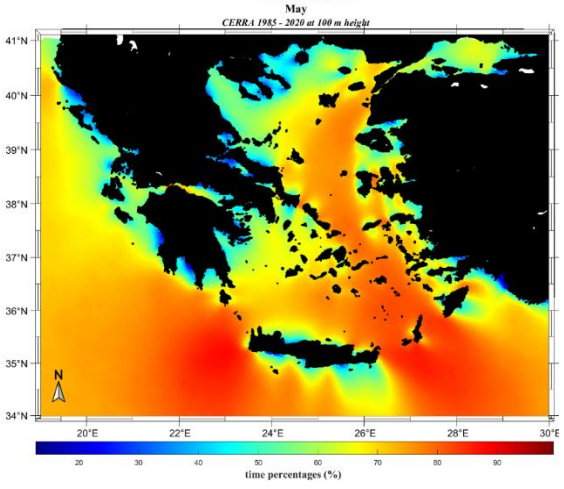
May
CERRA 1985 - 2020 at 100 m height
41°N
40°N
39°N
38°N
37°N
36°N
35°N
34°N
20°E
22°E
24°E
26°E
28°E
30°E
N
20
30
40
50
60
70
80
90
time percentages (%)

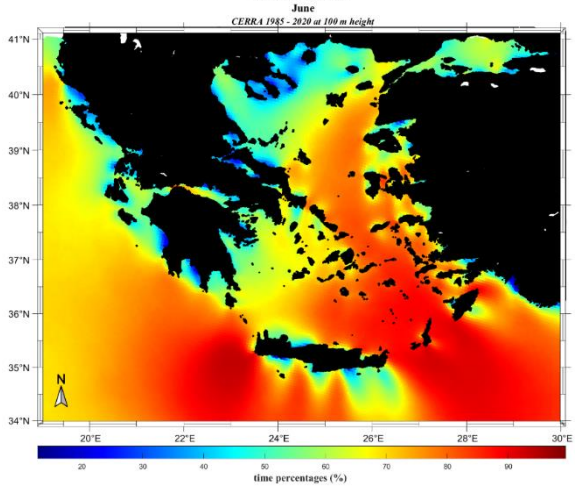
June
CERRA 1985 - 2020 at 100 m height
41°N
40°N
39°N
38°N
37°N
36°N
35°N
34°N
20°E
22°E
24°E
26°E
28°E
30°E
N
20
30
40
50
60
70
80
90
time percentages (%)

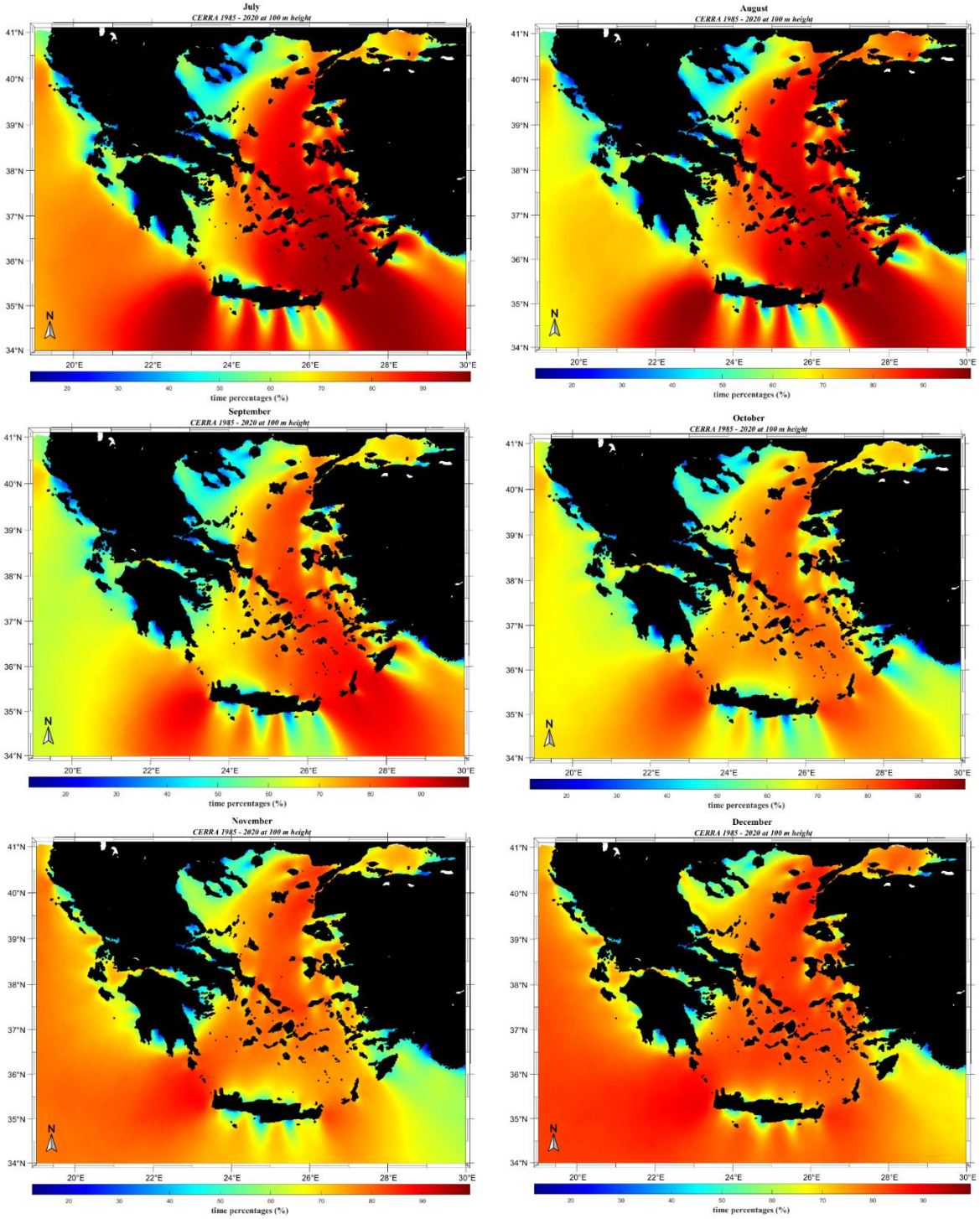

Figure 39. The spatial distribution of monthly time percentages from January to December, of wind speed within the operational limits of the NREL - 15 MW WT.

Regarding July, increased values of time percentages were emerged over the entire area of both the Aegean and the Ionian Seas. As anticipated, due to the fact that July was the month in which the highest wind speed values have been noticed, percentages exceeding 95% were observed, in the extended area between east coasts of Crete Isl., and south coasts of Rhodes Isl., including the offshore areas up to Astypalaia and Kos islands, with the overall highest percentage observed at point (34.70°N 27.79°E, ~99%). Similar spatial patterns, with some differences

appeared in August, with the overall highest values located at point 35.27°N 27.24°E, with values close to 99%, south of Karpathos Isl.

Lower, but not insignificant percentages, were observed over the entire north, specifically in the extended area between south of Samothrace and Chios islands (79 – 91%) and east Aegean, with values ranging from 67 – 94 %, with the lower located in the south coasts of Lesvos Isl. for both July and August. As for the Ionian, lower values were noticed, compared to July (~79%) for August (~70%), while low percentages were also emerged in the south and southeast coasts of Crete Isl. (~ 48 %), as well as in the eastern offshore areas of Peloponnese (~65 %) and Rhodes Isl. (~50% for July and 46% for August).

Regarding September, the highest percentage (decreased compared to July and August), was noted in the south offshore areas of Karpathos Isl. (35.28° N 27.19° E ~ 91%), while even lower values presented for October, with the overall maximum percentage located in the areas near west coasts of Crete Isl. (35.36 23.16 ~ 86.27%). The spatial distribution of the time percentages between these two months was quite different, September emerged with similar patterns with July and August, with high percentages in the central and eastern parts of the Aegean (69 – 85%) and lower to the western parts, while in October the highest values were appeared in both east and west coasts of Crete Isl., the northern parts of the Aegean and in the east regions of the central Aegean, exceeded 73%. For both September and October, the lowest percentages appeared in the south and SE areas near coasts of Crete Isl. (40 – 48 % and 33 – 55%, respectively), in the southeast areas of Rhodes Isl. (~ 52%), and in the northern parts of the north Aegean, east of Halkidiki and SW of Samothrace Isl., with values ranging from 40 to 60%, respectively.

As for November and December, higher values were observed compared to October, both for the Aegean and the Ionian, with the overall maximum percentage in the west coasts of Crete Isl., around the point 35.46 N 23.13 ~89%. In general, in December the higher percentages were emerged in the central, the west and the eastern parts of the Aegean, as well as in the northern regions, specifically in the surrounding area of Samothrace, Lemnos and Saint Efstratios islands, with values exceeded 80%. In November lower values were observed in the central (~ 75%), the eastern parts (~ 77%) and in the south regions of the Aegean (~65%).

Regarding the Ionian Sea, the percentages emerged for November were in a range between 65 to 80 %, with the highest values observed in the northern and southern regions, while higher time percentages were presented for December, exceeded 85%. The areas that showed the lowest time percentages were, the offshore areas east of Rhodes Isl. (55% for November and 65% for December), for both November and December the areas surrounding the coasts of Halkidiki and Peloponnese, with values lower than 60%, for December in some regions south of Crete Isl. (60 – 70%) and in November in the south coastal areas of Crete Isl. (43 – 60%).

In general, the patterns noticed in Figure 39, as it was expected, were following the patterns observed both in the spatial distribution of mean monthly WS and WPD. The overall maximum percentages were noticed in July, while the overall low in May. The Ionian has showed lower percentages compared to the Aegean, nevertheless, exceeded ~60 %. Furthermore, the highest values of percentages within the operational limits of the WT, were located in offshore areas with deep waters, either capable of hosting floating or inappropriate for the development of OWFs.

5.3.3. Seasonal time scale

The spatial distribution of the seasonal time percentages, is presented in Figure 40; the spatial results that was noticed in the monthly spatiotemporal analysis, were also observed in this time scale. Winter, including three months with high percentages, was emerged with high values that exceeded 80%, in the entire Aegean and lower in range between 76 to 83 % in the Ionian Sea.

The highest values were observed in the west parts of Crete Isl., covering the entire area up to south coasts of Kythera and the surrounding regions of Antikythera islands (81 – 89 %), while lower percentages were appeared in the south coasts of Crete Isl. (~67 %), east offshore areas of Rhodes Isl. (~68%) and in the northern Aegean, close to coasts of Halkidiki with values in range between 50 to 70%.

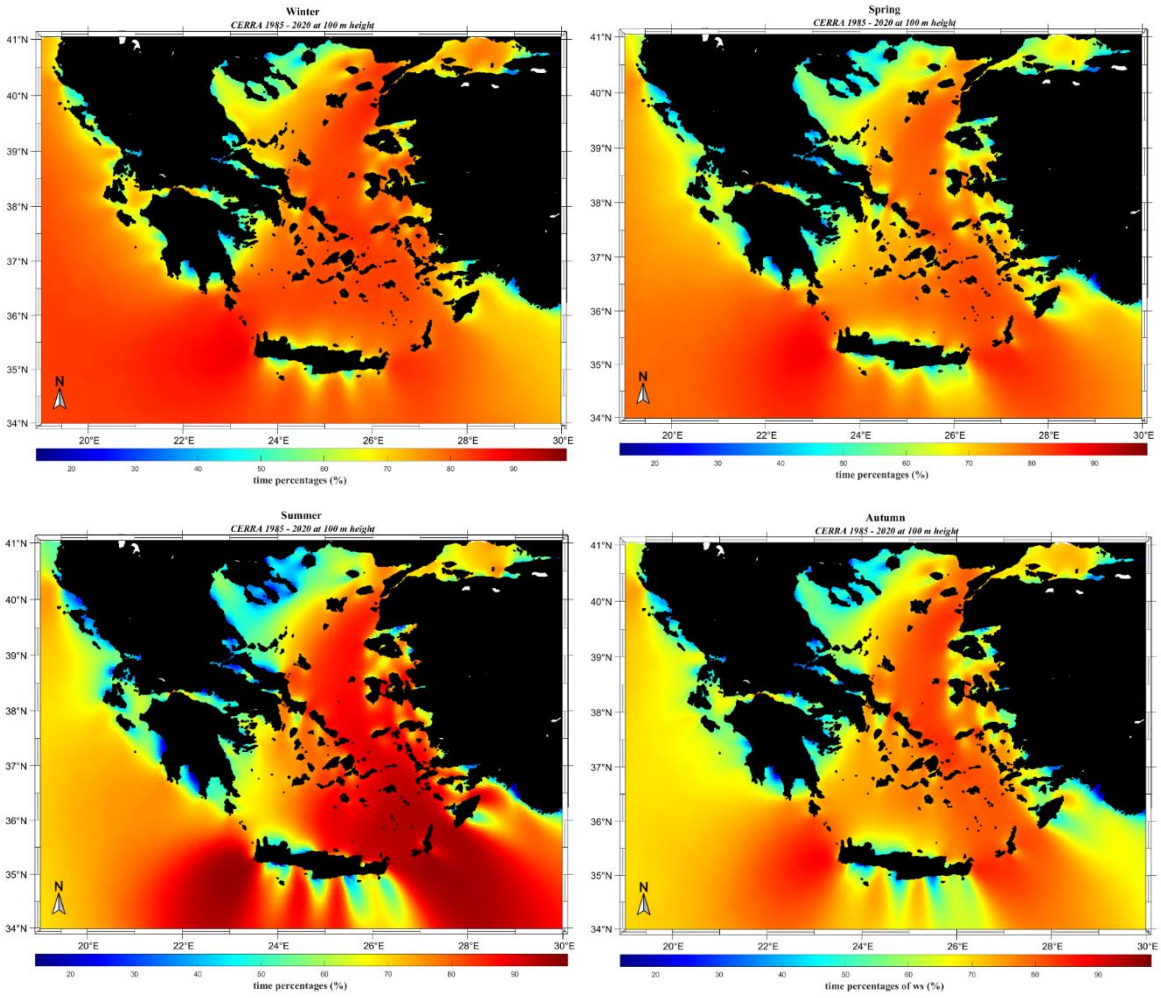

Figure 40. The spatial distribution of seasonal time percentages from winter to autumn, of wind speed within the operational limits of the NREL-15 MW WT.

Regarding Spring, lower percentages were observed compared to winter, with the overall highest values located near west coasts of Crete Isl. (~88%), while south and southeast coasts presented lower values ranging from 45 – 50%. The areas in which lower percentages observed were, the eastern regions of the Ionian, the northern parts of the north Aegean, as well as, areas

in the eastern Aegean, such as the extended area between Lesvos Isl. and Chios Isl. and the northern and eastern parts of Rhodes Isl., ranging from 40 – 70%.

As for the central Aegean, the lower percentages were observed in its western areas, with the overall lower located north of Kea Isl. (56%) and NE of Gyaros Isl. (62%), while in the eastern areas of the central Aegean, over Andros, Tinos, Mykonos islands, covering the area down to Astypalaia, Kasos and Karpathos islands, high percentages were observed, ranging from 70 – 80%.

Summer emerged with the overall maximum percentages compared to the rest seasons and followed the spatial patterns of the corresponded observed wind speeds in summer. The overall highest percentage was observed again, in the areas near west coasts of Crete Isl., while the south and southeast parts of the island, presented lower values ranging from 40 to 60%. The entire north and east central, as well as the eastern and the SE parts of the Aegean showed percentages that exceeded 80%, with the highest in the surrounding areas of Astypalaia Isl. in Kasos and Karpathos islands, and in the NE coasts of Crete Isl. with values ~92%, respectively.

Lower percentages were observed in the western regions of the central Aegean, expanded down to east offshore areas of Kythera Isl., Antikythera Isl. and the NW coasts of Crete Isl., ranging from 40 – 73%. In the eastern coasts of Rhodes Isl., were also emerged lower percentages (~55%), as well as for the Ionian with values under 75%.

The spatial distribution for Autumn indicated that lower percentages were emerged for both the Ionian and the Aegean Sea. The overall highest time percentages were again observed in the western and eastern offshore areas of Crete Isl. ~87% and 80 %, respectively, while the south and southeast parts presented low percentages ranging from 40 to 55%. For this season, slightly increased percentages were observed in the western parts of the central Aegean, where the lower percentages have been observed in summer, while in the east and southeast Aegean, where the maximum values have been located in summer, decreased percentages were noted, ~ 70 – 80%. The areas in which the lower percentages presented in Autumn were, the areas east of Rhodes Isl. (~52%), the extended area between north Evvoia and south coasts of Halkidiki (40 – 60%), and the entire area of the Ionian 60 – 75%, with the highest in the NW areas of Diapontian Islands.

5.4. The wind turbine performance in 30 selected areas in the Greek seas

In this section the assessment of wind speed, wind power density, the performance of the NREL - 15MW WT, was performed on an annual time scale, in order to evaluate the 30 potential areas that have been proposed for the development of OWFs. The aforementioned analysis includes one selected and representative point, for each of the 30 sites that have been emerged from the NDP – OWF by HEREMA [41].

Saint Efstratios Isl.

Saint Efstratios Isl., is located in the northern Aegean southern of Lemnos. The analysis of the WS and the WPD that preceded in previous sections, indicated that in the areas around Saint Efstratios Isl., high wind speeds and by extension, significant values of WPD and high time percentages for wind speeds within the operational limits of the WT, were observed in all the examined temporal scales. According to the plan of HEREMA, three polygons were corresponded to the aforementioned area; more details about each polygon are presented in Table 19.

Table 19. Information about the three polygons in Saint Efstratios Isl.

Polygon Name	**Size of Polygon** km^2	**Selected point**	**Prioritization**	**Installation type**	**Time percentages**
Saint Efstratios 1A	49.91	39.49°N 25.05°E	Long – term	Fixed – bottom	78.41%
Saint Efstratios 1B	74.76	39.57°N 25.14°E	Long – term	Floating	79.46%
Saint Efstratios 2	160.97	39.44°N 25.04°E	Long- term	Floating	78.94%

Regarding Saint Efstratios-1A, 4 points were available from the model inside the frame of the corresponded polygon, while for Saint Efstrations-1B, 7 points, and for Saint Efstratios-2, 15 points, respectively; the locations of the selected points for each polygon, are presented in Figure 41.

Table 20. The numerical results for the selected points of the polygons in Saint Efstratios Island

Polygon	**Energy** $MWh/year$	**CF** %	**WS**			**WPD**		
1A	58,508	44.52	**WS** m/s	**MAV** %	**IAV** %	**WPD** W/m^2	**MAV** %	**IAV** %
			7.95	55.72	3.80	629.39	153.55	10.69
1B	61,229	46.59	8.17	55.09	3.67	673.18	150.97	10.39
2	59,610	45.36	8.07	55.38	3.81	653.13	151.60	10.69

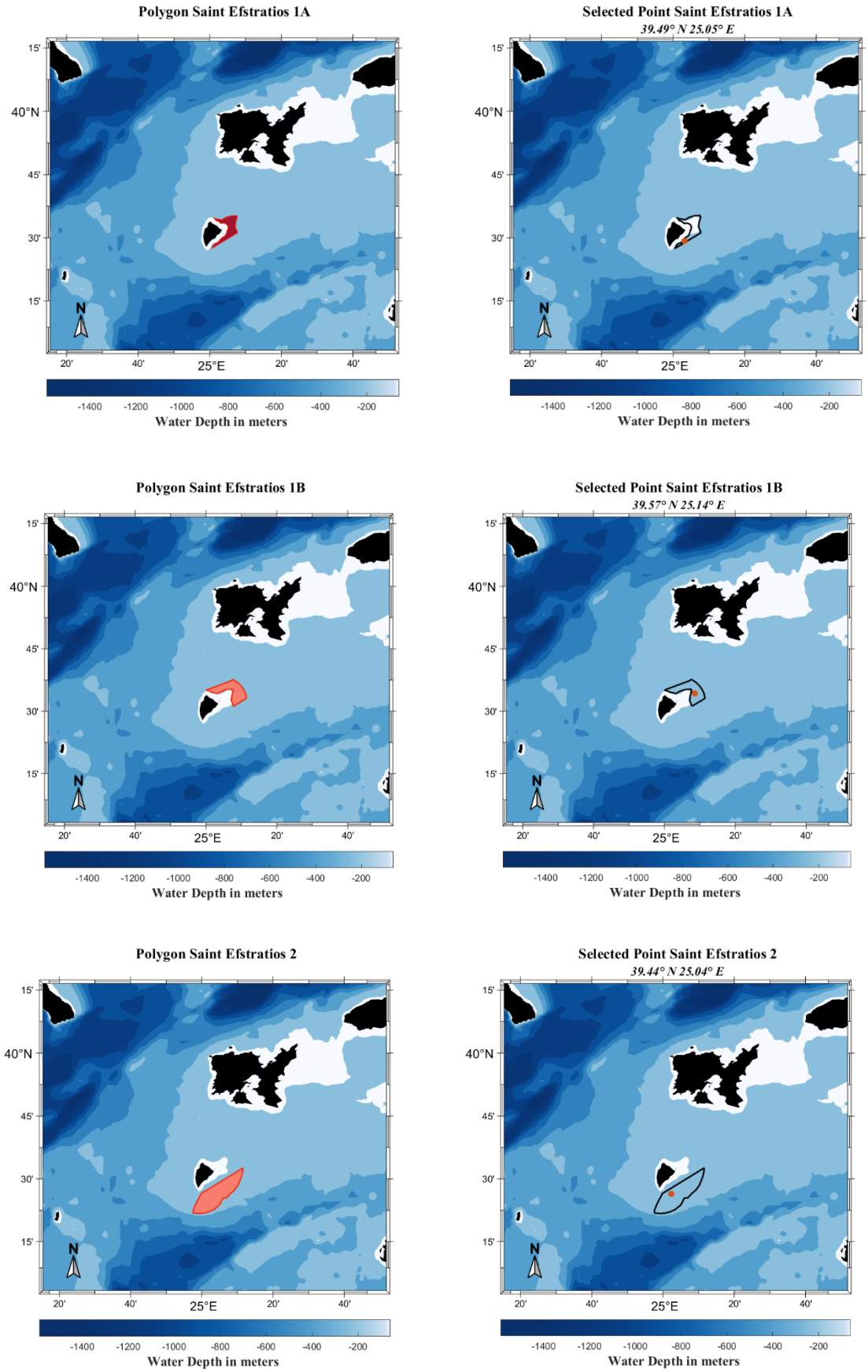

Figure 41. The location of the polygons Saint Efstratios 1A,1B and 2 and the corresponded examined points.

The results that were obtained from the analysis of the three corresponded points of each polygon (more details presented in Table 20), exhibited that the performance of the selected WT, is higher in Saint Efstratios-2, where the higher values of WS and WPD have been presented, as well as the lower corresponded MAV and IAV values for both of the examined aspects. The differences that have been observed between the 3 representative points, were not significant, nevertheless, the corresponded mean annual produced energy and CF, were emerged with higher values for the Saint Efstratios - 2. The estimated linear slopes for each site, indicated a further increase over time. The spot for Saint Efstratios-1A, emerged with a positive slope of (0.035 m/s/year), as well as for the extreme wind speeds (0.041 for the 95th and 0.0206 m/s/year for the 99th percentiles, respectively); Saint Efstratios-1B with corresponded values of ~ 0.0038 m/s/year, 0.0037 for the 95th and 0.0268 m/s/year for the 99th, respectively and Saint Efstratios – 2, with slopes 0.0038, 0.0254 and 0.0045 m/s/year, respectively.

Antikythera Isl.

Antikythera is located in the extended area between Kythera Isl. and NW coasts of Crete Isl. which emerged high values of wind speed to all the selected temporal scales. The time percentages for the wind speed within the operational limits of the WT, presented higher values compared to the polygons in Saint Efstratios, while there were 15 available points within the framework of the polygon from the model. Details about the polygon are given in Table 21, while the numerical results of the selected point, are presented in Table 22.

Table 21. Information about the polygon in Antikythera

Polygon Name	**Size of Polygon** km^2	**Selected point**	**Prioritization**	**Installation type**	**Time percentages**
Antikythera	160.97	35.84°N 23.23°E	Long – term	Floating	82.33%

Table 22.The numerical results for the selected points of the polygon in Antikythera.

Polygon	**Energy** $MWh/year$	**CF** %	**WS**			**WPD**		
Antikythera	59,448	45.23	**WS** m/s	**MAV** %	**IAV** %	**WPD** W/m^2	**MAV** %	**IAV** %
			7.94	49.91	1.95	554.94	139.41	6.34

From the analysis, was exhibited that in Antikythera, regarding the performance of the WT similar CF values with Saint Efstratios were observed, nevertheless, the potential mean annual produced energy, indicated lower production compared to the previous polygons. The numerical results for the selected point of Antikythera are given in Table 22, while the slopes emerged from the Theil Sen estimator, indicated increasing tendency over time, with positive values close to 0.0013 m/s/year, while for the extreme wind speeds the corresponded measures were, 0.0146 m/s/year for the 95th percentile and 0.0092 m/s/year for the 99th, thus the expected produced energy, could be higher in the future. Noteworthy was, that the selected point of this polygon emerged the overall lower IAV values.

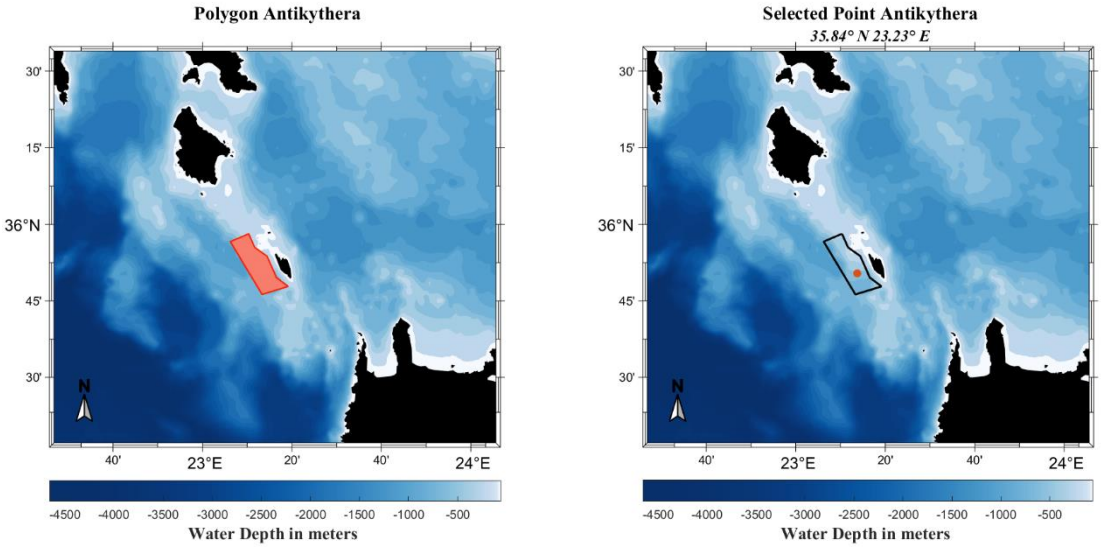

Figure 42. The location of polygon in Antikythera and the corresponded examined point.

Chios Isl.

Three available spots were noticed for Chios; for more information refer to Table 23; located in the northeastern parts of the Aegean and characterized by high values of wind speed and WPD, even when the surrounding regions didn't.

Table 23. Information about the polygon at Chios

Polygon Name	Size of Polygon km^2	Selected point	Prioritization	Installation type	Time percentages
Chios	65.54	38.59°N 25.81°E	Medium-term	Floating	79.13%

Table 24. The numerical results for the selected point of the polygon at Chios

Polygon	Energy $MWh/year$	CF %	WS			WPD		
			WS m/s	MAV %	IAV %	WPD W/m^2	MAV %	IAV %
Chios	58,003	44.14	7.72	52.82	3.01	541.43	147.20	9.06

Regarding the potential produced energy and the CF factors, decreased values emerged compared to the previous polygons examined. Furthermore, higher values of MAV and IAV presented for both wind speed and WPD, see more in Table 24; as well as tendency for decrease over time due to the negative slopes that emerged, with values of -0.0017 m/s/year for the mean wind speeds. Nevertheless, the extreme wind speeds showed increasing tendency, with the corresponded slopes of 95th percentile 0.0131 m/s/year and 0.0308 m/s/year for the 99th, respectively.

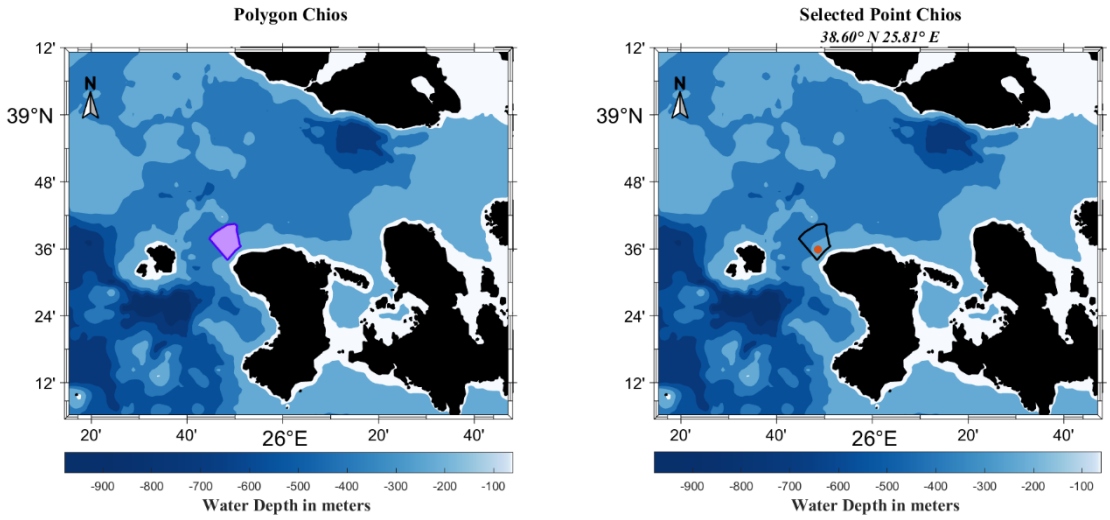

Figure 43. The location of the polygon in Chios and the corresponded examined point.

Crete Isl.

In the southern parts of the Aegean, Crete Isl. is located, the largest island of Greece, with 6 corresponding potential areas for the development and installation of OWFs. A noteworthy about Crete was that each coast of it, has been exhibited different patterns and statistical characteristics. The location of each polygon in Crete is depicted in Figure 44 and Figure 45, while further information is given in Table 25.

Table 25. Information about the polygons in Crete

Polygon Name	Size of Polygon km^2	Selected point	Prioritization	Installation type	Time percentages
Crete 1	118	35.07°N 26.34°E	Medium– term	Floating	76.37%
Crete 2A	187.26	35.31°N 25.80°E	Medium – term	Fixed bottom	79.75%
Crete 2B		35.36°N 25.82°E		Floating	80.76%
Crete 3	40.06	35.36°N 26.06°E	Long – Term	Floating	78.34
Crete 4A	40.63	34.97°N 26.06°E	Long – Term	Floating	65.47
Crete 4B		34.98°N 26.25°E		Floating	78.51

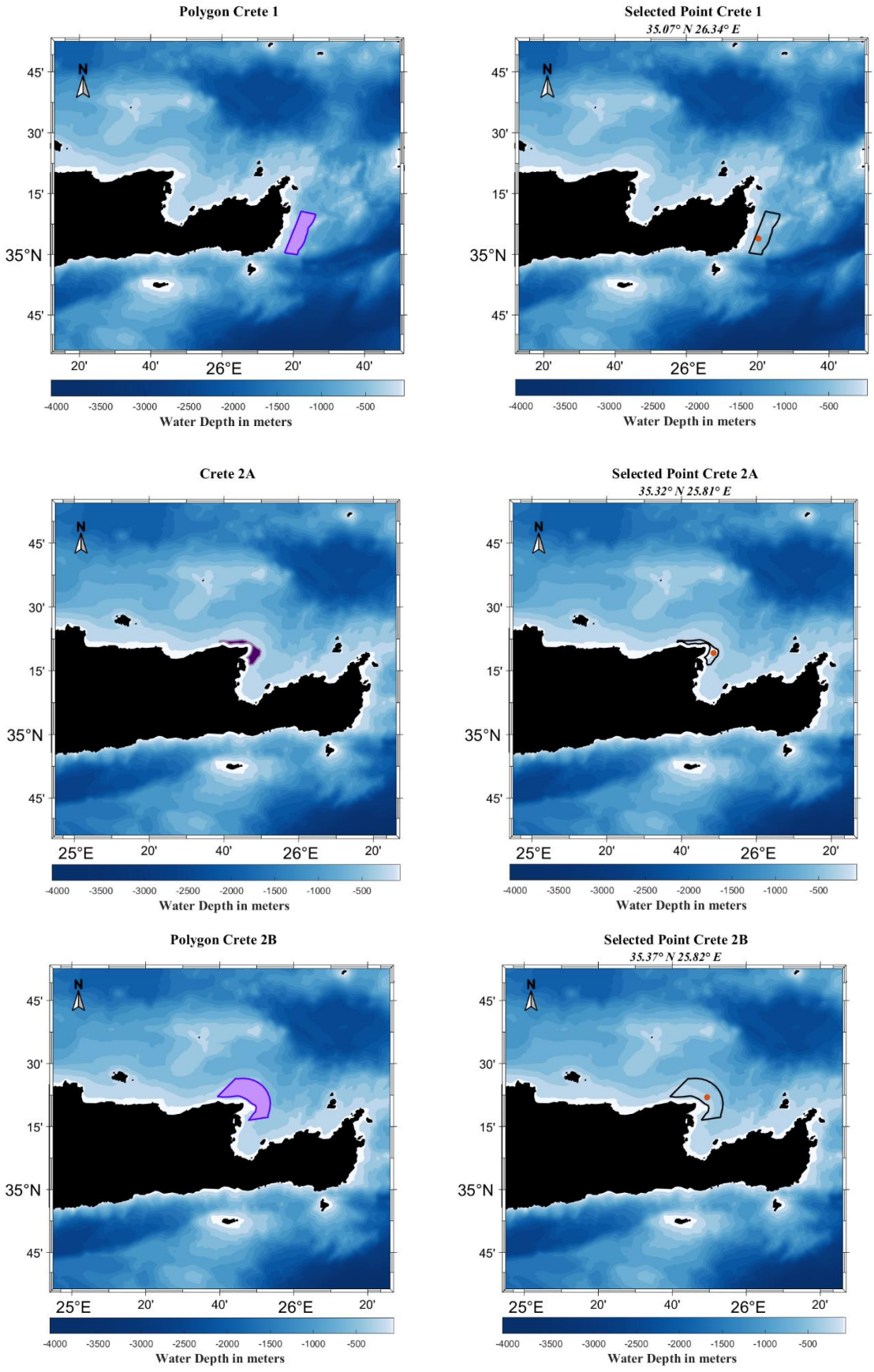

Figure 44. The locations of the three of the polygons in Crete and the corresponded examined points.

Each of the polygons in Crete, presented different scheme, thus the available points for each polygon were different; more specific, for Crete-1, the available points were 10, while for Crete -2A were 7, Crete-2B were 14, as for Crete-3, 4A and 4B, the available points emerged were, 2,1 and 2, respectively. From the numerical results that obtained in Table 26, as expected, the higher energy produced in Crete-1, which is located in the eastern parts of Crete coasts. The eastern part of Crete exhibited high values of wind speed and WPD during the 36 - years, nevertheless the slopes emerged from the analysis, indicated a tendency for decrease with values close to -0.0104 m/s/year for the mean annual wind speed, -0.0167 for the 95th percentiles and -0.0254 m/s/year for the really extreme wind speeds of the 99th percentiles, while MAV values for wind speed observed higher, compared to the previous examined sites.

Table 26.The numerical results for the selected points of the polygons in Crete Isl.

Polygon	**Energy** $MWh/year$	**CF** %	**WS**			**WPD**		
Crete 1	65,919	50.16	**WS** m/s	**MAV** %	**IAV** %	**WPD** W/m^2	**MAV** %	**IAV** %
			8.47	58.53	4.41	782.51	134.73	11.70
Crete 2A	59,540	45.31	7.69	47.91	3.97	487.91	117.45	9.32
Crete 2B	61,414	46.73	7.58	49.53	3.95	518.75	115.25	9.43
Crete 3	58,568	44.57	6.97	69.54	4.35	467.37	118.34	10.65
Crete 4A	46,823	35.63	7.07	71.36	5.28	572.97	182.28	14.61
Crete 4B	47,026	35.78	6.57	60.59	5.16	553.29	184.05	14.48

The second highest energy produced in Crete-2B, in the northern coasts of Crete, where lower wind speeds and WPD values have been noted, compared to Crete-1, nevertheless, decreased values of MAV and IAV were also observed. As for the corresponded linear slopes, negative tendency was also appeared, with the slopes of mean annual wind speed close to -0.0058 m/s/year. As for the extreme wind speeds, negative slopes emerged for the 95th percentiles with values -0.00580 m/s/year, while increased tendency appeared for the 99th, 0.0030 m/s/year.

The analysis of the representative point in Crete-2A, emerged with lower values of energy and CF, compared to Crete-1 and Crete-2A, while negative slopes observed for the mean annual wind speed (-0.0041 m/s/year), as well as for the higher extreme wind speeds of the 99th percentiles, with corresponded slope -0.0075 m/s/year, while the extreme wind speeds emerged from the 95th percentiles, emerged with positive slope 0.0053 m/s/year.

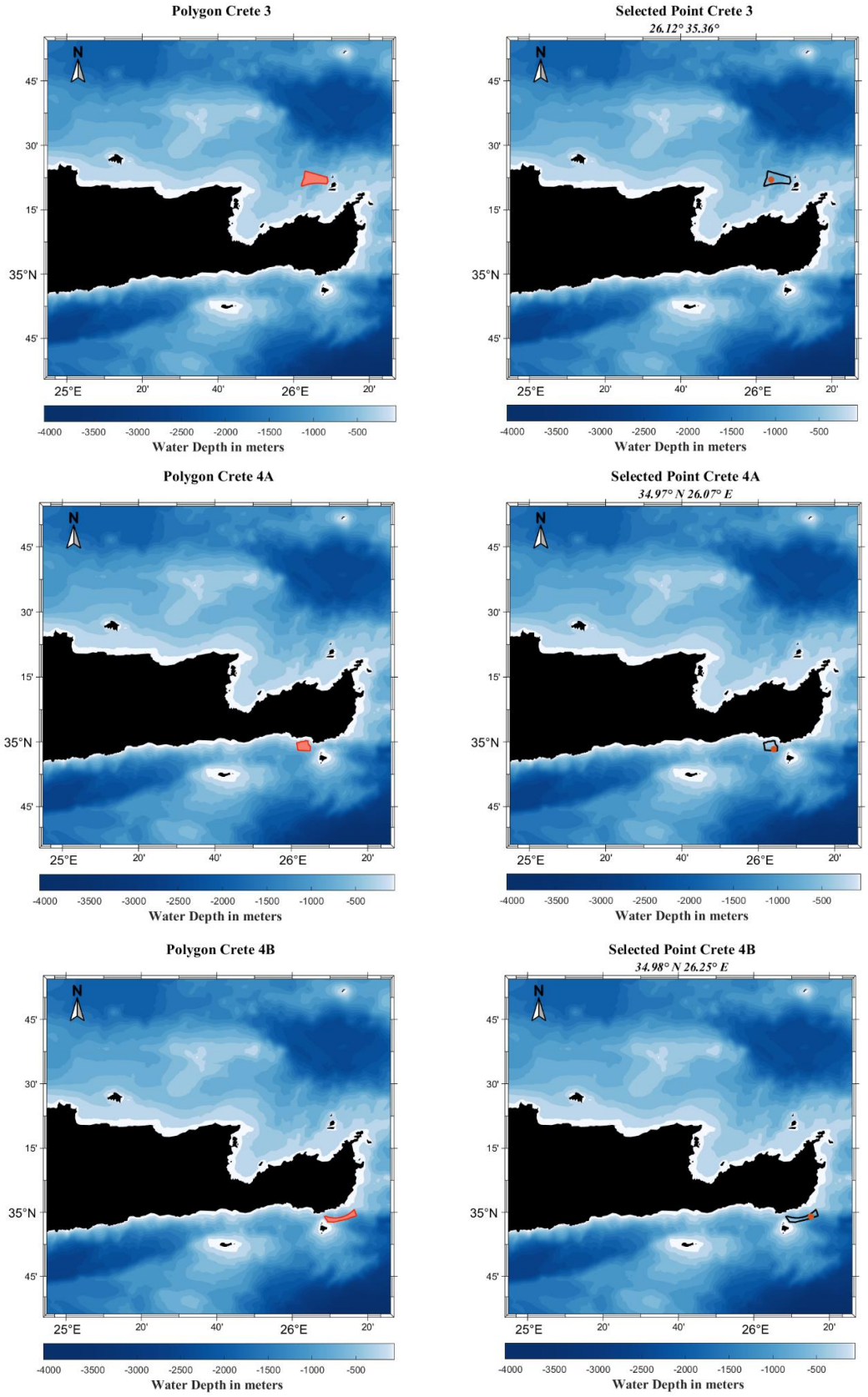

Figure 45.The locations of three of the polygons in Crete and the corresponded examined points.

Regarding the polygon Crete-3, noteworthy was the significant higher value of MAV regarding the WS close to 70% and decreasing tendency presented for the mean annual wind speeds in this point, with slope -0.0043 m/s/year, as well as for the 99th percentiles, with value -0.0089 m/s/year, while for the 95th a positive slope emerged 0.0056 m/s/year.

The two polygons located in the southeast coasts of the island, emerged with high values of MAV and IAV for both WS and WPD, while the selected point of Crete-4A, presented the overall maximum value of MAV, compared to the 30 examined sites. Furthermore, lower values of annual produced energy and CF, indicated the lower performance of the WT compared to the other polygons in Crete. The southern regions of Crete, corresponded to high variability and lower energy values, thus the area presented uncertainties to the installation of a profitable OWF.

Negative slopes appeared in Crete 4A (-0.0084 m/s/year), as well as a decreased tendency for the extreme wind speeds with values -0.0340 and -0.0387 for the 95th and the 99th percentiles, respectively. As for polygon Crete 4B, negative slopes appeared for both of the mean annual and the extremes of the 95th and 99th percentiles, with values -0.0102, -0.0337 and -0.0386 m/s/year, respectively.

Diapontian Islands

From the statistical analysis of the WS and WPD, one of the areas that presented both high values of the examined aspects, as well as a tendency for increase over time, was in the northern parts of the Ionian, in Diapontian Islands (see more in Table 27); with 3 available points from the model within the framework of the polygon. As it was expected, lower values of WS and WPD were emerged compared to the polygons in the Aegean, with corresponded higher variability coefficients.

Table 27. Information about the polygon at Diapontian Islands in the Ionian Sea.

Polygon Name	**Size of Polygon** km^2	**Selected point**	**Prioritization**	**Installation type**	**Time percentages**
Diapontian Islands	54.34	39.87°N 19.48°E	Medium– term	Fixed - Bottom	68.81%

Table 28. The numerical results for the selected points of the polygons at Diapontian Islands

Polygon	**Energy** $MWh/year$	**CF** %	**WS**			**WPD**		
			WS m/s	**MAV** %	**IAV** %	**WPD** W/m^2	**MAV** %	**IAV** %
Diapontian Islands	46,333	35.48	6.57	60.59	4.43	390.10	161.33	10.77

The produced energy that emerged from the analysis, was lower compared to the previous sites, nevertheless, the linear slopes of the mean annual WS, indicated a tendency for increase, with values 0.0069 m/s/year, 0.0185 and 0.0152 m/s/year for the extreme wind speeds, respectively; for more statistical parameters refer to Table 28. Noteworthy was the fact that the estimated

energy in Diapontian Isl., was similar to the corresponded energies that have been observed in Crete-4A and Crete-4B.

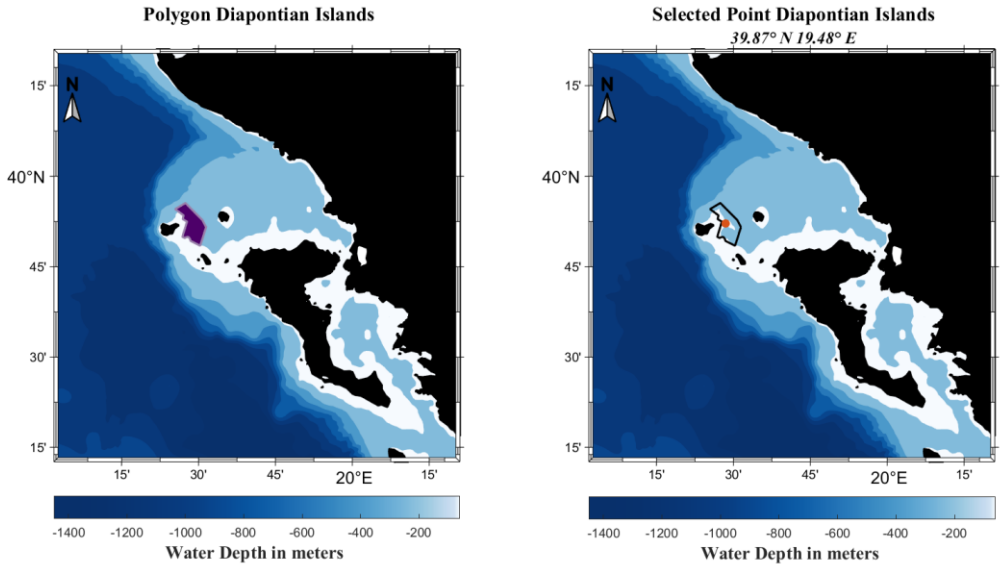

Figure 46. The location of the polygon in Diapontian Islands and the corresponded examined point.

Donousa Isl.

Two polygons emerged from the NWP – OWF regarding Donousa, which is a little island of Cyclades, located east of Naxos Isl. For more information about each polygon refer to Table 29, corresponded to 7 and 3 available points from the model, respectively. The locations of each representative point are presented in Figure 47.

Table 29. Information about the two polygons in Donousa Isl.

Polygon Name	Size of Polygon km^2	Selected point	Prioritization	Installation type	Time percentages
Donousa 1	107.79	37.21°N 25.76°E	Long– term	Floating	83.46%
Donousa 2	65.03	37.08°N 25.91°E	Medium – term	Floating	84.42%

Table 30. The numerical results for the selected points of the polygons in Donousa Isl.

Polygon	Energy $MWh/year$	CF %	WS			WPD		
			WS m/s	MAV %	IAV %	WPD W/m^2	MAV %	IAV %
Donousa 1	69,172	50.16	8.42	47.13	4.22	614.66	115.13	9.78
Donousa 2	70,730	45.31	8.55	46.27	3.12	643.21	113.25	9.47

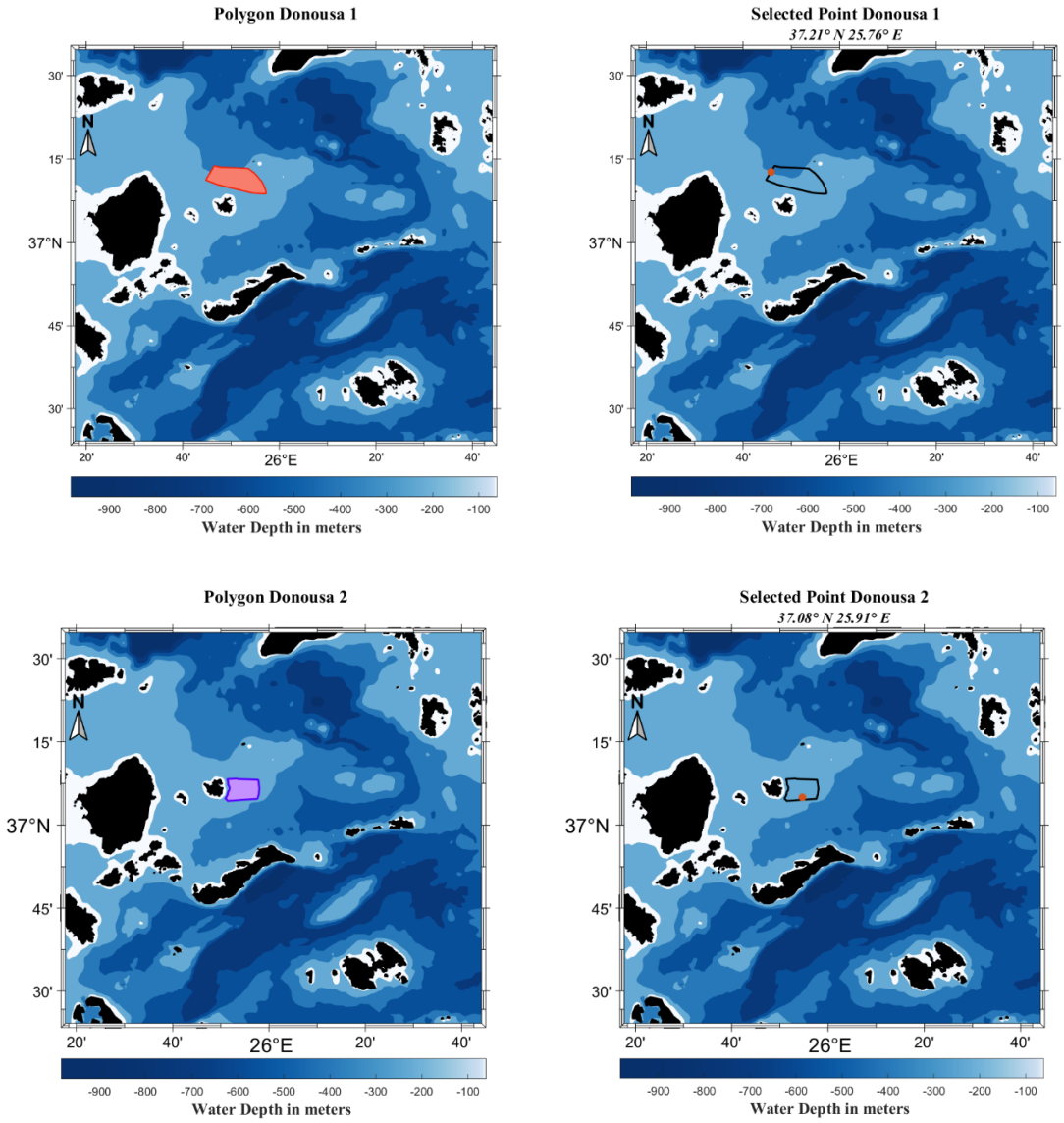

Figure 47. The location of the polygons in Donousa and the corresponded examined points.

In the eastern parts of the central Aegean in general high values of WS and WPD were noticed. From the numerical results obtained for the selected points (Table 30), in both of the polygons in Donousa, high produced energy, CF factors, corresponded to low variability coefficients. Regarding Donousa-1, negative slopes appeared from the analysis of the mean wind speed close to -0.0030 m/s/year, as well as for the 99th percentiles -0.0105 m/s/year. Nevertheless, the linear slopes for the 95th percentiles emerged with a tendency for increase 0.000949 m/s/year, for the examined 36 – year period.

As for Donousa-2, lower variability measures were observed compared to Donousa-1, while the performance of the WT emerged higher. Negative slopes of the mean annual wind speed were also appeared in this site for both the mean annual WS (-0.0031 m/s/year) and the 95th percentiles of annual WS (-0.0056 m/s/year), while for the extremer annual WS, corresponded to the 99th percentiles, increasing tendency was noted ~ 0.0039 m/s/year.

Gulf of Patras

The dominance of the spatial distribution of CERRA, was also supported from the fact that areas such as Gulf of Patras, close to land, and surrounding by complex geomorphological schemes, were emerged with a sufficient number of available points, 9 in this case. The location of the corresponded polygon is presented in Figure 48, while further information about the polygon and the representative point in Table 32.

Table 31. Information about the polygon in Gulf of Patras

Polygon Name	Size of Polygon km^2	Selected point	Prioritization	Installation type	Time percentages
Gulf of Patras	138.84	38.26°N 21.54°E	Medium– term	Fixed - bottom	60.50%

Table 32. The numerical results for the selected points of the polygons in Gulf of Patras

Polygon	Energy MWh/year	CF %	WS			WPD		
			WS m/s	MAV %	IAV %	WPD W/m^2	MAV %	IAV %
Gulf of Patras	42,463	32.31	5.95	68.69	5.04	349.70	200.24	14.22

The energy emerged for the selected point was lower compared to Diapontian Islands, where the lower values of energy observed so far. The numerical results indicated, high variability coefficients, for both annual and inter – annual temporal scales, corresponded with the overall minimum WS and WPD values, compared to all the examined sites.

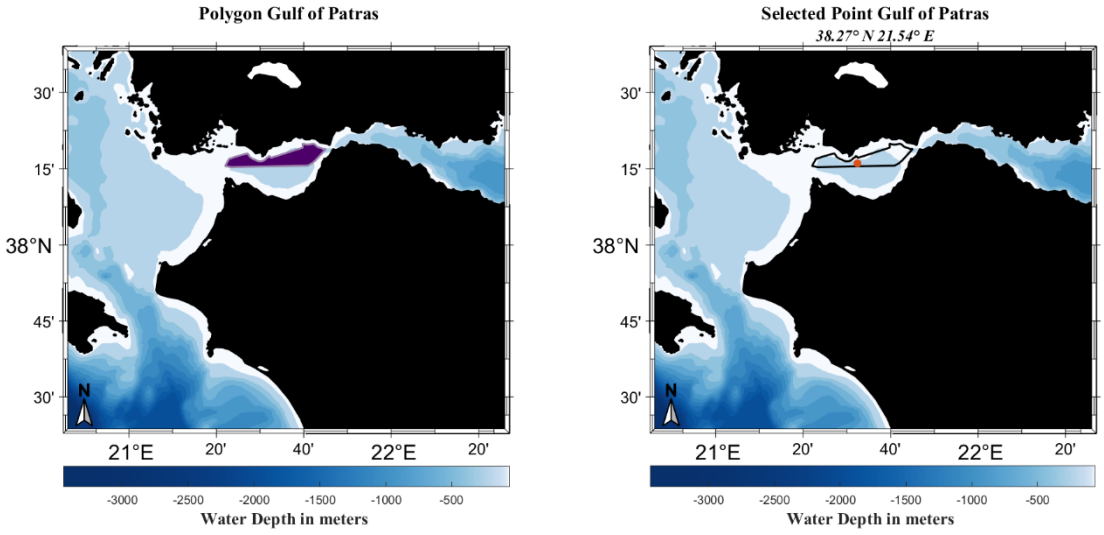

Figure 48. The location of the polygon in Gulf of Patras and the corresponded examined point.

Moreover, further decrease it is anticipated since negative slopes were appeared for the mean annual wind speed (-0.007 m/s/year), as well as for the 99th percentiles (-0.0279 m/s/year), while for the lower extreme wind speeds positive slopes were observed (0.0017 m/s/year). Noteworthy was that the selected point in Gulf of Patras was emerged with the overall highest IAV values regarding WS, compared to the rest 30 sites.

Gyaros Isl.

Gyaros Isl. has been mentioned several times both in the statistical analysis of WS and WPD, due to the high values that have been observed mainly in the northern offshore areas of the island. Three polygons are corresponded to the island which is located in the central Aegean, each one represented by 2 available points from the model, respectively. More information about the selected points, as well as for the location of each polygon, are represented in Table 33 and Figure 49.

Table 33. Information about the three polygons in Gyaros Island

Polygon Name	**Size of Polygon** km^2	**Selected point**	**Prioritization**	**Installation type**	**Time percentages**
Gyaros A	99.52	37.57°N 24.62°E	Medim - Term	Floating	76.91%
Gyaros B		37.66°N 24.71°E			76.14%
Gyaros C		37.63°N 24.57°E			76.72%

Table 34. The numerical results for the selected points of the polygons in Gyaros Island.

Polygon	**Energy** $MWh/year$	**CF** %	**WS**			**WPD**		
			WS m/s	**MAV** %	**IAV** %	**WPD** W/m^2	**MAV** %	**IAV** %
Gyaros A	63,706	48.48	8.16	55.54	5.02	659.73	128.08	11.91
Gyaros B	62,280	47.39	8.02	55.86	5.07	630.36	129.50	12.10
Gyaros C	63,929	48.65	8.25	56.74	5.14	700.65	132.17	12.59

From the numerical results that obtained in Table 34, high values of both produced energy and CF were emerged for each of the three polygons, with the highest observed in Gyaros-C, located in the NW offshore areas of the island. Despite the high energy production and the satisfying CF ratios, the WS, as well as the extreme wind speeds in the selected point, tended to decrease over time, with corresponded slopes, -0.0056, -0.0044 and -0.0169 m/s/year, respectively.

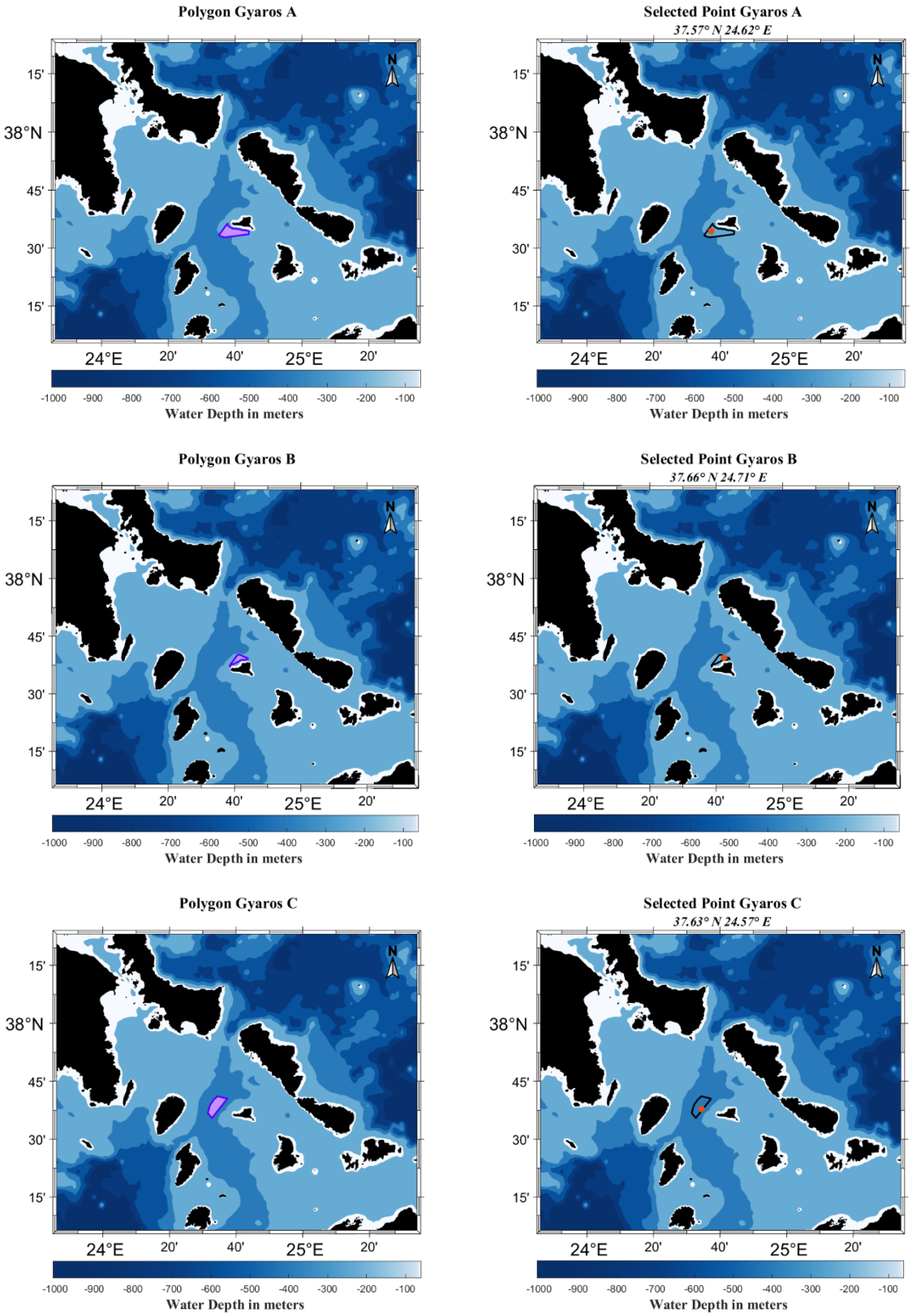

Figure 49. The location of polygons in Gyaros and the corresponded examined points.

The values of produced energy that was emerged was comparable with the values presented in the selected points of Saint Efstratios-1B and Crete-2B, while high variability coefficients were

also noted. Negative slopes for the mean annual wind speed characterized the selected point of Gyaros-A (-0.0029 m/s/year), as well as for the extreme wind speeds, with slopes -0.0019 and -0.0101 m/s/year, respectively. Regarding Gyaros-B, lower energy values were appeared compared to the previous polygon, while also negative slopes were emerged with corresponded values -0.0031, -0.0033, -0.0107 m/s/year, respectively.

Ikaria Isl.

In the eastern – central Aegean, Ikaria Isl. is located, in which two polygons were destined for the potential installation of OWFs; for more information refer to Table 35. The locations of the selected points are presented in Figure 50. The spatial analysis of the model, permitted the existence of 11 and 10 available points corresponded to each polygon, respectively.

Table 35. Information about the two polygons in Ikaria Isl.

Polygon Name	**Size of Polygon** km^2	**Selected point**	**Prioritization**	**Installation type**	**Time percentages**
Ikaria 1	181.07	37.48°N 25.91°E	Long– term	Floating	84.80%
Ikaria 2	170.83	37.52°N 26.23°E	Long – term	Floating	76.40%

Table 36. The numerical results for the selected points of the polygons in Ikaria Isl.

Polygon	**Energy** $MWh/year$	**CF** %	**WS**			**WPD**		
Ikaria 1	70,556	53.69	**WS** m/s	**MAV** %	**IAV** %	**WPD** W/m^2	**MAV** %	**IAV** %
			8.61	47.06	3.96	660.41	119.24	9.24
Ikaria 2	61,040	46.45	7.53	53.01	4.57	493.14	129.20	10.19

The offshore areas NW of the island, were emerged with greater amounts of produced energy, comparable to Donousa-2, as well as higher CF ratios, indicated that the prevailing site in Ikaria Isl., regarding the performance of the WT, was Ikaria-1. Furthermore, in the aforementioned point were presented lower variability coefficients, compared to the point in Ikaria-2. As for the trends of WS and the extreme wind speeds in Ikaria-1, negative slopes were appeared, for the mean annual WS (–0.0032 m/s/year), as well as for the WS ranging from 14 to 15 m/s with -0.0105 m/s/year, while for extremer WS that exceeded 18 m/s, an increasing tendency was observed (0.0045 m/s/year). Regarding Ikaria-2, negative slopes were appeared for both of the mean and the higher extremes WS, with corresponded values -0.0040 and -0.0104 m/s/year; while positive slopes were noticed in the area for the 95th percentile of wind speed 0.0063 m/s/year.

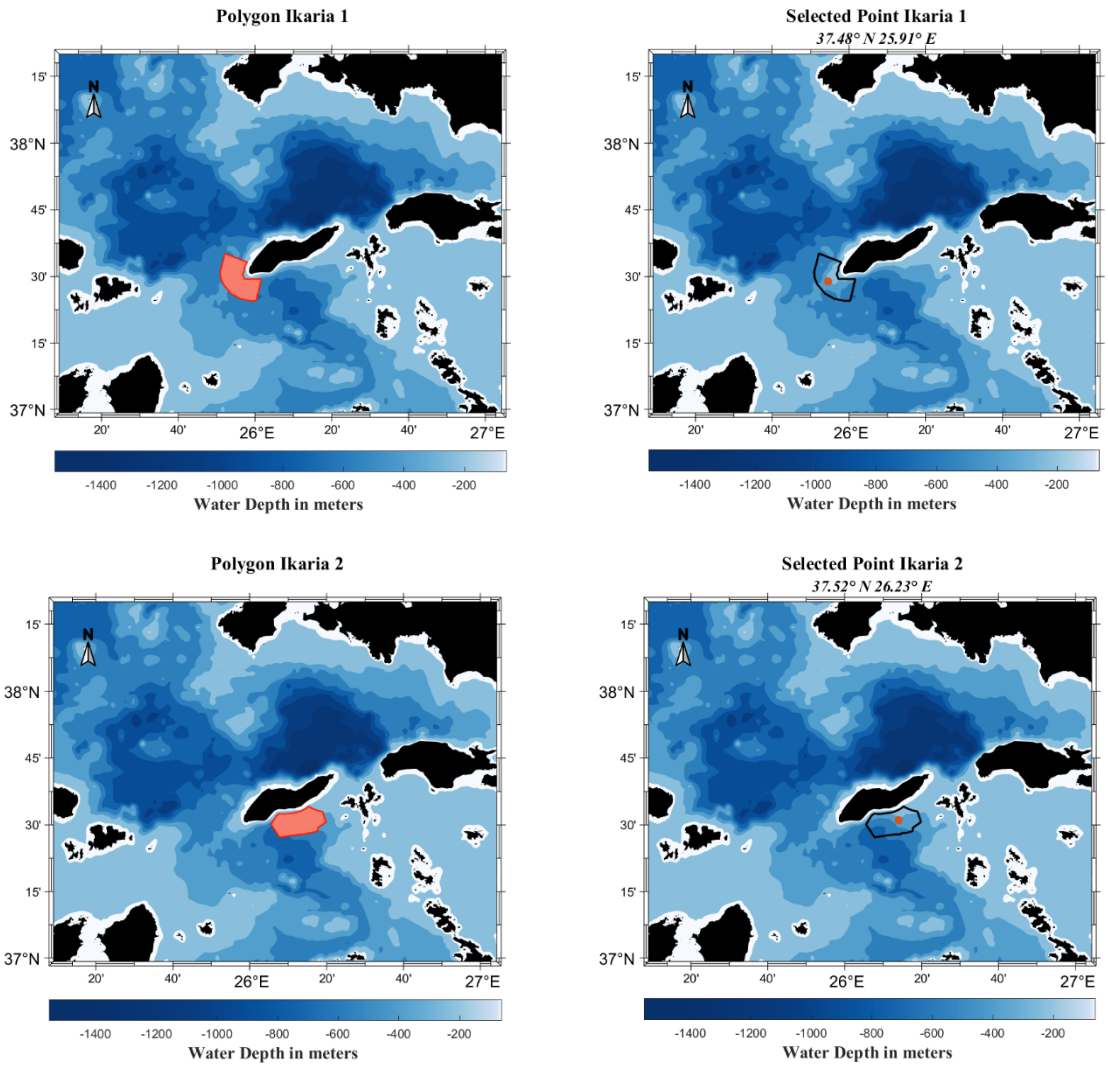

Figure 50. The location of polygons in Ikaria and the corresponded examined points.

Karpathos Isl.

Regarding Karpathos Isl., there were 9 available points from the model inside the framework of the polygon, while the selected point is depicted in Figure 51 and more information are provided in Table 37. In the extended area between east coasts of Crete Isl. and Karpathos Isl., high WS values were observed, corresponded to low measures of variability, thus, as it was expected, the produced energy and CF ratio at the point 35.97°N 27.23°E in Karpathos, as well as the values of WS, were also emerged high; more details are presented in Table 38.

The extreme wind speeds of the aforementioned site, is expected to increase, since positive slopes emerged for the 99th percentiles of the WS (0.0154 m/s/year). Nevertheless, the slopes for the mean annual wind speed and the 95th percentiles, were presented a tendency for decrease, with values close to -0.0136 and -0.0205 m/s/year, respectively.

Table 37. Information about the polygon in Karpathos Island

Polygon Name	Size of Polygon km^2	Selected point	Prioritization	Installation type	Time percentages
Karpathos	124.14	35.97°N 27.23°E	Long- term	Floating	84.11%

Table 38. The numerical results for the selected points of the polygon in Karpathos

Polygon	Energy $MWh/year$	CF %	WS			WPD		
			WS m/s	MAV %	IAV %	WPD W/m^2	MAV %	IAV %
Karpathos	65,763	50.04	8.14	47.12	4.34	563.33	126.41	10.96

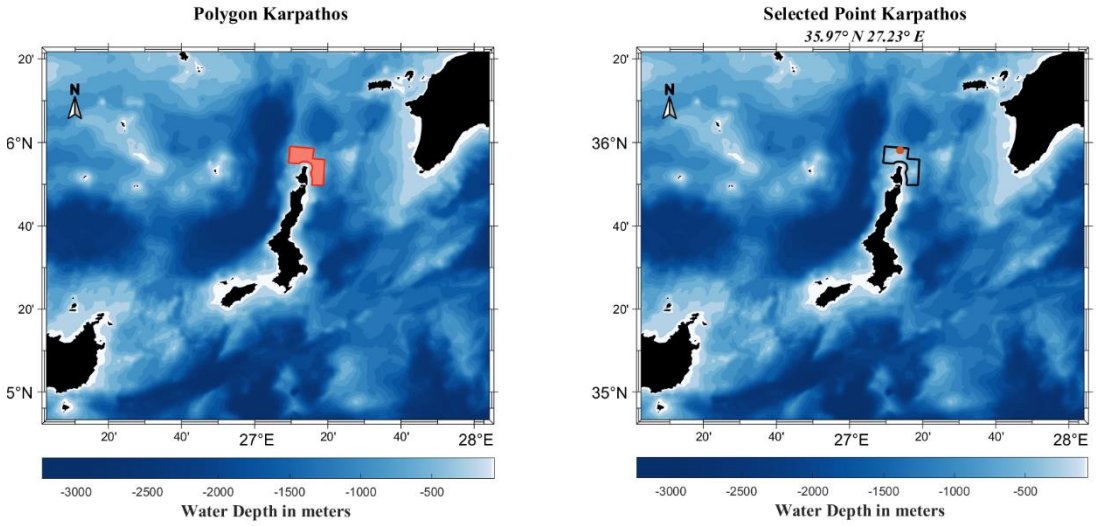

Figure 51. The location of polygon in Karpathos and the corresponded examined point.

Kasos Isl.

Kasos is also another island located in the SE Aegean in the extended area between east coasts of Crete Isl. and Rhodes Isl. Kasos Isl. offshore areas, were included into the prevailing areas in which the highest values of mean annual WS and WPD, have been observed. The available points from the model corresponded in Kasos were 12, while the selected and representative point of the area was, 35.26° N 26.82° E. The location of the potential polygon for the installation of a floating OWF, is depicted in Figure 52, while for more information refer to Table 39.

The numerical results obtained from the analysis at point 35.26° N 26.82° E are presented in Table 40. The overall maximum WS, WPD, produced energy and CF ratio, were observed. Kasos Isl., was emerged as the most favorable site between the 30 potential areas, since the WT, presented the greatest performance in the selected point. Moreover, a noteworthy fact was the low values of MAV that have been observed, indicated that winds over the particular area, were remaining steady for a significant span within a year for the examined period.

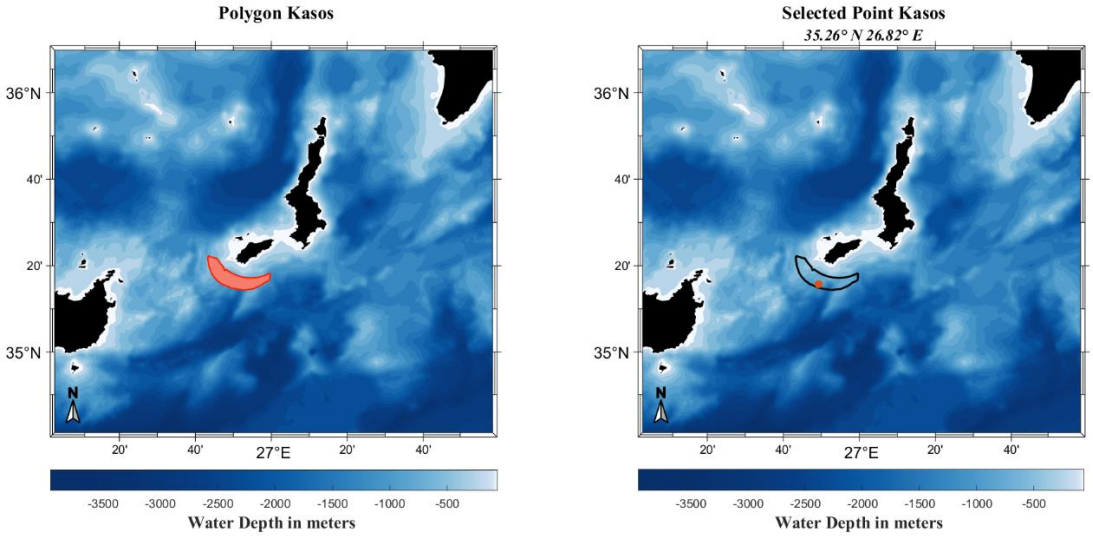

Figure 52.The location of the polygon in Kasos and the corresponded examined point.

The year-to-year variability of wind speed was also presented low values for the examined point in Kasos Isl., indicating a more stable estimation of the potential produced energy and the relevant cost of the OWF. Despite the great statistical characteristics that obtained from the analysis in Kasos Isl., the linear slopes for the mean annual WS, were emerged with negative slopes -0.0077 m/s/year, for the 36 – year period. Furthermore, the extreme WS, were emerged with decreasing tendency for both the 95th and 99th percentiles of wind speeds, with corresponded slopes -0.0129 and -0.0020 m/s/year, respectively. The results of the analysis at this point indicated that more extensive and in-depth assessments, combined with in – situ measures required, to confirm that the potential installation of an OWF will be as beneficial as it showed from the analysis.

Table 39. Information about the polygon in Kasos Island.

Polygon Name	**Size of Polygon** km^2	**Selected point**	**Prioritization**	**Installation type**	**Time percentages**
Kasos	141.01	35.26°N 26.82°E	Long– term	Floating	86.52%

Table 40. The numerical results for the selected points of the polygon in Kasos

Polygon	**Energy** $MWhyear$	**CF** %	**WS**			**WPD**		
			WS m/s	**MAV** %	**IAV** %	**WPD** W/m^2	**MAV** %	**IAV** %
Kasos	76,010	57.84	9.04	44.87	4.06	728.502	106.28	10.13

Kymi

In the central – east coasts of Evvoia, the polygon of Kymi is located, with 3 available points from the model with the corresponded and representative point in 38.58°N 24.27°E, as presented in Figure 53. The aforementioned polygon is among the few polygons presented positive trends for the mean annual WS, with slope 0.0021, while the extreme wind speeds emerged from the 95th and 99th percentiles, were presented a decreasing tendency, with corresponded slopes –0.0079 and -0.0025 m/s/year, respectively. Regarding the numerical results that are presented in Table 42, the performance of the WT in the selected point was lower compared to other sites, while the variability coefficients observed were in satisfactory levels.

Table 41. Information about the polygon in Kymi

Polygon Name	**Size of Polygon** km^2	**Selected point**	**Prioritization**	**Installation type**	**Time percentages**
Kymi	64.99	38.58°N 24.27°E	Long– term	Floating	78.66%

Table 42. The numerical results for the selected point of the polygon in Kymi

Polygon	**Energy** $MWh/year$	**CF** %	**WS**			**WPD**		
			WS m/s	**MAV** %	**IAV** %	**WPD** W/m^2	**MAV** %	**IAV** %
Kymi	54,772	41.68	7.43	50.68	3.93	456.44	134.03	10.74

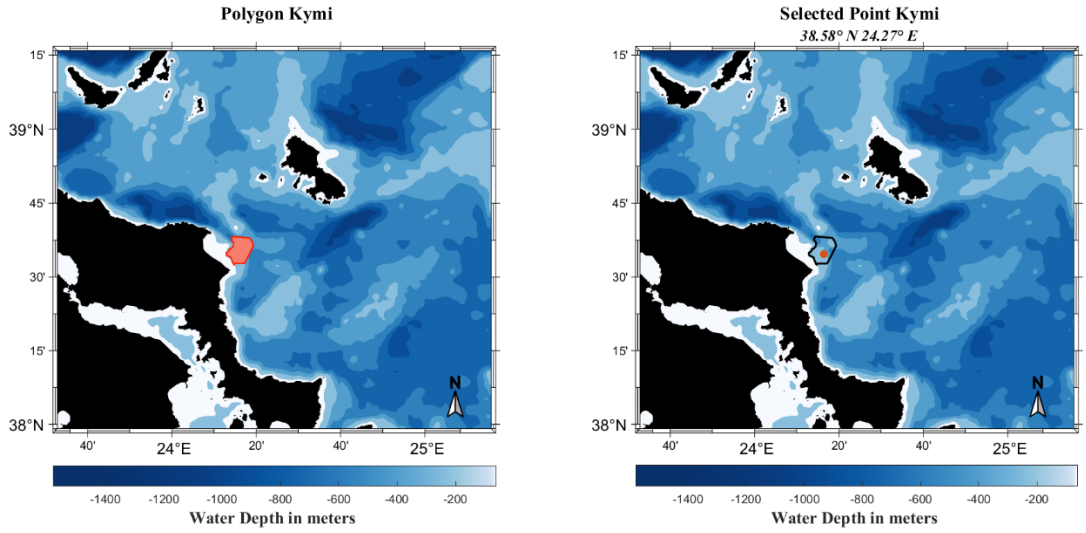

Figure 53. The location of polygon in Kymi and the corresponded examined point.

Psara Isl.

As mentioned earlier, in the eastern parts of the Aegean, and specifically in the extended area between Lesvos and Chios were presented high values of WS, and in for specific months, the overall highest. The western offshore areas of Chios Isl., hosts Psara Isl., which its location as well as the corresponded selected point from the 4 available from the model, are depicted in Figure 54, while further information is presented in Table 43.

Table 43. Information about the polygon in Psara Isl.

Polygon Name	Size of Polygon km^2	Selected point	Prioritization	Installation type	Time percentages
Psara	55.77	38.61°N 25.49°E	Long– term	Floating	82.63%

Table 44. The numerical results for the selected points of the polygon at Psara Isl.

Polygon	Energy $MWh/year$	CF %	WS			WPD		
			WS m/s	MAV %	IAV %	WPD W/m^2	MAV %	IAV %
Psara	66,297	50.45	8.43	49.52	3.36	651.49	127.83	7.89

The performance of WT at this point, was similar to the efficiency of the model in Karpathos and Crete-1, emerging comparable CF ratios and produced energy. The numerical results are presented in Table 44. The mean annual WS in Psara Isl., was emerged with increasing tendency (0.0016 m/s/year), while positive slopes were noticed regarding the extreme WS, 0.0104 and 0.0201 m/s/year for the 95th and the 99th percentiles, respectively. Noteworthy was the fact that Psara Isl., as well as Rhodes Isl., presented the highest positive slopes, compared to the rest of the examined sites.

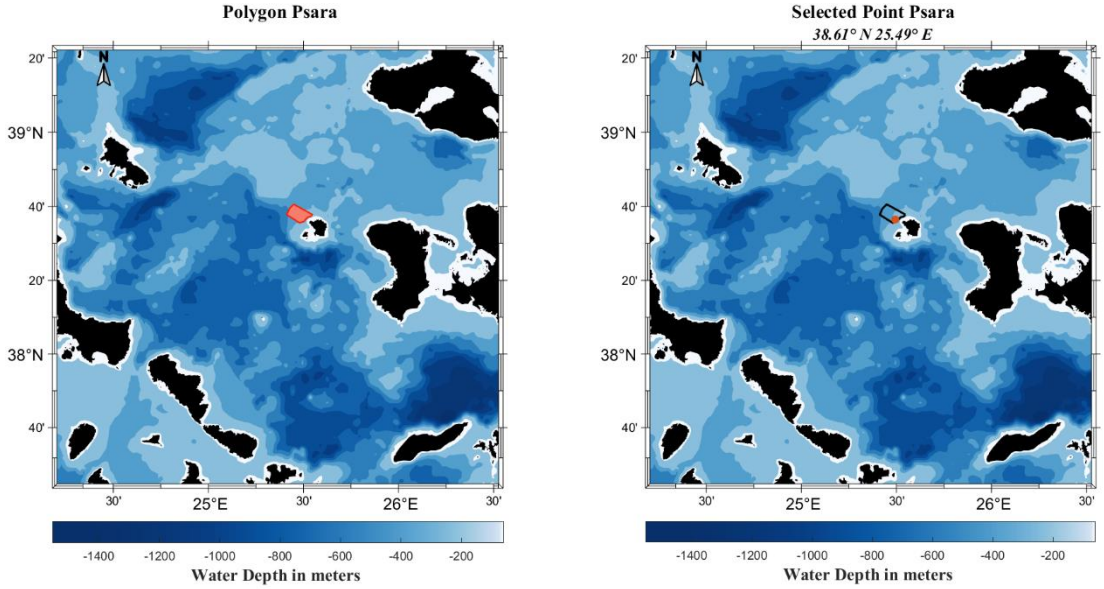

Figure 54. The location of the polygon in Psara and the corresponded examined point.

Rhodes Isl.

The polygon in Rhodes, is located near the SW coasts of the island, where high wind circulation between the complex of Kasos, Karpathos and Rhodes, create high WS channels, and therefore favorable wind potential for the installation of an OWF. The available points from the model were 5, and the examined point was, 35.87°N 27.69°E; for more details refer to Table 45.

Table 45. Information about the polygon in Rhodes Isl.

Polygon Name	Size of Polygon km^2	Selected point	Prioritization	Installation type	Time percentages
Rhodes	74.86	35.87°N 27.69°E	Medium– term	Floating	83.89%

Table 46. The numerical results for the selected points of the polygon in Rhodes Isl.

Polygon	Energy $MWh/year$	CF %	WS			WPD		
			WS m/s	MAV %	IAV %	WPD W/m^2	MAV %	IAV %
Rhodes	63,800	48.55	8.02	46.20	4.26	527.97	123.33	10,53

Regarding WT's performance in Rhodes Isl., the numerical results for the produced energy and the CF ratio (Table 46), were comparable with the three polygons in Gyaros Isl., indicating that the performance of the WT is similar in these islands. Nevertheless, the slopes that obtained from the analysis of the mean and the extreme WS, were emerged decreasing tendency regarding the mean and the less extreme wind speeds (95th percentile), -0.0150 and -0.0241 m/s/year, respectively, while positive slopes were observed for the higher extreme WS 0.0105 m/s/year.

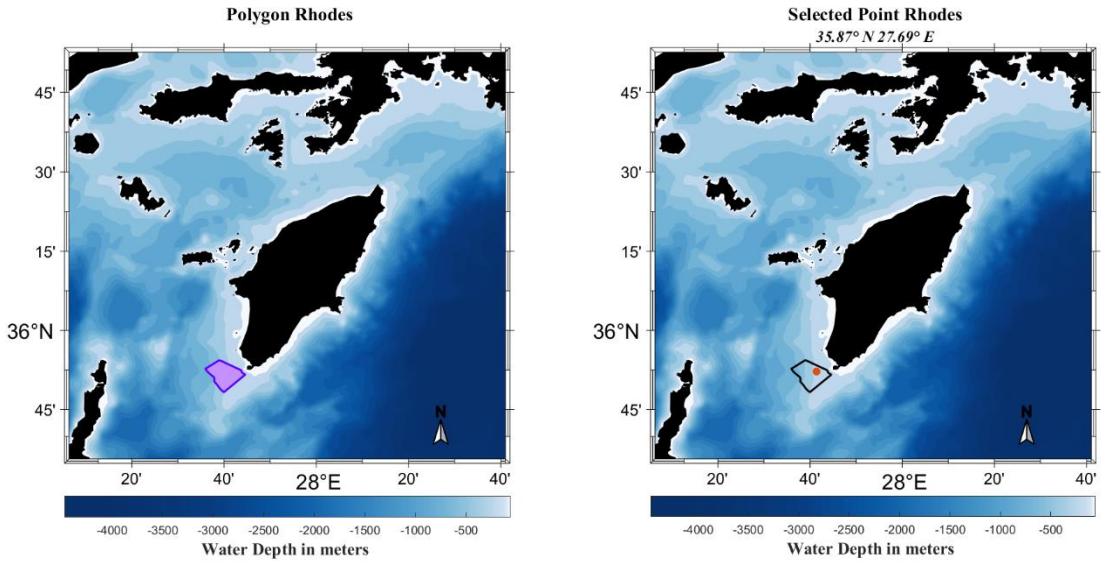

Figure 55. The location of the polygon in Rhodes and the corresponded examined point.

Saint Apostoloi

South of Kymi, another polygon (Saint Apostoloi) is located in the east offshore areas of Evvoia, with 8 available points from the model. From the numerical results presented in Table 48, the performance of the WT in Saint Apostoloi, was emerged high. Nevertheless, negative slopes were appeared in the area for both the mean annual WS (-0.038 m/s/year) and the extreme WS (-0.0167 for the 95th and -0.0113 m/s/year for the 99th percentiles). The location of the polygon is presented in Figure 56, while further information about the polygon in Table 47.

Table 47. Information about the polygon Saint Apostoloi

Polygon Name	**Size of Polygon** km^2	**Selected point**	**Prioritization**	**Installation type**	**Time percentages**
Saint Apostoloi	133.9	38.32°N 24.32°E	Medium– term	Floating	75.06%

Table 48. The numerical results for the selected point for the polygon Saint Apostoloi

Polygon	**Energy** $MWh/year$	**CF** %	**WS**			**WPD**		
			WS m/s	**MAV** %	**IAV** %	**WPD** W/m^2	**MAV** %	**IAV** %
Saint Apostoloi	55,075	41.88	7.37	54.74	4.34	479.95	136.47	11,80

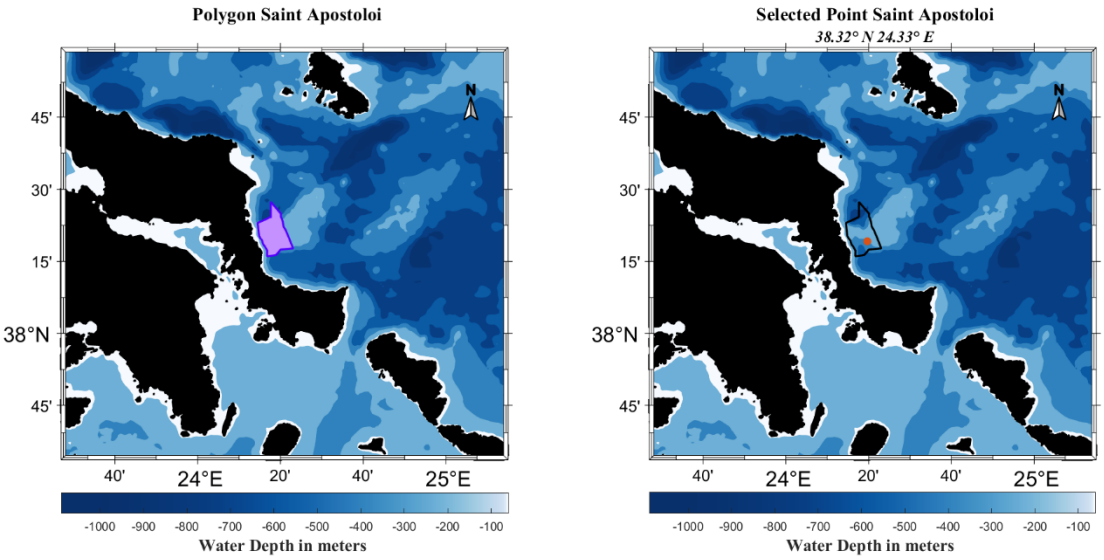

Figure 56. The location of the polygon in Saint Apostoloi and the corresponded examined point.

Pilot projects

Regarding the pilot projects, both for the statistical parameters of the wind climate and the performance of the WT, lower values were expected. Pilot projects are consisted by 4 polygons, located in the northern Aegean, two of which, near coasts of Evros, with 4 and 8 corresponded available points from the model, while the remaining two presented in the north parts of Samothrace Isl., with 4 and 7 points, respectively. The pilot projects have been designed in such a way that two polygons correspond to one project, nevertheless, in this study, the assessment of the WF and the statistical analysis of the wind aspects was performed for each site individually; for more details about the selected points, refer to Table 49.

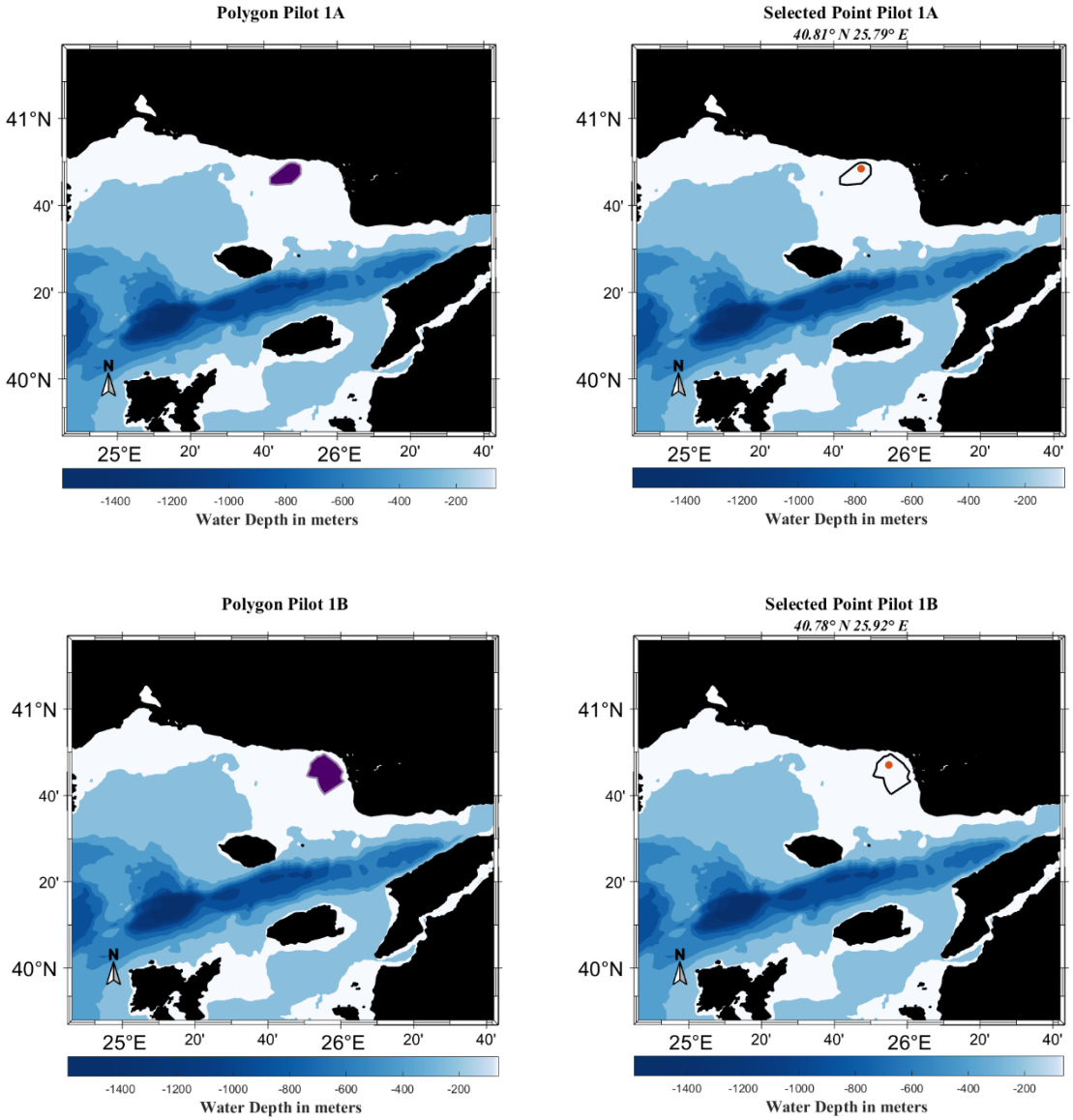

Figure 57. The locations of the polygons of the pilot project 1 and the corresponded examined points.

The numerical results obtained from the analysis, indicated that the performance of the WT for all the selected points, was extremely lower, compared to the other examined sites. Moreover, high coefficients of annual and inter – annual variability were noticed, as well as the lower values of WS and WPD, respectively.

Pilot-1A, presented the lower statistical parameters, as well as the overall minor performance of the WT between the 30 analyzed sites. Nonetheless, Pilot-1A emerged positive slopes, for both of the mean WS (0.0044 m/s/year) and the extreme wind speeds 0.0027 and 0.0193 m/s/year, for the 95th and 99th percentiles, respectively.

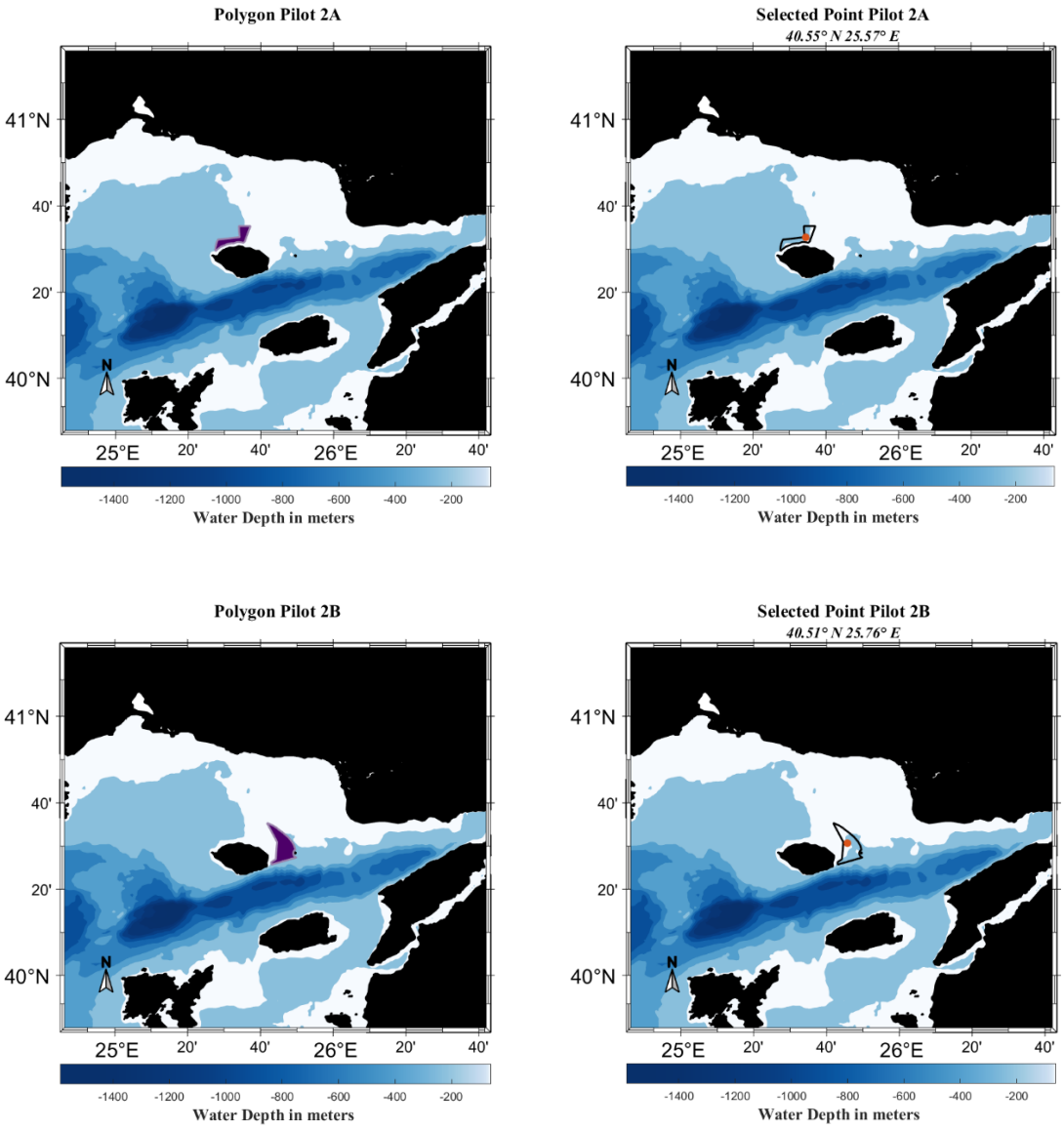

Figure 58. The locations of the polygons of the pilot project 2 and the corresponded examined points

Positive slopes were also emerged for Pilot-2A, where values of the order 0.0031 m/s/year spotted for the mean annual WS, as well as, for the higher extremes with slope 0.0145, and for winds ranging from 12 to 15 m/s, slope ~ 0.00035 m/s/year.

Table 49. Information about the pilot projects

Polygon Name	Size of Polygon km^2	Selected point	Prioritization	Installation type	Time percentages
Pilot 1A	219.42	40.81°N 25.79°E	Medium – term	Fixed -Bottom	63.90%
Pilot 1B		40.78°N 25.92°E			69.23%
Pilot 2A	133.98	40.55°N 25.57°E	Medium – term	Fixed - Bottom	66.37%
Pilot 2B		40.51°N 25.76°E			66.99%

The second pilot project, indicated highest values regarding the WT's performance, compared to Pilot-1, with corresponded higher variability measures. From the individual polygons, Pilot-2B, emerged with the higher standards regarding the produced energy and the CF ratio of the WT, since higher WS were also appeared in the area. Nevertheless, the variability coefficients for both of WS and WPD, were specified with higher values, compared to the other pilot polygons.

Both of the Pilot-2 project representative points were presented negative slopes for the mean annual WS and an increasing tendency regarding the extreme WS, which exceeded 16m/s (0.0099 m/s/year for Pilot 2A and 0.0184 m/s/year for Pilot 2B); while for the extreme speeds in range 12 – 15 m/s, negative slopes were appeared in both points, with slopes -0.00012 and -0.0029 m/s/year, respectively.

Table 50. The numerical results for the selected points on polygons for the Pilot projects

Polygon	Energy $MWh/year$	CF %	WS			WPD		
			WS m/s	MAV %	IAV %	WPD W/m^2	MAV %	IAV %
Pilot 1A	36,417	27.71.16	5.76	59.75	4.04	256.82	192.43	11.06
Pilot 1B	45,017	34.25	6.40	58.51	3.99	352.698	179.78	11.37
Pilot 2A	47,662	36.27	6.34	62.58	4.30	362.75	161.59	11.24
Pilot 2B	49,455	37.63	6.73	63.41	3.89	445.53	171.81	10.71

Conclusions and perspectives

In the present study, the statistical analysis of the offshore wind climate in Greece, for a 36 - year period (1985 – 2020) in 100 m height, above the sea level, was performed on three temporal scales (annual, monthly, seasonal). A detailed analysis, using the most recent regional reanalysis CERRA dataset, of the offshore WS, WD, WPD and the corresponded MAV and IAV variabilities was conducted, in order to evaluate the offshore wind climate in the Greek seas; the robust Thei Sen estimator was also applied, in order to estimate the linear slopes, i.e. the measure of tendency of wind speed for increase, decrease, or remain constant over time. The main purposes of this work were the evaluation and the analysis, of both of the entire offshore areas in Greece, and the potential sites emerged from the NDP – OWF 2023 by HEREMA for the development of OWFs, using the NREL -15MW WT. In order to compare the performance of the selected WT in the 30 sites of interest, apart from the statistical assessment the expected produced energy and the CF ratios were estimated on an annual scale for each of the 30 potential areas.

The spatial distribution of WS and WPD, were presented similar patterns for the three temporal scales. Regarding the annual scale, the most favorable areas, in terms of WS and WPD, were west and east coasts of Crete Isl., the offshore areas north of Kasos and Karpathos islands, as well as the eastern parts of the central Aegean, near Gyaros Isl. and east of Andros and Naxos islands, respectively. Significant values of WS and WPD were also noticed in the eastern and northern parts of the Aegean, while the Ionian Sea presented lower values; nevertheless, positive linear slopes were appeared for all the examined temporal scales in this region and specifically in its northern parts, in differ with the decrease tendency that emerged where the highest WS have been observed, in the Aegean Sea. Noteworthy, was that in several areas, such as SE Crete Isl., and the extended area between Psara and Chios islands, the extreme WS tended to increase over time, while the corresponded slopes for mean WS were negative.

Regarding the WS, WD and WPD analysis in the monthly and seasonal scale, the spatial distribution in the Greek seas from January to December indicated significant variations between individual months and seasons respectively, both in magnitude and spatially.

Specifically, the WS/WPD values followed a “circular” (seasonal) pattern, started in December with relatively high values. The highest WS values were observed in the northern and central Aegean, maintained until February (DJF), when peak values were observed for these months, with corresponding ENE wind directions. The pattern continues with a gradual decrease in March and April, with the highest WS/WPD shifted to the central Aegean in May, which is also the month with the overall lowest values of WS (MAM). Increased values were again observed in June, with the overall maximum in July and August, primarily distributed in the southeastern and central parts of the Aegean, with corresponded NNE WD in the northern parts of the Aegean, NW in the SE, and NW in the Ionian Sea with lower values of WS/WPD, compared to the Aegean. For JJA (summer), the highest WS/WPD were noticed in the SE Aegean, while noteworthy was that the corresponded slopes for this season were negative, indicating a decreasing tendency over time. In September abruptly decreased values of WS/WPD were observed, with a subsequent increase again in the northern Aegean and the Ionian in October. In November, a further increase was noticed in terms of WS/WPD and interesting WDs were observed in the Ionian Sea. The pattern, started again in December, with the highest WS noticed in the northern Aegean.

Regarding the assessment of the performance of the offshore NREL – 15 MW WT in the Greek Seas, the spatial distribution of the annual produced energy and CF ratios, have been followed

similar spatial and magnitude patterns. As for the 30 selected sites, the overall best performance of the WT was observed in Kasos Isl., along with the overall minimum value of MAV for both of WS and WPD, the highest mean annual WS which exceeded 9m/s, as well as, the highest time percentages of WS within the operational limits of the selected WT.

Apart from Kasos Isl., the WT showed great performance, in Donousa-2 and Ikaria-1, followed by Donousa-1, Psara and Crete-1. Nevertheless, despite Psara, the aforementioned areas presented decrease tendency over the 36-year period, fact that should be under consideration and further study, for the final installation of the potential OWFs. Antikythera was emerged with the overall minimum IAV values, while at the south coasts of Crete Isl., the representative point of the polygon Crete-4A, presented the overall highest; in each of the cases, both MAV and IAV constitute significant parameters for the development of an OWF, due to the fact that variability is directly associated with the assessment of long-term expected profits. Noteworthy was the fact that from all the examined areas, only 4 showed increasing trends regarding the mean annual WS, while the extreme wind speeds seemed to rise in most of these areas, in the 36-year period.

In general, the main conclusions of this study are summarized below:

- The Aegean Sea in terms of offshore wind energy significantly outperforms the Ionian.
- In the Aegean Sea were observed higher WS and WPD values with corresponded lower variability coefficients.
- Long-term increasing trends were observed in the Ionian Sea, while in the Aegean a general decrease. The highest negative slopes emerged in the areas where the highest values of WS observed.
- The highest WS values occurred in offshore areas with extremely deep depths, unsuitable for the installation of wind farms.
- Each coast of Crete Isl., presented different statistical characteristics and patterns.
- Positive slopes emerged for the 99^{th} percentiles in the eastern and central Aegean, with an exception the areas near east coasts of Crete Isl.; while negative slopes observed for the 95^{th} percentiles at several of the potential areas for the development of OWFs (Crete Isl., central Aegean, SW of Rhodes, surrounding areas of Kasos – Karpathos).
- The overall maximum time percentage where WS were within the operational limits of the NREL – 15 MW WT for the annual scale, was observed in areas west of Crete Isl., while for the monthly and seasonal scale, near Karpathos Isl., respectively.
- The spatial distribution of the WS/WPD regarding the monthly scale, showed a "circular" (seasonal) pattern both in magnitude and spatially. July and summer were characterized by the highest values of WS/WPD, respectively.
- Winter showed the most uniform spatial distribution for both WS and WPD, while summer seems to correspond to the most energetic season.
- The SW WDs observed in the Ionian Sea for November, combined with the NW winds noticed in the central Aegean, created over the southern Peloponnese to the west coast of Crete, formations similar to anticyclonic vortices, as noticed in west coasts of Crete Isl. of July.
- The potential sites of Crete Isl., showed significant statistical differences. The representative points of the southern coasts emerged with the overall highest values of IAV. The site where the WT presented its best performance was Kasos, where the highest values of WS, WPD, annual produced energy, CF, annual time percentages and corresponded low variability coefficients, observed.
- High values of annual energy produced by the NREL – 15 MW WT, observed in the entire Aegean, and lower in the Ionian Sea.
- The performance of the WT regarding the pilot projects was lower, compared to the rest sites. Nevertheless, increasing trends were noticed for these areas.

In the context of the analysis and the results discussed in this study, several perspectives emerge for future research, some of them presented below:

- Conducting in - situ measurements in the most favorable areas, in order to evaluate the reliability of the numerical data used in this study, mainly near the coasts and small straits.
- More extensive studies in the eastern side of the central Aegean for the identification of further potential areas for the development of OWFs.
- Studies on the potential impacts of climate change on Greece's offshore wind potential. In addition to the negative trends identified in this work, there are studies that show a decrease in the coming decades due to climate change.
- In-depth studies on the general conditions (geomorphological, socioeconomic, environmental, etc.) in the areas intended for the future installation of OWFs.
- Study of the cost of energy production, as well as its selling price.
- Assessment of synergies between OWE and offshore solar energy, with the aim of co-exploiting the maritime space, increasing the energy produced and reducing the related costs.

REFERENCES

1. Soukissian, T.H., et al., Marine Renewable Energy in the Mediterranean Sea: Status and Perspectives. Energies, 2017. **10**(10): p. 1512.
2. European Commission, Communication from the Commission to the European Parliament, the Council, the European Economic and Social Committee and the Committee of the Regions. An EU Strategy to harness the potential of offshore renewable energy for a climate neutral future. Brussels, 19.11.2020 COM(2020)741 final. . 2020.
3. European Commission; Communication from the commission to the european parliament, the council, the european economic and social committe of the regions: Blue Energy Action needed to deliver on the potential of ocean energy in European seas and oceans by 2020 and beyond /*COM/2014/08 final */. 2014 Publications Office of the European Union.
4. Appiott, J., A. Dhanju, and B. Cicin-Sain, Encouraging renewable energy in the offshore environment. Ocean & Coastal Management, 2013. **90**.
5. Soukissian, T., et al., European offshore renewable energy: Towards a sustainable future. 2023.
6. European Commission ; Horizon 2020 - Work Programme 2014 - 2025/ General Annexes/ Commission Decision C(2014)4995)
7. Portilla, J., J. Sosa, and L. Cavaleri, Wave energy resources: Wave climate and exploitation. Renewable Energy, 2013. **57**: p. 594-605.
8. Borthwick, A.G.L., Marine Renewable Energy Seascape. Engineering, 2016. **2**(1): p. 69-78.
9. European Commision;European Commision: The EU blue Economy Report 2023
10. Wang, L., et al., Flexible multibody dynamics modelling of point-absorber wave energy converters. Renewable Energy, 2018. **127**.
11. Tapoglou, E.G., A., Letout, S., Kuokkanen, A., Mountraki, A., Ince, E., Shtjefni, D., Joanny Ordonez, G., Eulaerts, O. and Grabowska, M., Clean Energy Technology Observatory: Ocean Energy in the European Union – 2022 Status Report on Technology Development, Trends, Value Chains and Markets, EUR 31219 EN. 2022, Publications Office of the European Union: Luxembourg.
12. Mutriku Wave Energy Plant. Spanish utility Ente Vasco de la Energía (EVE) officially commissioned the Mutriku Wave Energy Plant in July 2011., 2021.
13. Wello. The Penguin Wave Energy Converter Raw ocean power, direct to any grid. Available from: https://wello.eu/the-penguin-2/.
14. Marine Technology News,CorPower Ocean Installs First Commercial Wave Energy Converter Offshore Portugal. 2023.
15. Sgobbi, A.S., S.G.; Magagna, D.; Nijs, W., Assessing the Impacts of Technology Improvements on the Deployment of Marine Energy in Europe with an Energy System Perspective. 2016: p. 515–525.
16. Walters, R.A., et al., A study of tides and currents in Cook Strait, New Zealand. Ocean Dynamics, 2010. **60**(6): p. 1559-1580.
17. Coles, D., et al., A review of the UK and British Channel Islands practical tidal stream energy resource. Proceedings of the Royal Society A: Mathematical, Physical and Engineering Sciences, 2021. **477**(2255): p. 20210469.
18. Masood Ahmad, M., A. Kumar, and R. Ranjan, Recent Developments of Tidal Energy as Renewable Energy: An Overview, in River and Coastal Engineering: Hydraulics, Water Resources and Coastal Engineering, R. Jha, et al., Editors. 2022, Springer International Publishing: Cham. p. 329-343.
19. EMEC;Orbital multi - turbine tidal array to be delivered in new EU project. 2023.
20. Amir Garanovic;Minesto's 1.2MW tidal energy device on its way to Faroe Islands. 2023
21. PLOTEC: PLOCAN Tested Optimised Floating Ocean Thermal Energy Conversion Platform Available from: https://www.plymouth.ac.uk/research/materials-and-structures-research-group/research-projects/plotec-plocan-tested-optimised-floating-ocean-thermal-energy-conversion-platform.
22. Han, X.-W., et al., Review—Technologies and Materials for Water Salinity Gradient Energy Harvesting. Journal of The Electrochemical Society, 2021. **168**.
23. Oceans Energy; Leiden, The Netherlands; December 10, 2019 – Oceans of Energy successfully installed the first modules of the world's first offshore floating solar farm in the Dutch North

Sea. 2019; Available from: https://oceansofenergy.blue/2019/12/10/a-worlds-first-offshore-floating-solar-farm-installed-at-the-dutch-north-sea-2/.
24. Multiple Use of Space for Island Clean Autonomy - Blue Growth Solutions Available from: https://musica-project.eu/.
25. DHI; Develop offshore wind energy with respect for nature
26. Capps, S.B. and C.S. Zender, Estimated global ocean wind power potential from QuikSCAT observations, accounting for turbine characteristics and siting. Journal of Geophysical Research: Atmospheres, 2010. **115**(D9).
27. WindEurope, Wind energy in Europe: 2022 Statistics and the outlook for 2023-2027. 2022: p. 9 - 15; .
28. Jichuan Kang, L.S., C. Guedes Soares,, Fault Tree Analysis of floating offshore wind turbines,. Renewable Energy 2019. **133**: p. 1455 - 1467
29. Galparsoro, I., et al., Reviewing the ecological impacts of offshore wind farms. npj Ocean Sustainability, 2022. **1**(1): p. 1.
30. Bray, L., et al., Expected Effects of Offshore Wind Farms on Mediterranean Marine Life. Journal of Marine Science and Engineering, 2016. **4**(1): p. 18.
31. Kraus, S.D., R.D. Kenney, and L. Thomas. 2019. A Framework for Studying the Effects of Offshore Wind Development on Marine Mammals and Turtles. Report prepared for the Massachusetts Clean Energy Center, Boston, MA 2110, the Bureau of Ocean Energy Management 2019.
32. Arredondo-Galeana, A. and F. Brennan, Floating Offshore Vertical Axis Wind Turbines: Opportunities, Challenges and Way Forward. Energies, 2021. **14**(23): p. 8000.
33. Sánchez, S., et al., Foundations in Offshore Wind Farms: Evolution, Characteristics and Range of Use. Analysis of Main Dimensional Parameters in Monopile Foundations. Journal of Marine Science and Engineering, 2019. **7**(12): p. 441.
34. The Reservoir - Drops of knowledge; Decode offshore wind engineering challenges at every stage. Energy, Offshore wind; Available from: https://blog.dhigroup.com/decode-offshore-wind-engineering-challenges-at-every-stage/.
35. TGS 4C Offshore https://map.4coffshore.com/offshorewind/. 2023
36. Soukissian, T., et al., Assessment of offshore wind power potential in the Aegean and Ionian Seas based on high-resolution hindcast model results. AIMS Energy, 2017. **5**: p. 268-289.
37. Soukissian, T. and M.-A. Sotiriou, Long-Term Variability of Wind Speed and Direction in the Mediterranean Basin. Wind, 2022. **2**(3): p. 513-534.
38. Soukissian, T., et al., Offshore wind climate analysis and variability in the Mediterranean Sea. International Journal of Climatology, 2018. **38**(1): p. 384-402.
39. Kardakaris, K., I. Boufidi, and T. Soukissian, Offshore Wind and Wave Energy Complementarity in the Greek Seas Based on ERA5 Data. Atmosphere, 2021. **12**(10): p. 1360.
40. Polykarpou, M., et al., A Novel Data-Driven Tool Based on Non-Linear Optimization for Offshore Wind Farm Siting. Energies, 2023. **16**(5): p. 2235.
41. Hellenic Hydrocarbons and Energy Resources Management Company: National Development Program of offshore wind farms. 2023
42. S. Schimanke., L. Isaksson. , and L. Edvinsson Copernicus European Regional ReAnalysis (CERRA): product user guide. 2022
43. Parker, W., Reanalyses and Observations: What's the Difference? Bulletin of the American Meteorological Society, 2016. **97**: p. 160128144638003.
44. Hersbach, H., et al., The ERA5 global reanalysis. Quarterly Journal of the Royal Meteorological Society, 2020. **146**(730): p. 1999-2049.
45. Ulazia, A., et al., Global estimations of wind energy potential considering seasonal air density changes. Energy, 2019: p. 115938.
46. Hersbach, H., Bell, B., Berrisford, P., Biavati, G., Horányi, A., Muñoz Sabater, J., Nicolas, J., Peubey, C., Radu, R., Rozum, I., Schepers, D., Simmons, A., Soci, C., Dee, D., Thépaut, J-N. (2023): ERA5 hourly data on single levels from 1940 to present. Copernicus Climate Change Service (C3S) Climate Data Store (CDS), DOI: 10.24381/cds.adbb2d47 (Accessed on 12-01-2023).
47. Hersbach, H., Bell,, et al. ERA5 hourly data on single levels from 1940 to present. Copernicus Climate Change Service (C3S) .Climate Data Store (CDS), DOI: 10.24381/cds.adbb2d47 (Accessed on 23-01-2024). 2023.
48. Nezhad, M.M., et al., A new methodology for offshore wind speed assessment integrating Sentinel-1, ERA-Interim and in-situ measurement. Renewable Energy, 2021. **172**: p. 1301-1313.

49. Abdelaziz, S., et al., Assessing long-term future climate change impacts on extreme low wind events for offshore wind turbines in the UK exclusive economic zone. Applied Energy, 2024. **354**: p. 122218.
50. Copernicus Climate Change Service, Climate Data Store, (2019): Complete UERRA regional reanalysis for Europe from 1961 to 2019. Copernicus Climate Change Service (C3S) Climate Data Store (CDS). DOI:10.24381/cds.dd7c6d66 (Accessed on 23-1-2024).
51. Galanaki, E., et al., Validating the Copernicus European Regional Reanalysis (CERRA) Dataset for Human-Biometeorological Applications. 2023. **26**: p. 1-7.
52. Pelosi, A., Performance of the Copernicus European Regional Reanalysis (CERRA) dataset as proxy of ground-based agrometeorological data. Agricultural Water Management, 2023. **289**: p. 108556.
53. Giannaros, C., et al., Hourly values of an advanced human-biometeorological index for diverse populations from 1991 to 2020 in Greece. Scientific Data, 2024. **11**.
54. Schimanke S., et al. CERRA sub-daily regional reanalysis data for Europe on single levels from 1984 to present. Copernicus Climate Change Service (C3S) Climate Data Store (CDS), DOI: 10.24381/cds.622a565a (Accessed on 23-1-2024). 2021.
55. Wang, Z.Q. and R. Randriamampianina, The Impact of Assimilating Satellite Radiance Observations in the Copernicus European Regional Reanalysis (CERRA). Remote Sensing, 2021. **13**(3): p. 426.
56. Życzkowski, M., J. Szlapczynska, and R. Szlapczynski, Review of Weather Forecast Services for Ship Routing Purposes. Polish Maritime Research, 2019. **26**: p. 80-89.
57. Erni, B., F. Liechti, and B. Bruderer, The role of wind in passerine autumn migration between Europe and Africa. Behavioral Ecology, 2005. **16**(4): p. 732-740.
58. Gibb, R., et al., Remotely sensed wind speed predicts soaring behaviour in a wide-ranging pelagic seabird. Journal of The Royal Society Interface, 2017. **14**(132): p. 20170262.
59. Martinez, A. and G. Iglesias, Global wind energy resources decline under climate change. Energy, 2024. **288**: p. 129765.
60. Martinez, A. and G. Iglesias, Climate-change impacts on offshore wind resources in the Mediterranean Sea. Energy Conversion and Management, 2023. **291**: p. 117231.
61. Bonanno, R., F. Viterbo, and R.G. Maurizio, Climate change impacts on wind power generation for the Italian peninsula. Regional Environmental Change, 2022. **23**(1): p. 15.
62. Can, M., et al., The Impact of Meteorological Factors on Fine Particulate Pollution in Northeast China. Aerosol and Air Quality Research, 2020.
63. Pogumirskis, M., et al., PCA analysis of wind direction climate in the baltic states. Tellus A: Dynamic Meteorology and Oceanography, 2021. **73**(1): p. 1-16.
64. Casas-Prat, M., et al., Wind-wave climate changes and their impacts. Nature Reviews Earth & Environment, 2024. **5**.
65. Weisse, R., et al., Sea level dynamics and coastal erosion in the Baltic Sea region. Earth Syst. Dynam., 2021. **12**(3): p. 871-898.
66. Marchigiani, R., et al., Wind disasters: A comprehensive review of current management strategies. International journal of critical illness and injury science, 2013. **3**: p. 130-42.
67. Stathopoulos, T. and H. Alrawashdeh, Wind loads on buildings: A code of practice perspective. Journal of Wind Engineering and Industrial Aerodynamics, 2020. **206**: p. 104338.
68. He, Y., et al., Urban ventilation assessment with improved vertical wind profile in high-density cities – Comparisons between LiDAR and conventional methods. Journal of Wind Engineering and Industrial Aerodynamics, 2022. **228**: p. 105116.
69. Soukissian, T.H., Probabilistic modeling of directional and linear characteristics of wind and sea states. Ocean Engineering, 2014. **91**: p. 91-110.
70. Song, M., et al., Optimization of wind turbine micro-siting for reducing the sensitivity of power generation to wind direction. Renewable Energy, 2016. **85**: p. 57-65.
71. Díaz, H., et al., Micro sitting of floating wind turbines in a wind farm using a multi-criteria framework. Renewable Energy, 2023. **204**: p. 449-474.
72. Soukissian, T., F. Karathanasi, and P. Axaopoulos, Satellite-Based Offshore Wind Resource Assessment in the Mediterranean Sea. IEEE Journal of Oceanic Engineering, 2016. **42**: p. 1-14.
73. Melas, Dimitrios, Prodromos Zanis, and Anastasia Poupkou. "Present Climate Trend Analysis of the Etesian Winds in the Aegean Sea." Theoretical and Applied Climatology (2011): n. pag. Print.
74. Georgiou, S., et al., Climate variability and deep water mass characteristics in the Aegean Sea. Atmospheric Research, 2015. **152**: p. 146-158.

75. Kotroni, V., K. Lagouvardos, and D. Lalas, The effect of the island of Crete on the Etesian winds over the Aegean Sea. Quarterly Journal of the Royal Meteorological Society, 2001. **127**: p. 1917-1937.
76. Alpert, P., et al., A new seasons definition based on classified daily synoptic systems: An example for the Eastern Mediterranean. International Journal of Climatology - INT J CLIMATOL, 2004. **24**: p. 1013-1021.
77. Poupkou, A., et al., Present climate trend analysis of the Etesian winds in the Aegean Sea. Theoretical and Applied Climatology, 2011. **106**: p. 459-472.
78. Dafka, S., et al., Twenty-First-Century Changes in the Eastern Mediterranean Etesians and Associated Midlatitude Atmospheric Circulation. Journal of Geophysical Research: Atmospheres, 2019. **124**(23): p. 12741-12754.
79. Soukissian, T.H., F.E. Karathanasi, and D.K. Zaragkas, Exploiting offshore wind and solar resources in the Mediterranean using ERA5 reanalysis data. Energy Conversion and Management, 2021. **237**: p. 114092.
80. Berens, P., CircStat: A MATLAB Toolbox for Circular Statistics. Journal of Statistical Software, 2009. **31**(10): p. 1 - 21.
81. Theil, H., A Rank-Invariant Method of Linear and Polynomial Regression Analysis, in Henri Theil's Contributions to Economics and Econometrics: Econometric Theory and Methodology, B. Raj and J. Koerts, Editors. 1992, Springer Netherlands: Dordrecht. p. 345-381.
82. Sen, P.K., Estimates of the Regression Coefficient Based on Kendall's Tau. Journal of the American Statistical Association, 1968. **63**(324): p. 1379-1389.
83. Chervenkov, H. and K. Slavov, Theil–Sen estimator vs. Ordinary least squares — Trend analysis for selected ETCCDI climate indices. Comptes rendus de l'Académie bulgare des sciences: sciences mathématiques et naturelles, 2019. **72**: p. 47-54.
84. Conover, W.J., Practical Nonparametric Statistics. 1999: Wiley.
85. NREL (National Renewable Energy Laboratory). 2020. "2020 Annual Technology Baseline: Offshore Wind." Golden, CO: National Renewable Energy Laboratory. https://atb.nrel.gov/electricity/2020/index.php?t=ow. Accessed January 23, 2021.
86. Allen, Christopher, Anthony Viselli, Habib Dagher, Andrew Goupee, Evan Gaertner,Nikhar Abbas, Matthew Hall, and Garrett Barter. Definition of the UMaine VolturnUS-S Reference Platform Developed for the IEA Wind 15-Megawatt Offshore Reference Wind,Turbine. Golden, CO: National Renewable Energy Laboratory. NREL/TP-5000-76773..
87. Pawlowicz, R., 2020. "M_Map: A mapping package for MATLAB", version 1.4m, [Computer software], available online at www.eoas.ubc.ca/~rich/map.html.
88. Prezerakos, N. G. (2021). Etesian winds outbursts over the Greek Seas and their linkage with larger-scale atmospheric circulation features: Two real time data case studies. Atmósfera, 35(1), 89–110. https://doi.org/10.20937/ATM.52838.